Universidade do Minho
I3Bs - Instituto de Investigação em Biomateriais, Biodegradáveis e Biomiméticos

Carla Patrícia Martins Abreu

Strategies towards the recreation of a hair follicle regenerative microenvironment

Strategies towards the recreation of a hair follicle regenerative microenvironment

Carla Patrícia Martins Abreu

UMinho | 2020

Outubro de 2020

Universidade do Minho

I3Bs - Instituto de Investigação em Biomateriais, Biodegradáveis e Biomiméticos

Carla Patrícia Martins Abreu

Strategies towards the recreation of a hair follicle regenerative microenvironment

Tese de Doutoramento

Doutoramento em Engenharia de Tecidos, Medicina Regenerativa e Células Estaminais

Trabalho efetuado sob a orientação da

Doutora Alexandra Margarida Pinto Marques

Outubro de 2020

ACKNOWLEDGMENTS

This thesis represents a five-year journey and even though the present document is mainly intended to report all the scientific work performed, it indirectly reflects the people who professionally and/or personally were part of it, and to whom I am profoundly thankful.

It is my opinion that any doctorate should be based on hard and conscious work, but the materialization of this thesis also had some fortune associated. And my luckiest moment was having Dr Alexandra Marques appointed as my supervisor. She is, without question, the most passionate, hard worker and scientifically rigorous supervisor that I have ever met, and for those reasons, I will always look up for her as a role model. Thank you for all the time, dedication and knowledge you provided me with. To Professor Rui Reis I am truly grateful for the unique opportunity I found at 3Bs. Either through the attribution of a scholarship or by providing me with superior technical and financial resources to conduct my studies, this was a rare opportunity. I hope I have met his expectations and all the others that, in August 2015, evaluated me and decided I was worth giving a shot. I am also thankful to all the friends and colleagues that helped me during my doctoral years. This includes Manuela Lago, who always backed me up and constantly offered me help, and Mariana Cerqueira, Luca Gasperini, Lucília Silva and Rogério Pirraco who provided me with assistance and guidance whenever I needed.

Words are powerless to express my gratitude to my parents. One cannot control the family in which she is born, but I was fortunate to have the best parents with me all along. This last year was harsh by so many reasons, but they were one of my pillar stones, always there, always doing whatever they could to support me at different levels, even when they were the ones in need. I hope I can now dedicate more time to help you and Nuno instead. But my supportive network extends beyond my family and includes the friends I made at the beginning of this journey - Xana, Bárbara, Marta Casanova and Marta Guedes. Thank you for your support and patience, it would not have been the same without you and you know it. It also includes my beloved Ricardo. We meet each other in a difficult period, as two PhD students fighting for realization and ever since you have supported me through difficult times. Either celebrating my small victories or providing kind words in moments of distress you were always there. Let's hope we can now behave like a normal couple and enjoy our weekends.

STATEMENT OF INTEGRITY

I hereby declare having conducted this academic work with integrity. I confirm that I have not used plagiarism or any form of undue use of information or falsification of results along the process leading to its elaboration.

I further declare that I have fully acknowledged the Code of Ethical Conduct of the University of Minho.

ABSTRACT

The hair follicle (HF) is an exclusive skin appendage with important physiological and aesthetic functions including thermoregulation, physical protection, immunosurveillance and sensory perception. Despite its ability to undergo repeated lifelong cycles of regeneration, new HFs cannot be naturally formed after birth. After a significant injury, the repaired skin lacks this critical appendage, significantly compromising its functionality. In hair associated disorders, the success of the treatments is limited to autologous replacement therapies which are often compromised by the disease itself, including the lack of sufficient follicles available for transplantation. Hair development and cyclical growth are driven by the bidirectional signaling occurring between the epithelial and mesenchymal compartments of the HF. In this dynamic crosstalk, a key population of mesenchymal cells – the dermal papilla (DP) cells – instructs epithelial cells towards hair formation. So far, successful translation of regenerative strategies has been hampered by difficulties associated with the preservation of the trichogenic capacity of these cells during *in vitro* culture and expansion, which are required to obtain clinically relevant cell numbers.

In pursuit of a more accessible epithelial cell source, we explored the use of skin epidermal keratinocytes with stem cell characteristics (EpSIKCs), demonstrating their phenotypic similarity with follicular keratinocytes and capacity to crosstalk with DP cells. To counteract the loss of trichogenic properties that DP cells suffer in culture, we investigated the influence of skin keratinocyte-conditioned medium, physiological oxygen levels, as well as DP native extracellular matrix (ECM) features. We showed that DP cell inductivity and phenotype are partially recovered by culture with keratinocyte-conditioned medium or in ECM biomimetic peptide hydrogels. Moreover, we confirmed that physoxia (5% oxygen) improves the phenotype and functionality of DP cells, which is further enhanced when these cells are directly interacting with melanocytes. Finally, the generation of a human skin *in vitro* model bearing HF-like structures was pursued. A microfabrication technique was used to support the physical interaction between DP cells and keratinocytes and further elicit their critical crosstalk in a standard organotypic skin model, contributing to the recreation of a HF regenerative microenvironment *in vitro*.

The distinct strategies explored in this thesis provide valuable knowledge, which in the future may contribute to the bioengineering of complete human HFs *in vitro* or to promote the much desired HF regeneration or HF neoformation *in situ*.

Keywords: Epithelial-mesenchymal crosstalk, hair follicle, hair regeneration, *in vitro* models, peptide-based hydrogels, physoxia.

RESUMO

O folículo piloso (FP) é um apêndice da pele com importantes funções fisiológicas e estéticas incluindo termoregulação, proteção física, imunovigilância e perceção sensorial. Apesar do seu crescimento cíclico, em humanos não é possível formar novos FPs após o nascimento. Após uma lesão grave a nova pele não terá FPs, comprometendo a sua funcionalidade. Além disso, em doenças de foro capilar, o sucesso dos tratamentos é limitado a terapias de substituição autólogas, muitas das vezes comprometidas pela própria doença. A formação e crescimento do pelo são impulsionados pela sinalização bidirecional que ocorre entre os compartimentos epitelial e mesenquimal do FP. Nesta comunicação dinâmica, uma população chave de células mesenquimais – as células da papila dérmica (PD) – instruem as células epiteliais para a formação de pelo. No entanto, a translação de estratégias regenerativas tem sido impedida pela dificuldade em preservar a tricogenicidade destas células durante a sua expansão *in vitro*, a qual é necessária para obter um número de células clinicamente relevante.

Dada a necessidade de uma fonte de células epiteliais mais acessível do que o FP, demonstrámos que uma subpopulação de queratinócitos da pele com características estaminais é fenotipicamente semelhante aos queratinócitos foliculares e capaz de comunicar com as células da PD. No sentido de contrariar a perda de capacidade tricogénica que as células da PD sofrem em cultura, investigámos a influência do meio condicionado de queratinócitos da pele, de níveis de oxigénio fisiológicos (5% oxigénio, O_2) e o papel de elementos da matriz extracelular (MEC) da PD no mesmo. Quer a cultura das células da PD com o meio condicionado, quer em hidrogéis funcionalizados com péptidos que mimetizam a MEC da PD, permitiram recuperar parcialmente a indutividade e propriedades nativas destas células. Mais ainda, as condições de 5% O_2 melhoraram o fenótipo e funcionalidade das células da PD, efeito este que é realçado quando estas contactam diretamente com melanócitos. Por fim, explorámos a criação de um modelo *in vitro* de pele humana contendo estruturas morfologicamente semelhantes a FPs. A interação física entre as células da PD e os queratinócitos e, consequentemente, a comunicação entre ambos foi promovida pela microfabricação do hidrogel base de um modelo organotípico de pele, permitindo assim a recriação de um microambiente regenerativo de FP *in vitro*.

As diferentes estratégias exploradas nesta tese permitiram obter novos conhecimentos que, no futuro, poderão contribuir para a bioengenharia de FP humanos *in vitro* ou para a promoção da tão desejada regeneração ou neoformação de FPs *in situ*.

Palavras-chave: condições fisiológicas de oxigénio, folículo piloso, hidrogéis baseados em péptidos, modelos *in vitro,* regeneração de pelo, sinalização epitelial-mesenquimal.

TABLE OF CONTENTS

CHAPTER III - INTERFOLLICULAR EPIDERMAL STEM-LIKE CELLS FOR THE RECREATION OF THE HAIR FOLLICLE EPITHELIAL COMPARTMENT

CHAPTER IV - RESCUING KEY NATIVE TRAITS IN CULTURED DERMAL PAPILLA CELLS FOR HUMAN HAIR REGENERATION

CHAPTER V - GELLAN GUM-DERIVED HYDROGELS SUPPORT THE RECREATION OF THE DERMAL PAPILLA MICROENVIRONMENT

CHAPTER VII - MICROSCOPY-GUIDED LASER ABLATION FOR THE CREATION OF COMPLEX SKIN MODELS WITH FOLLICULOID APPENDAGES

CHAPTER VIII -GENERAL CONCLUSIONS AND FUTURE PERSPECTIVES

LIST OF ABBREVIATIONS

°C – Degree Celsius

2D – Two-dimensional

3D – Three-dimensional

α-MEM – Alpha-Minimum Essential Medium

α-SMA – Alpha-smooth muscle actin

λem – Emission wavelength

λex - Excitation wavelength

μg – Microgram

μJ – Microjoule

μL – Microliter

μm – Micrometer

μM – Micromolar

A

AB – Antibiotic and antimycotic solution

ABTS – 2, 2'-azinobis (3-ethylbenzothiazoline-6-sulfonic acid)

AF – Alexa Fluor

ALI – Air-liquid interface

ALP – Alkaline phosphatase

AM – Acetoxymethyl

ANOVA – Analysis of variance

APC – Allophycocyanine

APM – Arrector pili muscle

Arg – Arginine

Asp – Aspartic acid

B

BCA – Bicinchoninic acid protein

BCPI – 5-bromo-4-chloro-3-indolyl phosphate

bFGF – Basic fibroblast growth factor (also known as FGF2)

BIO – 6-bromoindirubin-3'-oxime

BMP – Bone morphogenetic protein

BPE – Bovine pituitary extract

bri – Staining brighter than the negative control

BSA – Bovine serum albumin

C

CD184 – CXC chemokine receptor type 4

CD29 – Integrin β1

CD49f – Integrin α6

CD71 – Transferrin receptor

CISH – Chromogenic *in situ* hybridization

CM – Conditioned medium

cm^2 – Square centimeter

COL – Collagen

cRGDfC – Cyclo [Arg-Gly-Asp-(D-Phe)-Cys]

CTRL – Control

Cys – cysteine

D

DAPI – 4′,6-diamidino-2-phenylindole

DCF – Dichlorodihydrofluorescein

DCFH – 2',7'-dichlorodihydrofluorescin

DE – Dermal equivalent

DFbs – Dermal fibroblasts

DI – Deionized

Diff – Differentiated

dim – Staining slightly increased than the negative control

DM – Degree of modification

DMEM – Dulbecco's modified Eagle's medium

DMMB – Dimethylmethylene blue

DNA – Deoxyribonucleic acid

DP – Dermal papilla

DS – Dermal sheath

dsDNA – Double strained DNA

DSHB – The Developmental Studies Hybridoma Bank

DVS – Divinyl sulfone

DWT – Dermal white adipose tissue

E

e.g. – "for example", from latin *exempli gratia*

ECM – Extracellular matrix

Eda – Ectodysplasin

Edar – Ectodysplasin receptor

EDTA – Ethylenediamine tetraacetic acid

EGF – Epidermal growth factor

ELISA – Enzyme-linked immunosorbent assay

EMI – Epithelial-mesenchymal interaction

EpSC – Epidermal stem cell

EpSlKC – Epidermal keratinocyte with stem-like features

et al. – And others

F

FABP4 – Fatty acid-binding protein 4

FACS – Fluorescence-activated cell sorting

FBS – Fetal bovine serum

FCT – Fundação para a Ciência e a Tecnologia

FGF – Fibroblast growth factor

FITC – Fluorescein isothiocyanate

FL – Fluorescent

Fn – Fibronectin

G

G – Gauge

g – Gram(s)

GAG – Glycosaminoglycan

GG – Gellan gum

GG-DVS – Gellan gum-divinyl sulfone

Glu – Glutamic acid

Gly – Glycine

GSK3 – Glycogen synthase kinase-3

H

h – Hour

H&E – Hematoxylin and eosin

HEM – Human epidermal melanocytes

HepIII – Cys-Gly-Glu-Phe-Tyr-Phe-Asp-Leu-Arg-Leu-Lys-Gly-Asp-Lys

HF – Hair follicle

HHFKC – Human hair follicular keratinocyte

hMel – Human melanocytes

HRP – Horseradish peroxidase

I

i.e –"that is", from latin *id est*

ICC – Immunocytochemistry

IFE – Interfollicular epidermis

IHC – Immunohistochemistry

IL-6 – Interleukin 6

IRS – Inner root sheath

J

JAK/STAT – Janus kinase/signal transducers and activators of transcription

K

K – Keratin

KC – Keratinocyte

KCs-CM – Conditioned medium collected from keratinocytes

kg – Kilograms

KGF – Keratinocyte growth factor

kHz – Kilohertz

kN – Kilonewton

KSFM – Keratinocyte Serum-free Medium

L

L – Liter

LDH – Lactate dehydrogenase

L-DOPA – L-3,4-dihydroxyphenylalanine

LEF1 – Lymphoid enhancer-binding factor 1

Leu – Leucine

LRP4 – Low-density lipoprotein receptor-related protein 4

Lys – Lysine

M

m – Meter

M – Molar

mg – Milligram

MGLA – Microscopy guided laser ablation

min – Minute(s)

miRNA – Micro-ribonucleic acid

mL – Milliliter

mm – Milimiter

mM – milimolar

mRNA - Messenger ribonucleic acid

Ms – Mouse

N

N – Newton

NA – Not applicable

NAC – N - acetyl cysteine

NBT – p - nitroblue tetrazolium chloride

NCOL – Non-collagenous

nd – Bellow the assay detection level

NF-κB – nuclear factor-kappa B

ng – Nanograms

NL - Netherlands

nm – Nanometers

O

OD – Optical density

ORS – Outer root sheath

P

p – Statistical level of significance

PBS – Phosphate buffered saline

PBST – Phosphate-buffered saline with 0.1% Tween 20

PDGF-A – Platelet-derived growth factor A

PE – Phycoerythrin

PenStrep – Penicillin and streptomycin solution

pg – Picogram

pH – Potential hydrogenionic

Phe – Phenylalanine

PI – Propidium iodide

R

Rb – Rabbit

rcf – Relative centrifugal force

rEGF – Recombinant epidermal growth factor

RM – Repeated measures

RNA – Ribonucleic acid

RNS – Reactive nitrogen species

ROS – Reactive oxygen species

rpm – Rotations per minute

RT – Room temperature

S

s – Second(s)

SA-β-GAL – Senescence-associated β-galactosidase

SCBT – Santa Cruz Biotechnology

SDS – Sodium dodecyl sulfate

SEM – Standard error of the mean

SG – Sebaceous gland

Shh – Sonic hedgehog

T

T150 – Tissue culture flask with a growth area of 150 cm_2

T75 – Tissue culture flask with a growth area of 75 cm^2

TA – Transit amplifying

TBS – Tris-buffered saline

TERM – Tissue engineering and regenerative medicine

TGF – Transforming growth factor

TMB – 3,3′,5,5′-tetramethylbenzidine

TRITC – Tetramethylrhodamine

Tyr – Tyrosine

TYR – Tyrosinase activity

U

UK – United Kingdom

USA – United States of America

V

v/v – Volume/volume

VCAN_V1 – V1-isoform of versican

VCAN_V2 – V2-isoform of versican

VD3 – 1α,25-dihydroxyvitamin D3

VEGF – Vascular endothelial growth factor

W

w/v – Weight/volume

LIST OF FIGURES

LIST OF SUPPLEMENTARY FIGURES

LIST OF TABLES

SHORT *CURRICULUM VITAE*

Carla Abreu was born on the 1st of March 1990, in Santo Tirso (Portugal). She started her graduate academic education at the Faculty of Pharmacy of the University of Porto (Portugal), where she enrolled in a five-year Integrated Master's in Pharmaceutical Sciences in 2008. During this period, Carla started her contact in research as a trainee at the Pharmacology Department of the same Faculty, under the supervision of Dr Manuela Morato and Dr Carmen Diniz. In the final year of this Master's degree, she got the opportunity to perform a training abroad at INSERM - *Institut National de la Santé et de la Recherche Médicale* (Marseille, France), within the scope of the Erasmus Program. During this three-month training, she not only got in touch with top-level research, in an international research dedicated institute, as also became acquainted with techniques that proven to be essential later on in her studies.

After concluding this Master's degree in 2013, she started working as an undergraduate researcher at the Department of Experimental Biology of the Faculty of Medicine of the University of Porto (Portugal), supervised by Dr Isaura Tavares and Dr Marisa Oliveira. This opportunity enabled her to deepen her knowledge and experience with previously acquired techniques, including cell culture, and to explore complementary skills such as *in vivo* testing and cellular/molecular characterization.

In September of 2015, she was awarded a PhD scholarship from the *Fundação para a Ciência e a Tecnologia* (FCT) to enroll in the Tissue Engineering, Regenerative Medicine & Stem Cells Doctoral Program of the University of Minho (Portugal). Ever since she has been conducting her PhD studies at the Institute for Biomaterials, Biodegradables and Biomimetics of the University of Minho, under the supervision of Dr Alexandra P. Marques.

While a PhD student, Carla Abreu has been interested in exploring both cellular and biomaterial strategies for a physiological-driven recreation of the hair follicle microenvironment. Moreover, she has also been actively involved in other scientific activities, as a member of organizing committees of conferences held by her research group, and in the foundation and development of *PhDynamics*, a science dissemination and soft-skills program organized by PhD students. She has also been participating in the scientific community, either by acting as referee of scientific papers of her area of research, as well as through participation in several important meetings in the Tissue Engineering and Regenerative Medicine field, including the 2019 TERMIS-EU Chapter.

LIST OF PUBLICATIONS

The work performed during the PhD period resulted in the publications listed below.

Papers in international scientific journals with referees (as first author)

1. **C. M. Abreu**, R. Pirraco, R. L. Reis, M. T. Cerqueira F.M., A. P. Marques. Interfollicular epidermal stem-like cells for the recreation of the hair follicle epithelial compartment. Submitted (2020)

2. **C. M. Abreu**, M. T. Cerqueira, R. Pirraco, L. Gasperini, R. L. Reis, A. P. Marques. Rescuing key native traits in cultured dermal papilla cells for human hair regeneration. Accepted for publication in *Journal of Advanced Research* (2020)

3. **C. M. Abreu**, M.E.L. Lago, J. Pires, R. L. Reis, L.P. da Silva, A. P. Marques. Gellan gum-based hydrogels support the recreation of the dermal papilla microenvironment. Submitted (2020)

4. **C. M. Abreu**, R. L. Reis, A. P. Marques. Dermal papilla cells and melanocytes response to physiological oxygen levels depends on their Interactions. Submitted (2020)

5. **C. M. Abreu**, L. Gasperini, M.E.L. Lago, R. L. Reis, A. P. Marques. Microscopy-guided laser ablation for the creation of complex skin models with folliculoid appendages. Accepted for publication in *Bioengineering & Translational Medicine* (2020)

6. **C. M. Abreu**, R. L. Reis, A. P. Marques. Bioengineering human hair follicle models: where do we stand? Submitted (2020)

Conference oral presentations (as first author and speaker)

1. **C. M. Abreu**, M. T. Cerqueira, R. P. Pirraco, R. L. Reis, F. Watt, A. P. Marques. Effect of EpSCs conditioned medium on dermal papilla cells. *TERMIS EU*. Rhodes, Greece, May, (2019) in: *European Cells and Materials*, Collection 3, 376 (2019)

2. **C. M. Abreu**, M. E. L. Lago, L. P. da Silva, H. R. Moreira, M. T. Cerqueira, R. L. Reis, A. P. Marques. Gellan gum-based hydrogels as a suitable platform to recreate the hair follicle 3D compartments. *Chem2Nature First School*. Guimarães, Portugal (2016)

3. **C. M. Abreu**, M. T. Cerqueira, R. P. Pirraco, R. L. Reis, A. P. Marques. Effect of epidermal-stem like cells conditioned medium on dermal papilla cells. *Gene2Skin Final Conference*. Guimarães, Portugal (2018)

Conference oral presentations (as co-author)

1. L. P. da Silva, G. Paulat, M. E. L. Lago, **C. M. Abreu**, A. F. Carvalho, R. L. Reis, A. P. Marques. Complex bioprinted skin analogue. *9th Conference of the European Wound Management Association*. Gothenburg, Sweden (2019)

2. M. E. L. Lago, **C. M. Abreu**, L. P. da Silva, M. T. Cerqueira, R. P. Pirraco, R. L. Reis, A. P. Marques. 3D constructs as cell-based regenerative approaches and *in vitro* patforms to study the crosstalk between dermal white adipose tissue and dermal papilla cells. *Gene2Skin Final Conference*. Guimarães, Portugal (2018)

3. L. P. da Silva, G. Paulat, M. E. L. Lago, **C. M. Abreu**, A. F. Carvalho, R. L. Reis, A. P. Marques. Skin-tailored bioinks. *Gene2Skin Final conference*. Guimarães, Portugal (2018)

4. L. P. da Silva, G. Paulat, M. E. L. Lago, **C. M. Abreu**, A. F. Carvalho, R. L. Reis, A. P. Marques. Tailoring bioink biofeatures to meet skin microenvironments specificities. *5th TERMIS World Congress*. Kyoto, Japan (2018)

5. L. P. da Silva, M. E. L. Lago, **C. Abreu**, R. L. Reis, A. P. Marques. Biofunctionalized gellan gum hydrogels as tailored platforms for skin regenerative purposes. *TERMIS EU*. Davos, Switzerland (2017) in: *European Cells and Materials*, Collection 2, 306 (2017)

Conference posters (as first author)

1. **C. M. Abreu**, M. E. L. Lago, L. P. da Silva, R. L. Reis, A. P. Marques. Encapsulation of dermal papilla cells in functionalized-gellan gum hydrogels. *FoReCaST Second Workshop*. Porto, Portugal (2019)

2. **C. M. Abreu**, M. E. L. Lago, L. P. da Silva, R. L. Reis, A. P. Marques. Biofunctionalized gellan gum hydrogels for the recreation of the hair follicle mesenchymal compartment. *1st Discoveries Forum*. Porto, Portugal (2019)

3. **C. M. Abreu**, R. L. Reis, A. P. Marques. Study of the crosstalk between melanocytes and dermal papilla cells under hyperoxic and normoxic Culture Conditions. *Term Stem*, Braga, Portugal (2019)

4. **C. M. Abreu**, M. T. Cerqueira, R. P. Pirraco, R. L. Reis, F. M. Watt, A. P. Marques. Epithelial stem-Like cells for the recreation of the hair follicle epithelial compartment. *Gene2Skin Summer School*. Porto, Portugal (2018)

5. **C. M. Abreu**, M. E. L. Lago, L. P. da Silva, M. T. Cerqueira, R. L. Reis, A. P. Marques. Tailoring gellan gum-based hydrogels for the recreation of the hair follicle epithelial compartment. *Chem2Nature Second School.* Porto, Portugal (2017)

6. **C. M. Abreu**, M. T. Cerqueira, R. L. Reis, A. P. Marques. Co-culturing epidermal stem-Like cells with dermal papilla cells enhances both cell types proliferation. *Gene2Skin Winter School*. Porto, Portugal (2017)

7. **C. M. Abreu**, M. E. L. Lago, L. P. da Silva, H. R. Moreira, M. T. Cerqueira, R. L. Reis, A. P. Marques. Gellan gum-based hydrogels for the recreation of hair follicle microenvironments. *The Gene2Skin Conference*. Guimarães, Portugal (2016)

Conference posters (as co-author)

1. M. E. L. Lago, **C. M. Abreu**, A. F. Carvalho, L. P. da Silva, M. T. Cerqueira, R. P. Pirraco, R. L. Reis, A. P. Marques. *In vitro* platform to study the crosstalk between the dermal white adipose tissue and dermal papilla cells. *Term Stem*. Braga, Portugal (2019)

2. M. E. L. Lago, **C. M. Abreu**, L. P. da Silva, R. L. Reis, A. P. Marques. Sulfate-modified Gellan gum as a platform to recover the inductive potential of human dermal papilla cells. *Gene2Skin Summer School*. Porto, Portugal (2018)

3. L. P. da Silva, M. E. L. Lago, **C. M. Abreu**, A. F. Carvalho, R. L. Reis, A. P. Marques. Advances on bioprinting a complex skin analogue substitute. *EWMA 2018*. Krakow, Poland (2018)

4. L. P. da Silva, A. F. Carvalho, M. E. L. Lago, **C. M. Abreu**, R. L. Reis, A. P. Marques. Cell-laden gellan gum-based bioinks for bioprinting a skin analogue. *Gene2Skin Winter School*. Porto, Portugal (2017)

5. M. E. L. Lago, **C. M. Abreu**, L. P. da Silva, H. R. Moreira, M. T. Cerqueira, R. P. Pirraco, R L. Reis, A. P. Marques. 3D platform to evaluate the influence of intradermal adipose tissue on hair follicle cycle. *Chem2Nature Second School.* Porto, Portugal (2017)

Awards & grants

INTRODUCTION TO THE STRUCTURE OF THE THESIS

This thesis compiles distinct strategies that were explored for the *in vitro* recreation of the hair follicle (HF) cellular and extracellular matrix microenvironment using both cellular- and biomaterial-dedicated approaches.

The main concepts associated with the subjects that were investigated, and a fundamental literature overview of the currently existing HF *in vitro* models, are provided on **Chapter I**. This section starts by contextualizing the basic mechanisms underlying HF morphogenesis and its biological organization, including the cellular populations it encompasses, their main functions and the description of the associated signaling and the microenvironment where they lie. It also provides background information supporting the rationale of the performed studies and provides an updated state-of-the-art summary of the different approaches used so far for the recreation of the HF microenvironment, namely towards the creation of human HF *in vitro* models.

In **Chapter II**, a detailed and structured description of the methodologies used throughout the experimental work is presented. The main goal of this chapter is to provide a solid description of the materials and methods used and the rationale behind them, under the context of the main objective of the thesis. Even covering information present in the subsequent chapters, the methodological description present in this section is more detailed, better ensuring the reproduction of the methodologies used and/or developed.

The chapters that follow represent the main body of the thesis and are based on manuscripts that are submitted or accepted for publication in different journals. For each one of these chapters, the motivation of the work and a respective introduction to the subject is presented, followed by the materials and methods adopted, the description of the results and, finally, an integrated discussion of the obtained results and respective concluding remarks.

In **Chapter III**, epidermal keratinocytes with stem cell features (EpSIKCs) were isolated from adult skin and explored as an alternative cellular fraction for the recreation of the HF epithelial compartment. In turn, **Chapter IV and V** are devoted to the key HF mesenchymal compartment – the dermal papilla (DP) – and describe independent strategies towards the *in vitro* recovery of these cells properties, which are rapidly lost outside their native niche and upon culture. While in **Chapter IV** the conditioned medium collected from skin keratinocytes was used towards that goal, in **Chapter V** a 3D biomaterial-based culture strategy inspired in the DP extracellular matrix components was explored.

Given the importance of oxygen in regulating cells' functions and overall health, and the known HF physiological oxygen levels (physoxia, 5% O₂), **Chapter VII** addresses the use of physoxia as a more reliable culture environment for DP cells and, consequently, its effect on the interaction between DP cells and melanocytes, another specialized key cellular player of the HF.

Finally, in **Chapter VII,** a human skin model bearing HF-mimetic structures was developed using a biofabrication technology.

An overview of the developed works and their final remarks, highlighting its main accomplishments and significance for the field is provided in **Chapter VIII**, the last one of this thesis.
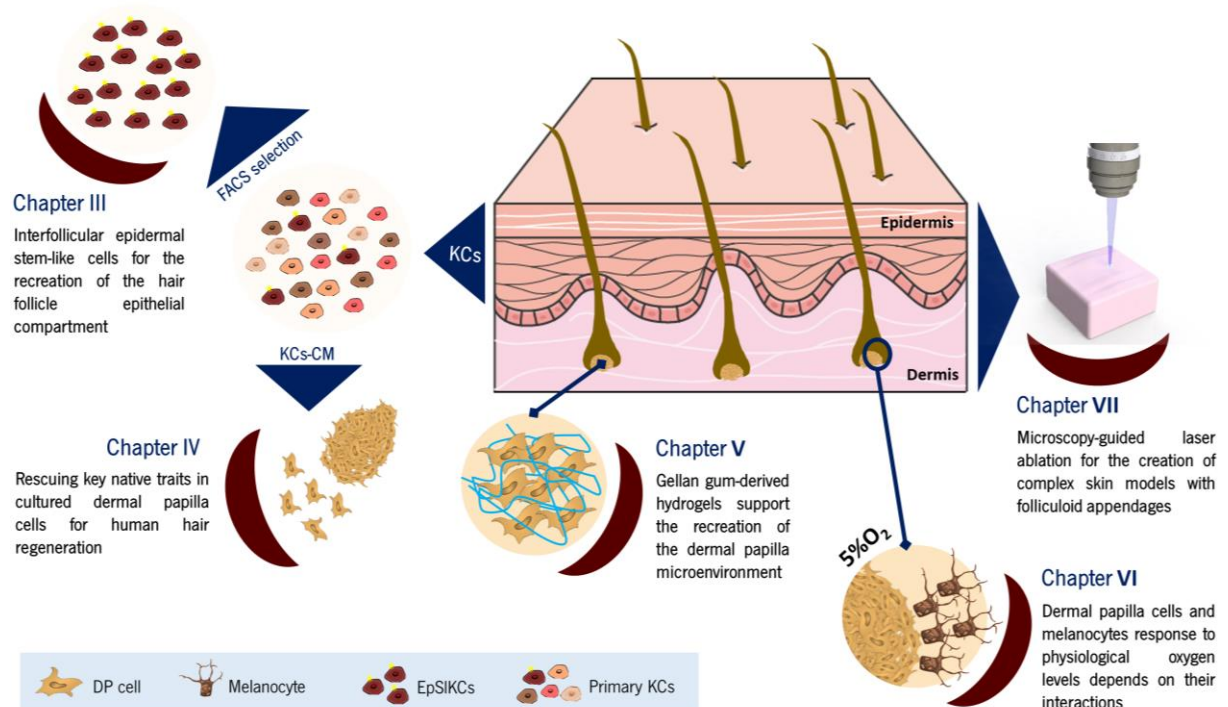
Scheme illustrating the different approaches used in this thesis towards the recreation of a HF microenvironment *in vitro*. FACS, Fluorescent-activated cell sorting; KCs, Keratinocytes; KCs-CM, Conditioned medium collected from keratinocytes; O₂, Oxygen

"Difficult roads often lead to beautiful destinations"

Zig Ziglar

CHAPTER I

GENERAL INTRODUCTION

CHAPTER I

GENERAL INTRODUCTION·

I-1. THE NEEDS AND DIFFICULTIES OF HUMAN HAIR FOLLICLE REGENERATION

Hair is a characteristic and unique trait of mammals with key physiological functions. Depending on the species and body distribution, the hair follicle (HF) has critical roles in thermoregulation, physical protection, immunosurveillance, relaying sensory perception and as a reservoir of stem cells that are necessary for both homeostasis and response to injury. Moreover, HF has an important aesthetic role for humans, being deeply involved in the individuals' non-verbal communication and well-being. Thereby, hair loss is invariably associated with a decline in skin function and, depending on the affected area, a profound physiological and psychosocial impact on patients [1].

The HF is an exquisite skin appendage that undergoes lifelong cyclical remodeling [2], which is reminiscent of the hair embryonic development and equally dependent on different stem cells and well-orchestrated epithelial-mesenchymal interactions (EMIs) [3–7]. However, and unlike what happens in some other mammals, in humans no additional HFs are naturally formed after birth [8]. When the hair growth machinery is compromised, such as in full-thickness skin defects or hair disorders, HFs cannot regenerate on their own [9]. In case of extensive injuries, such as severe burns and chronic wounds, the skin loses its regenerative power and autologous grafting is prevented by shortage of donor skin. Skin substitutes could be considered the ideal treatment, but current products only replicate the epidermal and dermal layers and have limited regenerative capacity, preventing appendages reformation [1]. Also, hair loss disorders, such as the highly prevalent androgenetic alopecia, still lack effective treatments. Hair growth-promoting drugs have an unpredictable and limited effect and the only effective treatment requires autologous transplantation of HFs from the healthy occipital area to the

---

· This chapter is based on the following publication:

C. M. Abreu, R. L. Reis, A. P. Marques. Bioengineering human hair follicle models: where do we stand? Submitted (2020)

affected site, a procedure to which not all patients are electable and that implies the creation of multiple donor sites.

Pioneering studies using rat vibrissa dermal papilla (DP), an inductive mesenchymal structure present at the base of the HF [10,11], demonstrated that it was possible to promote HF neogenesis with the transplantation of DP [11,12]. Ever since the inductive nature of dissociated murine DP and dermal sheath (DS, another mesenchymal compartment of the HF) cells was also demonstrated in combination with receptive epithelium cells [13]. However, it was only 30 years after the first experiments with murine cells that the inductive nature of intact human DS [14,15] and DP [16] was also demonstrated.

While these discoveries have opened possibilities in the development of human HF regenerative strategies, these have been hampered by successive challenges. Comparably to murine, human DP cells readily lose their intrinsic inductive properties when removed from their native environment and cultured *in vitro* [17]. Indeed, successful human HF regenerative strategies have been hampered by the difficulty in preserving the trichogenic capacity of key mesenchymal and epithelial cells after isolation and/or expansion, both indispensable to obtain clinically relevant cell numbers for biomedical applications.

Along the years, murine models and cells have allowed gaining critical cellular and molecular knowledge on HF embryonic development, postnatal cyclical growth and even regeneration [18,19]. Nonetheless, there are fundamental interspecies differences that need to be considered. Rodents have different types of hair, some of them highly specialized (*e.g.* vibrissa), that display a regular distribution pattern and grow in a synchronized way. In contrast, human HFs act independently, have different hair cycle duration and are sensitive to androgens [20]. Therefore, given the expected low animal-to-human translational success rate, human-dedicated approaches and study platforms in which human HF development, growth and regeneration can be studied remain unfulfilled needs.

This chapter starts by contextualizing the basic mechanisms underlying HF morphogenesis and cycling and by describing its constituents, including the resident cellular populations, their niches and main functions. Next, relevant aspects associated with the creation of a HF regenerative microenvironment *in vitro* are discussed. The use of relevant mesenchymal and epithelial cells, the maintenance of their key properties, the importance of a supportive extracellular matrix (ECM) and the existing knowledge of HF-related signaling events are highlighted. The strategies attempted so far to

3

bioengineer human HF models, or skin models capable of sustaining HF formation *in vitro*, are then described, emphasizing their achievements and limitations. Finally, general conclusions are drawn and future lines of investigation and important considerations for the field are put in perspective.

I-2.   BIOLOGY OF THE HUMAN HAIR FOLLICLE

I-2.1.   Embryonic Development

Depending on their embryonic origin, stem cells can differentiate into the epithelial (ectoderm), mesenchymal (mesoderm) or melanocyte (ectoderm derived neural-crest cells) lineages that constitute the HF [21–24]. The HF originates from neuroectodermal-mesodermal interactions (Figure I-1A), which in humans start by week 12 of the fetal development [21] when a yet unknown signal, considered to arise from the dermis, causes the formation of spaced thickenings in the ectoderm-derived epithelium, the hair placodes [25,26] (Figure I-1B). At this point, mesenchymal cells located bellow the stabilized placodes receive epidermal signals to start to aggregate into dermal condensates (Figure I-1C), establishing the location of the future HF [27]. Under highly-coordinated bidirectional ectoderm-mesoderm interactions, that are triggered by a second dermal signal, the epithelium forms a mass of cells (the hair peg, Figure I-1D) that grows towards the dermis and eventually surrounds and encloses the dermal condensate. During this process, ectoderm-derived progenitors give rise to epithelial stem cells (EpSCs) that stay located in the upper part of the incipient HF, in an area called the bulge, providing rapidly dividing cells that allow the downward epithelial movement [28]. In a parallel process, ectoderm-derived neural crest cells differentiate into melanocyte stem cells, which will reside in the hair bulge and act as the source of the head cells for the pigmentary unit, the melanocytes [2]. By the time epithelial cells engulf the dermal condensate, it differentiates into a specialized mesenchymal population, the dermal papilla (DP) [3,25,26] forming, together with the migrating melanocytes, the hair bulb. The hair bulb becomes fully mature when it reaches the dermis base and the DP becomes established as a permanent part of the HF [4] providing the inductive signals necessary to complete HF formation [25,26]. Along this process, another population of mesoderm-derived cells surrounds the incipient HF, from the bulge level down to the stalk, bordering the DP and forming the dermal sheath (DS), also known as connective tissue layer. A well-controlled epidermal-mesenchymal constant

4

intercommunication (Figure I-1E) will then be responsible for lifelong hair growth, generating the hair shaft, the part of the HF that is projected beyond the skin and becomes visible on the body surface.
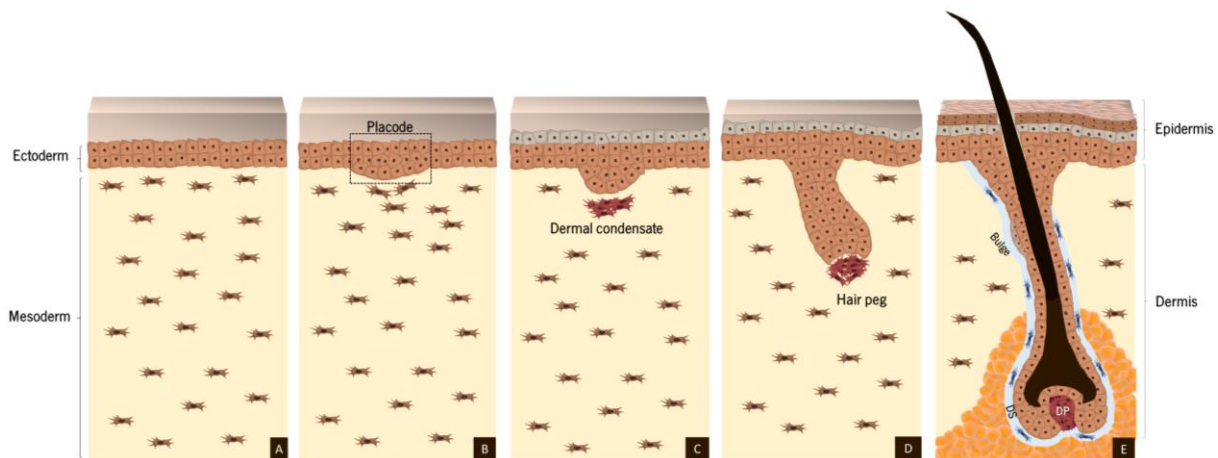
Figure I-1 - Hair follicle embryonic development. A) The epithelial and mesenchymal components of the HF are derived respectively from the ectoderm and mesoderm germ layers. B) Initially, a dermal signal derived from mesodermal cells promotes the formation of spaced thickenings of epidermal progenitors, known as placodes. C) In response, an epithelial signal stimulates the dermal cells to cluster bellow the placode, giving rise to the dermal condensate. D) After a second dermal signal, placode cells start to proliferate and invade the dermis, originating the hair peg. E) After continuous downward proliferation, the epithelial cells eventually engulf the dermal condensate, which develops into the dermal papilla (DP), allowing the establishment of epithelial-mesenchymal interactions that will further promote the proliferation and differentiation of the epithelial cells into the different structural layers of the mature HF, ultimately leading to the formation of the hair fiber.

I-2.2. Anatomical Components

The HF is a singular entity that, together with the sebaceous gland (SG) and arrector pili muscle (APM) forms the pilosebaceous unit [29] (Figure I-2A). Anatomically, the HF can be divided into different areas: the infundibulum, isthmus, suprabulbar region and bulb. The infundibulum is in the upper part of the HF, extending from the interfollicular epidermis (IFE) to the sebaceous duct, while the isthmus is located between the SG and the APM, accommodating the bulge. Some literature also refers to the upper part of the isthmus as a separated compartment termed junctional zone (or upper bulge) [30,31]. Below the isthmus lies the suprabulbar area, followed by the hair bulb, the lowest portion of the HF and the one responsible for its active growing (Figure I-2A).

The hair bulb is divided into two compartments separated by the fictional line of Auber. The DP, the mitotically active epithelial cells that colonize the matrix area (commonly referred to as matrix or germinative keratinocytes) and the neural-crest derived melanocytes are present below this line (Figure

I-2B). The two latter are the respective offspring of keratinocytes and melanocytes progenitors that previously migrated from the bulge through the outer root sheath (ORS), a layer of proliferative epithelial cells that extends down to the hair bulb and divides locally [32,33]. Above Auber's line lies the offspring of matrix keratinocytes, which differentiated together with ORS cells due to the action of factors released by DP [34,35], generating an upward movement through the follicle lumen.
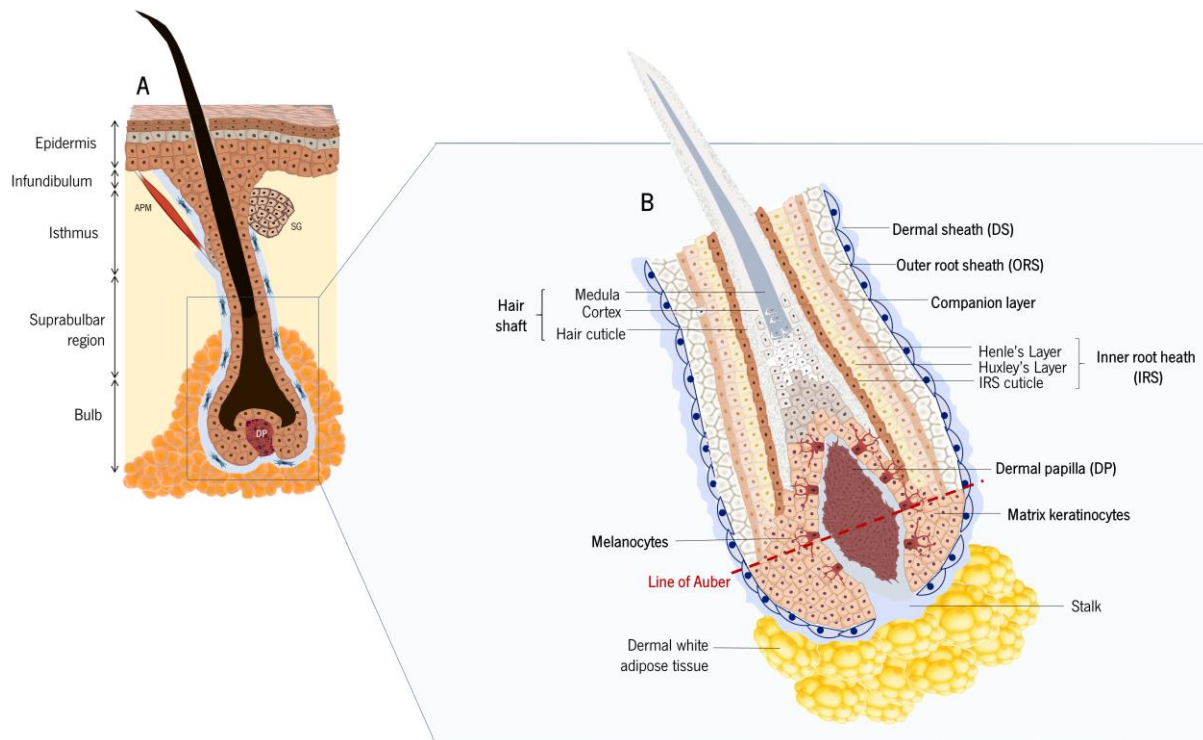
Figure I-2 – Anatomic representation of the (A) pilosebaceous unit and (B) lower hair follicle.

When matrix cells progeny migrate out of the bulb their proliferation stops and, as keratinization occurs, they give rise to the epithelial cells that form the remaining concentric layers of the HF, namely the hair shaft, the inner root sheath (IRS) and the companion layer [2,5,36], respectively organized from the HF lumen to its periphery. The IRS is structurally divided in the cuticle and the Huxley's and Henley's layers [2] and represents a channel that guides and protects the hair shaft upward growth [37]. The cells lying in the IRS are responsible for producing keratins and trichohyalin that hold, mold and reinforce the hair shaft involving structure [38]. In turn, the Henley's layer is intimately connected to the companion layer, an independent layer [39] that provides a slippage plane between the two epithelial compartments (ORS and IRS) [2]. In what concerns the HF shaft, it is divided into three regions: the cuticle, the cortex and, in certain cases, the medulla. The cuticle works as a protective

barrier, shielding the hair from external insults [2,38] and protecting the cortex, a well-defined structure of keratin fibers that confers physical and mechanical properties to the hair fiber. In opposition, loose keratinocytes without any specific organization compose the medulla at the core of the hair shaft.

I-2.3. Cycling

Conventionally, a hair growth cycle is divided into three phases: anagen (growing phase), catagen (transition phase) and telogen (resting phase) [25,40]. During each cycle, the lower part of the HF self-regenerates, while the upper region, from the bulge level up, remains constant [7,25]. During anagen, and under highly regulated EMIs, the hair shaft erupts from the skin and the hair fiber grows. In pigmented hairs this stage is also characterized by the production of melanin by melanocytes and its transfer to the cortical and medullar keratinocytes of the growing hair shaft, making it visible [41].

After anagen, which in humans can last between 3 to 10 years [42], the mature HF entries into catagen [43]. In this destructive phase, generally lasting for 2-3 weeks [42], the activity of matrix epithelial cells and melanocytes gradually slows down eventually stopping with the cells entering in an apoptotic state [2]. As a consequence, the bulb size decreases dramatically and the DP, that was deeply rooted in the dermal white adipose tissue [44], regresses and moves upward to the dermis as the remaining epithelial strand regresses [45]. This leads to the formation of the hair germ, constituted by bulge-derived keratinocytes and other follicular stem cells, localized between the bulge and the DP [46,47]. At this stage, melanin production ceases, remaining absent through the 2-4 months of telogen [5,42]. Likewise, the DP remains in a quiescent state in close proximity to the HF stem cells during telogen [46].

The shedding of the club hair (telogen hair shaft), initially thought to be a passive process, is now known to be a controlled process and thus considered an independent phase of the hair cycle, the exogen [48]. After exogen, the HF can initiate a new cycle and regenerate its lower portion by entering in a new anagen phase, which requires the activation of the hair germ [29,46]. Then, the HF epithelium lengthens downward, pushing down the DP and reestablishing the different epithelial layers. At the end, the new hair bulb, necessary to produce a new hair shaft, is reconstituted [5,46].

I-2.4.   Stem Cell Niches

The unique ability of the HF to self-regenerate cyclically relies on different stem cell populations, located in distinct follicular niches, which coordinate or provide the necessary cellular material for the continuous turnover and replacement of differentiated cells [49].

The bulge is a particularly privileged structure, comprising multipotent stem cells that can give rise to the different HF lineages. In fact, the majority of the clonogenic cells in the HF are derived from this area [50,51]. EpSCs reside in the bulge as long-lived quiescent cells [31,52] and, as previously mentioned, their offspring is responsible for reconstituting the lower HF apparatus and the derived epithelial layers upon anagen onset [53–55]. Moreover, bulge EpSCs can also replenish extrafollicular cellular compartments, including the IFE and SG [56,57]. Melanocyte stem cells also make their permanent residence in the HF bulge and sub-bulge region, after migrating from the perinatal dermis and epidermis [58]. In an analogous way to what happens with epithelial stem cells, melanocyte stem cells give rise to transit-amplifying melanocyte progenitors, which proliferate and migrate along with the ORS, differentiating into the melanin-producing melanocytes that during anagen co-inhabit the hair bulb with matrix keratinocytes [58–60]. These die by apoptosis throughout catagen, being afterwards replenished by the bulge melanocyte stem cells in the following cycle [61]. Other neural crest-like multipotent adult stem cells have been suggested to reside within the bulge, since murine [23,62,63] and human [64,65] cells derived from this area demonstrated the capacity to differentiate *in vitro* into both neural and mesodermal progeny, including cells from the adipogenic, myofibroblastic, glial, myogenic and neuronal lineages. Nevertheless, *in vivo* lineage tracing or *in vivo* functional assays still need to be carried out to confirm the existence and role of these populations in humans.

The bulge is classically considered the HF stem cell reservoir, but during the past decade evidence collected from adult murine has demonstrated the presence of epidermal stem cell populations among other HF regions, including the infundibulum, SG, junctional zone and isthmus [29,66–69]. Under homeostatic conditions each subcompartment generally produces a subset of epidermal cells but, upon injury, the different subpopulations can also contribute to a broader range of epidermal lineages [67]. Although markers of those subpopulations have not been described or confirmed so far in humans [69], they are most likely contributing to the stem cell heterogeneity in the pilosebaceous unit and maintenance of the different epithelial regions.

Along the hair cycle, the DP suffers volume and cell number fluctuations [70] while DS regresses during catagen [71]. Although both DP and DS are known to hold dermal stem cells [71–73], DP cells rarely display proliferative features [70]. Different studies showed that stem cells present in the DS possess the capacity both to regenerate a new DS and supply cells to the DP whenever necessary [15,71,74–76]. However, this relation may be more elaborated, since DP cells can themselves contribute to DS renewal during anagen [77], suggesting cellular interchangeability and cellular plasticity [70]. The future identification of distinctive stemness-related markers and its link to the mesenchymal progeny of the HF might allow to further understand this dynamic and/or potentially identify other critical niches and functions.

I-3.   CELLULAR REQUIREMENTS FOR HAIR FOLLICLE REGENERATION

The continuous reconstitution of the HF and its growth machinery after each cycle is dependent on elementary EMIs, implying the need to combine inductive mesenchymal cells and responsive epithelial cells as building blocks in HF regenerative strategies.

I-3.1.   Mesenchymal Cells

Although the hair mesenchyme is composed by both the DP and DS compartments, DP cells are considered the prime inductive players given their role in the initiation and control of hair formation and growth [78–80]. The inductive capacity of the peribulbar portion of the DS is sufficient to replace the DP and to regenerate new HFs both in rodents [14,74] and humans [15]. However, dissociated rat [81] and mouse [75] DS cells commonly fail to induce hair growth, suggesting that DS-to-DP cell transition may be lost upon culture and in the absence of influence from the adjacent epithelium.

The current major challenge associated with the application of human DP cells for HF regenerative purposes is the loss of their inductive phenotype after 2D culture [17,82]. Therefore, the use of human DP cells for the recreation of the HF microenvironment relies on the recovery and/or maintenance of their native properties *in vitro*. Up to now, the gold-standard strategy to preserve human DP cell inductivity is to artificially promote their native intercellular organization and aggregation into 3D spheroids [83–89], which partially restores DP cell features [87] and molecular signature [17].

Depending on the spheroid's size, oxygen (O_2) diffusion might be progressively decreased and whether this play a role in rescuing DP cell properties *in vitro* has to be further understood. Cell culture is typically performed under atmospheric O_2 levels (21% O_2, normoxia) but *in vivo* physiological levels usually range between 1% O_2 to 11% O_2 [90]. Comparably to cells cultured under normoxia, human DP cells cultured in 2% O_2 showed a significant increase in alkaline phosphatase (ALP) activity, a recognized DP cell inductive marker [75,91], suggesting improved hair inductive capacity. This was confirmed *in vivo*, where DP spheroids formed from cells cultured under 2% O_2 were able to sustain hair neogenesis, unlike normoxia-cultured cells [92].

Others have considered DP and bulbar epithelial cells proximity and signaling during anagen, to design new approaches capable of rescuing or preserving native DP cell features *in vitro*. The culture of DP cells with conditioned medium collected from keratinocytes (KCs-CM), for example, was already suggested to trigger epithelial-mesenchymal paracrine signaling. Inamatsu *et al.* [93] showed that KCs-CM improved the growth rate of rat DP cells in culture and, importantly, their capacity to induce HF-like structures *in vivo*. Studies with human DP cells also demonstrated KCs-CM positive effect over DP cell proliferation [94,95], but its influence on the hair-inductive capacity of DP cells has not been investigated. Interestingly, the supplementation of human DP cell culture with $1\alpha,25$-dihydroxyvitamin D3 (VD3), a compound identified in KCs-CM, leads to improved ALP activity [113]. The analysis of possible mechanisms of action revealed that VD3 significantly upregulated Wnt 10b and TGF-β2 gene expression in a dose-dependent manner. However, Wnt inhibition did not hinder VD3 effects on ALP activity. Moreover, as TGF-β2 upregulation was also maintained and TGF-β2-mediated signaling is crucial hair folliculogenesis and maturation [96], it was suggested that VD3 beneficial effects might involve this growth factor pathway.

Despite these discoveries, strategies that directly target HF signaling pathways known to be downregulated in 2D culture, such as Wnt/β-catenin, bone morphogenetic protein (BMP) and fibroblast growth factor (FGF) [82] are more commonly explored to revert the loss of human DP cell inductivity in culture. Adding Wnt 1a to the culture medium of human DP cells restores the expression of hair induction-related genes, namely versican, lymphoid enhancer binding factor-1 (LEF1), patched homolog-1 and GLI-Kruppel family member GLI-1, previously inhibited with dihidrotestosterone [98]. Also, human cell treatment with Wnt 3a- and Wnt 7b-enriched extracellular vesicles improved versican, ALP and β-catenin protein expression and LEF1, vascular endothelial growth factor (VEGF) and keratinocyte growth

factor (KGF) transcripts [99]. An alternative strategy to improve Wnt/β-catenin activation in DP cells comprises blocking glycogen synthase kinase-3 (GSK3), a key enzyme responsible for the degradation of cytoplasmic β-catenin. So far, molecules successfully used to this end include valproic acid and 6-bromoindirubin-3'-oxime (BIO). Treatment with valproic acid improved ALP activity and quantity in cultured human DP cells, concomitantly with the upregulation of β-catenin [100]. In turn, BIO has been mainly used in combination with other factors as a strategy to target multiple signalling pathways. An optimized combination of BIO with recombinant BMP2 and basic FGF (bFGF) maintained the expression of human DP signature genes and improved ALP activity [82]. Increased ALP activity and quantity were also confirmed with the supplementation of the culture medium only with BIO and bFGF [101]. A combined approach showed that VD3, BMP6 – a key molecule in maintaining mice DP cell inductive capacity [102] – and valproic acid further enhanced versican expression and ALP activity in comparison to Wnt 3a treatment [103].

Another pathway more recently associated with hair growth control is the Janus kinase/Signal transducers and activator of transcription (JAK/STAT), whose pharmacological inhibition has been demonstrated to promote robust hair regrowth in patients with alopecia areata, an autoimmune hair-loss disorder [104–106]. The impact of JAK/STAT inhibitors on the inductive capacity of human DP cells eas showed when tofacitinib-treated DP spheroids displayed improved HF induction rate than those treated with ruxolitinib, which performed similarly to non-treated spheroids [107]. The treatment with tofacitinib upregulated TGF-β2, BMP6, and LEF1 expression whilst ruxolitinib improved β-catenin gene expression but decrease TGF-β2 expression [108]. This suggests a TGF-β2 mediated hair growth after inhibition of the JAK/STAT signaling pathway.

Despite the different rationales and strategies that have been explored so far for the recovery of the inductive phenotype of DP cells, further studies will be needed to select or develop the most promising one(s).

I-3.2. Epithelial Cells

Epithelial cells isolated both from follicular and interfollicular sources possess the capacity to differentiate into follicular epithelium under proper DP cell signaling. Among the follicular sources already described are the bulge [56,107], ORS [108–110] or bulb [111]. Besides, skin epithelial cells

have also been successfully combined with DP cells to regenerate HFs, even when isolated from glabrous skin sources such as foreskin [112].

The differentiation level of the epithelial cells, however, deeply affects their response to inductive dermal cell stimuli and consequently, their trichogenic capacity. Murine K15 positive cells support HF formation when co-transplanted with neonatal dermal cells, but the same is not observed when the whole epidermal population is used [56]. This was also demonstrated with human epithelial cells from neonatal skin that, in combination with murine DP cells, led to a higher number of HF-like structures than adult skin cells, which lose their trichogenicity after the second passage [112]. Indeed, few studies demonstrated *de novo* HF formation from dissociated human cells and most of them report the use of human DP cells with the skin of mouse embryos [113] or embryonic [114]/newborn [83,115] skin epithelial cells. To date, entirely human HF regeneration was only succeeded when using epithelial cells from fetal origin [116,117] or neonatal/children skin [91,118]. While these keratinocytes display higher competence than adult cells [110], the use of newborn cells for regenerative purposes cannot be completely dissociated to ethical concerns.

Besides preserving epithelial cells undifferentiated state, it is also most advantageous to maintain or promote the trichogenic capacity of the cells in culture. Studies with human cells showed that a follicular-fate and the trichogenic capacity of keratinocytes can be promoted by co-culture with inductive dermal cells. The expression of the epidermal differentiation markers keratin 1 and profillagrin was downregulated in bulge-derived keratinocytes indirectly co-cultured with human DP cells, whereas the expression of the companion layer-specific K75 (formerly known as K6hf) significantly increased, demonstrating that the cells engage in a follicular-type of differentiation under DP cell stimuli [119]. The upregulation of keratins predominantly or exclusively expressed in the HF epithelium, namely K6, K16, K17 and K75, in high passage rat ORS keratinocytes expanded in 3T3 feeders was also reported after co-culture with DP cells [110]. Moreover, keratinocytes co-cultured with DP cells were able to support the formation of new HFs, which was not observed when only clonal expansion in feeders was performed. Similar results were observed when human ORS were grafted with newborn mice DP cells [120]. More recently, follicular keratinocytes co-cultured with a mice CD49f^{high} dermal subpopulation in Matrigel[®] co-led the formation of bud-like structures with an improved expression of Sox9 and ectodysplasin A receptor (Edar), a marker of the developing hair placode [121]. Nevertheless, *in vivo* demonstration or translation of those results to human cells has not been performed so far.

Others have shown that the enrichment of murine IFE cells in the bulge markers integrin α6+/CD34+ improves cellular trichogenicity, as demonstrated by the increased number of follicles formed after co-grafting with freshly isolated neonatal murine fibroblasts [122].

Overall, the literature demonstrates that different epithelial cell sources may be used for HF regeneration but those with higher undifferentiated status and clonogenic capacity exhibit improved hair regenerative efficiency. Moreover, maintaining in culture the characteristic signalling receptiveness of follicular keratinocytes, or pre-disposing non-follicular undifferentiated cells towards a follicular fate, may prove beneficial in improving trichogenic capacity of epithelial cells in culture.

I-4.   HUMAN HAIR FOLLICLE-RELATED SIGNALING

The events regulating human hair morphogenesis and cycling are still largely unknown. However, it is well-established that HF formation and growth involves different conserved signaling pathways including, but not limited to, Wnt/β-catenin, Sonic hedgehog (Shh)/PDGF-A, FGF, BMP, TGF-β, and Edar/nuclear factor-kappa B (NF-κB) pathways. Although the dissection of the mechanisms regulating HF is beyond the scope of this thesis (for more details please see [6,79,123,124]) the knowledge generated so far regarding each one of these signalling pathways, may present opportunities for HF regenerative strategies.

The Wnt/β-catenin signaling pathway is highly involved in hair development, growth and cycling [125–127]. The activation of this pathway, and β-catenin stabilization, direct epidermal cells towards a follicular phenotype [128,129]. Transient β-catenin activation in mice epidermis promotes HF neogenesis and induces anagen in follicles in the telogen phase, by improving cell proliferation and outgrowth both from the epidermis and existing ORS [129]. Wnt/β-catenin signaling is also critical in the *de novo* HF formation during wound healing, which reproduces the HF embryonic development [128]. *In vitro*, β-catenin activation and nuclear translocation were linked to the upregulated expression of follicular-specific epithelial markers in keratinocytes co-cultured with DP cells [110,119]. Thus, the role of different Wnt proteins in promoting epithelial cell differentiation has been addressed. Recombinant Wnt 10b, for example, was shown to be necessary to initiate HF development in mouse embryonic skin organ cultures. Moreover, hair formation in mice was observed only when neonatal epithelial cells and fibroblasts were co-grafted with a fibroblast cell line transfected to produce Wnt 10b

[130]. *In vitro*, Wnt 10b supplementation, contrarily to Wnt 3a, Wnt 5a and Wnt 11, promoted advanced follicular differentiation of primary IFE keratinocytes, suppressing their proliferation and inducing the expression of late differentiation markers, including cortex (mHa5 and mHb5) [131] and IRS (AE13 an AE15) [132] specific markers. Moreover, Wnt ligands also seem to maintain DP cell inductivity *in vitro*, which suggests that these molecules may be used as a strategy to direct keratinocytes follicular differentiation and preserve DP cells identity *in vitro*.

NF-κB activation through Eda (ectodysplasin)/Edar signaling is also acknowledged as crucial for HF morphogenesis, namely for placode formation, stabilization and patterning [133–135]. Eda-A1 is expressed in the epidermis and hair placodes whereas Eda-A2 is only expressed after, in the hair bulb epithelium [136]. Probably for this reason, Eda-1 seems to be required for ectodermal differentiation, as shown by the inhibition of hair development after mutation of the Eda-A1 isoform and its receptor [137]. Nevertheless, both Eda-A1 and Eda-A2 isoforms are capable of enhancing the number of epidermal invaginations in skin organ cultures, despite the superior effect of Eda-A2 [136]. Conversely, postnatal Eda signaling is linked to HF cycle control, particularly in promoting catagen onset and progression [138,139]. Exploration of possible mechanisms *in vitro* demonstrated that Eda-A2 stimulates apoptosis in cultured human ORS keratinocytes and DP cells [139,140]. Although the role of Eda/Edar signaling has been mainly explored in rodents, its promising capacity to trigger HF morphogenesis might prove advantageous if explored for human regenerative strategies.

PDGF-A and Shh are required to promote DP development and HF maturation [141–143]. PDGF-A is expressed in the embryonic epidermis and developing HF epithelium and acts directly in receptors present in the underlying mesenchyme, promoting their proliferation and the normal development of all skin mesenchymal compartments: DP, DS and dermis [144]. Thus, PDGF-A deficiency results in dermal hypoplasia and impaired DP and DS formation, with animals exhibiting a scarce and thinner hair coat. Shh is required to drive DP formation from dermal condensates, reason why its deficiency blocks hair formation at an early stage [142–144]. Postnatal PDGF-A ligands are still required to maintain DP cell function and receptor deficiency results in a progressive depletion of the HF dermal stem cell pool [145] and disturbs both dermal connective tissue development and hair canal formation [146]. In addition, local injection of PDGF ligands in mice skin induces anagen, which was associated with an upregulation of Shh, Wnt 5a and LEF1 at the injection sites [147].

14

In the mature HF, the activation of BMP signaling is crucial to promote HF differentiation and maturation [26,148], but it needs to be initially counteracted for anagen entry [149]. Noggin, a protein that neutralizes BMP, is exclusively produced in the HF mesenchyme and is necessary to stimulate postnatal hair induction [149,150]. On the other hand, transgenic mice expressing noggin are characterized by excessive proliferation of matrix keratinocytes and prevention of hair shaft maturation [151], clearly demonstrating that a tight control between BMPs and their inhibitors need to be carefully achieved for their effective use in the recreation of functional hairs.

From the TGF-β family, only the TGF-β2 isoform is indispensable to promote hair development, playing a specific role in hair morphogenesis induction that is not shared with other isoforms [152]. Indeed, TGF-β2 treatment in embryonic skin organ cultures significantly increased the number of hair buds and their development stage, whereas TGF-β1 reduced it [152]. *In vitro*, TGF-β2 secretion by DP cells significantly increased when these were cultured with human epidermal KCs-CM. Moreover, when TGF-β2 signal was inhibited in mice, HF formation by human DP cells was impaired [96]. TGF-β1, in turn, acts as a negative regulator of keratinocytes proliferation, promoting instead their differentiation and even apoptosis [153,154], being commonly appointed as a catagen regulator [154].

Different elements of the FGF family can also have quite distinct hair regulatory effects. FGF7, also known as KGF, is an important mitogenic factor for keratinocytes and is normally secreted within the DP, contributing to the proliferation of the hair germ cells and activation of a new hair cycle. Its expression increases in telogen but, on its own, is not enough to promote anagen [46]. In turn, topical application of FGF1, FGF2 and FGF10 was shown to promote hair growth by inducing early anagen and prolonging its duration [155]. A similar role was observed for FGF18, whose subcutaneous injection in mice uncovered a potential role in promoting telogen-to-anagen transition [156]. Contrariwise, FGF5 regulates catagen onset in human HF organ cultures. Mutations in this growth factor are associated with increased HF lengthening in humans. [157]. *In vitro* studies demonstrated that FGF2 increases the proliferation of both DP and DS cells [158] and, interestingly, the addition of FGF2 to terminally differentiated human epidermal keratinocytes promoted their dedifferentiation towards an early proliferative [159]. This increase in the proliferative capacity of both cell types might explain their capacity to induce anagen.

Besides the modulation of hair-related pathways, there are other signaling molecules known to impact hair development and growth. Although classically associated with oxidative stress, reactive

oxygen species (ROS) at physiological levels play an important role in hair formation. Bulbar epithelial cells produce high amounts of ROS during hair growing [160] and studies using human *ex vivo* HFs organ cultures proved that transient endogenous ROS production promotes HF stem cell activation and anagen entry, which was associated with the activation of Wnt transcriptional factors [161]. Corroborating these observations, Hamanaka and coworkers [162] showed that mice genetically manipulated to prevent mitochondrial ROS generation in basal epithelium displayed impaired development of epidermis, HF and SG.

MicroRNA (miRNA), involved in the post-transcriptional genetic control of multiple biological processes, also play a role in controlling HF organogenesis and postnatal growth (reviewed in [163]). For example, miRNA-203 targets p63, a transcriptional factor highly expressed in the innermost basal keratinocytes, and its upregulation is associated with a decrease of the clonogenic capacity of keratinocytes [164]. This explains why its expression is intensified in differentiating cells of the HF [165]. Similarly, miRNA-24 was demonstrated to block the keratinocyte stemness regulator Transcription Factor 3, which is induced during hair differentiation [166]. In turn, miRNA-125b is implicated in stem cells maintenance and its sustained expression, in engineered transgenic mice, blocks hair growth by repressing hair stem cell differentiation [167]. Noteworthy, miRNA-31 is associated with HF cycle progression, increasing during anagen and decreasing afterwards, and administration of an antisense inhibition was associated with hair shaft defects and ORS hyperplasia in mice [168]. Exploration of the underlying mechanisms showed that miRNA-31 acted by targeting the expression of structural keratins in keratinocytes [168]. Thought the incorporation of relevant HF miRNA in HF regenerative strategies may still be in its theoretical steps, in the future, with an increased understanding of the mechanisms involved, miRNA modulation may represent an additional and precise tool to control HF cell.

I-5. THE IMPORTANCE OF THE EXTRACELLULAR MATRIX WHEN BIOENGINEERING HAIR FOLLICLES

In addition to the critical homotypic or heterotypic cell-cell communication, cell-ECM interactions in the HF are crucial not only to maintain the specific cell phenotype and role within the individual compartments but are also involved in physiological (hair cycle) and pathophysiological (hair associated disorders) environment alterations [84,169]. The epithelial and mesenchymal compartments of the HF

are separated by a highly-specialized ECM basement membrane rich in collagen IV, fibronectin and laminin [170]. The DP ECM also has a prominent expression of these basement membrane elements, comparably to the non-follicular dermis, along with collagen III, collagen I, versican and glycosaminoglycans [78,171–173].

The basement membrane ECM is particularly relevant for epithelial cells differentiation state. Like in the skin, HF basal keratinocytes engagement in a differentiation pathway is associated with the loosening of their interaction with the basement membrane, whilst the maintenance of the epidermal reservoir is connected to the anchored stem cells [174–176]. ORS keratinocytes interact with the basement membrane via α2β1, α3β1 and α6β4 integrins, which are differentially expressed along the HF epithelium, most likely reflecting their differentiation along the HF [177]. Collagen XVII (COL17A1) is highly expressed in bulge epithelial stem cells and represents a specific stem-cell anchoring protein required to maintain epithelial and melanocyte stem cell quiescence. COL17A1-null mice suffer from premature hair loss and hair greying, which is associated with bulge depletion of epithelial stem cells and also of melanocytes stem cells, which do not express COL17A1 but directly adhere to epithelial stem cells, being also lost in the process. In humans, mutations in this protein lead to atrophic hair loss associated with generalized atrophic benign epidermolysis bullosa [178,179]

The HF ECM is also a key player in the regulation of HF development, hair cycle and signaling. The disruption of the DP ECM and the basal lamina by dispase, a fibronectinase and type IV collagenase, inhibited bulb growth in *ex vivo* HF cultures. This confirms the importance of the ECM in supporting hair growth and that the paracrine signaling between epithelial and mesenchymal compartments is not sufficient [180]. Laminin-511 is prominently expressed in the basement membrane of the hair germ. Its blockage in embryonic human scalp xenografts induces alopecia, suggesting a role in hair development [181]. Indeed, mice lacking laminin-511 have impaired hair development, contained fewer hair germs and exhibit a defective basement membrane compared to wild type, features that can be reverted with exogenous laminin-511 treatment [181]. Moreover, laminin-511 is required for the expression of noggin and downstream regulators, which are necessary for DP maturation during HF development [182].

Decorin, expressed in the HF epithelium and ECM of the DP, has been suggested to play a role in anagen maintenance [183,184]. This is confirmed by the higher expression of this proteoglycan during the anagen phase, and by the accelerated anagen onset in follicles at telogen phase after injection of human decorin in mice, and delayed transition to catagen in those at the anagen stage [184].

17

Moreover, decorin-knockout mice showed shortened anagen, as well as downregulated β-catenin signaling. *In vitro* results showed that upregulation of β-catenin in ORS cells overexpressing decorin occurs together with LEF1 and Wnt 10b [183]. This effect was also associated with increased proliferation and migration of ORS keratinocytes [183].

A similar impact could be attributed to hyaluronic acid owed to the enhanced ORS growth observed in a hair germ model *in vitro* [103]. Hyaluronic acid, like fibronectin and the proteoglycans aggrecan or biglycan, stimulate human DP cell proliferation *in vitro* [103]. Interestingly, DP cell motility is diminished on collagen IV, laminin and collagen I coated surfaces [185], while melanocytes migration is enhanced on collagen IV but not on fibronectin or laminin [186]. Interestingly, both RAD16-I peptide [187], a synthetic peptide that shares structural similarity with the integrin receptor-binding site RGD present in several ECM proteins [188], and collagen type IA [114] hydrogels improved ALP activity and versican expression in DP cells, suggesting an effect on their inductive potency by these ECM-replacing matrices *in vitro*. In turn, the ECM derived from DP cells supported enhanced tyrosinase activity in melanocytes [189], the rate-limiting enzyme for melanin production [190]. This effect was higher than the one observed in melanocytes cultured onto a DP feeder layer or with DP cell-CM, further demonstrating the vital role of the ECM that other signaling mediators cannot replace.

Altogether, these studies highlight the importance of the HF ECM components in balancing epithelial cell growth and differentiation, modulating HF development and EMIs and influencing cell-specific function and properties, including the inductive properties of DP cells.

I-6.   DEVELOPMENTS IN THE BIOENGINEERING OF HAIR FOLLICLES OR HAIR-BEARING SKIN MODELS

Unquestionably, the development of HF regenerative strategies would benefit from the existence of reliable and representative *in vitro* models allowing, in a standardized way, to test new bioactive compounds to modulate hair growth or to study the biological and molecular events regulating hair morphogenesis and growth.

Along the years, the development of HF *in vitro* models was looked from different perspectives. From simple systems where 3D cultured epithelial cells and DP cells were assembled in close proximity, to models that mimicked the spatial organization of the cells within the HF bulb and, more

recently, to more elaborate platforms in which HF recreation was viewed not as an isolated structure but instead integrated with the skin.

The first attempts to construct human HF models were focused in creating 3D systems where the close contact between epithelial and DP cells was reestablished. These constructs depicted simplified spatial organizations and were elementary in what concerns the recapitulation of the HF structure. They involved the co-culture of the cells in Matrigel®, collagen I or other matrices with different spatial arrangements [108,191–194] (Table I-1). Despite the recreation of the signaling in these systems, the epithelial cells often formed cyst-like spheroidal structures and a follicular-type differentiation was not observed or confirmed. Therefore, their functionality was short and their use might be restricted to testing simple features, such as the effect of hair growth modulatory agents in epithelial cell proliferation or the expression of specific markers expression, more closely resembling co-culture systems than *in vitro* models of HF.
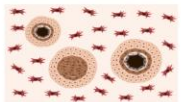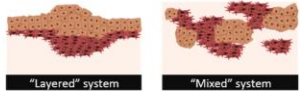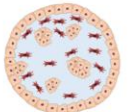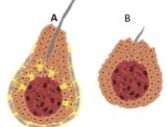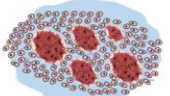
More complex approaches allowed to create *in vitro* models in which unpigmented hair fiber-like structures were formed. In one method DP spheroids formed on top of Matrigel® were directly co-cultured with matrix keratinocytes [84] while, in a slightly more elaborated strategy, DP cell aggregates were coated with basement membrane molecules (collagen IV, laminin, fibronectin) and only then cultured with matrix keratinocytes and melanocytes [109]. The formation of "microfollicles" with a proper topological cellular arrangement in these models represented a substantial improvement in the fulfilment of criteria steps towards HF formation. In another endeavor, a simple *in vitro* DP organoid model, characterized by enhanced expression of inductive markers and epithelial proliferation, was developed [195]. Here, DP spheroids were encapsulated in silk-gelatin hydrogels together with normal HF keratinocytes and HF stem cells, to mimic the HF bulb cellular environment.
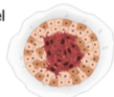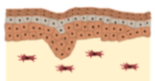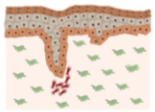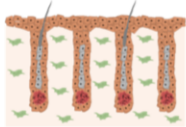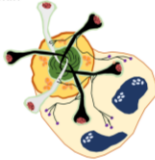
Instead of bioengineering HFs as a single independent structure, others have developed or incorporated HFs in skin constructs, better reproducing the native tissue and, thereby, improving the model functionality and translational value. In a first approximation, DP cells' paracrine signalling was explored for the promotion of epidermal keratinocytes organization and formation of tubular epidermal invaginations in an organotypic skin model. Both DP cell- and fibroblast-laden collagen matrices were permissive to this effect although the latter still required the presence of DP cells-conditioned medium in the culture [196]. Similar epithelial invasion of the dermis was demonstrated when DP cells and follicular keratinocytes enriched in stem cells were seeded in different sides of a porcine acellular

dermal matrix [197]. Also, a more robust epidermal protrusion directed toward DP cells was observed when DP spheroids were incorporated within the dermal equivalents of a standard organotypic skin model [198]. While epithelial invagination and formation of an epithelial column are required for HF morphogenesis, DP spheroids rapidly dissociate when placed within collagen matrices [118], which might be compromising DP cell inductivity and model progression. Bearing this in mind, another strategy, in which DP spheroids integrity was maintained, allowed creating a skin model with follicular units capable of generating an unpigmented hair shaft. Micromolding was used to create, in fibroblast-populated collagen I hydrogels, defined microwells in which DP spheroids were formed *in situ.* Keratinocytes were then seeded on top, engulfing the spheroids and differentiating into proper follicular layering over the control of the inductive DP cells. Hair shafts were only formed occasionally in these models thus, to further enhance DP cell inductivity, a subpopulation of LEF1 overexpressing DP cells was also used, significantly improving HF induction efficiency and the expression of hair lineage-specific genes.

However, the most complete *in vitro* recreation of human HF achieved so far was developed entirely using pluripotent stem cell lines. In a quite distinct and successful approach, hair-bearing skin organoids akin to 18-week human fetal skin were produced. The formation of a cyst-like skin organoid was attained from aggregates of pluripotent stem cells and using a step-by-step modulation of the TGF-β, BMP and FGF signalling pathways, to promote ectoderm and cranial-neural crest induction [199]. The formation of pigmented HFs within the skin organoids was observed after a 4/5-month culture period. Importantly, the skin organoids also display a stratified epidermis and a dermis with SGs and neural innervation, linked to adjacent fat tissue. This study clearly demonstrates the relevance of selective modulation of hair development signalling pathways, as well as the advantage of reconstructing embryonic events guiding the natural development of the skin and associated appendages. Still, the long preparation time and associated costs represent considerable disadvantages comparably to the use of dissociated primary cells.

Table I-1 - Reported bioengineered human HF or hair-bearing skin *in vitro* models

Structures formed *in vitro*	Strategy	*In vitro* experimental findings	*In vivo* outcomes	References
Epidermoid cyst-like spheroids	DP cells were: • co-cultured with ORS or /IFE keratinocytes inside Matrigel and layered above cell-free collagen I gels; • embedded in collagen I hydrogels and overlaid with IFE or ORS cells in Matrigel.	Independently of their location, DP cells accelerated epithelial cells proliferation. Both epithelial cell types formed aggregates (larger in ORS cells) but these displayed an epidermis-type of stratification towards the center instead of a follicle-type of development	NA	[191]
"Folliculoid sandwiches" "Layered" system "Mixed" system	Dermal fibroblasts were mixed with collagen I and covered on top by: • a Matrigel network with DP cells, where ORS cells were seeded on top (layered system) • a Matrigel network were both DP cells and ORS were encapsulated (mixed system).	The cells remained in close contact and ORS keratinocytes were capable of proliferating and forming epithelial aggregates rather than generating an epidermis-like stratified epithelia.	NA	[192]
HF-like structures	DP or DS cells were encapsulated in a collagen I gel and different epithelial cells – IFE keratinocytes, ORS keratinocytes (superior or inferior anatomical location) or matrix keratinocytes – were seeded on top.	The combination of both ORS and DS cells led the formation of structures with inward oriented epithelial concentric layers, which was not reported for DP cells.	Yes, simple HF-like structures mainly observed when DP cells and superior ORS keratinocytes were co-transplanted.	[108]
"Folliculoid" microsphere	DP cells and ORS keratinocytes were encapsulated in a matrix mixture of collagen I and Matrigel (4:1 ratio) and casted as small droplets.	Small aggregates of DP cells expressing versican or ORS cells positively staining for K6 and displaying proliferative properties were observed, but a HF type of organization was not observed	NA	[193]
Tubular structures	DP cells were embedded in collagen I hydrogels and IFE keratinocytes seeded on top. Alternatively, DP cells were replaced by their conditioned medium in the culture.	Both DP cells and their conditioned medium induced the projection of keratinocytes into the collagen matrix, forming tubular structures that resembled hair germ formation during embryogenesis.	NA	[196]
Unpigmentated fiber-producing structures	A) DP aggregates were coated with basement membrane proteins (collagen IV, laminin and fibronectin) and ORS keratinocytes and melanocytes were added to the culture afterwards.	Formation of organoids in which DP cells were surrounded by concentric epithelial layers, including a K15 and a trichohyalin-positive layers. Melanocytes remained in close proximity with DP cells and the formation of unpigmented hair-like fibers was observed.	NA	[109]
	B) DP cells spheroids were formed on top of Matrigel and matrix keratinocytes were posteriorly added	Formation of structures capable of generating a colorless hair-like fiber	NA	[84]
Follicular DP structures	DP cells and IFE keratinocytes were encapsulated in different domains of water-soluble chitin (polycation), separated by a sodium alginate solution (polyanion) and brought together to form an insoluble fibrous hydrogel by interfacial polyelectrolyte complexation.	DP cells self-assembled into aggregates, while the adjacent epithelial layers remained in close contact, but only partially surrounding the DP-spheroids.	Yes, formation of rudimentary HF-like structures.	[194]

Structures formed in vitro	Strategy	In vitro experimental findings	In vivo outcomes	References
HF organoid model	DP-spheroids were encapsulated in a silk-gelatin hydrogel and co-cultured with both HF stem cells and HF keratinocytes. In a biomaterial-free approach, DP-spheroids were directly cultured with both epithelial cells	Formation of an in vitro HF-organoid model in which cellular proliferation and the expression of DP cell signature genes versican (ALP, BMP4 and β-catenin) were significantly higher in the presence of hydrogel support	NA	[195]
Reconstructed skin with invaginations A) B)	A) DP cells were cultured in porcine acellular dermal matrices and follicular keratinocytes enriched in stem cells were posteriorly seeded on the opposite side.	Constructs gave rise to a stratified epidermis with invaginations that resembled embryonic hair bud-like structures. The expression of the companion layer keratin K6hf within the constructs indicated commitment to follicular lineage.	Yes, presence of hair bud-like inclusions in constructs where follicular keratinocytes enriched in stem cells were used	[197]
	B) DP spheroids were incorporated between layers of fibroblast-embedded collagen I hydrogels, which were used then used to produce standard reconstructed skin.	DP spheroids within dermal equivalents stimulated epidermal downward movement and dermis invasion. These epidermal invaginations were composed of an inner K15-positive layer, an outer K10-positive layer and displayed a basement membrane rich in collagen IV and laminin.	NA	[198]
HF generation within reconstructed skin	3D-printed molds were used to produce dermal equivalents with microwells of controlled dimensions, inside which DP cells (transfected or not with a LEF1 vector) spontaneously formed spheroids. Neonatal keratinocytes were then seeded over the dermal constructs.	The keratinocytes encased the DP cell-spheroids, forming an epithelial column that initiated HF-specific differentiation, expressing hair lineage markers and occasionally forming colorless hair fibers. DP cells overexpressing LEF-1 synergistically improved HF differentiation and hair shaft formation. Dermal vascularization was observed in the constructs used for in vivo implantation.	Yes, vascularized constructs induced the formation of unpigmented hairs, but DS reformation in the grafts was not observed	[118]
Hair-bearing skin organoids	Human embryonic (WA25) or induced pluripotent (DSP-GFP) stem cell lines were used to form aggregates and cultured with 2% Matrigel, bFGF, BMP4 and a TGF-β inhibitor. Afterwards, a BMP inhibitor and bFGF were added to the culture. The resultant organoid structures were culture and matured over 140 days.	Independently of the cell line used organoids acquired a bipolar organization, with a chondral tail and an epidermal cyst head, which developed in complete stratified skin with HFs. The recreated HFs featured all the cellular layers (except the medullar layer), were embedded in a lipid-rich dermis, in which hairs were associated with SGs and a neuronal network. The number of HFs was higher in WA25 organoids, whilst a higher number of pigmented hairs were observed in the DSP-GFP organoids.	Yes, organoids without the cartilaginous tail were engrafted in nude mice. In 55% of the xenografts, hair shaft growing perpendicular to the skin surface was observed	[199]

22

Instead of bioengineering HFs as a single independent structure, which would be unnatural and poorly representative, some groups have tried to develop or incorporate HFs in skin constructs, better reproducing the HF native tissue and, thereby, improving the model functionality and translational value. In a first approximation, epidermal keratinocytes seeded on top of DP cell-laden collagen matrices were able to invade those matrices and form tubular epidermal invaginations [208]. Interestingly, this effect was also observed when collagen hydrogels were populated with dermal fibroblasts instead of DP cells, but DP cells-conditioned medium was used in the construct culture, demonstrating the importance of DP cells paracrine signalling for the induction of the structures. Similar, epithelial invasion of the dermis was demonstrated when DP cells and follicular keratinocytes enriched in stem cells were seeded in different sides of a porcine acellular dermal matrix [209]. A more robust epidermal protruding into the dermis was observed when DP spheroids were incorporated between the dermal equivalents of standard organotypic skin model, with the epidermal downward movement being detected towards the spheroid prior location [210]. While epithelial invagination and formation of an epithelial column are required for HF morphogenesis, DP spheroids rapidly dissociate when placed within collagen matrices [122], which might be compromising DP cell inductivity and model progression. Bearing this in mind, Abaci *et al.* [122] developed a strategy in which DP spheroid integrity was maintained and allowed the formation of a skin model with follicular units capable of producing an unpigmented hair shaft. They used micromolding to fabricate defined microwells in fibroblast-populated collagen I hydrogels in which DP spheroids were produced *in situ.* Keratinocytes were then seeded on top, engulfing the spheroids, and differentiating into proper follicular layering over the control of the inductive DP cells and, occasionally forming hair shafts. Further, to enhance DP cell inductivity, a subpopulation of LEF1 overexpressing DP cells was also used, significantly improving HF induction efficiency and the expression of hair lineage-specific genes.

However, the most complete *in vitro* recreation of human HF achieved so far was developed entirely using pluripotent stem cell lines. In a quite distinct and successful approach, hair-bearing skin organoids akin to 18-week human fetal skin were produced. The formation of a cyst-like skin organoid was attained from aggregates of pluripotent stem cells and using a step-by-step modulation of the TGF-β, BMP and FGF signalling pathways, to promote ectoderm and cranial-neural crest induction [211]. The formation of pigmented HFs within the skin organoids was observed after a 4/5-month culture period. Importantly, the skin organoids also display a stratified epidermis and a dermis with SGs and neural innervation, linked to adjacent fat tissue. This study clearly demonstrates the relevance of

selective modulation of hair development signalling pathways, as well as the advantage of reconstructing embryonic events guiding the natural development of the skin and associated appendages. Still, the long preparation time and associated costs represent considerable disadvantages comparably to the use of dissociated primary cells.

I-7.   CONCLUSION AND FUTURE TRENDS

The need for human HF regenerative strategies, and *in vitro* models has been mostly nourished by the growing evidence that murine and human skin and HFs are dissimilar.

Evidences so far have highlighted the importance of combining inductive DP cells and immature epithelial cells with a high proliferative capacity for the recreation of the HF cellular compartments, pushing efforts towards the maintenance of the trichogenic capacity of human cells *in vitro*. Even so, human hair regeneration promoted entirely from human adult cells is yet to be achieved. In truth, the literature concerning hair regeneration continues to be dominated by murine cell-studies or chimeric human-murine combinations, instead of purely human approaches. On the other hand, poor success may also be partially explained by the lack of integrative approaches that go beyond the segregated exploitation of strategies to improve either the inductivity of DP cells or the competence of epithelial cell. In the future, comparative studies capable of identifying the most promising trichogenic combinations may allow significant developments in the field.

Meanwhile, other mesenchymal and epithelial human cell sources may be considered for HF regeneration. Human bone marrow or umbilical cord-derived cells were able to induce HF formation after co-transplantation with human ORS keratinocytes in mice, and to promote hair bulb reformation in an *ex vivo* assay with transected human HFs [200]. Furthermore, human adipose-derived stem cells (ASCs) overexpressing PDGF-A, Sox2 and β-catenin showed higher ALP expression levels than the non-transfected counterparts or DP cells [201] thus representing a potential, and easily available, mesenchymal cell source for HF reformulation. In an era of stem cell engineering, the use of iPSCs from available and more easily reprogrammable autologous epithelial and mesenchymal sources, may also rapidly expand and led to important breakthroughs, such as the recently reported hair-bearing skin organoids [199]. Nonetheless, some constraints should be first overcome, such as the differentiation of

the iPSCs towards the phenotypes of interest. We still have a long road ahead to achieve such goal, but the work by Lee *et al.* [199] provide hope for iPSCs future applications in the HF regenerative field.

Besides the cellular counterparts, the HF microenvironment constitutes, by itself, a challenge when bioengineering HFs. The ECM, in particular, has a key role in directing hair growth and the maintenance of cell function, which also varies with physiological HF cycling. Despite the knowledge generated on this subject, its translation has been limited and bioengineered HF models continue to be elementary and lacking an appropriate recreation of the complexity of the ECM or the native signaling molecules involved in hair control.

The most complex and functional HF models achieved so far comprise the whole skin with HF appendage reformation. Besides HF integration in a supportive biomimetic skin, the inclusion of other HF specialized cell populations, such as neuronal cells and melanocytes or melanocyte precursors in the models are necessary to bioengineer functional and aesthetically acceptable hairs. Also, other elements of the HF macroenvironment, such as the adipose tissue, which has an important regulatory role in hair development and growth, should be considered in future strategies.

Ultimately, the techniques and knowledge generated when pursuing HF recreation *in vitro* also hold potential for regenerative purposes. Although only theoretical for now, the use of small amounts of donor HF samples to isolate, propagate and even genetically manipulate relevant cell populations *in vitro* would be ideal. These could then be used to promote HF *de novo* formation *in situ*, or to bioengineer HFs, allowing the production of ready-to-use follicular units that could be transferred back to the patient for hair restoration. Another important milestone would be the incorporation of HF-like structures in skin substitutes, or the inclusion of cellular and/or bioactive clues that could sustain HF regeneration after implantation, also contributing to their functionality. Additionally, and depending on the cellular populations used and their stemness, a variable degree of self-regeneration capacity could be granted to the skin substitutes, making them more likely to reach long-term use and representing a more effective treatment for patients with severe skin damage.

Future research may even provide knowledge to reprogram the patient's resident skin cells and recreate hair morphogenic events *in situ* [202]. The complexity and spatio-temporal controlled nature of the HF signaling interactions imply that this type of intervention would most likely require the modulation of multiple signalling pathways and to be addressed in a timely manner, making it less likely to succeed compared to autologous cell-based therapies. Nonetheless, there are conditions where

simpler signalling modulation with inductive factors may prove sufficient to promote hair restoration or cycle reactivation in pre-existing HFs. For example, hair miniaturization and loss observed in common baldness have been associated with a defective conversion of bulge stem cells into proliferative progenitor cells [203], representing a prime example of a condition that can eventually be reversed by pharmacological intervention. Also, the knowledge that during wound [128] and increased β-catenin activity [204] neofollicle formation can occur from the IFE, and not from adjacent bulge stem cells, encourage further exploration of these mechanisms in humans.

New and more effective treatment options for hair loss disorders are a major target of the pharmaceutical and cosmetic industry. Similarly, skin substitutes with increased functionality have long been a pressing requirement for effective cutaneous wound healing. The work performed in the last years in the bioengineering of purely human HFs *in vitro* and, particularly in the knowledge regarding HF regeneration have paved the way for future approaches with a high potential to result in clinically applicable solutions.

I-8. REFERENCES

1. Mahjour, S. B., Ghaffarpasand, F. & Wang, H. Hair follicle regeneration in skin grafts: current concepts and future perspectives. *Tissue Eng Part B Rev* **18**, 15–23 (2012).

2. Schneider, M. R., Schmidt-Ullrich, R. & Paus, R. The Hair Follicle as a Dynamic Miniorgan. *Curr Biol* **19**, R132–R142 (2009).

3. Sennett, R. & Rendl, M. Mesenchymal-epithelial interactions during hair follicle morphogenesis and cycling. *Semin Cell Dev Biol* **23**, 917–927 (2012).

4. Balana, M. E., Charreau, H. E. & Leiros, G. J. Epidermal stem cells and skin tissue engineering in hair follicle regeneration. *World J Stem Cells* **7**, 711–727 (2015).

5. Stocum, D. L. Regenerative Medicine of Epidermal Structures. in *Regenerative Biology and Medicine* 261–284 (Elsevier, 2012).

6. Schmidt-Ullrich, R. & Paus, R. Molecular principles of hair follicle induction and morphogenesis. *BioEssays* **27**, 247–261 (2005).

7. Stenn, K. S. & Paus, R. Controls of hair follicle cycling. *Physiol Rev* **81**, 449–494 (2001).

8.   Jönsson, E. H. *et al.* The relation between human hair follicle density and touch perception. *Sci. Rep.* **7**, 2499 (2017).

9.   Martin, P. Wound Healing–Aiming for Perfect Skin Regeneration. *Science.* **276**, 75–81 (1997).

10.   Oliver, R. F. Whisker growth after removal of the dermal papilla and lengths of follicle in the hooded rat. *J. Embryol. Exp. Morphol.* **15**, 331–347 (1966).

11.   Oliver, R. F. The induction of hair follicle formation in the adult hooded rat by vibrissa dermal papillae. *Development* **23**, 219–236 (1970).

12.   Oliver, R. F. The induction of hair follicle formation in the adult hooded rat by vibrissa dermal papillae. *J. Embryol. Exp. Morphol.* **23**, 219–36 (1970).

13.   Yang, C.-C. & Cotsarelis, G. Review of hair follicle dermal cells. *J. Dermatol. Sci.* **57**, 2–11 (2010).

14.   Jahoda, C. A. B., Oliver, R. F., Reynolds, A. J., Forrester, J. C. & Horne, K. A. Human Hair Follicle Regeneration Following Amputation and Grafting into the Nude Mouse. *J. Invest. Dermatol.* **107**, 804–807 (1996).

15.   Reynolds, A. J., Lawrence, C., Cserhalmi-Friedman, P. B., Christiano, A. M. & Jahoda, C. A. Trans-gender induction of hair follicles. *Nature* **402**, 33–34 (1999).

16.   Jahoda, C. A. B. *et al.* Trans-species hair growth induction by human hair follicle dermal papillae. *Exp. Dermatol.* **10**, 229–237 (2001).

17.   Higgins, C. A., Chen, J. C., Cerise, J. E., Jahoda, C. A. B. & Christiano, A. M. Microenvironmental reprogramming by three-dimensional culture enables dermal papilla cells to induce de novo human hair-follicle growth. *Proc. Natl. Acad. Sci.* **110**, 19679–19688 (2013).

18.   Porter, R. M. Mouse models for human hair loss disorders. *J. Anat.* **202**, 125–131 (2003).

19.   Philpott, M. P. Culture of the human pilosebaceous unit, hair follicle and sebaceous gland. *Exp. Dermatol.* **27**, 571–577 (2018).

20.   Oh, J. W. *et al.* A Guide to Studying Human Hair Follicle Cycling In Vivo. *J. Invest. Dermatol.* **136**, 34–44 (2016).

21.   Kent M. Van De Graaff Christopher H. Creek, D. S. *Human Anatomy.* (The McGraw–Hill Companies, 2001).

22.   Turksen, K. Revisiting the bulge. *Dev. Cell* **6**, 454–456 (2004).

23.   Sieber-Blum, M., Grim, M., Hu, Y. F. & Szeder, V. Pluripotent neural crest stem cells in the adult hair follicle. *Dev. Dyn.* **231**, 258–69 (2004).

24.   Christiano, A. M. Epithelial Stem Cells. *Cell* **118**, 530–532 (2004).

25.   Hardy, M. H. The Secret Life of the Hair Follicle. *Trends Genet.* **8**, 55–61 (1992).

26.   Millar, S. E. Molecular mechanisms regulating hair follicle development. *J Invest Dermatol* **118**, 216–225 (2002).

27.   Paus, R. *et al.* A comprehensive guide for the recognition and classification of distinct stages of hair follicle morphogenesis. *J Invest Dermatol* **113**, 523–532 (1999).

28.   Nowak, J. A., Polak, L., Pasolli, H. A. & Fuchs, E. Hair follicle stem cells are specified and function in early skin morphogenesis. *Cell Stem Cell* **3**, 33–43 (2008).

29.   Gonzales, K. A. U. & Fuchs, E. Skin and Its Regenerative Powers: An Alliance between Stem Cells and Their Niche. *Dev. Cell* **43**, 387–401 (2017).

30.   Garcin, C. L. & Ansell, D. M. The battle of the bulge: re-evaluating hair follicle stem cells in wound repair. *Exp. Dermatol.* **26**, 101–104 (2017).

31.   Purba, T. S. *et al.* Human epithelial hair follicle stem cells and their progeny: Current state of knowledge, the widening gap in translational research and future challenges. *Bioessays* **36**, 513–525 (2014).

32.   Legue, E. Hair follicle renewal: organization of stem cells in the matrix and the role of stereotyped lineages and behaviors. *Development* **132**, 4143–4154 (2005).

33.   Cotsarelis, G. Epithelial Stem Cells: A Folliculocentric View. *J. Invest. Dermatol.* **126**, 1459–1468 (2006).

34.   Jahoda, C. A. B., Horne, K. A. & Oliver, R. F. Induction of hair growth by implantation of cultured dermal papilla cells. *Nature* **311**, 560–562 (1984).

35.   Reynolds, A. J., Oliver, R. F. & Jahoda, C. A. Dermal cell populations show variable competence in epidermal cell support: stimulatory effects of hair papilla cells. *J. Cell Sci.* **98**, 75–83 (1991).

36.   Mesler, A. L., Veniaminova, N. A., Lull, M. V. & Wong, S. Y. Hair Follicle Terminal Differentiation

Is Orchestrated by Distinct Early and Late Matrix Progenitors. *Cell Rep.* **19**, 809–821 (2017).

37. Fuchs, E. Skin stem cells: rising to the surface. *J. Cell Biol.* **180**, 273–284 (2008).

38. Buffoli, B. *et al.* The human hair: from anatomy to physiology. *Int J Dermatol* **53**, 331–341 (2014).

39. Sequeira, I. & Nicolas, J.-F. Redefining the structure of the hair follicle by 3D clonal analysis. *Development* **139**, 3741–3751 (2012).

40. Messenger, A. G. The control of hair growth: an overview. *J Invest Dermatol* **101**, 4S-9S (1993).

41. Slominski, A. *et al.* Hair follicle pigmentation. *J Invest Dermatol* **124**, 13–21 (2005).

42. Schwartzenfeld, D. M. & Karamikian, J. Hair Transplantation. in *Plastic Surgery Secrets Plus* 123–127 (Elsevier, 2010).

43. Whitting, D. A. *Hair Growth and Disorders*. *Hair, Hair Growth and Hair Disorders* (Springer Berlin Heidelberg, 2008).

44. Driskell, R. R., Jahoda, C. A. B., Chuong, C.-M., Watt, F. M. & Horsley, V. Defining dermal adipose tissue. *Exp. Dermatol.* **23**, 629–631 (2014).

45. Yang, C.-C. & Cotsarelis, G. Review of hair follicle dermal cells. *J. Dermatol. Sci.* **57**, 2–11 (2010).

46. Greco, V. *et al.* A two-step mechanism for stem cell activation during hair regeneration. *Cell Stem Cell* **4**, 155–169 (2009).

47. Hsu, Y. C., Pasolli, H. A. & Fuchs, E. Dynamics between stem cells, niche, and progeny in the hair follicle. *Cell* **144**, 92–105 (2011).

48. Higgins, C. A., Westgate, G. E. & Jahoda, C. A. B. From Telogen to Exogen: Mechanisms Underlying Formation and Subsequent Loss of the Hair Club Fiber. *J. Invest. Dermatol.* **129**, 2100–2108 (2009).

49. Stenn, K. S. & Cotsarelis, G. Bioengineering the hair follicle: fringe benefits of stem cell technology. *Curr Opin Biotechnol* **16**, 493–497 (2005).

50. Tumbar, T. *et al.* Defining the epithelial stem cell niche in skin. *Science.* **303**, 359–363 (2004).

51. Braun, K. M. & Watt, F. M. Epidermal Label-Retaining Cells: Background and Recent

Applications. *J. Investig. Dermatology Symp. Proc.* **9**, 196–201 (2004).

52. Cotsarelis, G., Sun, T. T. & Lavker, R. M. Label-retaining cells reside in the bulge area of pilosebaceous unit: implications for follicular stem cells, hair cycle, and skin carcinogenesis. *Cell* **61**, 1329–1337 (1990).

53. Fuchs, E., Tumbar, T. & Guasch, G. Socializing with the neighbors: stem cells and their niche. *Cell* **116**, 769–778 (2004).

54. Taylor, G., Lehrer, M. S., Jensen, P. J., Sun, T. T. & Lavker, R. M. Involvement of follicular stem cells in forming not only the follicle but also the epidermis. *Cell* **102**, 451–461 (2000).

55. Oshima, H., Rochat, A., Kedzia, C., Kobayashi, K. & Barrandon, Y. Morphogenesis and renewal of hair follicles from adult multipotent stem cells. *Cell* **104**, 233–245 (2001).

56. Morris, R. J. *et al.* Capturing and profiling adult hair follicle stem cells. *Nat. Biotechnol.* **22**, 411–417 (2004).

57. Ohyama, M. Hair follicle bulge: a fascinating reservoir of epithelial stem cells. *J Dermatol Sci* **46**, 81–89 (2007).

58. Nishimura, E. K. *et al.* Dominant role of the niche in melanocyte stem-cell fate determination. *Nature* **416**, 854–860 (2002).

59. Tobin, D. J. & Bystryn, J.-C. Different Populations of Melanocytes Are Present in Hair Follicles and Epidermis. *Pigment Cell Res.* **9**, 304–310 (1996).

60. Sarin, K. Y. & Artandi, S. E. Aging, Graying and Loss of Melanocyte Stem Cells. *Stem Cell Rev.* **3**, 212–217 (2007).

61. Tobin, D. J., Hagen, E., Botchkarev, V. A. & Paus, R. Do hair bulb melanocytes undergo apoptosis during hair follicle regression (catagen)? *J. Invest. Dermatol.* **111**, 941–947 (1998).

62. Amoh, Y., Li, L., Katsuoka, K., Penman, S. & Hoffman, R. M. Multipotent nestin-positive, keratin-negative hair-follicle bulge stem cells can form neurons. *Proc. Natl. Acad. Sci.* **102**, 5530–5534 (2005).

63. Mignone, J. L. *et al.* Neural Potential of a Stem Cell Population in the Hair Follicle. *Cell Cycle* **6**, 2161–2170 (2007).

64. Yu, H., Kumar, S. M., Kossenkov, A. V, Showe, L. & Xu, X. Stem cells with neural crest

characteristics derived from the bulge region of cultured human hair follicles. *J Invest Dermatol* **130**, 1227–1236 (2010).

65. Clewes, O. *et al.* Human epidermal neural crest stem cells (hEPI-NCSC)–characterization and directed differentiation into osteocytes and melanocytes. *Stem Cell Rev* **7**, 799–814 (2011).

66. Solanas, G. & Benitah, S. A. Regenerating the skin: a task for the heterogeneous stem cell pool and surrounding niche. *Nat Rev Mol Cell Biol* **14**, 737–748 (2013).

67. Watt, F. M. Mammalian skin cell biology: at the interface between laboratory and clinic. *Science* **346**, 937–40 (2014).

68. Page, M. E., Lombard, P., Ng, F., Gottgens, B. & Jensen, K. B. The epidermis comprises autonomous compartments maintained by distinct stem cell populations. *Cell Stem Cell* **13**, 471–482 (2013).

69. Kretzschmar, K. & Watt, F. M. Markers of Epidermal Stem Cell Subpopulations in Adult Mammalian Skin. *Cold Spring Harb. Perspect. Med.* **4**, a013631–a013631 (2014).

70. Tobin, D. J., Gunin, A., Magerl, M. & Paus, R. Plasticity and cytokinetic dynamics of the hair follicle mesenchyme during the hair growth cycle: implications for growth control and hair follicle transformations. *J Investig Dermatol Symp Proc* **8**, 80–86 (2003).

71. Rahmani, W. *et al.* Hair Follicle Dermal Stem Cells Regenerate the Dermal Sheath, Repopulate the Dermal Papilla, and Modulate Hair Type. *Dev. Cell* **31**, 543–558 (2014).

72. Vapniarsky, N., Arzi, B., Hu, J. C., Nolta, J. A. & Athanasiou, K. A. Concise Review: Human Dermis as an Autologous Source of Stem Cells for Tissue Engineering and Regenerative Medicine. *Stem Cells Transl Med* **4**, 1187–1198 (2015).

73. Agabalyan, N. A., Rosin, N. L., Rahmani, W. & Biernaskie, J. Hair follicle dermal stem cells and skin-derived precursor cells: Exciting tools for endogenous and exogenous therapies. *Exp. Dermatol.* **26**, 505–509 (2017).

74. Horne, K. a & Jahoda, C. A. Restoration of hair growth by surgical implantation of follicular dermal sheath. *Development* **116**, 563–71 (1992).

75. McElwee, K. J., Kissling, S., Wenzel, E., Huth, A. & Hoffmann, R. Cultured peribulbar dermal sheath cells can induce hair follicle development and contribute to the dermal sheath and

dermal papilla. *J Invest Dermatol* **121**, 1267–1275 (2003).

76. Matsuzaki, T. & Yoshizato, K. Role of hair papilla cells on induction and regeneration processes of hair follicles. *Wound Repair Regen* **6**, 524–530 (1998).

77. Jahoda, C. A. Induction of follicle formation and hair growth by vibrissa dermal papillae implanted into rat ear wounds: vibrissa-type fibres are specified. *Development* **115**, 1103–9 (1992).

78. Ohyama, M., Zheng, Y., Paus, R. & Stenn, K. S. The mesenchymal component of hair follicle neogenesis: background, methods and molecular characterization. *Exp. Dermatol.* **19**, 89–99 (2010).

79. Rendl, M., Lewis, L. & Fuchs, E. Molecular Dissection of Mesenchymal–Epithelial Interactions in the Hair Follicle. *PLoS Biol.* **3**, e331 (2005).

80. Driskell, R. R., Clavel, C., Rendl, M. & Watt, F. M. Hair follicle dermal papilla cells at a glance. *J. Cell Sci.* **124**, 1179–1182 (2011).

81. Jahoda, C. A. B., Reynolds, A. J. & Oliver, R. F. Induction of Hair Growth in Ear Wounds by Cultured Dermal Papilla Cells. *J. Invest. Dermatol.* **101**, 584–590 (1993).

82. Ohyama, M., Kobayashi, T., Sasaki, T., Shimizu, A. & Amagai, M. Restoration of the intrinsic properties of human dermal papilla in vitro. *J. Cell Sci.* **125**, 4114–25 (2012).

83. Lin, B. *et al.* Surface Tension Guided Hanging-Drop: Producing Controllable 3D Spheroid of High-Passaged Human Dermal Papilla Cells and Forming Inductive Microtissues for Hair-Follicle Regeneration. *ACS Appl Mater Interfaces* **8**, 5906–5916 (2016).

84. Miao, Y., Sun, Y. B., Liu, B. C., Jiang, J. D. & Hu, Z. Q. Controllable production of transplantable adult human high-passage dermal papilla spheroids using 3D matrigel culture. *Tissue Eng Part A* **20**, 2329–2338 (2014).

85. Osada, A., Iwabuchi, T., Kishimoto, J., Hamazaki, T. S. & Okochi, H. Long-term culture of mouse vibrissal dermal papilla cells and de novo hair follicle induction. *Tissue Eng* **13**, 975–982 (2007).

86. Young, T. H., Lee, C. Y., Chiu, H. C., Hsu, C. J. & Lin, S. J. Self-assembly of dermal papilla cells into inductive spheroidal microtissues on poly(ethylene-co-vinyl alcohol) membranes for hair

follicle regeneration. *Biomaterials* **29**, 3521–3530 (2008).

87.   Higgins, C. A., Richardson, G. D., Ferdinando, D., Westgate, G. E. & Jahoda, C. A. Modelling the hair follicle dermal papilla using spheroid cell cultures. *Exp Dermatol* **19**, 546–548 (2010).

88.   Hsieh, C. H., Wang, J. L. & Huang, Y. Y. Large-scale cultivation of transplantable dermal papilla cellular aggregates using microfabricated PDMS arrays. *Acta Biomater* **7**, 315–324 (2011).

89.   Huang, Y. C. *et al.* Scalable production of controllable dermal papilla spheroids on PVA surfaces and the effects of spheroid size on hair follicle regeneration. *Biomaterials* **34**, 442–451 (2013).

90.   Carreau, A., Hafny-Rahbi, B. El, Matejuk, A., Grillon, C. & Kieda, C. Why is the partial oxygen pressure of human tissues a crucial parameter? Small molecules and hypoxia. *J. Cell. Mol. Med.* **15**, 1239–1253 (2011).

91.   Thangapazham, R. L. *et al.* Dissociated human dermal papilla cells induce hair follicle neogenesis in grafted dermal-epidermal composites. *J Invest Dermatol* **134**, 538–540 (2014).

92.   Zheng, M. *et al.* Hypoxia improves hair inductivity of dermal papilla cells via nuclear NADPH oxidase 4-mediated reactive oxygen species generation'. *Br. J. Dermatol.* **181**, 523–534 (2019).

93.   Inamatsu, M., Matsuzaki, T., Iwanari, H. & Yoshizato, K. Establishment of Rat Dermal Papilla Cell Lines that Sustain the Potency to Induce Hair Follicles from Afollicular Skin. *J. Invest. Dermatol.* **111**, 767–775 (1998).

94.   Warren, R. & Wong, T. K. Stimulation of human scalp papilla cells by epithelial cells. *Arch. Dermatol. Res.* **286**, 1–5 (1994).

95.   Won, C. H. *et al.* Hair-growth-promoting effect of conditioned medium of high integrin α6 and low CD 71 (α6bri/CD71dim) positive keratinocyte cells. *Int. J. Mol. Sci.* **16**, 4379–4391 (2015).

96.   Inoue, K. *et al.* TGF-beta is specifically expressed in human dermal papilla cells and modulates hair folliculogenesis. *J. Cell. Mol. Med.* **13**, 4643–56 (2009).

97.   Aoi, N. *et al.* 1α,25-Dihydroxyvitamin D3 Modulates the Hair-Inductive Capacity of Dermal Papilla Cells: Therapeutic Potential for Hair Regeneration. *Stem Cells Transl Med* **1**, 615–626 (2012).

98.   Dong, L. *et al.* Treatment of MSCs with Wnt1a-conditioned medium activates DP cells and

promotes hair follicle regrowth. *Sci. Rep.* **4**, 5432 (2015).

99. Rajendran, R. L. *et al.* Macrophage-Derived Extracellular Vesicle Promotes Hair Growth. *Cells* **9**, 856 (2020).

100. Lee, S.-H. *et al.* Valproic Acid Induces Hair Regeneration in Murine Model and Activates Alkaline Phosphatase Activity in Human Dermal Papilla Cells. *PLoS One* **7**, e34152 (2012).

101. Yamauchi, K. & Kurosaka, A. Inhibition of glycogen synthase kinase-3 enhances the expression of alkaline phosphatase and insulin-like growth factor-1 in human dermal papilla cell culture and maintains mouse hair bulbs in organ culture. *Arch. Dermatol. Res.* **301**, 357–365 (2009).

102. Rendl, M., Polak, L. & Fuchs, E. BMP signaling in dermal papilla cells is required for their hair follicle-inductive properties. *Genes Dev* **22**, 543–557 (2008).

103. Kalabusheva, E., Terskikh, V. & Vorotelyak, E. Hair Germ Model In Vitro via Human Postnatal Keratinocyte-Dermal Papilla Interactions: Impact of Hyaluronic Acid. *Stem Cells Int.* **2017**, 1–14 (2017).

104. Kennedy Crispin, M. *et al.* Safety and efficacy of the JAK inhibitor tofacitinib citrate in patients with alopecia areata. *JCI Insight* **1**, (2016).

105. Jabbari, A. *et al.* An Open-Label Pilot Study to Evaluate the Efficacy of Tofacitinib in Moderate to Severe Patch-Type Alopecia Areata, Totalis, and Universalis. *J. Invest. Dermatol.* **138**, 1539–1545 (2018).

106. Liu, L. Y., Craiglow, B. G., Dai, F. & King, B. A. Tofacitinib for the treatment of severe alopecia areata and variants: A study of 90 patients. *J. Am. Acad. Dermatol.* **76**, 22–28 (2017).

107. Toyoshima, K. *et al.* Fully functional hair follicle regeneration through the rearrangement of stem cells and their niches. *Nat. Commun.* **3**, 784 (2012).

108. Wu, J.-J. *et al.* Hair follicle reformation induced by dermal papilla cells from human scalp skin. *Arch. Dermatol. Res.* **298**, 183–190 (2006).

109. Lindner, G., Horland, R., Wagner, I., Ataç, B. & Lauster, R. De novo formation and ultra-structural characterization of a fiber-producing human hair follicle equivalent in vitro. *J. Biotechnol.* **152**, 108–112 (2011).

110. Chan, C. C., Fan, S. M., Wang, W. H., Mu, Y. F. & Lin, S. J. A Two-Stepped Culture Method for

Efficient Production of Trichogenic Keratinocytes. *Tissue Eng Part C Methods* **21**, 1070–1079 (2015).

111.   Nilforoushzadeh, M. *et al.* Hair follicle generation by injections of adult human follicular epithelial and dermal papilla cells into nude mice. *Cell J.* **19**, 259–268 (2017).

112.   Ehama, R. *et al.* Hair follicle regeneration using grafted rodent and human cells. *J Invest Dermatol* **127**, 2106–2115 (2007).

113.   Qiao, J. *et al.* Hair follicle neogenesis induced by cultured human scalp dermal papilla cells. *Regen Med* **4**, 667–676 (2009).

114.   Kageyama, T., Yan, L., Shimizu, A., Maruo, S. & Fukuda, J. Preparation of hair beads and hair follicle germs for regenerative medicine. *Biomaterials* **212**, 55–63 (2019).

115.   Kang, B. M., Kwack, M. H., Kim, M. K., Kim, J. C. & Sung, Y. K. Sphere formation increases the ability of cultured human dermal papilla cells to induce hair follicles from mouse epidermal cells in a reconstitution assay. *J Invest Dermatol* **132**, 237–239 (2012).

116.   Wu, X., Scott, L., Washenik, K. & Stenn, K. Full-Thickness Skin with Mature Hair Follicles Generated from Tissue Culture Expanded Human Cells. *Tissue Eng. Part A* **20**, 3314–3321 (2014).

117.   Yoshida, Y., Soma, T., Matsuzaki, T. & Kishimoto, J. Wnt activator CHIR99021-stimulated human dermal papilla spheroids contribute to hair follicle formation and production of reconstituted follicle-enriched human skin. *Biochem. Biophys. Res. Commun.* **516**, 599–605 (2019).

118.   Abaci, H. E. *et al.* Tissue engineering of human hair follicles using a biomimetic developmental approach. *Nat. Commun.* **9**, 5301 (2018).

119.   Roh, C., Tao, Q. & Lyle, S. Dermal papilla-induced hair differentiation of adult epithelial stem cells from human skin. *Physiol. Genomics* **19**, 207–217 (2005).

120.   Bak, S. S. *et al.* Restoration of hair-inductive activity of cultured human follicular keratinocytes by co-culturing with dermal papilla cells. *Biochem. Biophys. Res. Commun.* **505**, 360–364 (2018).

121.   Yang, Z. *et al.* CD49fhigh Defines a Distinct Skin Mesenchymal Stem Cell Population Capable of Hair Follicle Epithelial Cell Maintenance. *J. Invest. Dermatol.* **140**, 544-555.e9 (2020).

122. Chacon-Martinez, C. A., Klose, M., Niemann, C., Glauche, I. & Wickstrom, S. A. Hair follicle stem cell cultures reveal self-organizing plasticity of stem cells and their progeny. *EMBO J* **36**, 151–164 (2017).

123. Sennett, R. & Rendl, M. Mesenchymal–epithelial interactions during hair follicle morphogenesis and cycling. *Semin. Cell Dev. Biol.* **23**, 917–927 (2012).

124. Rishikaysh, P. *et al.* Signaling Involved in Hair Follicle Morphogenesis and Development. *Int. J. Mol. Sci.* **15**, 1647–1670 (2014).

125. Andl, T., Reddy, S. T., Gaddapara, T. & Millar, S. E. Wnt signals are required for the initiation of hair follicle development. *Dev. Cell* **2**, 643–653 (2002).

126. Huelsken, J., Vogel, R., Erdmann, B., Cotsarelis, G. & Birchmeier, W. β-Catenin Controls Hair Follicle Morphogenesis and Stem Cell Differentiation in the Skin. *Cell* **105**, 533–545 (2001).

127. Van Mater, D. Transient activation of beta -catenin signaling in cutaneous keratinocytes is sufficient to trigger the active growth phase of the hair cycle in mice. *Genes Dev.* **17**, 1219–1224 (2003).

128. Ito, M. *et al.* Wnt-dependent de novo hair follicle regeneration in adult mouse skin after wounding. *Nature* **447**, 316–320 (2007).

129. Celso, C. Lo. Transient activation of -catenin signalling in adult mouse epidermis is sufficient to induce new hair follicles but continuous activation is required to maintain hair follicle tumours. *Development* **131**, 1787–1799 (2004).

130. Ouji, Y., Yoshikawa, M., Shiroi, A. & Ishizaka, S. Promotion of hair follicle development and trichogenesis by Wnt-10b in cultured embryonic skin and in reconstituted skin. *Biochem. Biophys. Res. Commun.* **345**, 581–587 (2006).

131. Ouji, Y. *et al.* Wnt-10b, uniquely among Wnts, promotes epithelial differentiation and shaft growth. *Biochem. Biophys. Res. Commun.* **367**, 299–304 (2008).

132. Ouji, Y., Yoshikawa, M., Shiroi, A. & Ishizaka, S. Wnt-10b promotes differentiation of skin epithelial cells in vitro. *Biochem. Biophys. Res. Commun.* **342**, 28–35 (2006).

133. Botchkarev, V. A. & Fessing, M. Y. Edar Signaling in the Control of Hair Follicle Development. *J. Investig. Dermatology Symp. Proc.* **10**, 247–251 (2005).

134. Mustonen, T. Ectodysplasin A1 promotes placodal cell fate during early morphogenesis of ectodermal appendages. *Development* **131**, 4907–4919 (2004).

135. Laurikkala, J. *et al.* Regulation of hair follicle development by the TNF signal ectodysplasin and its receptor Edar. *Development* **129**, 2541–53 (2002).

136. Yan, M. Two-Amino Acid Molecular Switch in an Epithelial Morphogen That Regulates Binding to Two Distinct Receptors. *Science.* **290**, 523–527 (2000).

137. Srivastava, A. K. *et al.* Ectodysplasin-A1 is sufficient to rescue both hair growth and sweat glands in tabby mice. *Hum. Mol. Genet.* **10**, 2973–2981 (2001).

138. Fessing, M. Y., Sharova, T. Y., Sharov, A. A., Atoyan, R. & Botchkarev, V. A. Involvement of the Edar Signaling in the Control of Hair Follicle Involution (Catagen). *Cytokines, Cell Cycle Mol.* **169**, 2075–2084 (2006).

139. Kwack, M. H., Kim, J. C. & Kim, M. K. Ectodysplasin-A2 induces apoptosis in cultured human hair follicle cells and promotes regression of hair follicles in mice. *Biochem. Biophys. Res. Commun.* **520**, 428–433 (2019).

140. Kwack, M. H., Jun, M. S., Sung, Y. K., Kim, J. C. & Kim, M. K. Ectodysplasin-A2 induces dickkopf 1 expression in human balding dermal papilla cells overexpressing the ectodysplasin A2 receptor. *Biochem. Biophys. Res. Commun.* **529**, 766–772 (2020).

141. Karlsson, L., Bondjers, C. & Betsholtz, C. Roles for PDGF-A and sonic hedgehog in development of mesenchymal components of the hair follicle. *Development* **126**, 2611–21 (1999).

142. Chiang, C. *et al.* Essential role for Sonic hedgehog during hair follicle morphogenesis. *Dev. Biol.* **205**, 1–9 (1999).

143. St-Jacques, B. *et al.* Sonic hedgehog signaling is essential for hair development. *Curr. Biol.* **8**, 1058–1069 (1998).

144. Karlsson, L., Bondjers, C. & Betsholtz, C. Roles for PDGF-A and sonic hedgehog in development of mesenchymal components of the hair follicle. *Development* **126**, 2611–21 (1999).

145. González, R. *et al.* Platelet-derived growth factor signaling modulates adult hair follicle dermal stem cell maintenance and self-renewal. *npj Regen. Med.* **2**, 11 (2017).

146. Takakura, N., Yoshida, H., Kunisada, T., Nishikawa, S. & Nishikawa, S.-I. Involvement of Platelet-

Derived Growth Factor Receptor-α in Hair Canal Formation. *J. Invest. Dermatol.* **107**, 770–777 (1996).

147. Tomita, Y., Akiyama, M. & Shimizu, H. PDGF isoforms induce and maintain anagen phase of murine hair follicles. *J. Dermatol. Sci.* **43**, 105–115 (2006).

148. Kulessa, H., Turk, G. & Hogan, B. L. M. Inhibition of Bmp signaling affects growth and differentiation in the anagen hair follicle. *EMBO J.* **19**, 6664–6674 (2000).

149. Botchkarev, V. A. *et al.* Noggin is a mesenchymally derived stimulator of hair-follicle induction. *Nat. Cell Biol.* **1**, 158–164 (1999).

150. Botchkarev, V. A. *et al.* Noggin is required for induction of the hair follicle growth phase in postnatal skin. *FASEB J.* **15**, 2205–2214 (2001).

151. Kulessa, H. Inhibition of Bmp signaling affects growth and differentiation in the anagen hair follicle. *EMBO J.* **19**, 6664–6674 (2000).

152. Foitzik, K., Paus, R., Doetschman, T. & Paolo Dotto, G. The TGF-β2 Isoform Is Both a Required and Sufficient Inducer of Murine Hair Follicle Morphogenesis. *Dev. Biol.* **212**, 278–289 (1999).

153. Inui, S., Fukuzato, Y., Nakajima, T., Yoshikawa, K. & Itami, S. Androgen-inducible TGF-beta1 from balding dermal papilla cells inhibits epithelial cell growth: a clue to understand paradoxical effects of androgen on human hair growth. *FASEB J.* **16**, 1967–1969 (2002).

154. Foitzik, K. *et al.* Control of murine hair follicle regression (catagen) by TGF-β1 in vivo. *FASEB J.* **14**, 752–760 (2000).

155. Lin, W. *et al.* Fibroblast Growth Factors Stimulate Hair Growth through β -Catenin and Shh Expression in C57BL/6 Mice. *Biomed Res. Int.* **2015**, 1–9 (2015).

156. Kawano, M. *et al.* Comprehensive Analysis of FGF and FGFR Expression in Skin: FGF18 Is Highly Expressed in Hair Follicles and Capable of Inducing Anagen from Telogen Stage Hair Follicles. *J. Invest. Dermatol.* **124**, 877–885 (2005).

157. Higgins, C. A. *et al.* FGF5 is a crucial regulator of hair length in humans. *Proc. Natl. Acad. Sci.* **111**, 10648–10653 (2014).

158. Katsuoka, K., Schell, H., Hornstein, O. P. & Wessel, B. Epidermal growth factor and fibroblast growth factor accelerate proliferation of human hair bulb papilla cells and root sheath tibroblasts

cultured in vitro. *Br. J. Dermatol.* **116**, 464–465 (1987).

159. Sun, X. *et al.* Dedifferentiation of Human Terminally Differentiating Keratinocytes into Their Precursor Cells Induced by Basic Fibroblast Growth Factor. *Biol. Pharm. Bull.* **34**, 1037–1045 (2011).

160. Lemasters, J. J. *et al.* Compartmentation of Mitochondrial and Oxidative Metabolism in Growing Hair Follicles: A Ring of Fire. *J. Invest. Dermatol.* **137**, 1434–1444 (2017).

161. Calvo-Sánchez, M. I., Fernández-Martos, S., Montoya, J. J. & Espada, J. Intrinsic activation of cell growth and differentiation in ex vivo cultured human hair follicles by a transient endogenous production of ROS. *Sci. Rep.* **9**, 1–9 (2019).

162. Hamanaka, R. B. *et al.* Mitochondrial Reactive Oxygen Species Promote Epidermal Differentiation and Hair Follicle Development. *Sci. Signal.* **6**, ra8–ra8 (2013).

163. Andl, T. & Botchkareva, N. V. MicroRNAs (miRNAs) in the control of HF development and cycling: The next frontiers in hair research. *Exp. Dermatol.* **24**, 821–826 (2015).

164. Lena, A. M. *et al.* miR-203 represses 'stemness' by repressing ΔNp63. *Cell Death Differ.* **15**, 1187–1195 (2008).

165. Yi, R., Poy, M. N., Stoffel, M. & Fuchs, E. A skin microRNA promotes differentiation by repressing 'stemness'. *Nature* **452**, 225–229 (2008).

166. Amelio, I., Lena, A. M., Bonanno, E., Melino, G. & Candi, E. miR-24 affects hair follicle morphogenesis targeting Tcf-3. *Cell Death Dis.* **4**, e922–e922 (2013).

167. Zhang, L., Stokes, N., Polak, L. & Fuchs, E. Specific microRNAs are preferentially expressed by skin stem cells to balance self-renewal and early lineage commitment. *Cell Stem Cell* **8**, 294–308 (2011).

168. Mardaryev, A. N. *et al.* Micro-RNA-31 controls hair cycle-associated changes in gene expression programs of the skin and hair follicle. *FASEB J.* **24**, 3869–3881 (2010).

169. Watt, F. M. Engineered Microenvironments to Direct Epidermal Stem Cell Behavior at Single-Cell Resolution. *Dev. Cell* **38**, 601–609 (2016).

170. Messenger, A. G., Elliott, K., Westgate, G. E. & Gibson, W. T. Distribution of extracellular matrix molecules in human hair follicles. *Ann. N. Y. Acad. Sci.* **642**, 253–62 (1991).

171. Messenger, A. G., Elliott, K., Temple, A. & Randall, V. A. Expression of basement membrane proteins and interstitial collagens in dermal papillae of human hair follicles. *J Invest Dermatol* **96**, 93–97 (1991).

172. Jahoda, C. A., Mauger, A., Bard, S. & Sengel, P. Changes in fibronectin, laminin and type IV collagen distribution relate to basement membrane restructuring during the rat vibrissa follicle hair growth cycle. *J. Anat.* **181**, 47–60 (1992).

173. Soma, T., Tajima, M. & Kishimoto, J. Hair cycle-specific expression of versican in human hair follicles. *J. Dermatol. Sci.* **39**, 147–154 (2005).

174. Hotchin, N. A., Gandarillas, A. & Watt, F. M. Regulation of cell surface beta 1 integrin levels during keratinocyte terminal differentiation. *J. Cell Biol.* **128**, 1209–1219 (1995).

175. Zhu, A. J., Haase, I. & Watt, F. M. Signaling via 1 integrins and mitogen-activated protein kinase determines human epidermal stem cell fate in vitro. *Proc. Natl. Acad. Sci.* **96**, 6728–6733 (1999).

176. Watt, F. M. Role of integrins in regulating epidermal adhesion, growth and differentiation. *EMBO J.* **21**, 3919–3926 (2002).

177. Commo, S. & Bernard, B. A. The distribution of α2β1, α3β1 and α6β4 integrins identifies distinct subpopulations of basal keratinocytes in the outer root sheath of the human anagen hair follicle. *Cell. Mol. Life Sci.* **53**, 466–471 (1997).

178. McGrath, J. A. *et al.* Mutations in the 180–kD bullous pemphigoid antigen (BPAG2), a hemidesmosomal transmembrane collagen (COL17A1), in generalized atrophic benign epidermolysis bullosa. *Nat. Genet.* **11**, 83–86 (1995).

179. La Placa, M. Generalized atrophic benign epidermolysis bullosa. *J. Eur. Acad. Dermatology Venereol.* **7**, 167–170 (1996).

180. Link, R. E., Paus, R., Stenn, K. S., Kuklinska, E. & Moellmann, G. Epithelial Growth by Rat Vibrissae Follicles In Vitro Requires Mesenchymal Contact via Native Extracellular Matrix. *J. Invest. Dermatol.* **95**, 202–207 (1990).

181. Li, J. Laminin-10 is crucial for hair morphogenesis. *EMBO J.* **22**, 2400–2410 (2003).

182. Gao, J. *et al.* Laminin-511 is an epithelial message promoting dermal papilla development and

function during early hair morphogenesis. *Genes Dev.* **22**, 2111–2124 (2008).

183. Zhou, L., Jing, J., Wang, H., Wu, X. & Lu, Z. Decorin promotes proliferation and migration of ORS keratinocytes and maintains hair anagen in mice. *Exp. Dermatol.* **27**, 1237–1244 (2018).

184. Jing, J. *et al.* Expression of decorin throughout the murine hair follicle cycle: hair cycle dependence and anagen phase prolongation. *Exp. Dermatol.* **23**, 486–491 (2014).

185. Young, T.-H. *et al.* The enhancement of dermal papilla cell aggregation by extracellular matrix proteins through effects on cell–substratum adhesivity and cell motility. *Biomaterials* **30**, 5031–5040 (2009).

186. Morelli, J. G., Yohn, J. J., Zekman, T. & Norris, D. A. Melanocyte movement in vitro: Role of matrix proteins and integrin receptors. *J. Invest. Dermatol.* **101**, 605–608 (1993).

187. Betriu, N., Jarrosson-Moral, C. & Semino, C. E. Culture and Differentiation of Human Hair Follicle Dermal Papilla Cells in a Soft 3D Self-Assembling Peptide Scaffold. *Biomolecules* **10**, 684 (2020).

188. Zhang, S., Gelain, F. & Zhao, X. Designer self-assembling peptide nanofiber scaffolds for 3D tissue cell cultures. *Semin. Cancer Biol.* **15**, 413–420 (2005).

189. Buffey, J. A. *et al.* Extracellular matrix derived from hair and skin fibroblasts stimulates human skin melanocyte tyrosinase activity. *Br. J. Dermatol.* **131**, 836–842 (1994).

190. Tobin, D. J. The cell biology of human hair follicle pigmentation. *Pigment Cell Melanoma Res.* **24**, 75–88 (2011).

191. Limat, A. *et al.* Outer root sheath (ORS) cells organize into epidermoid cyst-like spheroids when cultured inside Matrigel: a light-microscopic and immunohistological comparison between human ORS cells and interfollicular keratinocytes. *Cell Tissue Res.* **275**, 169–176 (1994).

192. Havlickova, B. *et al.* A Human Folliculoid Microsphere Assay for Exploring Epithelial–Mesenchymal Interactions in the Human Hair Follicle. *J. Invest. Dermatol.* **129**, 972–983 (2009).

193. Havlickova, B., Biro, T., Mescalchin, A., Arenberger, P. & Paus, R. Towards optimization of an organotypic assay system that imitates human hair follicle-like epithelial-mesenchymal interactions. *Br. J. Dermatol.* **151**, 753–765 (2004).

194. Lim, T. C. *et al.* Follicular dermal papilla structures by organization of epithelial and mesenchymal cells in interfacial polyelectrolyte complex fibers. *Biomaterials* **34**, 7064–7072 (2013).

195. Gupta, A. C. *et al.* Establishment of an in vitro organoid model of dermal papilla of human hair follicle. *J. Cell. Physiol.* **233**, 9015–9030 (2018).

196. Chermnykh, E. S. *et al.* Dermal papilla cells induce keratinocyte tubulogenesis in culture. *Histochem. Cell Biol.* **133**, 567–576 (2010).

197. Leirós, G. J. *et al.* Dermal Papilla Cells Improve the Wound Healing Process and Generate Hair Bud-Like Structures in Grafted Skin Substitutes Using Hair Follicle Stem Cells. *Stem Cells Transl. Med.* **3**, 1209–1219 (2014).

198. Vahav, I. *et al.* Reconstructed human skin shows epidermal invagination towards integrated neopapillae indicating early hair follicle formation in vitro. *J. Tissue Eng. Regen. Med.* **14**, 761–773 (2020).

199. Lee, J. *et al.* Hair-bearing human skin generated entirely from pluripotent stem cells. *Nature* **582**, 399–404 (2020).

200. Yoo, B.-Y. *et al.* Application of mesenchymal stem cells derived from bone marrow and umbilical cord in human hair multiplication. *J. Dermatol. Sci.* **60**, 74–83 (2010).

201. Choi, N. *et al.* Generation of trichogenic adipose-derived stem cells by expression of three factors. *J. Dermatol. Sci.* **92**, 18–29 (2018).

202. Mohammadi, P., Youssef, K. K., Abbasalizadeh, S., Baharvand, H. & Aghdami, N. Human Hair Reconstruction: Close, But Yet So Far. *Stem Cells Dev.* **25**, 1767–1779 (2016).

203. Garza, L. A. *et al.* Bald scalp in men with androgenetic alopecia retains hair follicle stem cells but lacks CD200-rich and CD34-positive hair follicle progenitor cells. *J. Clin. Invest.* **121**, 613–622 (2011).

204. Silva-Vargas, V. *et al.* β-catenin and hedgehog signal strength can specify number and location of hair follicles in adult epidermis without recruitment of bulge stem cells. *Dev. Cell* **9**, 121–131 (2005).

CHAPTER II

MATERIALS AND METHODS

MATERIALS AND METHODS

This chapter aims to describe the experimental procedures used throughout the work reported in this thesis. Although each experimental chapter of this thesis contains a materials and methods section, providing details for each experimental setup, this particular one provides a general perspective of materials and methods complemented with the rationale for the selection of the materials and cells, and the characterization techniques used.

II-1.   BIOMATERIALS

II-1.1.   Gellan Gum

Gellan gum (GG) is an anionic polysaccharide produced by the non-pathogenic gram - bacteria *Sphingomonas elodea* [1]. It consists of linear repetitions of tetrasaccharide units composed of 1,3-β-D-glucose, 1,4-β-D-glucuronic acid, 1,4-β-D-glucose and 1,4-α-L-rhamnose and it can exist in two different forms – native or deacetylated [2] (Figure II-1). In the native form, or high acyl form, GG presents two acyl groups in the glucose residues, which are absent in the deacetylated form, which can be achieved using an alkaline treatment [3].
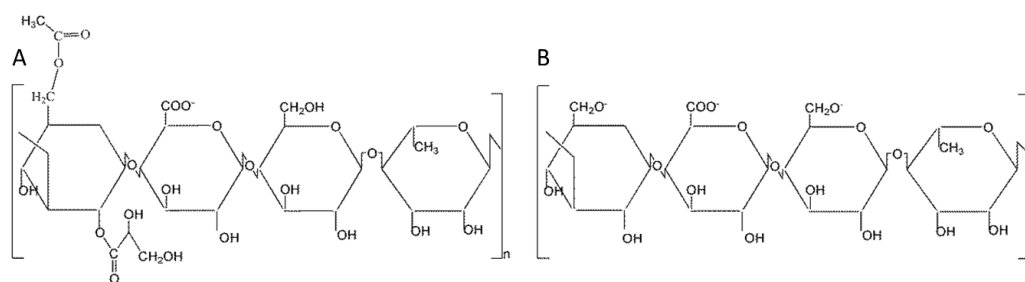
Figure II-1 - Chemical structure of the (A) native and (B) deacetylated gellan gum.

GG attractiveness for Tissue Engineering and Regenerative Medicine (TERM), or other biomedical applications, rely firstly on its gelation properties. In short, GG can be dissolved in water at high temperatures (> 40°C), displaying a disordered conformation (random coil) that gradually becomes

more ordered during cooling, allowing the formation of a hydrogel under mild conditions [3]. Moreover, GG can be crosslinked in the presence of low concentrations of divalent (*e.g.* Ca^{2+}, Mg^{2+}) or monovalent cations (*e.g* Na^+, K^+) present for example in standard cell culture media [4], favoring its combination with different types of cells. GG hydrogels are also relatively stable when cultured for long periods since, being only susceptible to hydrolysis [5] or enzymatic degradation by enzymes such as lysozyme, amylase or trypsin [6,7].

The GG used in this thesis studies was purchased in the deacetylated form with the designation of Gelzan™ CM from Sigma-Aldrich (USA).

II-1.1.1. Gellan gum modification

Contrarily to other polysaccharides, GG has no cell-adhesive sites which represents a major drawback for TERM mostly dependent on the use of anchorage-dependent cells. To overcome this limitation and incorporate cell-adhesive sites, GG was chemically modified and coupled to peptide sequences present in two relevant HF proteins: collagen type IV and fibronectin. Collagen IV is abundantly expressed in the basement membrane separating the HF epithelial and mesenchymal cellular compartments, and in the dermal papilla (DP) extracellular matrix (ECM), while fibronectin is present on the ECM of the DP [8]. Considering this, the HepIII sequence, a heparin-binding peptide sequence located in the $\alpha 1$ (IV) triple-helical region of collagen type IV [9] and a synthetic cyclic form of RGD (cRGDfC), a known peptide sequence of fibronectin that mediates cells adhesion [10], were used.

Firstly, GG was conjugated with a divinyl sulfone (DVS) group, using Michael-type addition chemistry following a previously published protocol [11]. The DVS group works as an intermediary moiety since hydroxyl groups of GG reacts with it, establishing a covalent link. Peptides containing cysteine residues can then react with the DVS group, yielding a very stable thiol-ether linkage [11]. In detail, Gelzan™ CM powder (0.25% w/v) was dissolved in deionized (DI) water under stirring at 90°C. After dissolution, the temperature was lowered to room temperature (RT), and the pH adjusted to 12 with 0.1 N sodium hydroxide (PanReac AppliChem, USA). DVS (Sigma-Aldrich, USA) was then added in excess (molar ratio of 30:1) and left to react 1 hour (h) under stirring. GG modified with DVS (GG-DVS, Figure II-2) was then purified by a series of dialysis against DI water at RT combined with precipitation in cold diethyl ether (1:5). The purified GG-DVS was filtered with a 0.22 μm filter and freeze-dried for further characterization and use.
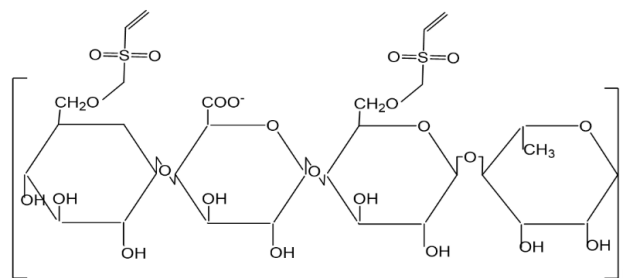
Figure II-2 - Chemical structure of gellan gum modified with divinyl sulfone.

For the functionalization with the peptides, GG-DVS (at 0.75 or 1.25% w/v) and the HepIII (400 µM; Cys-Gly-Glu-Phe-Tyr-Phe-Asp-Leu-Arg-Leu-Lys-Gly-Asp-Lys) and cRGDfC (800 µM; Cyclo[Arg-Gly-Asp-(D-Phe)-Cys]) peptides (≥ 95% purity per manufacturer, GeneCust, France) were separately dissolved in a 0.25 M solution of sucrose at pH ≥ 8.3 (Sigma-Aldrich, USA), which allows controlling the osmotic pressure [12] and avoid cell disruption when the hydrogels are used for cell encapsulation. Upon dissolution, the peptide and the GG-DVS solutions (volume ratio 30:70) were slowly mixed and left to react for 1h at RT, under gentle stirring. The GG-DVS-peptide solution was dialyzed against DI water at RT for 3 days, to remove unbound peptide, and then freeze-dried for further characterization and use. GG-DVS-HepIII and GG-DVS-cRGDfC were used to prepare hydrogels that recreate the DP ECM microenvironment.

II-2.   CELL SOURCES, ISOLATION AND/OR EXPANSION

Hair follicle (HF) embryogenesis and cyclical activity are dependent on the bidirectional signaling occurring between its epithelial and mesenchymal compartments (EMIs) [13–17]. Therefore, the recreation of a HF regenerative microenvironment requires the use of relevant epithelial and mesenchymal cells as building blocks. From its privileged position at the bottom of the HF, the DP represents a specialized mesenchymal compartment responsible for the coordination of the HF development and growth [18,19]. Therefore, cells isolated from this structure have a key role in HF induction and are commonly combined with follicular epithelial cells as a strategy to rescue EMIs and regenerate hairs [20]. In this thesis, we used DP cells as mesenchymal effectors but, regarding the epithelial counterpart, we hypothesized that interfollicular epidermal KCs with stem-like features (EpSlKCs) could be considered as a novel and more accessible epithelial cell source for follicular regeneration, due to their undifferentiated state. Epidermal stem cells (EpSCs) represent a minor skin

46

subpopulation, embodying only 1% to 10% of the skin basal keratinocytes (KCs) [21], Moreover, the panel of markers defining pure EpSCs is not consensual, which represent an additional challenge regarding their selection and the maintenance of an immature state *in vitro*. Despite this, it is known that the expression of α6-integrin (CD49f) diminishes when EpSCs differentiate, while the expression of the transferrin receptor (CD71) increases when EpSCs give rise to daughter transiently amplifying (TA) cells [22]. Therefore, these two markers allow the separation of epidermal KCs into three categories:

- epidermal stem cells - express high levels of α6 integrin and low levels of the transferrin receptor (CD49f^{high}/CD71^{dim} subpopulation);

- transit-amplifying (TA) cells - express high levels of both α6 integrin and the transferrin receptor (CD49f^{high}/CD71^{high} subpopulation);

- differentiated cells – characterized by low levels of α6 integrin (CD49f^{dim}).

The separation of the CD49f+/CD71- epidermal-like stem cells fraction from the whole interfollicular KCs population mixture was previously adapted by our group and performed through immunomagnetic selection [23]. In this thesis, fluorescent-activated cell sorting (FACS, section II-2.1.2.1.2.) was used to improve the yield of the separation process. Additionally, the sorted cells were cultured on J2 3T3 mouse fibroblast feeders (section II-2.1.2.1.1.) to preserve their stem-like features.

In addition to the cells of the HF mesenchymal and epithelial compartments, melanocytes are also an important cellular player in HF formation. These neural crest-derived cells [24] colonize the hair bulb within each anagen phase of the hair cycle and are responsible for hair pigmentation [25]. Despite the current understanding of melanocytes-KCs interactions, and melanin transfer from bulbar melanocytes to the KCs of the growing hair shaft, less is known about the interaction between human DP cells and human melanocytes (hMel). In this thesis, we focused on further enlightening this crosstalk adding to other studies that have previously provided evidence of the involvement of DP cells in melanocytes migration, proliferation and/or melanogenic activity [26–28].

Besides the abovementioned skin and follicular cells, dermal fibroblasts (DFbs) and epidermal KCs [29] were also used in this thesis (Table II-1), as the representative cellular components of the main skin layers. They were applied during the construction of a skin organotypic model and, in the case of the KCs, to provide paracrine signaling capable of recovering DP cell phenotype in culture. The organotypic model aimed to recreate the complexity of the HF environment within the surrounding

dermal compartment, as well as the link between the epithelial compartment of the HF and the epidermis, then generating a skin model bearing HF-mimetic structures.

Table II-1 - Summary of the cell types used and their tissues of origin

Cell name	Cell type	Tissue source	Abbreviation
Keratinocytes	Primary	Adult human skin	KCs
Hair follicular keratinocytes	Primary	Adult human scalp samples	HHFKCs
Epidermal KCs with stem-like features	Primary	Adult human skin	EpSlKCs
Dermal fibroblasts	Primary	Adult human skin	DFbs
Dermal papilla cells	Primary	Adult human scalp samples	DP cells
Melanocytes	Primary	Neonatal human foreskin	hMel

All human biological samples were obtained under collaboration protocols approved by the ethical committees of the involved institutions and after informed consent from patients. Adult human skin samples were obtained from routine programmed surgeries, performed at Hospital da Prelada (Porto, Portugal) or Hospital Narciso Ferreira (Braga, Portugal). Adult human scalp HF samples were collected from the occipital area of patients who underwent hair transplantation surgeries at Sanare Unicapilar (Porto, Portugal).

II-2.1.   Epithelial Cells

II-2.1.1. Human follicular keratinocytes

HHFKCs were purchased from ScienCell (USA) at passage 2, plated on poly-L-lysine coated flasks (2 µg/cm^2) (ScienCell, USA) and cultured in the recommended Keratinocyte Medium (ScienCell, USA). Cells were cultured under standard culture conditions (37°C, 5% CO_2) with medium changes every 2-3 days and used up to passage 4.

II-2.1.2. Human epidermal keratinocytes

Adult human skin samples were collected in sterile recipients containing 100 mL of phosphate-buffered saline (PBS; Gibco, USA) with 10% (v/v) antibiotic/antimycotic solution (AB; Gibco, USA) after abdominoplasty surgery. The samples were stored at 4°C, transported in a cooler and processed within 24h after collection.

Upon arrival, skin samples were washed in PBS, the adjacent adipose tissue was removed, and two additional washes in PBS were performed to clean the sample from tissue's debris. The skin was then cut in small fragments (of approximately 1 cm^2) and incubated overnight with dispase (2.5 units/mL, 4°C) (Corning, USA), to promote the cleavage of the dermal-epidermal junction. In the next day, the skin fractions were transferred to Petri Dishes and the epidermis was peeled off, using forceps, and digested with trypsin/ethylenediaminetetraacetic acid (EDTA) (0.05%; Gibco, USA) for 7-8 minutes (min) at 37°C. The epidermis fragments were then scraped and pipetted up-and-down several times to promote cell detachment, filtered through a sterile 100 μm cell strainer and centrifuged at 300 relative centrifugal force (rcf) for 5 min. Dissociated KCs were then resuspended in Keratinocyte Serum-Free Medium (KSFM; Gibco, USA) supplemented with human recombinant epidermal growth factor (rEGF) (5 ng/mL; Gibco, USA), bovine pituitary extract (BPE) (50 μg/mL; Gibco, USA), 1% (v/v) penicillin-streptomycin (PenStrep) solution (Lonza, Switzerland) and the ROCK pathway inhibitor Y-27632 (10 μM; STEMCELL Technologies, Canada). 5x10^6 cells KCs were plated per each tissue culture flask with a growth area of 150 cm^2 (T150 flask) and cultured under standard culture conditions (37°C, 5% CO$_2$) with the first medium change being performed 4 days after plating, and every 2-3 days afterwards.

II-2.1.2.1 *Epidermal keratinocytes with stem-like features*

II..2.1.2.1.1 J2 3T3 mouse culture and feeder layer preparation

The culture of growth-arrested feeder cells is used to support the survival and proliferation of other cell types, through the release of growth factors, adhesion molecules and ECM proteins [30]. They can also perform as a substrate for cell attachment and detoxicate the culture medium, by removal of toxic or inhibitory factors [30,31]. Feeder cells proliferation is usually prevented by gamma irradiation or with a mitomycin-C treatment, which mitotically inactivates the cells while keeping them viable [32]. The J2 strain of 3T3 mouse fibroblasts is commonly employed to support the expansion of primary KCs, by

keeping them in a proliferative undifferentiated phenotype [33]. In this thesis, the J2 clone of random-bred Swiss mouse 3T3 cells - kindly provided by Prof. Fiona Wat lab (Wattlab; King's College London, UK) - were used as feeder cells capable of providing optimal support for epithelial stem cells collected after FACS.

Feeder cells were initially subcultured in high glucose DMEM (Sigma-Aldrich, USA) supplemented with 10% (v/v) bovine serum (Gibco, USA) and 1% PenStrep and cryopreserved at a density of $1x10^6$ cells/mL in a 90% (v/v) bovine serum and 10% (v/v) dimethyl sulfoxide (VWR, USA) solution in liquid nitrogen, to create a working stock. For routine culture, cells were thawed and subcultured every week at a density of $1.0-2.0x10^5$ cells per each tissue culture flask with a growth area of 75 cm^2 (T75 flask). Cells were used until passage 10-11 at most.

II..2.1.2.1.2   Selection and culture of interfollicular epidermal keratinocytes with stem-like features

FACS is a specialized type of flow cytometry that allows to physically sort a heterogeneous mixture of cells based upon their size, granularity and/or fluorescence [34]. It is considered a high yield method to obtain purified populations, particularly when the target subpopulation is fairly expressed within the original population, such as in the case of EpSCs. For this reason, FACS was used in this thesis to isolate EpSlKCs based on the expression of CD49f and CD71 markers (section II-2.) from the whole epidermal KCs population. The sorted subpopulation was then cultured onto J2 3T3 mouse fibroblasts feeders to maintain their proliferative undifferentiated state (Figure II-3).

After isolation from skin samples (section II-2.1.2.), KCs were cultured until 80-90% confluence was reached. At this point, the cells were resuspended at a density of $5.0x10^6$ cells/mL in KSFM and incubated with antibodies against CD71-PE (1:200) (BioLegend, USA) and CD49f-APC (1:85) (eBioscience, USA). To establish the settings in the sorting equipment, $2x10^5$ cells were resuspended in 100 µL of culture media (KSFM) and used to identify the autofluorescence of the cells (negative control), or labelled with the CD49f and CD71 antibodies to define the different subfractions of interest (section II-2.). The labelling with the antibodies was carried out for 30 min at RT in the dark. Upon incubation, 2 mL of PBS were added and the cell suspension was centrifuged (300 rcf, 5 min). The obtained pellet was then resuspended in KSFM and the subfraction of KCs with stem cell features – $CD49f^{bri}/CD71^{dim}$ profile – was selected using a FACSAria™ III Cell Sorter (BD Biosciences, USA).

For cell collection, cell sorter tubes were coated with a 2% (w/v) bovine serum albumin (BSA) solution in PBS (1h, RT), to prevent cells from adhering to the tube walls. The subfraction of interest

was then recovered in 1 mL of complete FAD medium, comprising 1 part Ham's F12 medium (Sigma-Aldrich, USA) and 3 parts DMEM (Sigma-Aldrich, USA) supplemented with 1.8×10^4 M adenine (Sigma-Aldrich, USA), 10% (v/v) non-inactivated FBS, 0.5 μg/μL hydrocortisone (Sigma-Aldrich, USA), 5 μg/mL insulin (Sigma-Aldrich, USA), 10^{10} M cholera toxin (Sigma-Aldrich, USA), 10 ng/mL epidermal growth factor (EGF, Peprotech, UK), 1.8 mM calcium chloride (Merck, Germany) and 1% (v/v) PenStrep. After collection, cells were centrifuged (300 rcf, 5 min) and 1.4×10^5 cells were seeded onto each T75 flask previously prepared with an inactivated feeder layer. Cultures were kept in FAD medium and the first medium change was performed after 3 days. By day 4 it was already possible to observe small EpSIKCs-derived colonies growing and, approximately one week after, cells were ready to be harvested.
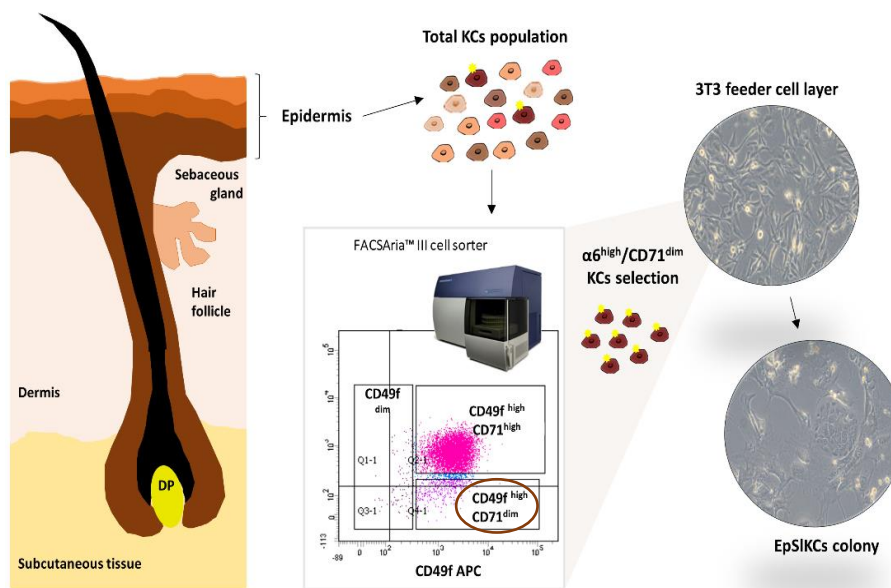
Figure II-3 - Representation of the different steps followed to establish primary EpSIKCs cultures. Isolated human KCs containing a heterogeneous mixture of cells in various differentiation states were labelled with the fluorescent CD71 and CD49f antibodies and the subpopulation of interest – CD49f ᴴⁱᵍʰ/CD71ᵈⁱᵐ profile – was selected using a FACS procedure. The subfraction of interest was then seeded in a J2-3T3 inactivated feeder layer.

II-2.2.   Mesenchymal Cells

II-2.2.1. Human dermal fibroblasts

Human DFbs were isolated from the remaining dermal fragments obtained from the processed skin samples after epidermis peeling (section II-2.1.2). Enzymatic treatment was performed by incubation with 0.1% (w/v) collagenase type I solution (Sigma-Aldrich, USA) in PBS for 3h (37°C, with agitation), to promote the loosening of the tissue. At the end of this step, the fragments were

mechanically dissociated and filtered through a 100 μm strainer to obtain a cellular suspension. After a 450 rcf centrifugation step for 5 min, the cell pellet was resuspended in Minimum Essential Medium-Alpha Modification (α-MEM; Gibco, USA), supplemented with 10% (v/v) fetal bovine serum (FBS; Gibco, USA) and 1% (v/v) AB. Afterwards, 1-2x10^6 DFbs were plated per each T150 flask. The cells were cultured under standard culture conditions (37°C, 5% CO_2), with medium changes every 2-3 days and used from passage 3 to 4.

II-2.2.2. Human dermal papilla cells

DPs were obtained from HF scalp samples using the microdissection technique, which was established for the first time in the lab (Figure II-4) and based on previously published protocols [35,36]. First, HFs were transected above the bulb area and the DPs were manually separated from the dermal sheath and hair epithelial matrix using 27 G needles. 4-6 DPs were then transferred to 6-well plates, scratched against the bottom of the well with a needle to fix their position, and cultured in DMEM supplemented with 20% (v/v) FBS and 1% (v/v) AB. The DPs were left untouched for 5-6 days before the first medium replenishment. Approximately between day 7 and 10, cells started to migrate out of the DP explant and were subcultured when their confluence reached 70-80%.
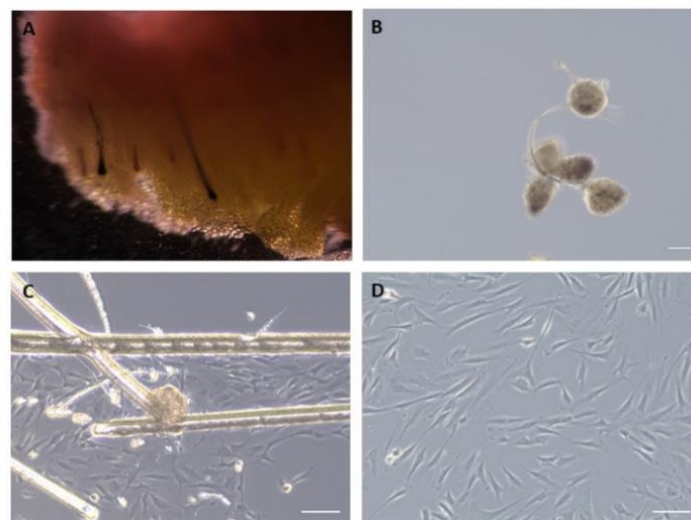
Figure II-4 - Images representing the different stages of the microdissection method used to establish primary human DP cell cultures. (A) Human scalp sample before processing, with visible hair bulbs embedded in the subcutaneous adipose tissue. (B) Isolated DPs with typical pear-shape morphology and (C) the initial outgrowth of DP cells promoted by fixing DP on the culture surface with a needle scrap. (D) DP cells cultures. Scale bar= 100 μm.

After the first passage, DP cells were expanded in flasks coated with a commercial bovine collagen-coating solution (Sigma-Aldrich, USA). In brief, the flasks were incubated with the solution for a minimum of 1h at RT and washed twice with PBS to remove unbound collagen before cell seeding. DP cells were cultured in DMEM with 10% (v/v) FBS and 1% (v/v) AB, with medium changes every 2-3 days and used from passage 4 to 7.

II-2.3.   Human Epidermal Melanocytes

Neonatal cryopreserved human epidermal melanocytes (hMel) were bought from Cell Applications (USA) at passage 2 and cultured in the recommended Melanocyte Growth Medium supplemented with Melanocytes Growth Supplements (HEM medium; Cell Applications, USA). Cells were cultured under standard culture conditions (37°C, 5% CO_2) with medium changes every 2-3 days and used up to passage 4.

II-3.   IN VITRO CULTURE METHODOLOGIES

II-3.1.   Dermal Papilla Spheroids Production

DP cells rapidly lose their intrinsic inductivity and phenotype when cultured under standard 2D culture conditions, hampering their use in TERM strategies [37]. So far, the best strategy to rescue human DP cell native features is by artificially promoting their self-aggregation in 3D spheroids [37–39]. Even representing only a partial restoration of the DP transcriptional signature [37], this is so far the best strategy to culture human DP cells *in vitro*.

To produce DP cell spheroids, $1x10^4$, $5x10^3$ or $3x10^3$ DP cells, depending on the use of the produced spheroids, were resuspended in 50 µL of DMEM with 10% FBS and seeded in round bottom ultra-low attachment 96-well plates (Corning, USA). Independently of the number of cells used, DP spheroids were always visible in the day after seeding (Figure II-5).
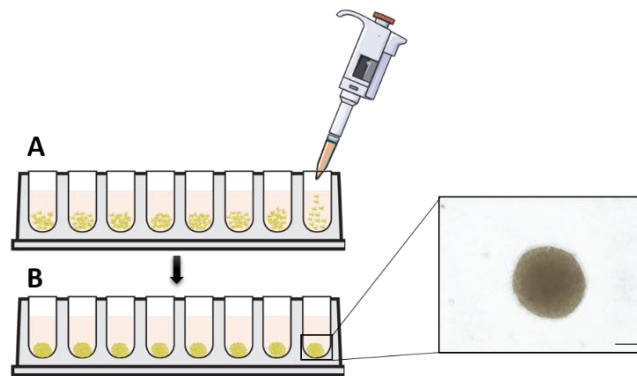
Figure II-5 - Production of DP cell spheroids. (A) A 50µL suspension of DP cells was seeded in low-attachment round wells and left untouched overnight. **(B)** 24h after seeding, DP cell spheroids displaying a smooth and compact shape (close-up, light microscopy image) were already visible. Scale bar =50 µm.

II-3.2.   Co-Culture Systems

II-3.2.1. Co-culture of EpSIKCs with dermal papilla cells

Considering that the success of using EpSIKCs to recreate the HF epithelial compartment depends on their capability to communicate with DP cells, the crosstalk between EpSIKCs and DP cells, and its putative effects on both cellular populations were studied in indirect co-cultures. EpSIKCs that were growing in 3T3-inactivated feeders (section II-2.1.2.1.1.) were collected by firstly removing feeder cells with a 5 min treatment with Versene at 37°C, followed by a trypsinization step (Trypsin/EDTA) for up to 10 min, also at 37°C. EpSIKCs were then centrifuged at 1000 rotations per minute (rpm) for 5 min, resuspended in KSFM with Y-27632, and seeded in tissue culture plates at a density of 500 cells/cm². Next day, Transwell® inserts (0.4 µm pore; Corning, USA) were placed on those culture plates and DP cells seeded into the inserts at a density of 1000 cells/cm². Co-culture medium consisted of an equal mixture of DMEM plus 10% FBS and KSFM with Y-27632 (DMEM: KSFM). Single cell-type cultures were prepared as controls, by culturing cells in their regular medium or the co-culture medium, the latter to control possible medium effects on the cells. Medium change was performed every 3 days.

II-3.2.2. Co-culture of dermal papilla cells with melanocytes

To explore DP cell capacity to influence hMel, and study how these cells response to physoxia was affected by their interaction, both direct and indirect co-cultures were established with these cells.

54

Indirect co-cultures were established by seeding DP cells at a density of 2×10^4 cells/cm^2 in DMEM with 10% FBS overnight. Transwell® inserts (0.4 µm pore; Corning, USA) were then placed in the culture plates and hMel were seeded into the inserts, also at a density of 2×10^4 cells/cm^2. Monocultures of each cell type were prepared as controls, either by culturing cells in their regular medium, or in the medium used to establish the co-culture, which consisted in an equal mixture of DMEM 10% FBS with HEM medium.

Direct co-cultures were established by seeding 3×10^3 DP cells in 50 µL of DMEM with 10% FBS in round bottom ultra-low attachment 96-wells (Corning, USA) overnight to allow cell aggregation (section II-3.1.). In the following day, 1.5×10^3 hMel were resuspended in 25 µL of HEM medium and directly seeded in the wells. Both co-cultures were kept for further 3 days.

II-3.2.3. Co-culture of dermal papilla cells with keratinocytes

To mimic the DP and follicular KCs compartmentalized architectural arrangement within the HF bulb, direct co-culture systems were used to prepare DP-KCs aggregates. These were firstly established by preparing DP cell spheroids as described in section II-3.1 and using 3×10^3 DP cells/spheroid. Two days after seeding, 7.5×10^3 KCs were resuspended in 125 µL of KSFM, added to the wells and further cultured for 2 days.

II-3.3. Culture of Dermal Papilla Cells with Conditioned Medium Collected from Keratinocytes

The cells secretome is rich in metabolites, growth factors, cytokines and ECM proteins, which act as paracrine mediators of information between different cell types [40]. Considering that the loss of inductivity that DP cells suffer in culture is linked with the absence of contextual epithelial influence [37], the capacity of conditioned medium collected from KCs (KCs-CM) to rescue DP cell phenotype and inductivity was studied.

KCs were removed from feeder layers (as described for EpSIKCs in section II-3.2.1.) and cultured in KSFM with Y-27632 (1.67×10^4 cells/cm^2). Considering that the conditioned medium (CM) collection should be harvested from cells in their exponential growth phase, and not in confluent cells to ensure that no inhibitory or deleterious signals are present, the medium was replaced at day 4 and KCs were

further cultured for 48h. Then, the supernatant of the cells was collected, filtered through a 0.22 µm syringe filter, aliquoted and stored at -20°C until further use.

DP cells were initially seeded at a density of $1x10^4$ cells/cm^2 and cultured in DMEM with 10% FBS overnight. In the following day, the medium was replaced by the collected CM mixed with an equal volume of fresh DMEM 10% FBS (KCs-CM). DP cells cultured in their regular medium (DMEM), or DMEM mixed with an equal volume of KSFM with Y-27632 (Medium CTRL), were prepared as controls. Culture media were refreshed every other day up to 5 days.

II-3.4. Cell Culture under Physiological Oxygen Conditions

The oxygen (O_2) level of the tissues plays a vital role in the regulation of cellular functions, their overall health and ultimately survival. Nonetheless, each tissue has its oxygenation status. In the DP and skin, the oxygen level is about 5% O_2 (physoxia) [41,42], which is also considered the best oxygen level to recreate peripheral tissues physiological oxygen levels [43]. Nevertheless, and despite researchers concern to provide cultured cells with *in vitro* physiological conditions, tightly controlling parameters such as temperature, pH, CO_2 or glucose, most cellular experiments are performed under atmospheric oxygen levels (21% O_2, normoxia) instead of using oxygen levels that replicate the cell native microenvironment. Taking this into account, the putative effect of physoxia on both DP cells and hMel was investigated under a 5% O_2 atmosphere, and compared with standard culture conditions under a 21% O_2 atmosphere.

After a trypsinization step with TrypLE™ Express (Thermo Fisher Scientific, USA) at RT, DP cells were resuspended in DMEM with 10% FBS, seeded in culture well-plates at a density of $2x10^4$ cell/cm^2 and cultured under a 5% O_2 environment (5% CO_2, 37°C) using a hypoxic chamber (Coy O2 Control Glove Boxe, Coy Laboratory Products, USA). hMel were trypsinized at RT with a Trypsin/EDTA (0.025%) solution (Gibco, USA), centrifuged at 220 rcf (5 min) and resuspended in HEM medium. Next, hMel were seeded at $2x10^4$ cell/cm^2 and cultured under physoxia, as for the DP cells. Cells cultured under normoxia were used as controls.

II-3.5. Encapsulation of Dermal Papilla Cells in Gellan Gum-Derived Hydrogels

To specifically recreate the DP ECM microenvironment, GG was biofunctionalized with the HepIII and cRGDfC peptide motifs of collagen IV and fibronectin. Before encapsulation, DP cells were trypsinized, centrifuged at 270 rcf for 5 min and cell pellets resuspended in the GG-DVS-peptide solutions prepared as described in section II-1.1.1. For the preparation of 1.0% and 0.75% cell-laden hydrogels, DP cell-containing GG-DVS-peptide suspensions and unmodified GG, prepared by dissolving GG at 90°C in a 0.25 M sucrose solution, were mixed in equal volumes.

Independently of the conditions tested (Table II-2), DP cells were encapsulated at a density of 1×10^4 cells/µL hydrogel. Cell-laden hydrogels were prepared at a volume that ranged from 10-15 µL and were cultured in DMEM with 10% FBS. DP encapsulated in unmodified GG hydrogels (GG control) or GG-DVS hydrogels (DVS control) were also prepared as experimental controls.

Table II-2 - Formulations of the different GG-derived hydrogels used to encapsulate DP cells

Formulation	Final concentration in the hydrogel		Peptide concentration)
	GG (w/v)	GGDVS (w/v)	
GG_0.75%	0.75%	0.375%	—
GG_1.25%	1.25%	0.625%	—
GGDVS_ 0.75%	0.75%	0.375%	—
GGDVS_1.25%	1.25%	0.625%	—
GGDVS-HepIII_0.75%	0.75%	0.375%	HepIII (400 µM)
GGDVS-HepIII_1.25%	1.25%	0.625%	HepIII (400 µM)
GGDVS-cRGDfC_0.75%	0.75%	0.375%	cRGDfC (800 µM)
GGDVS-cRGDfC_1.25%	1.25%	0.625%	cRGDfC (800 µM)

II-3.6. Modified Organotypic Skin Model

Skin organotypic systems have been used as 3D models to study the mechanisms involved in skin morphogenetic, function and homeostasis [44]. Traditionally, the dermal equivalent (DE) is firstly produced using DFbs embedded in a collagen type I matrix, followed by the seeding, on top, of epidermal KCs, which posteriorly stratify by cultivation at the air-liquid interface (ALI) [44]. In this thesis,

modified versions of the standard skin organotypic model [44] were used for the incorporation and functionality assessment of DP-cell laden hydrogels, or as the foundation to create a complex skin model with follicular units.

II-3.6.1. Preparation of the model containing dermal papilla cell-laden hydrogels

The preparation of a 3D reconstructed skin model was based on what is established for standard skin organotypic co-cultures [44]. First, a collagen solution was prepared by mixing α-MEM (10x) with 1 N sodium hydroxide (Sigma-Aldrich, USA) and slowly adding rat tail collagen type I (3 mg/mL, Invitrogen, USA), at a ratio of 10:2.5:87.5, respectively. The solution was prepared on ice, to prevent collagen polymerization, and 250 μL were then cast onto 12-well polyester inserts (0.4 μm pore, Corning, USA) to produce an acellular layer that acts as an attachment substrate for the layers produced above [45]. The acellular layer was then incubated for 30-40 min at 37°C to allow the gel to polymerize. A similar collagen solution incorporating DFbs at a density of 7.5×10^4 cells/mL was then prepared and 750 μL were added on top of the acellular layer. This fibroblast-populated cellular layer was let to polymerized for 2h in the incubator and then α-MEM with 10% FBS was added to the wells. Next day, DP cell-laden hydrogels were incorporated in the DE (Figure II-6). For that, 1 μL of 1.25% GG solution (prepared as described on section II-3.5) containing DP cells at a density of 1×10^4 cells/μL was dispensed inside the cellular collagen layer using a 10 μL viscous pipette (Gilson, USA). At this point, the medium was changed to DMEM with 10% FBS and medium changes were performed every 2-3 days up to 7 days. For epidermis reconstruction, 5×10^4 KCs were re-suspended in 30-50 μL of KSFM and seeded on top of the cellular layer of the prepared DE. The whole model was then further cultured for one week using KSFM on the insert and DMEM 10% FBS in the bottom well. The model was then lifted to ALI and cells were fed from bellow with FAD medium to induce the differentiation of the epidermal cells and the formation of a stratified epidermis. During the 14 days of ALI, the medium was changed every 1-2 days.
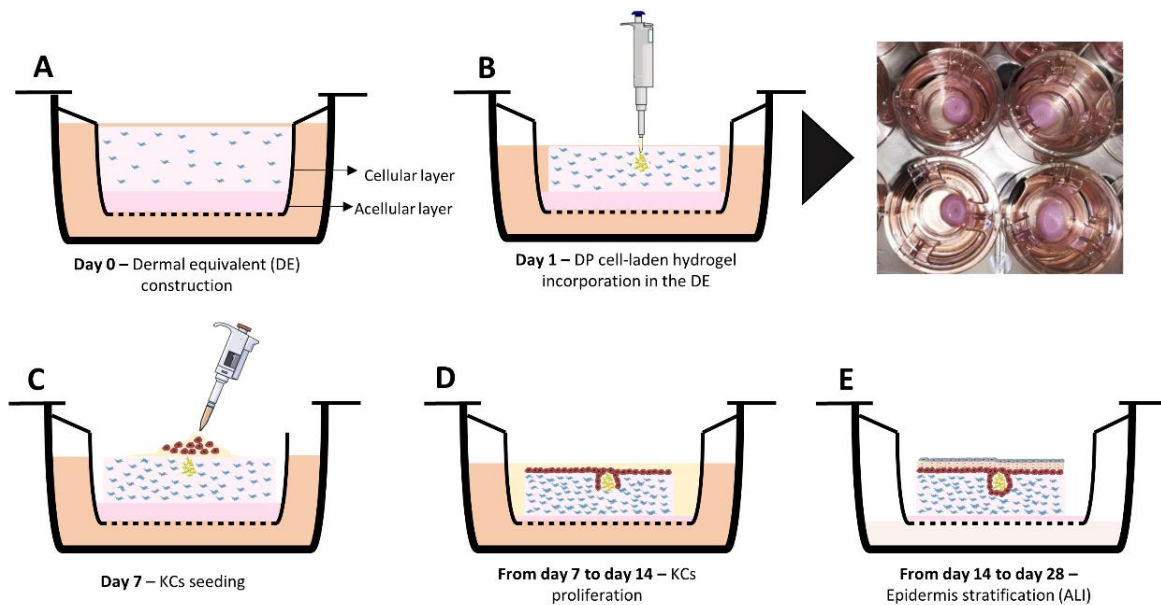
Figure II-6 - Schematic representation of the successive steps followed to prepare the skin model containing DP cell-laden hydrogels. (A) The construction of the skin organotypic model started with the production of the DE into which, after 24h (B), DP cell-laden GG suspensions were injected using a viscous micropipette. The formed DP cell-laden GG hydrogels were visible within the constructs (right-hand side image). (C) At day 7, a KCs suspension was seeded on top of the constructs, (D) which were kept under submerged conditions for one week. (E) The constructs were raised to the air-liquid interface (ALI) at day 14 and nourished from the bottom until day 28, to allow the formation of a stratified epidermis.

II-3.6.2. Preparation of the model containing dermal papilla-keratinocytes aggregates

The organotypic model was prepared as described in section II-3.6.1. but with modifications in the construction of the cellular layer. First, 500 µL of the collagen-DFbs solution was dispensed on top of the acellular layer and allowed to polymerize. Afterwards, 1-2 DP-KCs aggregates (section II-3.2.3) were placed on top, and a second cellular layer (250 µL) was slowly added and allowed to polymerize as well. The constructs were cultured submerged in DP cell medium (DMEM with 10% FBS) for 5 days. After the ablation procedure (section II-3.6.2.1.), the constructs were placed back in the inserts and 5×10^4 KCs were seeded on top in 30 µL of KSFM. Constructs were then cultured and allowed to attain epidermis stratification as described in section II-3.6.1.

II-3.6.2.1   *Microscopy-guided laser ablation*

Microscopy-guided laser ablation (MGLA) is a non-contact technique that allows the removal of material by irradiation with a pulsed laser beam. In this process, the energy of the laser photons is transferred to the electrons of the target material increasing the temperature until the material vaporizes

[46]. In this thesis, MGLA was used to microfabricate the model containing DP-KCs aggregates, by creating microchannels to connect the aggregates to the surface of the construct. The goal was to guide the migration and downgrowth of the KCs posteriorly seeded on top of the constructs, promoting the necessary conditions to generate a skin model with follicular appendages. For that, the MGLA system – a UGA-42 Caliburn motorized laser focus and a 355 nm, 1 kHz, 42 µJ/pulse pulsed laser (Rapp Optoelectronic, Germany) directly coupled to an Axio Observer 7 inverted microscope (Zeiss, Germany) – was first calibrated following the procedure provided by the producer of the equipment. The constructs with the DP-KCs aggregates were then turned upside down in a sterile three-well chamber microscopy glass slide (Ibidi, Germany) with culture medium and sealed under sterile conditions. For each construct, the end ablation plan (*x, y* and *z* position) was fixed by focusing the center of the cellular aggregate (20 x magnification). Then, the focus plan was moved to the surface of the construct in contact with the glass slide. To determine the starting ablation *z*-plane we first focused the microscope on the glass slide and ablated a small spot, confirmed by the presence of corrugations and the change in the transparency of the ablated surface. The focus plan was then moved 5 µm away to ablate another area. This procedure was repeated until no sign of ablated glass was seen, thus establishing the starting plan for the ablation of the hydrogel. The ablation of 150 µm diameter sections was repeated along different planes towards the cellular aggregate and up to the end ablation plane. Each ablation removed 30 µm of material, in depth.

II-4. *IN VIVO* METHODOLOGIES

II-4.1. Silicone Chamber Model

The silicone chamber model is a well-established hair reconstitution *in vivo* assay that allows assessing the hair inductive capacity of dissociated epidermal and dermal cell populations [47]. It was firstly introduced by Lichti and Weinberg [48,49] and consists in implanting a silicone chamber onto the back of recipient immunocompromised mice, which protects and restricts the movement of the grafted cells within the wound bed [50,51]. The chamber is held in place with sutures, and different epidermal and/or dermal populations are directly injected in the chamber to test their trichogenic capacity. In this thesis, the chamber model was used to assess the capacity of EpSIKCs to support hair formation after co-grafting with DP, as well as the capacity of CM-precultured DP cells to promote hair induction.

For the *in vivo* experiments, male nude Balb/C mice were purchased from Charles River Laboratories (France) and all the experimental protocols were approved by the *Direção-Geral de Alimentação e Veterinária*, the Portuguese National Authority for Animal and Health, and performed according to the applicable national regulations, respecting international welfare rules. Nude Balb/C mice strain has a mutation in the gene FOXN1, which is crucial for the development of thymus and several immune responses, especially T-cell mediated [52]. As a consequence, the animals lack the thymus and have a critically reduced T cell population, making them a good xenografic model.

The animals were randomly divided into the experimental groups, anaesthetized with a mixture of ketamine (75 mg/kg; Merial Portuguesa, Portugal) and medetomidine (1 mg/kg; Esteve Farma, Portugal), and their back disinfected with betaisodona. Then, a biopsy punch was used to make a 6 mm full-thickness wound on the mice upper back and the silicon chambers were inserted under the skin surface. Cell mixtures of 5.0×10^6 dermal cells (DP cells) and 2.5×10^6 epidermal cells (EpSIKCs or KCs) were re-suspended in 100-120 µL of complete FAD medium and injected into the silicon chamber using a 1 mL syringe with a 19 G needle (Figure II-7). Cell suspensions of 5×10^6 dermal cells or only vehicle (control group) were injected as negative controls. After the surgeries, the animals were kept separately and had free access to food and water. After one week, the top of the silicon chamber was cut-off to allow the wound to dry out, which facilitates the healing process, and after two weeks the chambers were removed [53]. The animals were euthanized six weeks after the initial grafting procedure, by CO_2 inhalation.
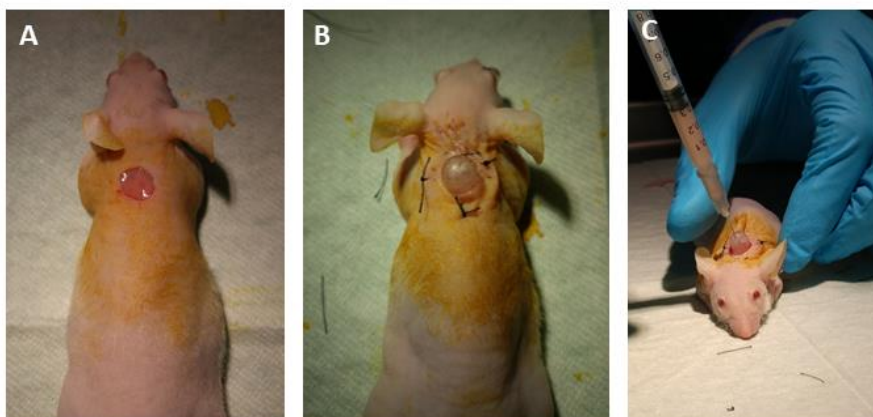
Figure II-7 - Silicone chamber model. (A) A biopsy punch was used to make 6 mm full-thickness wound on the mice upper Back and (B) the silicon chambers were inserted under the skin surface. (C) The cell suspension was slowly injected into the silicon chamber.

II-5. METHODOLOGIES FOR BIOMATERIAL AND BIOLOGICAL CHARACTERIZATION

II-5.1. Biomaterial Characterization

II-5.1.1. Compressive modulus

Hydrogels have been frequently used in TERM to provide cells with a 3D culture environment that better simulates their native ECM [54,55]. Besides providing a more natural culture system, the hydrogel physical-mechanical properties can also affect cellular viability, differentiation, proliferation and function, therefore representing a major role in directing the cells' phenotype and in the overall functionality of the biomaterials used [56].

Given the importance of 3D culture conditions in the recovery of DP cell native phenotype and properties *in vitro* [37,38], ECM-biomimetic GG-derived hydrogels were used to culture DP cells. However, the use of different amounts of GG, as well as its chemical conjugation with other molecules, may affect GG physical- and/or ionic-crosslinking, thus altering the mechanical properties of the produced hydrogels. Since this could lead to changes in cell behavior, the mechanical properties of the different GG-derived hydrogels proposed in this thesis (Table II-2) were tested. Compressive characterization was selected given that tensile testing (extensiometry) can only be performed in specific hydrogel geometries, such as strips or rings [57,58], which does not apply to the produced hydrogels.

The unconfined static compressive mechanical properties of GG-derived hydrogels were analyzed using an INSTRON 5543 universal mechanical testing equipment (load cell 1 kN, Instron Int. Ltd., USA). GG-derived hydrogels were prepared in round-shaped molds (10x6 mm), as described in section II-1.1.1., and equilibrated in DMEM with 10% FBS for 48h at 37°C prior testing. Samples were submitted to a pre-load of 0.1 N and were tested up to 60% of strain, at a loading rate of 2 mm/min. The compressive modulus was determined from the slope of compressive stress *vs* compressive strain graphics, at 1% of compressive strain.

II-5.1.2. Micro-Bicinchoninic Acid Protein™ assay

Micro Bicinchoninic Acid Protein (Micro BCA™) is a colorimetric assay that allows protein quantification. It is based on the specific reduction of Cu^{+2} to Cu^{+1} by proteins in an alkaline environment and the high specificity of BCA for Cu^{+1} [59]. The chelation of Cu^{+1} by two molecules of BCA results in the formation of a purple-colored reaction product, which is linear to the amount of protein.

Micro-BCA assay (Thermo Fisher Scientific, USA) was used to determine the amount of peptide (HepIII, cRGDfC) that reacted with GG-DVS, *i.e.* the modification efficiency. Calibration curves were prepared with the respective peptide (ranging from 0 to 200 µg/mL), and GGDVS-HepIII and GGDVS-cRGDfC (ranging from 1 and 0.5 mg/mL) solutions. The working reagent was prepared by mixing Micro BCA Reagent MA, MB and MC at the proportions of 25:24:1. Afterwards, 150 µL of the sample (GG-DVS-peptide), control (GG-DVS) and standards were mixed with 150 µL of working reagent in a multi-well, mixed thoroughly on a plate shaker, and incubated at 37°C for 2h. The plate was then cooled to RT and the absorbance was read at 562 nm in a microplate reader (Synergy HT, BioTek, USA). The modification efficiency yield was determined by the ratio of the mass of peptide linked to GGDVS determined by µBCA ($m_{measured\ pept}$) and the mass of peptide that was used for the reaction with GGDVS ($m_{initial\ pept}$), through the following calculation:

$$\text{Efficiency (\%)} = \frac{m_{measured\ pept} \times 100}{m_{initial\ pept}}$$

II-5.2. Biological Characterization

II-5.2.1. Quantitative analysis

II-5.2.1.1 *Deoxyribonucleic acid quantification*

Deoxyribonucleic acid (DNA) measurement was performed using the Quant-iT™ PicoGreen® Assay Kit (Thermo Fisher Scientific, USA). This kit applies a fluorescent nucleic acid stain that specifically binds to double-stranded DNA (dsDNA) in solution, emitting fluorescence that can be read at 480 nm

(excitation) and 520 nm (emission). In the context of this thesis, DNA quantification was used as a tool to assess cell proliferation, by comparing the dsDNA content of the cells along with different time points and/or between different experimental groups. For such, at each experimental time point, the cells were washed twice with PBS and lysed by addition of ultra-pure water with 0.01% sodium dodecyl sulfate (SDS) (NZYTech, Portugal), incubated for 1h at 37°C, and then frozen at -80°C. Before quantification, samples were allowed to thaw at RT. Samples from 2D cultures were assayed directly, while samples from 3D culture conditions (cells encapsulated within GG-derived hydrogels or spheroids) were sonicated on ice for 5 seconds (s) at a 40% amplitude using the VCX-130PB-220 ultrasonic processor (Sonics, USA) to guarantee a complete disintegration of the cell membranes and nuclear envelope. The DNA content was determined by adding, in 96-well white polystyrene plates, 28.7 µL of the sample (experimental, standard or blanks), mixed with 100 µL of 1x Tris-EDTA buffer (10 mM Tris-HCl, 1 mM EDTA, pH 7.5) and 71.3 µL of 1x Quant-iT™ PicoGreen® reagent. After 10 min of incubation at RT, the fluorescence was read at 480 nm (excitation) and 520 (emission) in the microplate reader. The dsDNA quantity was determined by interpolation from a standard curve ranging from 0 to 2 µg/mL, prepared with a DNA stock solution provided with the kit.

II-5.2.1.2 *Alkaline phosphatase quantification*

Alkaline phosphatase (ALP) is an enzyme whose expression is correlated with DP cell inductive properties [60,61]. Literature reports demonstrate that DP cells with higher ALP activity resulted in higher success rates in hair inductive assays, [62,63] therefore we used this marker to assess DP cell phenotype in culture.

The Alkaline Phosphatase Detection Kit (Sigma-Aldrich-Aldrich, USA) was used to quantify the amount of active ALP, since it is a fluorescent-based procedure that can be up to 100x more sensitive than the commonly used colorimetric assays. Considering that ALP is a highly stable enzyme, sample collection was performed in the same way as for DNA quantification (section II-5.2.1.1.) for cell lysis. For the quantification of active ALP, 20 µL of the sample (unknown, standard or blank) were added to 96-well white polystyrene plates and mixed with 20 µL of the kit Dilution Buffer and 160 µL of the Fluorescent Assay Buffer. The enzyme-substrate provided with the kit was then added to each well (1 µL substrate in 3 µL of deionized water) and the fluorescence was read at 360 nm (excitation) and 440 nm (emission) in the microplate reader. The amount of active ALP in DP cell lysates was determined by

interpolation from a standard curve ranging from 0 to 0.2 µg/mL, which was prepared with the active enzyme provided with the kit.

II-5.2.1.3 *Flow cytometry*

Flow cytometry is a multi-parameter technology capable of simultaneously measuring the optical and fluorescence characteristics of single cells, as these flow in suspension through the apparatus [64]. The most traditionally analyzed cell features are cell size, granularity and fluorescence, with the latter being widely used for analyzing the expression of specific markers. The principle relies on an immune reaction were fluorochrome-labelled antibodies are linked to the antigen of interest, allowing the identification and quantifications of those specific proteins within the analyzed cell subpopulation. Throughout this thesis, flow cytometry was used for the phenotypic characterization of both surface and intracellular markers expressed among different cell populations, including epithelial (EpSIKCs and HHFKCs) and mesenchymal cells (DP cells).

For surface markers analysis, the cells were resuspended in 100 µL of their respective medium and directly incubated with fluorescent-labelled antibodies (see Table II-3, "Surface staining") for 30 min at RT. For intracellular staining, the FIX&PERM™ Cell Permeabilization Kit (Thermo Fisher Scientific, USA) was used following the manufacturer's indications. In detail, cells were firstly fixed with the kit reagent A (15 min, RT), washed in PBS and then permeabilized with the kit reagent B, incubated in simultaneous with the fluorescent-labelled antibodies (see Table II-3, "Intracellular staining") for 20 min at RT. Independently of the above procedure, cells were then washed with PBS and fixed with a 1% (v/v) formalin solution in PBS overnight at 4°C and analyzed with the FACSCalibur flow cytometer (BD Biosciences, USA), using the Cell Quest Pro version 4.0.2 (BD Biosciences) software.

Table II-3 - Panel of antibodies and conditions used to characterize the different cell types by flow cytometry

Cell type	Antibody	Reference	Brand	Dilution	Type of staining
HHFKCs EpSIKCs	CD71-PE	334106	BioLegend, USA	1:66	Surface staining
	CD49f-APC	17-0495-82	eBiosciences, USA	1:33	
	CD29-PE	555443	BD Biosciences, USA	1:33	
	K14-FITC	MCA890F	Bio-Rad, USA	1:50	Intracellular Staining

	K19-AF488	A4-120-C100	ExBio, Czech Republic	1:20	
DP cells	CD184 -APC	306510	BioLegend, USA	1:20	Surface staining
	LRP4-PE	306510	Miltenyi Biotec, Germany	1:50	
	α-SMA-FITC	ab8211	Abcam, UK	1:33	Intracellular Staining
	LEF1-AF488	2230T	Cell Signalling, NL	1:50	

Legend: CD71 – transferrin receptor; CD49f – α6 integrin; CD29 – integrin β1; K14 – keratin 14; K19 – keratin 19, CD184 – chemokine receptor type 4; LRP4 – low-density lipoprotein receptor-related protein 4; α-SMA – alpha-smooth muscle actin; LEF1 – lymphoid enhancer-binding factor 1; PE – phycoerythrin, APC – allophycocyanin; FITC – fluorescein isothiocyanate; AF – Alexa Fluor

II-5.2.1.4 *Enzyme-linked immunosorbent assay*

Enzyme-linked Immunosorbent Assay (ELISA) is a type of antigen-antibody binding, with the particularity of being performed in solid-phase, that allows the detection and quantification of proteins, peptides or glycoproteins. In a sandwich ELISA, the variant used in this thesis, the target antigens bind to the primary antibody ("capture antibody") initially immobilized in the wells. Its identification follows the standard principle of using a secondary antibody ("detection antibody") coupled to an enzyme capable of converting a specific substrate into a colored product, measured using a spectrometer. Although commonly less specific than other antigen-antibody mediated assay, ELISA has the advantage of being a highly sensitive technique.

This technique was used to quantify the release of growth factors and/or cytokines by cultured DP cells, either in indirect co-culture with EpSIKCs or hMel, or after culture with KCs-CM. The supernatants of the cultures were collected, centrifuged (3000 rpm, 10 min), and stored at -80°C in single-use aliquots. ELISA kits were used following the manufacturers' procedures as summarized in Table II-4. Briefly, high protein-binding 96 well plates (Nunc-Immuno™ MicroWell™; Sigma-Aldrich, USA) were coated with the primary antibody (capture antibody) by overnight incubation. Next day, the wells were washed and posteriorly blocked, with the kit corresponding washing solution and blocking agent. After a new washing step, the samples and standards were added to the wells and allowed to bind to the capture antibody. The detection of bound antibody was performed by incubation with a biotinylated detection antibody, followed by the addition of a streptavidin/avidin-HRP conjugate, with the wells being thoroughly washed between each step to remove unbound molecules. Finally, the addition of a colorimetric subtract, and the subsequent enzyme catalysis, allowed the formation of a colored solution,

or a color shift, which was optically measured. The amount of growth factor or cytokine present in the sample was then determined by interpolation from a standard curve.

Table II-4 - Summary of the different ELISA procedures

	VEGF	BMP2	PDGF-A	IL-6	TGF-β1
Brand	PeproTech, USA		R&D Systems, USA		Thermo Fisher Scientific, USA
Reference	900-K10	900-K255	DY221	DY206	88-8350-88
Sensitivity (pg/mL)	10-1000	47-3000	10 - 1000	9.38 - 600	8 - 1000
Capture antibody	100 µL, immobilization overnight (RT)				100 µL; immobilization overnight (4°C)
Blocking	300 µL 1% BSA; 1h incubation (RT)		300 µL Reagent Diluent; 1h incubation (RT)		200 µL of ELISA Diluent; 1h incubation (RT)
Sample/standard	100 µL; 2h incubation (RT), washing				
Detection antibody	100 µL; 2h incubation (RT)				100 µL; 1h incubation (RT),
Enzyme	100 µL avidin-HRP; 30 min (RT, dark)		100 µL Streptavidin-HRP; 20 min (RT, dark)		100 µL avidin-HRP; 30 min (RT, dark)
Substract	100 µL ABTS Substrate (RT, dark)		100 µL Substrate; 20 min (RT, dark)		100 µL TMB solution; 15 min (RT, dark)
Stop Solution	————		50 µL		100 µL
Absorbance	OD: 405 nm - 605 nm		OD: 450 nm - 570 nm		

Legend: ABTS – 2, 2'-azinobis (3-ethylbenzothiazoline-6-sulfonic acid); BMP2 – bone morphogenetic protein 2; HRP – horseradish peroxidase; IL-6 – interleukin 6; OD – optical density; TGF-β1 – transforming growth factor β1; PGDF- A – platelet-derived growth factor A; TMB – 3,3′,5,5′-tetramethylbenzidine; VEGF – vascular endothelial growth factor.

II-5.2.1.5 *Dimethylmethylene blue assay*

The dimethylmethylene blue (DMMB) assay is based on the high affinity of the cationic dye 1,9-dimethyl-methylene blue zinc chloride to sulfated glycosaminoglycans (GAGs), resulting in an absorbance shift that can be quantified at 530 nm [65]. Therefore, it was used in the context of this thesis to quantify the total amount of sulfated GAGs produced by DP cells after culture with KCs-CM.

The protocol used in this thesis was based on the method described by Hollander and colleagues [66]. DMMB stock solution was prepared by dissolving 16 mg of DMMB powder (Sigma-Aldrich, USA) in 900 mL of distilled water containing 3.04 g of glycine (Sigma-Aldrich, USA) and 2.73 g of sodium

chloride (PanReac AppliChem, USA). The pH was adjusted to 3.0 with 1 N HCl (Honeywell, USA) to a final volume of 1 L, and the solution was stored at RT protected from light until further use. The coverslips where DP cells were grown were directly transferred into Eppendorf tubes and frozen at −80°C. After thawing, the cells were digested at 60°C (overnight) in a solution consisting of 0.05% of papain and 0.096% of *N*-acetyl cysteine prepared in 200 mM of phosphate buffer with 1 mM EDTA at pH 6.8 (all from Sigma-Aldrich, USA). The samples were then centrifuged (13000 rpm, 10 min) and the supernatants incubated with 250 µL of DMMB stock solution for 10 min at RT. The resultant DMMB-GAGSs complexes were quantified by measuring OD at 530 nm. The amount of sulfated GAGs was extrapolated from a chondroitin sulfate (EMD Millipore, USA) standard curve (ranging from 0 to 50 µg/mL), prepared using a 5 mg/ml chondroitin sulfate stock solution.

II-5.2.1.6 *Sirius Red/Fast Green staining*

Sirius Red binds specifically to collagen (COL), regardless of type, while Fast Green binds to non-collagenous components (NCOL). Since these dyes have different absorption wavelength in the visible light, the OD values of the extracted dyes can be used to calculate the COL ($\geq$ 3 µg/sample) and NCOL ($\geq$ 50 µg/sample) content of samples [67]. The semi-quantitative Sirius Red/Fast Green Collagen Staining Kit (Chondrex Inc., USA) was used to quantify the amount and type of ECM produced by DP cells (in 2D culture conditions or 3D hydrogels) or in DP-hMel cellular aggregates cultured under hypoxia and normoxia.

The production of and COL and NCOL proteins was studied using the Sirius Red/Fast Green Collagen Staining Kit (Chondrex Inc., USA). Adherent cells and spheroids were fixed in 10% formalin, washed in PBS and incubated with 200 µL of dye solution for 30 min at RT. The dye solution was then removed, and the samples were washed in water and observed under a light microscope (AxioVert A1 FL LED microscope, Zeiss, Germany). Further quantification was performed by extracting the dies using 1 mL of the destaining solution provided in the kit under mild stirring and until complete dye elution. The samples OD were measured at 540 nm (Sirius red) and 605 nm (fast green) using a microplate reader. The color equivalences [67] were used to calculate the quantity of COL and NCOL proteins (µg/mL) produced by DP cells, and the total protein content was obtained according to the following equations:

$$\text{COL (µg/sample)} = \frac{\text{OD 540 value} - (\text{OD 605 value} \times 0.291)}{0.0378}$$

$$\text{NCOL (µg/sample)} = \frac{\text{OD 605 value}}{0.00204}$$

$$\text{Total protein (µg/sample)} = \text{µg COL} + \text{µg NCOL}$$

II-5.2.1.7 *Bradford assay*

The Bradford protein assay is a rapid, accurate and routinely used method for the quantification of total protein. It applies the use of the Coomassie Brilliant Blue G-250 acidic dye, which forms a noncovalent complex with the carboxyl groups of proteins, causing an absorption shift of the dye from 465 to 595 nm [68]. This assay was used in DP cell spheroid lysates, to determine the effect of DP cell culture with KCs-CM on its protein production capacity.

Total protein quantification was performed using the Bio-Rad Protein Assay Dye Reagent Concentrate (Bio-Rad, USA). In detail, the samples were thawed on ice and 60 µL were diluted in 740 µL of a 0.01% Triton X-100 solution prepared in water. Afterwards, 200 µL of dye reagent were added and the samples were vortexed for dye homogenization and incubated for 5 min at RT. For quantification of the colored complexes, 100 µL of the mixture were added to 96-wells of a transparent polyester plate and the absorbance was read at 595 nm. For results interpolation, a BSA standard curve (ranging from 0 to 10 µg /mL) was prepared using a 2 mg/mL BSA stock solution (Thermo Fisher Scientific, USA).

II-5.2.1.8 *Lactate dehydrogenase assay*

Lactate dehydrogenase (LDH) is a cytosolic enzyme whose presence in the extracellular space indicates membrane damage, being used as an indicator of cytotoxicity. The Pierce LDH Cytotoxicity Assay Kit (Thermo Fisher Scientific, USA) was used for the colorimetric quantification of LDH in the supernatant of the cultures of DP cells encapsulated within GG-derived hydrogels, as an assessment of hydrogel cytotoxicity. Before each experimental time point, the culture medium was renewed and after 24h the supernatant was collected, centrifuged (250 rcf, 3 min) and 50 µL of each sample medium

was transferred to a transparent flat-bottom 96-well plate (TPP, Switzerland). The sample was let to react with 50 μL of the reaction mixture reagent in the dark for 30 min, after which was interrupted by adding 50 μL of stop solution. LDH amount was determined in the samples by subtracting the 680 nm absorbance value from the 490 nm value. Supernatants collected from acellular hydrogels maintained in the same experimental culture conditions were used as blanks. Maximum LDH amount was established for each experimental condition by promoting total LDH release with the incubation of the cell-laden hydrogels with the kit lysis buffer for 1h at 37°C. The cytotoxicity was then calculated using the following formula:

$$\% \text{ Cytotoxicity} = \frac{(\text{Sample LDH} - \text{blank LDH}) \times 100}{(\text{Maximum LDH} - \text{blank LDH})}$$

II-5.2.1.9   *Reactive-oxygen species quantification*

Reactive oxygen species (ROS) are normal side-products generated by the mitochondrial respiratory chain, being formed by the partial reduction of oxygen. Excessive ROS production is traditionally associated with oxidative stress however, increasing evidence demonstrates that endogenous ROS play a physiological role as signaling molecules [69,70]. In the HF, a transient elevation of ROS levels is necessary to promote hair growth during anagen [71]. Therefore, in this thesis, physoxia was used to better represent the native HF conditions and ROS analysis was performed to better understand how DP cell and hMel culture were affected and if that would impact the way these cells interact.

The production of ROS by cultured cells was quantified using the OxiSelect™ *In vitro* ROS/RNS assay kit (Cell Biolabs Inc., USA), which employs the use of a quenched fluorogenic probe, the 2′,7′-dichlorodihydrofluorescin (DCFH)-DiOxyQ. The probe is firstly primed with a quench removal reagent and subsequently stabilized in the highly reactive DCFH form, which is readily oxidized by ROS/RNS into the fluorescent dichlorodihydrofluorescein (DCF).

Cultured cells were lysed as described for DNA quantification (section II-5.2.1.1.). In 96-wells white polystyrene plates 50 μL of sample or standards were mixed with 50 μL of catalyst. After 5 min of

incubation at RT, 100 µL of the DCFH solution were added to the mixture and plates were further incubated for 45 min in the dark, also at RT. Fluorescence was then read at 480 nm (excitation) and 530 (emission) in the microplate reader and ROS/RNS relative levels were quantified by comparison with a DCF standard calibration curve.

II-5.2.1.10   *Tyrosinase activity quantification*

Melanin synthesis by melanocytes begins with the hydroxylation of L-tyrosine to L-DOPA (L-3,4-dihydroxyphenylalanine), a reaction that is catalyzed by tyrosinase in melanosomes. This is a rate-limiting step for melanin synthesis, as other enzymes involved in melanogenesis can only affect the quantity and type of melanin being synthesized [72,73]. Therefore, the quantification of melanocytes tyrosinase activity is a good indicator of their melanogenic capacity and tyrosinase is a frequent target for hypopigmentation therapies [72]. In this thesis, tyrosinase activity was determined as a functional indicator of hMel melanogenic capacity under physoxia.

For the quantification of tyrosinase activity in hMel, cells were rinsed twice in PBS and incubated for 5 min (ice) with a lysis buffer consisting of 20 mM Tris (hydroxyethyl) aminomethane (pH 7.5, Sigma-Aldrich, USA) containing 0.1% (v/v) Triton X-100 and a protease inhibitors cocktail (1:100, Sigma-Aldrich, USA). Cell lysates were then centrifuged at 14500 rcf (10 min, 4°C) and 70 µL of the supernatant was transferred to transparent 96-well plates. As a substrate for tyrosinase, a 0.1% (w/v) L-Dopa (Sigma-Aldrich, USA) solution was prepared in sodium phosphate buffer (pH 6.8; Sigma-Aldrich, USA) and 140 µL were added to each well containing the cell lysates or blanks (lysis buffer). After a gentle shake, the plates were directly incubated for 2h at 37°C in the microplate reader and the absorbance was measured at a wavelength of 475 nm. The results were presented as the relative values obtained from the absorbance readings.

II-5.2.1.11   *Migration assay*

To test hMel capacity to migrate, standard cell culture inserts for 24-well plates (8.0 µm pore size, Corning) were equilibrated with HEM medium for 30 min at 37°C. Afterwards, hMel were resuspended in basal HEM medium and seeded at a density of 4×10^4 cells/cm^2 in the inserts, whereas supplemented HEM medium was added to the bottom well. After 48h of culture, cells that migrated from the insert to

the bottom of the well were fixed with 10% formalin (15 min, RT) and counted by direct microscopic observation (AxioVert A1 FL LED) in twelve independent microscopic fields per triplicate.

II-5.2.2. Qualitative analysis

II-5.2.2.1   *Immunostaining*

Immunostaining, like flow cytometry, is an antibody-mediated antigen technique that allows the detection of specific antigens in fixed cells. The immune reaction is then exposed using an enzyme or fluorophore-mediated conjugation system that allows the visualization and examination of the target protein presence and location under a microscope.

Both immunohistochemistry (IHC) and immunocytochemistry (ICC) rely on this principle, but their main difference resides in the nature of the biological samples to be analyzed. ICC is performed in dissociated cells, cultured in monolayer or suspension, while IHC uses tissue sections, either paraffin-embedded or frozen, to preserve the tissues' morphology.

II..5.2.2.1.1   Immunohistochemistry

IHC was carried out in histological sections of human scalp sections and in explants from the *in vivo* assays. Paraffin-embedded sections (ranging from 4 to 10 µm) were dewaxed in xylene, rehydrated in graded series of ethanol solutions (100%, 95%, 70%) and water. Antigen retrieval was then performed in citrate buffer (pH 6.0) progressively heated in the microwave (2 min, 30 s heating intervals) by adding the tissue sections to the container and heating (4 min, 10-15 s heating intervals). After reaching RT, sections were washed with water before continuing with the permeabilization step, which was performed when the target marker was not on the cell surface. In case of intracellular staining, the samples were permeabilized with 0.2% (v/v) Triton X-100 (Sigma-Aldrich, USA) for 15 min at RT or, in the case of nuclear staining, with 1% Triton X-100 for 30 min at 4°C. To prevent unspecific binding of proteins, a blocking step was performed using a 3% (w/v) BSA (Sigma-Aldrich, USA) solution for 30-45 min at RT. Primary antibodies (Table II-5) were diluted in 1% BSA solution with 0.2% Triton X-100 and incubated for 1h at RT or overnight at 4°C. Samples were then washed three times with PBST (PBS with 0.1% Tween 20) to remove unbound antibodies, and incubated with AF (488/594)-conjugated secondary antibodies (1:500) (Molecular Probes, USA) for 1h at RT. Nuclear counterstain was

performed with 4',6-diamidino-2-phenylindole (DAPI) (0.02 mg/mL in PBS, Biotium, USA) for 15 min at RT. The samples were analyzed with an Axioplan Imager Z1m fluorescent microscope and representative images acquired with the ZEN 2.3 (blue) imaging software (Zeiss, Germany).

Table II-5 - Primary antibodies used for ICC and IHC

Markers group	Antibody	Host	Brand	Reference	Clonality	Dilution
Epidermal cells	Keratin 15	Ms	Abcam, UK	ab1385	Monoclonal	1:50
	Keratin 14	Rb	BioLegend, USA	905301	Monoclonal	1:800
	Keratin 10	Ms	Abcam, UK	ab9026	Monoclonal	1:100
	Keratin 6	Ms	Abcam, UK	ab75703	Monoclonal	1:200
	Keratin 25	Rb	Invitrogen, USA	PA5-62888	Polyclonal	1:1000
	Involucrin	Ms	Abcam, UK	Ab68	Monoclonal	1:25
	β-catenin	Ms	BD Biosciences, USA	Z031129-2	Monoclonal	1:100
DP cells	Versican V1	Rb	Abcam, UK	ab19345	Polyclonal	1:200
	Versican V2	Ms	DSHB, USA	12C5	Monoclonal	1:10
	α-SMA	Rb	Abcam, UK	Ab5694	Monoclonal	1:200
DP cells and hMel	Vimentin	Rb	Abcam, UK	ab92547	Monoclonal	1:50
	S100	Rb	Dako, Denmark	Z031129-2	Polyclonal	1:100
hMel	MelanA	Rb	Abcam, UK	ab51061	Monoclonal	1:250
	PMEL	Ms	Thermo Fisher Scientific, USA	MA1-34759	Monoclonal	1:100
	Tyrosinase	Ms	SCBT, USA	sc-20035	Monoclonal	1:100
ECM components	Collagen I	Rb	Abcam, UK	ab34710	Polyclonal	1:100
	Collagen IV	Ms	Abcam, UK	ab6311	Monoclonal	1:25
	Fibronectin	Rb	Abcam, UK	ab2413	Polyclonal	1:100
	Laminin	Ms	Sigma-Aldrich, USA	L8271	Monoclonal	1:100
Proliferation	Ki67	Rb	Abcam, UK	ab16667	Monoclonal	1:50
Gap junction	Connexin 43	Rb	Abcam, UK	ab11370	Polyclonal	1:500
Fat tissue	FABP4	Rb	Abcam, UK	ab66682	Polyclonal	1:400

Legend: SCBT – Santa Cruz Biotechnology, DSHB – The Developmental Studies Hybridoma Bank, FABP4 – Fatty acid-binding protein 4, Ms – mouse, Rb – rabbit.

II..5.2.2.1.2   Immunocytochemistry

Cells cultured under 2D conditions were washed in PBS twice and fixed in 10% formalin for 15 min at RT. After washing with PBS, the staining protocol was the same as described in section II-5.2.2.1.1. after antigen retrieval, which was not required. Moreover, the washing steps occurring after primary antibody incubation were performed with PBS, instead of PBST.

For the immunolabelling of cells entrapped in GG-derived hydrogels, the procedure was equivalent but the timing of the different steps was adjusted. In detail, 3D cultured cells were fixed with formalin for at least 1h and, when necessary, permeabilization was performed for 30 min on ice. After washing with PBS, the blocking step was performed for 1h at RT, followed by the incubation with primary antibodies for 18-24h at 4°C. The subsequent washing steps with PBS (up to the final step) were carried out under mild stirring for 15 min each. The incubation with the secondary antibody was performed overnight at 4°C and the counterstaining with DAPI was performed for 1h at RT.

Moreover, DP cell spheroids or DP-KCs/DP-hMel aggregates, although made from dissociated cells and not representing a tissue, were processed for paraffin inclusion after HistoGel™ (Thermo Fisher Scientific, USA) embedding, to facilitate their immunological analysis. The remaining process was the same as previously described in section II-5.2.2.1.1.

2D samples were analyzed with the Axioplan Imager Z1m microscope and representative images acquired with the ZEN 2.3 software, whilst 3D cultured cells were visualized with a Leica TCS SP8 confocal microscope and images acquired with the LEICA imaging software (Leica, Germany). Hematoxylin & Eosin staining

The Hematoxylin and Eosin (H&E) stain is the most widely used histological stain. It follows a standardized procedure that combines hematoxylin - which stains cell nuclei in blue - and eosin - which stains the ECM and cytoplasm in pink [74] - allowing the visualization of the tissues' morphology and organization in detail. In this thesis, it was used as a standard characterization method to assess tissue morphology in HF scalp samples, explants collected from the *in vivo* assays and to visualize cellular organization within the modified organotypic skin models.

Deparaffinized sections (as in II-5.2.2.1.1) were washed with distilled water, incubated with Mayer's Hematoxylin (Thermo Fisher Scientific, USA) for 5 min at RT and washed again under tap water. Samples were then incubated with eosin solution (Thermo Fisher Scientific, USA) for 1 min,

dehydrated with absolute ethanol, washed with xylene (Carlo Erba, Spain) and mounted using Entellan® (Merck, Germany).

II-5.2.2.2   *Chromogenic in situ hybridization*

Chromogenic *in situ* hybridization (CISH) is a cytogenic technique generally used to detect the presence or absence of specific nucleic acid sequences. It applies biotin- or digoxigenin-labelled DNA or RNA probes that link to specific nucleic acid sequences and that can be enzymatically detected with a peroxidase or ALP immunodetection system [75,76]. In this thesis, CISH was used to detect the presence of human cells in mice tissue explants six weeks upon human cell transplantation, using a DNA-probe corresponding to the human-specific Alu repeat sequence.

For that, the human-specific DNA labelled oligo probe (PanPath, NL) was used in combination with the BIO-AP REMBRANDT® Universal DISH & Detection kit (PanPath, NL). In detail, 5 µm-deparaffinized sections (see section II-5.2.2.1.1) were incubated with a 3% solution of hydrogen peroxide (H₂O₂; VWR, USA) for 15 min at RT to block endogenous peroxidase. Proteolytic digestion was then performed on the tissue sections using a pepsin-HCl solution for 30 min at 37°C, followed by dehydration in graded series of ethanol solutions. Samples were then air-dried and 1 drop of the probe was applied and covered with a coverslip. Samples were let at 95°C for 5 min for DNA denaturation, and then for 16h at 37°C in a moisturized environment for hybridization to occur. Samples were then washed in Tris-buffered saline (TBS) and incubated for 10 min with the stringency wash buffer. After rinsing with TBS, the detection was performed using the kit AEC substrate detection system. Color was let to develop for 10 min at 37°C in the dark. Samples were washed with water and observed under a DM750 light microscope (Leica).

II-5.2.2.3   *Alcian blue staining*

Alcian blue is a positively charged dye that links to all the negatively charged acid mucins. Depending on the pH at which it is prepared, alcian blue can be used to distinguish the type of acid mucins. At pH 2.5, all acidic mucins, either carboxylated or sulfated, ionize which is indicated by a turquoise blue color. When the pH is lowered to 1.0 the dye only interacts with sulfated mucins, while at pH 0.2 only strongly sulfated mucins are identified.

75

DP cells fixed with 10% formalin (15 min at RT) or 5 µm-HF tissue sections (deparaffinized as in II-5.2.2.1.1), were washed in PBS and briefly rinsed with 3% acetic acid (Fisher Chemical, USA) solution. Alcian blue 8GX (Sigma-Aldrich, USA) was prepared in a 3% acetic acid solution (pH 2.5) and used to incubate samples for 30 min (RT), followed by an additional rinse in 3% acetic acid. After washing with PBS, the samples were visualized under a DM750 Leica light microscope and representative images were acquired.

II-5.2.2.4 *Phalloidin-TRITC/DAPI staining*

Phalloidin–Tetramethylrhodamine B isothiocyanate (phalloidin-TRITC; Sigma-Aldrich, USA) is a low molecular weight toxin produced by the mushroom *Amanita phalloides* that specifically binds to polymeric F-actin. Throughout this thesis, phalloidin-TRITC was employed to visualize the organization of the cells' cytoskeleton and to analyze cellular morphology, both in 2D culture and in the 3D cell-laden hydrogels.

After fixation with 10% formalin for 15 min at RT, 2D cultured cells were washed in PBS and incubated with phalloidin-TRITC (0.1 mg/mL in PBS) for 1h at RT, after which cells were rinsed with PBS. Afterwards, the nuclei were counterstained with DAPI for 15 min at RT. For 3D cultured cells, incubation with the solutions of DAPI and phalloidin-TRITC was carried out in simultaneous. After a new rinse with PBS, the samples were observed under an Axioplan Imager Z1M microscope (2D cultured cells) or a TCS SP8 confocal microscope (cell-laden hydrogels), respectively.

II-5.2.2.5 *Live/dead staining*

The acetomethoxy derivate of calcein (calcein-AM) is a non-fluorescent and highly lipophilic dye that permeates most eukaryotic cells and is converted, by removal of the acetomethoxyl group by esterases, into the fluorescent calcein. Since dead cells do no possess active esterases, calcein green fluorescence (λex 490 nm, λem 515 nm) can be used to visualize live cells. PI, on the other hand, is a red fluorescent nuclear dye (λex 535 nm, λem 617 nm) that cannot cross viable cell membranes. However, it can pass through disorganized membranes of dead cells, it intercalates with the DNA double helix allowing their identification.

The viability of DP cells encapsulated in different GG hydrogels (described in section II-3.5.) was determined using the calcein and propidium iodide (PI) fluorescent dyes, to assess a potential negative effect of the encapsulation process, *e.g.* due to limited diffusion. For that, the 3D cell-laden hydrogels were incubated with calcein-AM (2 µg/mL, Molecular Probes, USA) and PI (1 µg/mL, Molecular Probes, USA) solutions prepared in DP cells medium (DMEM with 10% FBS) for 1h in the dark at 37°C and 5% CO_2. The live staining was then directly visualized under a TCS SP8 confocal microscope.

II-5.2.2.6   *Alkaline phosphatase staining*

The 5-bromo-4-chloro-3-indolyl phosphate and *p*-nitroblue tetrazolium chloride (NBT/BCIP) substrate system is used to detect non-specific alkaline phosphatase [77]. The BCIP acts a chromogenic substrate for ALP, to form a dephosphorylated intermediate that undergoes dimerization, resulting in an insoluble dark-blue indigo dye as an oxidation product of the reaction. The *p*-nitroblue tetrazolium chloride (NBT) is a potent redox indicator, acting as an electron acceptor and equally developing a dark-blue color, therefore increasing the sensitivity of the reaction. Besides being a very sensitive staining, the BCIP/NBT reaction results in little or no background staining [78] and is stable when exposed to light.

Since in the NBT/BCIP detection system color development only occurs in the presence of cells with metabolically active ALP (ALP-active cells), this allows to clearly visualize which cells retain ALP activity in culture. This is of key importance for DP cells since, as previously mentioned in section II-5.2.1.2., ALP activity is a major marker of these cells hair inductive potency, allowing their phenotype assessment.

The staining of ALP-active cells was performed in 10% formalin-fixed cells. After fixation, samples were washed in PBS were incubated for 20 min (dark, RT) with the NBT/BCIP substrate solution prepared by diluting 5 µL of NBT and 3.75 µL of BCIP (Roche, Switzerland) per 1 mL of NTMT solution, composed of 100 mM NaCl, 100 mM Tris-HCl pH 9.5 and 50 mM $MgCl_2$ (all from Sigma-Aldrich, USA) in water. Samples were then washed for 5 min in water before being observed under an inverted light microscope (AxioVert A1 FL LED).

II-5.2.2.7   *Senescence β-galactosidase staining*

Senescence is a state in which the cell remains metabolically active and viable but is no longer capable of dividing [79]. Primary cells have a limited replicative lifespan in culture, undergoing senescence after a limited number of passages, which can be identified by an increase in the senescence-associated β-galactosidase (SA-β-GAL) activity [80,81]. Considering that supraphysiological oxygen levels are associated with increased oxidative stress and DP cell senescence [82], we used the detection of SA-β-GAL activity to measure cellular senescence in DP cells cultured under physoxia/normoxia.

The detection of senescence cells was performed using the Senescence β-Galactosidase Staining Kit (Cell Signaling Technology, USA). DP cells were washed in PBS and fixed with 1x Fixative Solution for 15 min at RT. After two additional washing steps with PBS, cells were incubated with the β-Galactosidase Staining Solution for 24h at 37°C in a dry incubator. Afterwards, cells were once again rinsed with PBS and visualized under an inverted light microscope (AxioVert A1 FL LED) and, for each condition, twelve pictures per triplicate were taken at random microscopy fields. The images were used to quantify the number of cells stained and the total number of cells per field to determine the percentage of senescent cells as follows:

$$\% \text{ Senescent cells} = \frac{\text{number of stained cells} \times 100}{\text{total number of cells}}$$

II-5.2.3. Image analysis

II-5.2.3.1   *Self-aggregation quantification*

In the HF, the DP is organized as a cluster of cells and their tendency to aggregate, both *in vivo* and *in vitro*, is associated with their hair inducing ability [83,84]. For the quantification of DP cell self-aggregation capacity *in vitro*, cells were fixed with 10% formalin (15 min, RT), washed in PBS and incubated with DAPI for 15 min at RT. Samples were then examined under a fluorescence microscope

(Axio Observer, Zeiss, Germany) and, for each condition, ten pictures per triplicate were taken at random fields. The aggregation of DP in each condition was measured using the CellProfiler™ Software 3.0.0 [85]. The images were first converted to greyscale, and the signal of the nuclei was identified by applying Otsu thresholding algorithm to differentiate signal from the background [86]. Cells were regarded as adjacent if the distance between their nuclei was below ten pixels, and groups of 30 or more adjacent cells were counted as one aggregate

II-5.2.3.2   *Spheroid formation analysis*

To further understand the way DP cells self-aggregate under different conditions, the time taken to form the spheroids and their compactness were further analyzed. For that, $1x10^4$ DP cells were seeded in round bottom ultra-low attachment 96-well plates and the spheroid formation was recorded using time-lapse microscopy (Axio Observer, Zeiss, Germany) along 22h. Images of the center of the well were taken each 2h and the 2D area (mm^2) occupied by the cells was determined using the ZEN 2.3 (blue edition) image analysis module. The area occupied by the cells was manually encircled and then calculated by the software.

II-5.2.3.3   *Morphological characterization*

The quantification of morphology-related parameters was carried out in DP cells stained with phalloidin-TRITC/DAPI (section II-5.2.2.5.). For each condition and experiment, six different images of random fields were acquired, using a fluorescence microscope. Images were processed using the CellProfiler™ 3.0.0, where the nuclei of the cells were identified as the "Primary Object" using Otsu algorithm and the phalloidin-stained cytoskeleton the "Secondary Object" using a watershed gradient method. Data regarding the cell area, perimeter and major axis length was obtained using the software module "MeasureObjectSizeShape".

The data was provided in pixels (Figure II-8) and the posterior conversion into μm was performed by setting up the images scale bar in the ImageJ software (v1.51k).
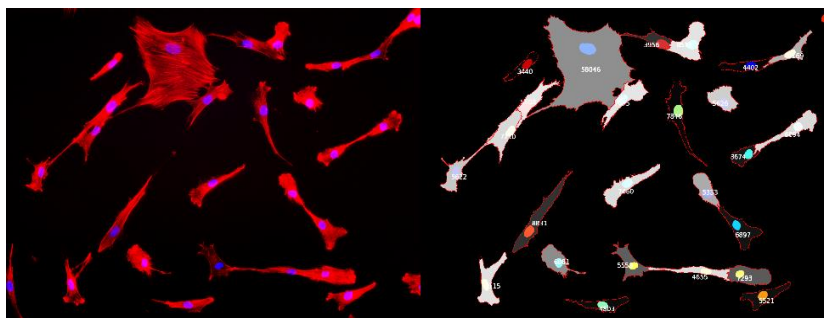
Figure II-8 – Representative pictures of DP cells stained with phalloidin/DAPI (left-hand side image) used to run the CellProfiler™. As output (right-hand side image), the cell nuclei were identified in different colors, while phalloidin staining was converted into the greyscale and the cell borders were limited by a red line, which was then used to calculate the relevant cell parameters.

II-5.2.3.4   *Quantification of dermal papilla-keratinocytes aggregates diameter*

Phase-contrast images of DP spheroids after KCs seeding, and of the formed multicellular aggregates (described on section II-3.2.3.), were acquired with an AxioVert.A1 microscope. The diameter of the cellular aggregates and DP spheroids was analyzed using the ZEN 2 software (blue edition; Zeiss, Germany),

II-5.2.3.5   *Live/dead cell quantification*

Dead and living cells were counted and the percentage of live cells was expressed as the ratio of living cells per the total number of cells in the total area or non-ablated areas around the microchannels. The total percentage of live cells, that also consider the cells in the ablated hole, does not significantly vary from the percentage present around the non-ablated area.

II-6.   STATISTICAL ANALYSIS

Statistical analysis was performed using GraphPad Prism 7.03. To determine if each subset of data followed a Gaussian distribution, the D'Agostino-Pearson omnibus test was performed. Nonparametric data were analyzed with a two-tailed Mann-Whitney test (two groups, unpaired) or with a Friedman (paired) or Kruskal-Wallis test (unpaired) when more than 2 groups were compared. Data that followed a Gaussian distribution were analyzed with a two-tailed Student's t-test (two groups, paired or

unpaired). The comparison of more than two groups was performed with an ordinary (unpaired) or RM (paired) one-way ANOVA (one independent variable) or two-way ANOVA (two independent variables). The data was expressed as mean ± standard error of the mean (SEM) and significance levels were set at: $^{*}p$ < 0.05, $^{**}p$ < 0.01, $^{***}p$ < 0.001 and $^{****}p$ < 0.0001.

II-7. REFERENCES

1. Pollock, T. J. Gellan-related polysaccharides and the genus Sphingomonas. *J. Gen. Microbiol.* **139**, 1939–1945 (1993).

2. Oliveira, J. T. *et al.* Gellan gum: A new biomaterial for cartilage tissue engineering applications. *J. Biomed. Mater. Res. - Part A* **93**, 852–863 (2010).

3. Ferris, C. J., Gilmore, K. J., Wallace, G. G. & Panhuis, M. In Het. Modified gellan gum hydrogels for tissue engineering applications. *Soft Matter* **9**, 3705 (2013).

4. Morris, E. R., Nishinari, K. & Rinaudo, M. Gelation of gellan – A review. *Food Hydrocoll.* **28**, 373–411 (2012).

5. Coutinho, D. F. *et al.* Modified Gellan Gum hydrogels with tunable physical and mechanical properties. *Biomaterials* **31**, 7494–7502 (2010).

6. Suri, S. & Banerjee, R. In vitro evaluation of in situ gels as short term vitreous substitutes. *J. Biomed. Mater. Res. Part A* **79A**, 650–664 (2006).

7. Xu, Z., Li, Z., Jiang, S. & Bratlie, K. M. Chemically Modified Gellan Gum Hydrogels with Tunable Properties for Use as Tissue Engineering Scaffolds. *ACS Omega* **3**, 6998–7007 (2018).

8. Messenger, A. G., Elliott, K., Westgate, G. E. & Gibson, W. T. Distribution of extracellular matrix molecules in human hair follicles. *Ann. N. Y. Acad. Sci.* **642**, 253–62 (1991).

9. Wilke, M. S. & Furcht, L. T. Human Keratinocytes Adhere to a Unique Heparin-Binding Peptide Sequence Within the Triple Helical Region of Type IV Collagen. *J. Invest. Dermatol.* **95**, 264–270 (1990).

10. D'Souza, S. E., Ginsberg, M. H. & Plow, E. F. Arginyl-glycyl-aspartic acid (RGD): a cell adhesion motif. *Trends Biochem. Sci.* **16**, 246–250 (1991).

11. da Silva, L. P. *et al.* Gellan Gum Hydrogels with Enzyme-Sensitive Biodegradation and Endothelial Cell Biorecognition Sites. *Adv. Healthc. Mater.* **7**, 1700686 (2018).

12. Carvalho, A. F., Gasperini, L., Ribeiro, R. S., Marques, A. P. & Reis, R. I. Control of osmotic pressure to improve cell viability in cell-laden tissue engineering constructs. *J. Tissue Eng. Regen. Med.* **12**, e1063–e1067 (2018).

13. Sennett, R. & Rendl, M. Mesenchymal-epithelial interactions during hair follicle morphogenesis and cycling. *Semin Cell Dev Biol* **23**, 917–927 (2012).

14. Balana, M. E., Charreau, H. E. & Leiros, G. J. Epidermal stem cells and skin tissue engineering in hair follicle regeneration. *World J Stem Cells* **7**, 711–727 (2015).

15. Stocum, D. L. Regenerative Medicine of Epidermal Structures. in *Regenerative Biology and Medicine* 261–284 (Elsevier, 2012).

16. Schmidt-Ullrich, R. & Paus, R. Molecular principles of hair follicle induction and morphogenesis. *BioEssays* **27**, 247–261 (2005).

17. Stenn, K. S. & Paus, R. Controls of hair follicle cycling. *Physiol Rev* **81**, 449–494 (2001).

18. Millar, S. E. Molecular Mechanisms Regulating Hair Follicle Development. *J. Invest. Dermatol.* **118**, 216–225 (2002).

19. Driskell, R. R., Clavel, C., Rendl, M. & Watt, F. M. Hair follicle dermal papilla cells at a glance. *J. Cell Sci.* **124**, 1179–1182 (2011).

20. Ohyama, M. & Veraitch, O. Strategies to enhance epithelial–mesenchymal interactions for human hair follicle bioengineering. *J. Dermatol. Sci.* **70**, 78–87 (2013).

21. Li, A., Simmons, P. J. & Kaur, P. Identification and isolation of candidate human keratinocyte stem cells based on cell surface phenotype. *Proc. Natl. Acad. Sci.* **95**, 3902–3907 (1998).

22. Webb, A., Li, A. & Kaur, P. Location and phenotype of human adult keratinocyte stem cells of the skin. *Differentiation* **72**, 387–395 (2004).

23. Cerqueira, M. T., Frias, A. M., Reis, R. L. & Marques, A. P. Boosting and Rescuing Epidermal Superior Population from Fresh Keratinocyte Cultures. *Stem Cells Dev.* **23**, 34–43 (2014).

24. Thomas, A. J. & Erickson, C. A. The making of a melanocyte: the specification of melanoblasts from the neural crest. *Pigment Cell Melanoma Res.* **21**, 598–610 (2008).

25.   Tobin, D. J. The cell biology of human hair follicle pigmentation. *Pigment Cell Melanoma Res.* **24**, 75–88 (2011).

26.   Lim, J., Ng, K. J. & Clavel, C. Dermal papilla regulation of hair growth and pigmentation. in *Advances in Stem Cells and their Niches* vol. 3 115–138 (Elsevier, 2019).

27.   Ideta, R., Soma, T., Tsunenaga, M. & Ifuku, O. Cultured human dermal papilla cells secrete a chemotactic factor for melanocytes. *J. Dermatol. Sci.* **28**, 48–59 (2002).

28.   Buffey, J. A. *et al.* Extracellular matrix derived from hair and skin fibroblasts stimulates human skin melanocyte tyrosinase activity. *Br. J. Dermatol.* **131**, 836–842 (1994).

29.   Ponec, M. Skin constructs for replacement of skin tissues for in vitro testing. *Adv. Drug Deliv. Rev.* **54**, S19–S30 (2002).

30.   Li, P. *et al.* Efficient feeder cells preparation system for large-scale preparation and application of induced pluripotent stem cells. *Sci. Rep.* **7**, 12266 (2017).

31.   Namba, M., Fukushima, F. & Kimoto, T. Effects of feeder layers made of human, mouse, hamster, and rat cells on the cloning efficiency of transformed human cells. *In Vitro* **18**, 469–475 (1982).

32.   Llames, S., García-Pérez, E., Meana, Á., Larcher, F. & del Río, M. Feeder Layer Cell Actions and Applications. *Tissue Eng. Part B Rev.* **21**, 345–353 (2015).

33.   Rheinwald, J. G. & Green, H. Serial cultivation of strains of human epidermal keratinocytes: the formation of keratinizing colonies from single cells. *Cell* **6**, 331–343 (1975).

34.   Basu, S., Campbell, H. M., Dittel, B. N. & Ray, A. Purification of Specific Cell Population by Fluorescence Activated Cell Sorting (FACS). *J. Vis. Exp.* **10**, 1546 (2010).

35.   Williams, D., Profeta, K. & Stenn, K. S. Isolation and culture of follicular papillae from murine vibrissae: an introductory approach. *Br. J. Dermatol.* **130**, 290–297 (1994).

36.   Topouzi, H., Logan, N. J., Williams, G. & Higgins, C. A. Methods for the isolation and 3D culture of dermal papilla cells from human hair follicles. *Exp. Dermatol.* **26**, 491–496 (2017).

37.   Higgins, C. A., Chen, J. C., Cerise, J. E., Jahoda, C. A. B. & Christiano, A. M. Microenvironmental reprogramming by three-dimensional culture enables dermal papilla cells to induce de novo human hair-follicle growth. *Proc. Natl. Acad. Sci.* **110**, 19679–19688 (2013).

38. Higgins, C. A., Richardson, G. D., Ferdinando, D., Westgate, G. E. & Jahoda, C. A. B. Modelling the hair follicle dermal papilla using spheroid cell cultures. *Exp. Dermatol.* **19**, 546–548 (2010).

39. Miao, Y., Sun, Y. Bin, Liu, B. C., Jiang, J. D. & Hu, Z. Q. Controllable Production of Transplantable Adult Human High-Passage Dermal Papilla Spheroids Using 3D Matrigel Culture. *Tissue Eng. Part A* **20**, 2329–2338 (2014).

40. Kim, H. O., Choi, S.-M. & Kim, H.-S. Mesenchymal stem cell-derived secretome and microvesicles as a cell-free therapeutics for neurodegenerative disorders. *Tissue Eng. Regen. Med.* **10**, 93–101 (2013).

41. Wang, W., Winlove, C. P. & Michel, C. C. Oxygen Partial Pressure in Outer Layers of Skin of Human Finger Nail Folds. *J. Physiol.* **549**, 855–863 (2003).

42. Lartigau, E. *et al.* Intratumoral oxygen tension in metastatic melanoma. *Melanoma Res.* **7**, 400–406 (1997).

43. McKeown, S. R. Defining normoxia, physoxia and hypoxia in tumours—implications for treatment response. *Br. J. Radiol.* **87**, 20130676 (2014).

44. Gangatirkar, P., Paquet-Fifield, S., Li, A., Rossi, R. & Kaur, P. Establishment of 3D organotypic cultures using human neonatal epidermal cells. *Nat. Protoc.* **2**, 178–186 (2007).

45. Carlson, M. W., Alt-Holland, A., Egles, C. & Garlick, J. A. Three-Dimensional Tissue Models of Normal and Diseased Skin. *Curr. Protoc. Cell Biol.* **41**, 19.9.1-19.9.17 (2008).

46. Hashida, M., Mishima, H., Tokita, S. & Sakabe, S. Non-thermal ablation of expanded polytetrafluoroethylene with an intense femtosecond-pulse laser. *Opt. Express* **17**, 13116 (2009).

47. Yang, C.-C. & Cotsarelis, G. Review of hair follicle dermal cells. *J. Dermatol. Sci.* **57**, 2–11 (2010).

48. Lichti, U. *et al.* In vivo regulation of murine hair growth: Insights from grafting defined cell populations onto nude mice. *J. Invest. Dermatol.* **101**, S124–S129 (1993).

49. Weinberg, W. C. *et al.* Reconstitution of Hair Follicle Development In Vivo: Determination of Follicle Formation, Hair Growth, and Hair Quality by Dermal Cells. *J. Invest. Dermatol.* **100**, 229–236 (1993).

50. Mahjour, S. B., Ghaffarpasand, F. & Wang, H. Hair follicle regeneration in skin grafts: current concepts and future perspectives. *Tissue Eng Part B Rev* **18**, 15–23 (2012).

51. Yang, C.-C. & Cotsarelis, G. Review of hair follicle dermal cells. *J. Dermatol. Sci.* **57**, 2–11 (2010).

52. Szadvaria, I., Krizanova, O. & Babula, P. Athymic Nude Mice as an Experimental Model for Cancer Treatment. *Physiol. Res.* **65**, S441–S453 (2016).

53. Jensen, K. B., Driskell, R. R. & Watt, F. M. Assaying proliferation and differentiation capacity of stem cells using disaggregated adult mouse epidermis. *Nat. Protoc.* **5**, 898–911 (2010).

54. Lee, J.-H. & Kim, H.-W. Emerging properties of hydrogels in tissue engineering. *J. Tissue Eng.* **9**, 204173141876828 (2018).

55. Guimarães, C. F., Gasperini, L., Marques, A. P. & Reis, R. L. The stiffness of living tissues and its implications for tissue engineering. *Nat. Rev. Mater.* **5**, 351–370 (2020).

56. Krishnamoorthy, S., Noorani, B. & Xu, C. Effects of encapsulated cells on the physical-mechanical properties and microstructure of gelatin methacrylate hydrogels. *Int. J. Mol. Sci.* **20**, (2019).

57. Ahearne, M., Yang, Y. & Liu, K.-K. Mechanical Characterisation of Hydrogels for Tissue Engineering Applications Hydrogels for Tissue Engineering. in *Tissue Engineering* vol. 4 (2008).

58. Vedadghavami, A. *et al.* Manufacturing of hydrogel biomaterials with controlled mechanical properties for tissue engineering applications. *Acta Biomater.* **62**, 42–63 (2017).

59. Smith, P. K. *et al.* Measurement of protein using bicinchoninic acid. *Anal. Biochem.* **150**, 76–85 (1985).

60. Handjiski, B. K., Eichmuller, S., Hofmann, U., Czarnetzki, B. M. & Paus, R. Alkaline phosphatase activity and localization during the murine hair cycle. *Br. J. Dermatol.* **131**, 303–310 (1994).

61. McElwee, K. J., Kissling, S., Wenzel, E., Huth, A. & Hoffmann, R. Cultured peribulbar dermal sheath cells can induce hair follicle development and contribute to the dermal sheath and dermal papilla. *J Invest Dermatol* **121**, 1267–1275 (2003).

62. Thangapazham, R. L. *et al.* Dissociated Human Dermal Papilla Cells Induce Hair Follicle Neogenesis in Grafted Dermal–Epidermal Composites. *J. Invest. Dermatol.* **134**, 538–540

(2014).

63. Kwack, M. H. *et al.* Overexpression of alkaline phosphatase improves the hair-inductive capacity of cultured human dermal papilla spheres. *J. Dermatol. Sci.* **95**, 126–129 (2019).

64. Adan, A., Alizada, G., Kiraz, Y., Baran, Y. & Nalbant, A. Flow cytometry: basic principles and applications. *Crit. Rev. Biotechnol.* **37**, 163–176 (2017).

65. Kubaski, F. *et al.* Glycosaminoglycans detection methods: Applications of mass spectrometry. *Mol. Genet. Metab.* **120**, 67–77 (2017).

66. Kafienah, W. & Sims, T. J. Biochemical Methods for the Analysis of Tissue-Engineered Cartilage. in *Biopolymer Methods in Tissue Engineering* 217–230 (Humana Press, 2003).

67. López-De León, A. & Rojkind, M. A simple micromethod for collagen and total protein determination in formalin-fixed paraffin-embedded sections. *J. Histochem. Cytochem.* **33**, 737–743 (1985).

68. Bradford, M. M. A rapid and sensitive method for the quantitation of microgram quantities of protein utilizing the principle of protein-dye binding. *Anal. Biochem.* **72**, 248–254 (1976).

69. Ray, P. D., Huang, B.-W. & Tsuji, Y. Reactive oxygen species (ROS) homeostasis and redox regulation in cellular signaling. *Cell. Signal.* **24**, 981–990 (2012).

70. Jagannathan, L., Cuddapah, S. & Costa, M. Oxidative Stress Under Ambient and Physiological Oxygen Tension in Tissue Culture. *Curr. Pharmacol. Reports* **2**, 64–72 (2016).

71. Carrasco, E. *et al.* Photoactivation of ROS Production In Situ Transiently Activates Cell Proliferation in Mouse Skin and in the Hair Follicle Stem Cell Niche Promoting Hair Growth and Wound Healing. *J. Invest. Dermatol.* **135**, 2611–2622 (2015).

72. Ando, H., Kondoh, H., Ichihashi, M. & Hearing, V. J. Approaches to Identify Inhibitors of Melanin Biosynthesis via the Quality Control of Tyrosinase. *J. Invest. Dermatol.* **127**, 751–761 (2007).

73. D'Mello, S., Finlay, G., Baguley, B. & Askarian-Amiri, M. Signaling Pathways in Melanogenesis. *Int. J. Mol. Sci.* **17**, 1144 (2016).

74. Fischer, A. H., Jacobson, K. A., Rose, J. & Zeller, R. Hematoxylin and Eosin Staining of Tissue and Cell Sections. *Cold Spring Harb. Protoc.* pdb.prot4986 (2008).

75. Lambros, M. B. K. *et al.* Unlocking pathology archives for molecular genetic studies: a reliable

method to generate probes for chromogenic and fluorescent in situ hybridization. *Lab. Investig.* **86**, 398–408 (2006).

76. Lambros, M. B. K., Natrajan, R. & Reis-Filho, J. S. Chromogenic and fluorescent in situ hybridization in breast cancer. *Hum. Pathol.* **38**, 1105–1122 (2007).

77. McGadey, J. A tetrazolium method for non-specific alkaline phosphatase. *Histochemie* **23**, 180–184 (1970).

78. De Jong, A. S. H., Van Kessel-Van Vark, M. & Raap, A. K. Sensitivity of various visualization methods for peroxidase and alkaline phosphatase activity in immunoenzyme histochemistry. *Histochem. J.* **17**, 1119–1130 (1985).

79. Goldstein, S. Replicative senescence: the human fibroblast comes of age. *Science.* **249**, 1129–1133 (1990).

80. Kuilman, T., Michaloglou, C., Mooi, W. J. & Peeper, D. S. The essence of senescence. *Genes Dev.* **24**, 2463–2479 (2010).

81. Dimri, G. P. *et al.* A biomarker that identifies senescent human cells in culture and in aging skin in vivo. *Proc. Natl. Acad. Sci.* **92**, 9363–9367 (1995).

82. Upton, J. H. *et al.* Oxidative Stress–Associated Senescence in Dermal Papilla Cells of Men with Androgenetic Alopecia. *J. Invest. Dermatol.* **135**, 1244–1252 (2015).

83. Jahoda, C. & Oliver, R. F. The growth of vibrissa dermal papilla cells in vitro. *Br. J. Dermatol.* **105**, 623–627 (1981).

84. Jahoda, C. A. B., Horne, K. A. & Oliver, R. F. Induction of hair growth by implantation of cultured dermal papilla cells. *Nature* **311**, 560–562 (1984).

85. Lamprecht, M. R., Sabatini, D. M. & Carpenter, A. E. CellProfiler™: free, versatile software for automated biological image analysis. *Biotechniques* **42**, 71–75 (2007).

86. Sankur, B. Survey over image thresholding techniques and quantitative performance evaluation. *J. Electron. Imaging* **13**, 146 (2004).

CHAPTER III

INTERFOLLICULAR EPIDERMAL STEM-LIKE CELLS FOR THE RECREATION OF THE HAIR FOLLICLE EPITHELIAL COMPARTMENT

CHAPTER III

INTERFOLLICULAR EPIDERMAL STEM-LIKE CELLS FOR THE RECREATION OF THE HAIR FOLLICLE EPITHELIAL COMPARTMENT†

ABSTRACT

Hair follicle (HF) development and growth are dependent on epithelial-mesenchymal interactions (EMIs). Dermal papilla (DP) cells are recognized as the key inductive mesenchymal player but the ideal source of receptive keratinocytes for human HF regeneration is yet to be defined. We herein investigated whether human interfollicular epidermal keratinocytes with stem-like features (EpSlKCs), characterized by $\alpha6^{high}$/$CD71^{dim}$ expression, can replace human hair follicular keratinocytes (HHFKCs) for the recreation of the HF epithelium and respective EMIs. The $\alpha6^{high}$/$CD71^{dim}$ cellular fraction was selected from the whole interfollicular keratinocytes population through fluorescent activated cell sorting and directly compared with HHFKCs regarding their proliferative capacity and phenotype. The crosstalk with DP cells was studied in indirect co-cultures, and EpSlKCs hair-forming capacity was tested in a hair reconstitution assay with DP cells. We show that EpSlKCs exhibited a phenotypic profile similar to HHFKCs, and were capable of increasing DP cell proliferation and their alkaline phosphatase activity, suggesting an inductivity improvement. Moreover, the recreation of immature HFs and sebaceous glands was observed after EpSlKCs and DP cells co-grafting in mice. Our results suggest that EpSlKCs are akin to HHFKCs and can crosstalk with DP cells, contributing to HF morphogenesis *in vivo*, thus representing an attractive epithelial cell source for hair regeneration strategies.

III-1.   INTRODUCTION

The hair follicle (HF) singular capacity to continually self-renew and undergo repeated cycles relies on the reciprocal interactions that occur between its mesenchymal and epithelial compartments [1,2]. Therefore, successful strategies aiming to promote HF regeneration rely on the combination of relevant dissociated cell populations to rescue epithelial-mesenchymal interactions (EMIs) [3,4]. The HF mesenchyme is usually recreated with specialized dermal papilla (DP) cells, whereas the epithelial fraction is commonly reconstructed using keratinocytes (KCs) isolated from different follicular sources, including the bulge [5], the outer root sheath (ORS) [6–10] or the hair bulb [8,11]. Yet, the ideal epithelial source is not identified. Although representing a stem cell niche, the bulge can only be accessed from intact HF [12], which is hindered by fairly indistinguishable anatomical boundaries [13]. Hence, KCs are frequently obtained from the hair bulb or ORS of plucked HFs, an easier access source. However, their isolation relies on the rough HF transection, followed by enzymatic digestion or cells outgrowth [12,14,15]. This represents a low yield process [16] where population purity is reduced due to the contamination with other cell fractions. Moreover, the isolated cells are at distinct differentiation stages, most of them being transit-amplifying (TA) cells, with shorter culture lifespan in comparison to stem cells [12].

Human interfollicular epidermal cells have also been used for HF regeneration, but successful strategies rely on their combination with murine DP cells [17], that better retain inductivity than human cells. Neonatal epithelial cell sources are potentially the most useful due to the immature state of the cells, however, accessibility and ethical constraints still feed the gap between demand and supply. Knowing that epidermal stem cells express high levels of α6-integrin, and can be distinguished from other basal cells based on their lower expression of the transferrin receptor (CD71) [18,19], we previously demonstrated that the α6^{high}/CD71^{dim} subpopulation of interfollicular epidermal stem-like cells can be isolated from adult skin [19]. Considering their undifferentiated state and high clonogenic capacity [19], we hypothesized that these epidermal KCs with stem-like features (EpSlKCs) can replace follicular keratinocytes in the recreation of the HF epithelium and respective EMIs with DP cells, promoting HF formation. EpSlKCs were isolated by fluorescent activated cell sorting (FACS) based on their α6^{high}/CD71^{dim} profile, and their proliferative capacity and phenotype were directly compared with the commonly used human hair follicular keratinocytes (HHFKCs). Next, EpSlKCs capacity to affect and communicate with DP cells was tested in indirect co-cultures focusing on cell proliferation, phenotype

and release of the HF-related growth factors PDGF-A, VEGF and BMP2. Finally, EpSlKCs hair trichogenic capacity was assessed in a hair inductive assay in combination with human DP cells.

III-2. MATERIAL AND METHODS

Human skin was obtained from abdominoplasties, performed at Hospital da Prelada (Porto, Portugal), while human occipital scalp samples from hair transplantation surgeries at Sanare Unicapilar (Porto, Portugal). Samples were obtained under a collaboration protocol approved by the ethical committees of the involved institutions and after written informed consent from patients. Animal experimentation was approved by the local Animal Welfare Body.

III-2.1. Cell isolation and culture

KCs were isolated as previously described [19] and cultured in Keratinocyte Serum-Free Medium (KSFM, Gibco) with 1% penicillin-streptomycin solution (PenStrep, Gibco) and WITH the ROCK pathway inhibitor Y-27632 (10 μM, STEMCELL Technologies). HHFKCs were purchased from ScienCell (USA) and cultured in the supplied keratinocyte medium. DPs were microdissected [20] from occipital scalp samples. The explants were cultured in Dulbecco's Modified Eagle's Medium (DMEM, Sigma-Aldrich) supplemented with 20% FBS and 1% antibiotic-antimycotic solution (Gibco). Cells growing out of the explant were further expanded in collagen (Sigma-Aldrich)-coated flasks and cultured in DMEM with 10% FBS and 1% antibiotic-antimycotic solution. Cell culture was conducted under standard conditions ($37°C$, 5% CO_2) in a humidified atmosphere and with medium change every 2-3 days.

III-2.2. Feeder layer preparation

J2-3T3 mouse fibroblasts were cultured in DMEM with 10% bovine serum (Life Technologies). Cells were then inactivated with mitomycin C (4 μg/mL, Sigma-Aldrich) for 2h30 min at $37°C$ [21]. Feeder layers were prepared by seeding the inactivated 3T3 fibroblasts at a density of 2.4×10^4 cells/cm^2.

III-2.3. Selection of the α6^{bri}/CD71^{dim} cellular subpopulation

A suspension of primary KCs with $5.0x10^6$ cells/mL was incubated with CD71-PE (1:200, BioLegend) and CD49f-APC (1:85, eBioscience) for 30 min at room temperature (RT). The selection of α6^{bri}/CD71^{dim} cells was performed using a FACSArialII Cell Sorter and FACSDiva software (BD Biosciences). Sorted α6^{bri}/CD71^{dim} cells were plated at $1.8x10^3$ cells/cm² onto the feeder layer and cultured in FAD medium [1-part Ham's F-12 and 3-parts DMEM supplemented with 10% non-inactivated FBS, $1.8x10^4$ M adenine, 0.5 μg/ml hydrocortisone, 5 μg/mL insulin, 10^{10} M cholera toxin (Sigma-Aldrich), 10 g/ml epidermal growth factor (Peprotech), 1.8 mM $CaCl_2$ (Merck) and 1% PenStrep].

III-2.4. Flow cytometry analysis

For surface marker analysis (Table II-3), cell suspensions were directly incubated with fluorochrome-labelled antibodies for 30 min at RT. For intracellular staining, cells were firstly fixed with the FIX&PERM™ Cell Permeabilization Kit Reagent A (Life Technologies) for 15 min at RT, and then permeabilized with Reagent B and simultaneously incubated with the intracellular-labelled antibodies (20 min, RT). Cells were analyzed with FACSCalibur flow cytometer in CellQuest software.

III-2.5. Indirect co-culture

EpSlKCs were harvested from the feeder layer [21], resuspended in KSFM with Y-27632 and seeded at a density of 500 cells/cm². Co-cultures were established in the next day, using Transwell® inserts (0.4 μm pore, Corning). DP cells were plated in the insert at a density of 1000 cells/cm². Co-culture medium consisted of an equal mixture of DMEM 10% FBS and KSFM with Y-27632 (DMEM: KSFM). Single cell-type cultures were prepared as controls, by culturing cells in their regular medium and in the co-culture medium, the latter to control possible medium effects on the cells.

III-2.6. DNA and alkaline phosphatase quantification

At each experimental time point, cells were washed with PBS and lysed with 0.01% sodium dodecyl sulfate (NZYteck). DNA was quantified using the Quant-iT™ PicoGreen® dsDNA kit (Thermo Fisher

Scientific), and active ALP was quantified using the ALP Fluorescent Detection Kit (Sigma-Aldrich), both following the manufacturer's instructions.

III-2.7. Enzyme-linked immunosorbent assay

Growth factors present in the supernatants of the 48h homotypic cultures or co-cultures were quantified using vascular endothelial growth factor (VEGF) ELISA Development Kit (Peprotech), bone morphogenetic protein 2 (BMP2) ELISA Development Kit (Peprotech) and platelet-derived growth factor A (PDGF-A) DuoSet (R&D Systems), according to the manufacturer's instructions. DNA values were used to normalize results.

III-2.8. Hair reconstitution assay

Athymic male nude Balb/C mice (Charles River, 9 weeks) were randomly divided into three experimental groups: control, DP cells and DP cells with EpSlKCs ($n = 4$, each group). The silicone chamber model was set and used as previously described [22]. Cell suspensions with 5.0×10^6 DP cells (DP cells group) and 2.5×10^6 EpSlKCs (experimental group), or vehicle (FAD medium, control group) were injected in the chamber. The top of the chamber was cut-off after one week and the chamber was fully removed after two weeks. Animals were euthanized six weeks after surgery to harvest the wound area for histological analysis.

III-2.9. Immunofluorescence and histological analysis

Cells from the *in vitro* experiments were washed in PBS and fixed in 10% formalin for 15 mins (RT). Cell permeabilization was performed with 0.2% Triton X-100 for 15 min (RT, intracellular staining) or 30 min (4°C, nuclear staining), and blocking with a 3% BSA solution for 30 min (RT). Samples were then incubated with primary antibodies (Table II-5) diluted in 1% BSA for 1h (RT). After washing with PBS, Alexa Fluor (594/488)-conjugated secondary antibodies (1:500; Molecular Probes) were applied. Cellular morphology was observed after staining F-actin with phalloidin-TRITC (1:100, Sigma-Aldrich) for 1h (RT) and nuclear counterstain performed using DAPI (0.02 mg/mL, Biotium) for 15 min (RT). Images were acquired with an Axio Imager Z1m microscope (Zeiss).

For histological analysis, 4 µm paraffin-embedded sections were stained with Hematoxylin & Eosin (H&E) and analyzed with a DM750 microscope (Leica). For immunofluorescence studies, heat-mediated antigen retrieval was performed in the deparaffinized sections using the citrate buffer (pH 6.0) and the remaining procedure was performed as above described for the *in vitro* ones.

III-2.10. Statistical analysis

Statistical analysis was performed using GraphPad Prism 7.03. To test if data followed a Gaussian distribution the D'Agostino & Pearson normality test was used. Nonparametric data were analyzed with a Mann-Whitney t-test (two groups, unpaired); Kruskal-Wallis (three groups, unpaired) or Friedman test (three groups, paired) were used coupled with Dunn's post-test. Parametric data were analyzed using a one-way ANOVA (two groups, paired) or RM two-way ANOVA (three groups, paired) in combination with Tukey's post-test. Differences with $p < 0.05$ were considered significant.

III-3. RESULTS

III-3.1. EpSlKCs and HHFKCs are phenotypically similar

The isolated interfollicular KCs comprehended a low percentage of epidermal stem cells ($4.62 \pm 1.47\%$; $\alpha6^{high}/CD71^{dim}$ fraction) and differentiated cells ($3.72 \pm 0.47\%$; $\alpha6^{dim}$ subpopulation), while TA cells ($78.44 \pm 3.26\%$; $\alpha6^{high}/CD71^{high}$ subpopulation) represented the majority of the population (Supplementary Figure III-1A), as expected [18]. The selected $\alpha6^{high}/CD71^{dim}$ cells where cultured on feeders (Supplementary Figure III-1B and C), and the obtained cells – EpSlKCs – were directly compared to HHFKCs. Most EpSlKCs and HHFKCs were small and bright cells displaying a cobblestone morphology (Figure III-1A), characteristic of undifferentiated epithelial cells. However, cellular heterogeneity was higher for HHFKCs cultures, with the presence of large size cells, representative of differentiated cells. Nevertheless, both cell types proliferated at similar rates (Figure III-1B), although at day 3 HHFKCs numbers were higher than EpSlKCs. The percentage of $\alpha6^{high}/CD71^{dim}$ cells in both cell types was similar, as was the expression of the basal epidermal markers β1-integrin (CD29) and keratin (K) 14 (Figure III-1C). The expression of K19, typically considered a stem cell marker whose expression decreases with age [23], was also similar among cell types. Immunocytochemistry analysis confirmed

94

their immature phenotype, with positive staining for the basal-specific markers K15, K6 and K14, and absence of the differentiation marker K10 (Figure III-1D). Additionally, most cells were positive for the proliferation-associated marker Ki67. Together, these results demonstrate that EpSlKCs and HHFKCs proliferative capacity and phenotype are equivalent.

	α6high/CD71dim	CD29	K19	K14
EpSlKCs	5.82 ± 1.26 %	99.90 ± 0.06 %	5.18 ± 0.67 %	99.24 ± 0.29 %
HHFKCs	6.90 ± 3.54 %	99.88 ± 0.09 %	7.19 ± 0.36 %	99.02 ± 0.49 %
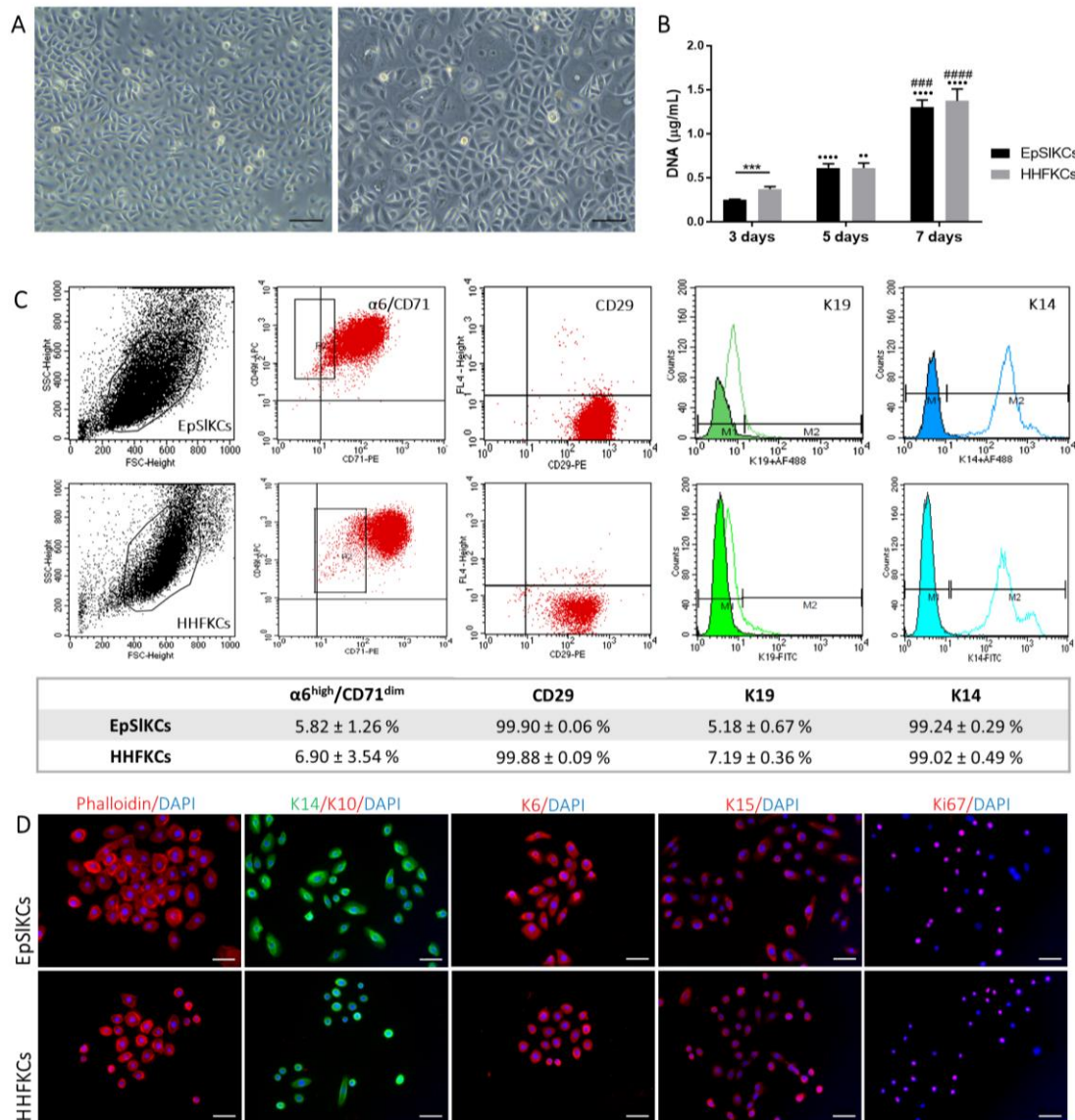
Figure III-1 - Morphology, proliferation and phenotype of EpSlKCs and HHFKCs. (A) Representative light microscopy images of human epidermal stem-like keratinocytes (EpSlKCs) and human hair follicular keratinocytes (HHFKCs) culture. (B) DNA quantification of the cells along the culture time. (C) Representative flow cytometry histograms and respective quantification regarding the percentage of α6high/CD71dim cells, and those positive for integrin β1 (CD29), keratin 19 (K19) and keratin 14 (K14) in EpSlKCs and HHFKCs cultures after one week. (D) Immunofluorescence staining of β-actin filaments (phalloidin), keratin 14 (K14), keratin 10 (K10), keratin 6 (K6), keratin 15 (K15) and the proliferation-associated marker Ki67 in EpSlKCs and HHFKCs. DAPI was used as nuclear counterstainer. *** $p < 0.001$; ·· $p < 0.01$ and ···· $p < 0.0001$ *vs.* day 3; ### $p < 0.001$ and #### $p < 0.0001$ *vs.* day 5. Scale bars are 100 μm for (A) and 50 μm for (D).

III-3.2. EpSlKCs support DP cell growth and a partial restoration of their native phenotype

To study EpSlKCs capacity to communicate with DP cells, an indirect co-culture was established (Figure III-2A). After co-culture, EpSlKCs remained small and exhibited a cuboidal morphology (Figure III-2B). In the conventional culture medium (KSFM), EpSlKCs displayed a cobblestone morphology and were slightly brighter and smaller than in co-culture. Despite this, co-cultured EpSlKCs were different from those kept in the co-culture medium (DMEM: KSFM), whose morphology, larger size and lower brightness evidenced a more differentiated state. Co-culture with DP cells also prevented the differentiation of EpSlKCs, expected to be induced by DMEM components, such as calcium [24,25]. Furthermore, co-culture conditions were able to sustain EpSlKCs proliferation along with culture, as demonstrated by the similar DNA amounts of the co-culture and KSFM, both significantly higher than in the medium control (Figure III-2C).
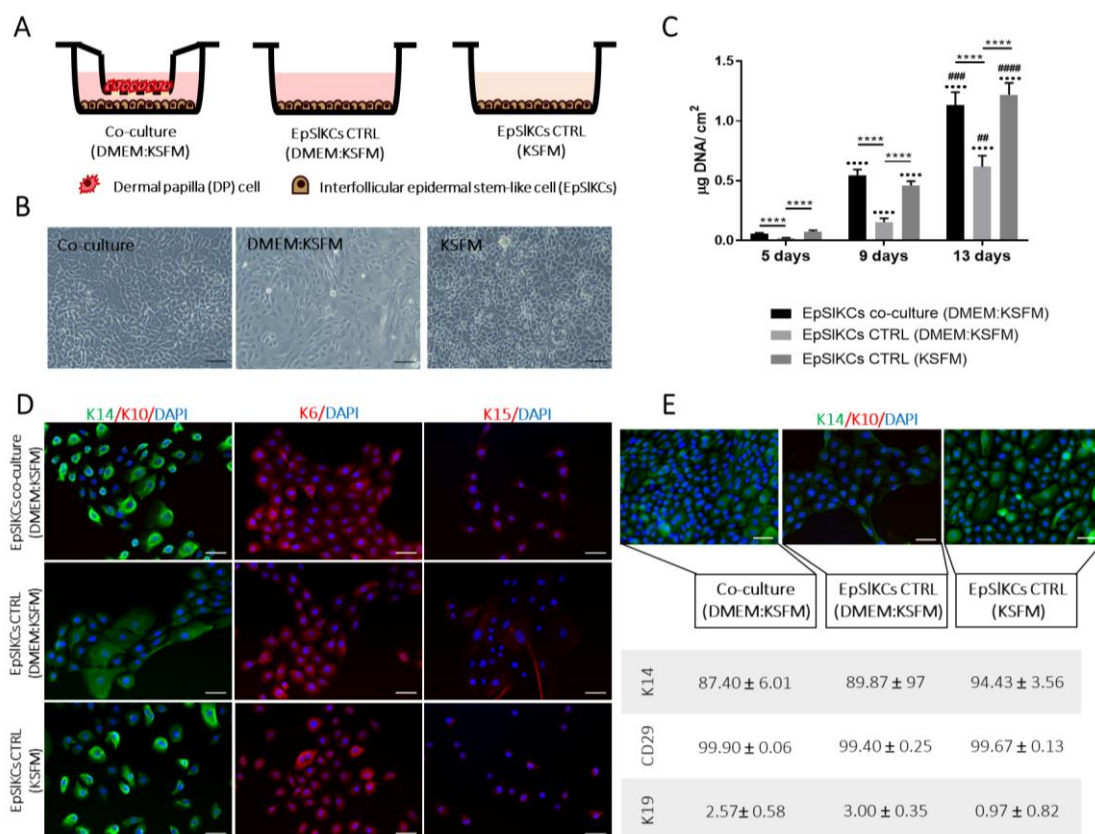
Figure III-2 - Characterization of EpSlKCs co-cultured with DP cells. (A) Schematic representation and (B) light microscopy images of EpSlKCs in co-culture with dermal papilla (DP) cells and the respective monoculture controls. (C) DNA quantification of EpSlKCs after 5, 9 and 13 days of culture. (D) Representative images of immunofluorescence staining against the epithelial markers K14 and K10, K6 and K15 after 5 days in culture. (E) Immunostaining against K14 staining in EpSlKCs after 13 days in culture and the respective flow cytometry quantitative data (n = 3). DAPI was used as nuclear counterstaining. **** $p < 0.0001$; ···· $p < 0.0001$ *vs.* day 5; ## $p <0.01$, ### $p < 0.001$ and #### $p < 0.0001$ *vs.* day. Scale bars are 100 μm for (B) and 50 μm for (D, E).

Further evaluation of DP cell effects on EpSlKCs differentiation showed that K14 expression was similar in the co-cultures and the monoculture established with KSFM. In contrast, K14-bright positive cells were not found in the monocultures of EpSlKCs in control medium (Figure III-2D). Nevertheless, K6 and K15 staining were similar among conditions, with cells stained for K6 but weakly expressing K15. After 13 days in co-culture, most cells were K14-positive, as confirmed by flow cytometry analysis, but K14-bright cells were only observed for EpSlKCs cultured in KSFM (Figure III-2E). Independently of the culture conditions, EpSlKCs retained β1-integrin expression while K19 expression was almost absent.

	α-SMA	CD184	LRP4
DP cells co-culture (DMEM:KSFM)	0.50 ± 0.29	21.57 ± 9.36	0.50 ± 0.45
DP cells CTRL (DMEM:KSFM)	16.30 ± 9.39	14.43 ± 4.11	0.37 ± 0.09
DP cells CTRL (DMEM)	29.13 ± 12.78	27.80 ± 7.30	1.50 ± 0.71
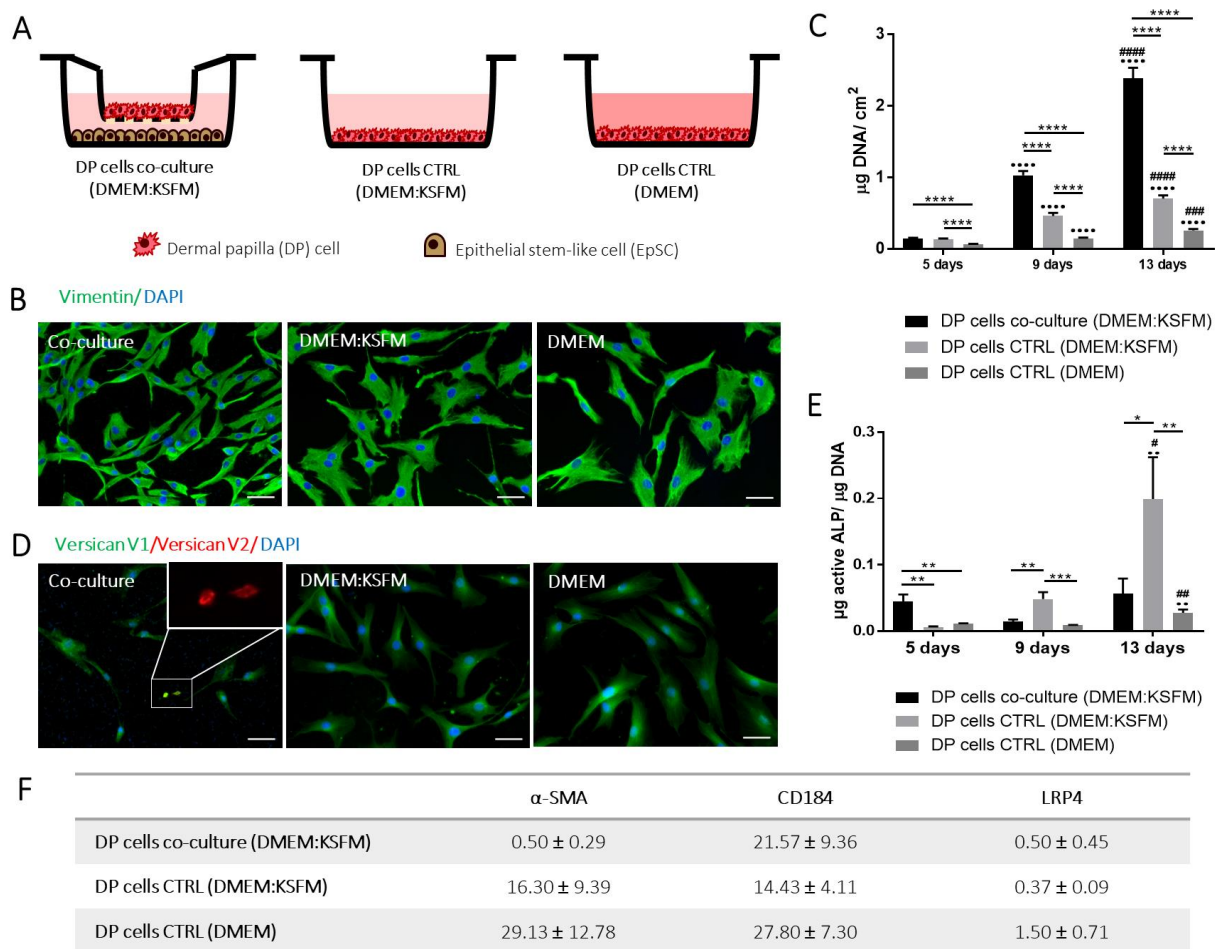
Figure III-3 – Characterization of DP cells co-cultured with EpSlKCs. (A) Schematic representation of the co-culture established with DP cells and EpSlKCs and the respective monoculture controls. **(B)** Representative images of DP cell morphology after staining against the mesenchymal cytoskeleton marker vimentin. **(C)** DNA quantification of DP cells along the culture time. **(D)** Expression of the versican V1 and V2 isoforms by DP cells in the different cultures conditions at day 5 of culture. The presence of versican V2-positive cells was observed when DP cells were co-cultured with EpSlKCs (zoomed-in image). Images were counterstained with DAPI. **(E)** The inductivity of DP cells was assessed through the quantification of active alkaline phosphatase. **(F)** Quantitative flow cytometry data. * $p < 0.05$, ** $p < 0.01$, *** $p < 0.001$, **** $p < 0.0001$; ·· $p < 0.01$ and ···· $p < 0.0001$ *vs.* day 5; # $p < 0.05$, ## $p < 0.01$ and #### $p < 0.0001$ *vs.* day 9. Scale bars are 50 μm.

In addition to the effect of the co-culture over EpSlKCs, we looked to potential alterations on DP cells (Figure III-3A). In DMEM, most of the cells exhibited a flattened and enlarged morphology, typical of higher passage cells, while in co-culture they were smaller, with a polygonal or spindle-shaped morphology (Figure III-3B), evidencing a healthier state [26,27]. When cultured in the control medium, DP cells had an intermediate morphology. Likewise, the cell number at each time point was successively higher from DMEM to the co-culture conditions revealing an increased proliferation capacity both due to the culture medium and presence of EpSlKCs (Figure III-3C). The expression of the V1-isoform of versican was uniform among conditions, whereas the *in vivo* predominant V2-isoform [28] was only observed in co-cultured DP cells (Figure III-3D). Moreover, the amount of active alkaline phosphatase (ALP) in co-culture was significantly higher than in the controls after 5 days in culture, although this effect was not sustained over time (Figure III-3E). A decrease in α-SMA expression was also observed in co-culture, although CD184 and LRP4 expression was not restored (Figure III-3F).

III-3.3. EpSlKCs and DP cells co-culture impacts the release of EMIs mediators

To study if DP cells and EpSlKCs could communicate through the release of mediators, as seen in the native HF EMIs, we studied the release of PDGF-A, VEGF and BMP2, known to influence hair growth [29–31].

PDGF-A production was higher in the co-culture than in the other conditions although successively lower levels were detected along with the culture (Figure III-4A). EpSlKCs in KSFM were also able to secrete PDGF-A, which was at a constant level along the culture time. Secretion of PDGF-A by DP cells was only detected at 9 and 13 days of culture in DMEM. However, in the monocultures established to control medium effects (DMEM: KSFM), PDGF-A values were below the detection level for EpSlKCs, and lower than standard culture for DP cells from day 9 onward. Considering this, it seems that the interaction between EpSlKCs and DP cells in co-culture promotes PDGF-A production, particularly at early time points.

VEGF levels in the co-culture increased with time, and both EpSlKCs and DP cells secreted more VEGF when cultured in the medium used for the co-culture (DMEM: KSFM) than in KSFM and DMEM, respectively (Figure III-4B). Moreover, the amount of VEGF secreted by EpSlKCs decreased along with the culture and increased for DP. Despite this, VEGF levels in co-cultures and in monocultures of DP cells in the same medium were similar independently of the time of culture. Except at day 5, at which

the VEGF amount was significantly lower in the co-culture than in EpSIKCs cultures established in the co-culture medium, it seems that the co-culture does not affect VEGF secretion.
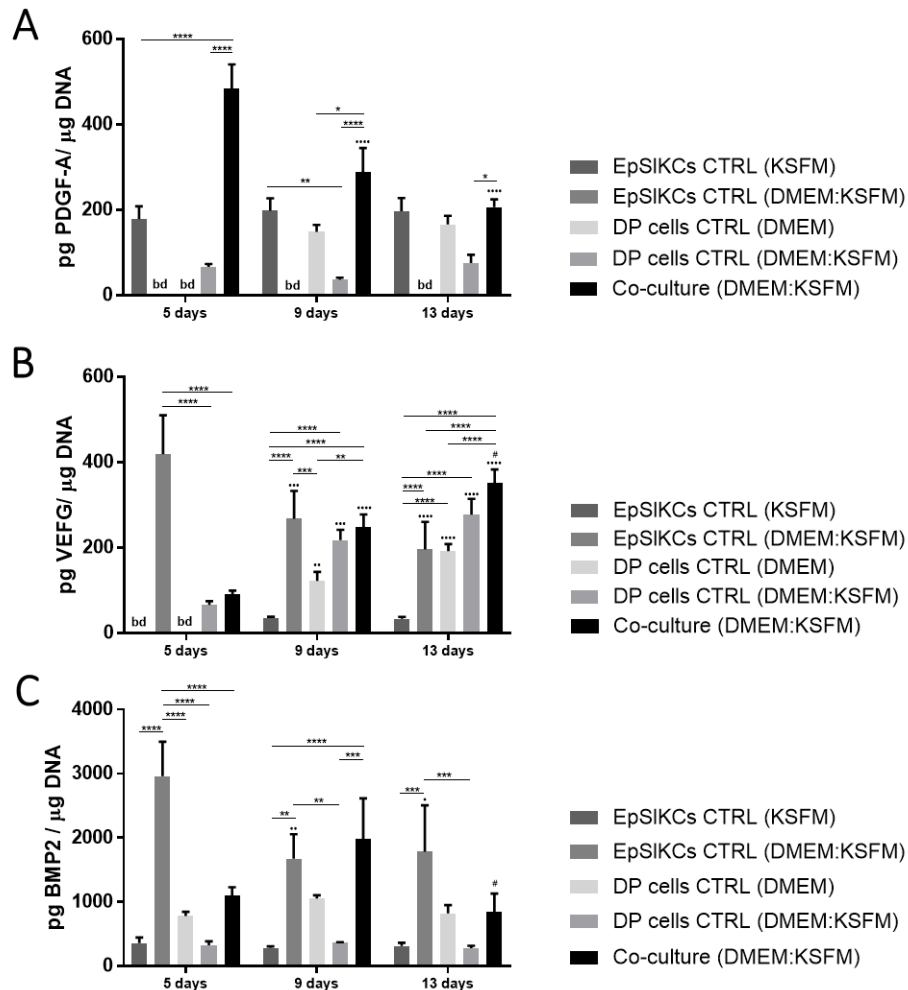
Figure III-4 – Quantification of the amount of (A) PDGF-A, (B) VEGF and (C) BMP2 released by both co-cultured cells and monocultured EpSIKCs and DP cells by ELISA . * p < 0.05, **p < 0.01, *** p < 0.001, **** p < 0.0001; · p < 0.05, ·· p < 0.01, ··· p < 0.001, ···· p < 0.0001 *vs.* day 5; # p < 0.05 *vs.* day 9. bd - bellow detection level.

In what concerns BMP2 secretion, the levels detected in the co-culture peaked on day 9 (Figure III-4C). The amount of BMP2 in the monocultures of EpSIKCs in KSFM was lower than in the monoculture of DP cells in DMEM, and none varied with time. However, the medium used to establish the co-culture had contrary effects on each cell type, respectively promoting and diminishing BMP2 secretion by EpSIKCs and DP cells. Except for day 9, BMP2 levels in the co-cultures were always lower than in the monocultures of EpSIKCs established with the same medium. This indicates that cells in co-culture are communicating, and suggests that DP cells may be responsible for the overall decreased BMP2 production in co-culture.

III-3.4. Generation of HF- and sebaceous gland-like structure by co-grafted EpSIKCs and DP cells

Six weeks after EpSIKCs and DP cells transplantation in mice, we observed the formation of structures that morphologically resembled HF and sebaceous glands (SG) in 3 out of 4 animals (Figure III-5A).
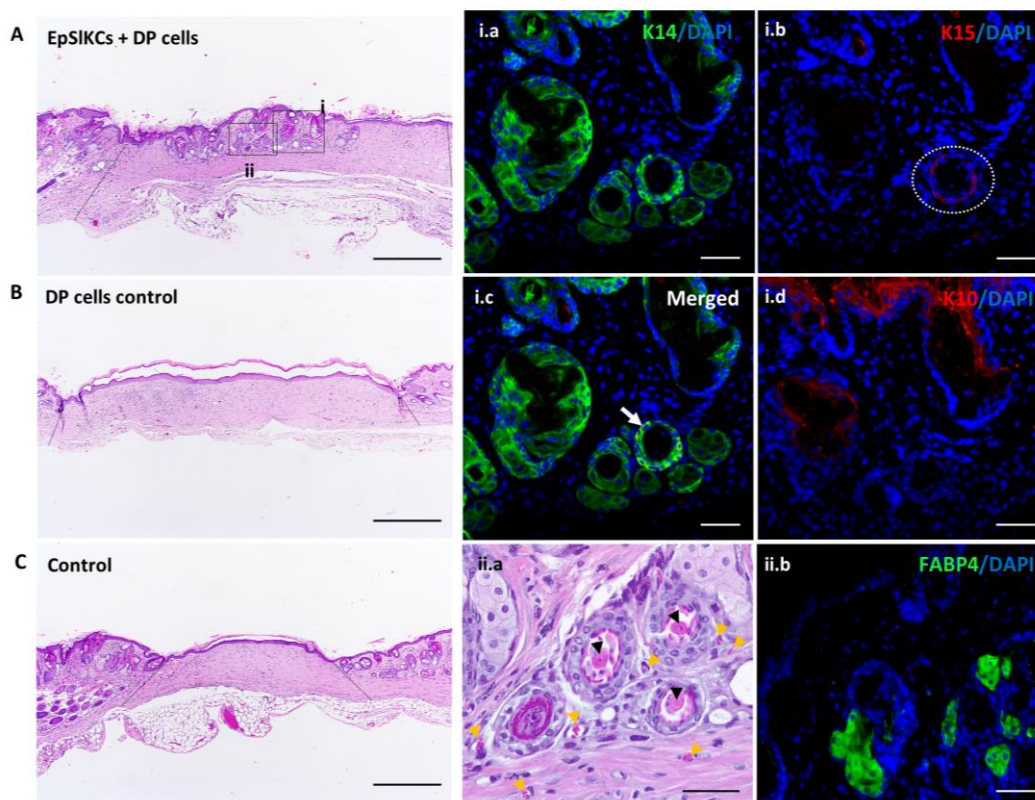
Figure III-5 – HF and SG induction in mice. (A) Representative hematoxylin and eosin (H&E) images of the area where EpSIKCs and DP cells, (B) DP cells alone or (C) vehicle were transplanted (dashed lines indicating the wound area). Immunostaining of the recreated hair follicle (HF)- and sebaceous gland (SG)-like structures against the epithelial markers (i.a) K14, (i.b) K15 (dashed circle) or (i.c) both (white arrow). (i.d) Expression analysis of the differentiation marker K10 within the wound area (ii.a). H&E higher magnification image evidencing an apparently differentiated core (black arrowheads) within the formed structures, and the presence of small vessels around them (yellow arrowheads). (ii.b) Immunodetection of the fatty acid-binding protein 4 (FABP4) within the structures resembling SGs. Scale bars are 500 μm for (A-C) and 50 μm for (i.a-i.d, ii.a-ii.b).

These structures were not observed in the controls (Figure III-5B and C). Immunohistochemical analysis of the recreated structures showed the presence of epithelial layers positive for the basal markers K14 and K15 (Figure III-5 i.a, b), in some cases co-expressed (Figure III-V5 i.c, white arrow), whereas K10 was observed in the skin outermost layer and some of the structures' core (Figure III-5 i.d). The presence of multiple concentric epithelial layers, some of them with what appears to be a

100

keratinized core (Figure III-5 ii.a, black arrowhead) was also observed. This suggests that the differentiation process was initiated but remained incomplete, since features of mature HFs, including hair shaft formation, were not observed. Moreover, small vessels were observed around the recreated structures (Figure III-5 ii.a, yellow arrowhead), while in the SG-like structures the expression of the adipocyte marker FABP4 (Figure III-5 ii.b) demonstrates sebocyte lineage differentiation. Labelling with a DNA-human specific probe failed to detect the presence of human cells within the recreated structures (Supplementary Figure III-2). Nevertheless, the absence of structures in the controls suggests that the human EpSIKCs were critical for HF and SG induction process.

III-4. DISCUSSION

Despite the advances in rodent HF regeneration, through the combination of receptive-epithelial and inductive-mesenchymal cells, human HF regeneration remains elusive. Major hurdles reside in the lack of tissue sources capable of providing immature epithelial cells, and of suitable culture conditions capable of minimizing cell differentiation *in vitro*. Here, we propose the use of EpSIKCs as an alternative to HHFKCs for the recreation of the HF epithelial compartment. Compared to HHFKCs, EpSIKCs represent a more homogeneous cell fraction and larger numbers of EpSIKCs can be obtained from surgically discarded skin, enabling hair regeneration studies/therapies.

Despite their undifferentiated profile and high clonogenic capacity [19], using EpSIKCs for the recreation of the HF epithelial compartment depends on their capacity to crosstalk with DP cells. We showed that DP cells promoted an increase in EpSIKCs numbers, which is in agreement with previous studies confirming that DP cells enhance the growth of co-cultured ORS cells [32,33]. For longer culture times, EpSIKCs in co-culture increased in size and K14-bright cells were lost, suggesting differentiation. Despite this, their proliferation was not affected, which seems to indicate that DP cells are tightly balancing EpSIKCs division and differentiation. This is important considering that DP controls the number of bulb KCs [34], whose continuous proliferation and differentiation are required for hair growth. Another indicator of this control was the release of VEGF and BMP2 by co-cultured cells. Epidermal VEGF is mainly expressed in the upper-to-middle epidermal layers, supporting a positive correlation between VEGF release and epithelial cell differentiation [35,36]. This is also supported by the higher amount of VEGF detected in EpSIKCs cultured in the co-culture medium, in which EpSIKCs have a more differentiated phenotype. Interestingly, VEGF levels in the co-culture increased with time,

which may indicate that EpSIKCs differentiation is occurring. However, their proliferative capacity remained unaffected, once again indicating that EpSIKCs differentiation and proliferation is balanced by DP cells. Also, BMP expression is subtle among proliferating epithelial cells and higher in differentiating cells [37]. Herein we showed that BMP2 secretion in the co-cultures peaked at day 9 while decreasing in the EpSIKCs monocultures established in the same medium, reinforcing the influence of DP cells.

EpSIKCs also improved DP cell proliferation, an effect already reported for rodent KCs [38]. To this might have contributed the marked increase in PDGF-A levels observed in the co-culture, particularly up to 9 days of culture. PDGF-A is a mitogenic factor typically produced by epidermal [39] and follicular keratinocytes [40], capable of stimulating mesenchymal cells proliferation [41]. Most importantly, PDGF-A receptor is activated in the DP during anagen [42] and PDGF-A administration has been demonstrated to induce anagen [42,43]. This suggests that PDGF-A increase in co-culture may not only promote DP cell proliferation but also stimulate their hair growth capacity. In fact, co-culture conditions positive effect on DP cell phenotype was demonstrated by the loss of α-SMA expression. Although commonly referred as a DP cell marker [44], α-SMA is only expressed in 2D cultured DP cells and not *in situ* [45], therefore its near absence in the co-cultures seems an indicator that EpSIKCs are positively influencing DP cells. ALP activity and versican expression, in turn, are well-established markers of DP cell inductivity [44]. The presence of the V2-isoform of versican at early culture times, which is predominant in the native DP [28], and the increased of active ALP in DP cells also suggest an improvement in these cells inductivity. Nevertheless, ALP activity is known to vary along the HF cycle, and differences in DP spatial-temporal ALP activity might correlate with distinct functions along the cycle [44,46]. Furthermore, the release profile of BMP2 also suggests a hair inductive profile by co-cultured DP cells. BMP signaling is an anagen negative regulator [31,47], which needs to be counteracted for HF induction to occur [31,48,49]. Therefore, the lower BMP2 expression observed at day 5, associated with increased PDGF-A levels, suggest that EpSIKCs-DP cells communication *in vitro* may be mimicking early anagen features. This is interesting considering previous reports where ORS cells co-culture with DP cells, precisely for 4-5 days, restored ORS cells trichogenic ability, with DP cells influencing their competence [50,51]. They also demonstrated that previously co-cultured ORS cells promoted HF formation, whereas monocultured ORS cells failed to do it. Remarkably, we observed the recreation of HF- and SG-like structures upon co-grafting of EpSIKCs and human DP cells, regardless of not having been co-cultured, which suggests that EpSIKCs can acquire follicle-specific competence *in vivo* upon interaction with DP cells.

The capacity of interfollicular epidermal cells to differentiate into follicular structures was already demonstrated in the chamber model, after their combination with murine DP cells [17]. However, to our knowledge, this is the first study to demonstrate the recreation of HF- and SG-like structures upon grafting adult human interfollicular KCs and DP cells. Additionally, the capacity of human epithelial cells to generate HF-like structures is higher for neonatal cells than for adult or passaged cells [17], supporting the importance of EpSlKCs immature state. We demonstrated that KSFM-cultured EpSlKCs, as performed before grafting, are kept in a high proliferative state. Moreover, these cells are characterized by high production of PDGF-A, a factor involved in HF formation, and low secretion of the anagen inhibitor BMP2, which may have contributed to the observed response. The recreated structures displayed common features of the native HF, including the presence of cell layers co-expressing K15 and K14, as observed in the bulge and upper ORS, or only expressing K14 as in the HF lower ORS and respective progeny. We also observed the presence of blood vessels around the structures, likely a consequence of EpSlKCs and DP cells production of VEGF, essential to induce and maintain the microvasculature around the HF and in the dermal compartment [30,52]. Nevertheless, the follicle-like structures failed to produce a hair shaft, demonstrating that hair formation remained incomplete. Furthermore, we did not detect human cells within the recreated structures or in the grafting area, which has potentially limited the required signaling for the complete hair formation. The absence of the transplanted cells is not completely unexpected considering that, unlike other models, the chamber assay represents a wound healing environment [4], with high cellular turnover. Moreover, although the chamber prevents the contribution of host cells for the initial regenerative process, dissociated human cells are easily replaced by host KCs after wound closure in this model [53]. Nonetheless, the lack of structures in the controls demonstrates that human EpSlKCs were critical for hair neogenesis initial steps.

III-5. CONCLUSIONS

Taken together, our results show that EpSlKCs are phenotypically similar do HHFKCs and can crosstalk and beneficially impact DP cells *in vitro*. When combined with cultured DP cells *in vivo*, EpSlKCs demonstrated their competence by promoting the recreation of structures that resembled the HF and SG initial morphogenetic events. Thus, EpSlKCs represent an alternative immature and available epithelial cell fraction for the recreation of the HF epithelial compartment.

III-6. REFERENCES

1. Millar, S. E. Molecular Mechanisms Regulating Hair Follicle Development. *J. Invest. Dermatol.* **118**, 216–225 (2002).

2. Sennett, R. & Rendl, M. Mesenchymal–epithelial interactions during hair follicle morphogenesis and cycling. *Semin. Cell Dev. Biol.* **23**, 917–927 (2012).

3. Ohyama, M. & Veraitch, O. Strategies to enhance epithelial-mesenchymal interactions for human hair follicle bioengineering. *Journal of Dermatological Science* **70**, 78–87 (2013).

4. Balañá, M. E. Epidermal stem cells and skin tissue engineering in hair follicle regeneration. *World J. Stem Cells* **7**, 711–727 (2015).

5. Leirós, G. J. *et al.* Dermal Papilla Cells Improve the Wound Healing Process and Generate Hair Bud-Like Structures in Grafted Skin Substitutes Using Hair Follicle Stem Cells. *Stem Cells Transl. Med.* **3**, 1209–1219 (2014).

6. Limat, A. *et al.* Outer root sheath (ORS) cells organize into epidermoid cyst-like spheroids when cultured inside Matrigel: a light-microscopic and immunohistological comparison between human ORS cells and interfollicular keratinocytes. *Cell Tissue Res.* **275**, 169–176 (1994).

7. Havlickova, B., Biro, T., Mescalchin, A., Arenberger, P. & Paus, R. Towards optimization of an organotypic assay system that imitates human hair follicle-like epithelial-mesenchymal interactions. *Br. J. Dermatol.* **151**, 753–765 (2004).

8. Wu, J.-J. *et al.* Hair follicle reformation induced by dermal papilla cells from human scalp skin. *Arch. Dermatol. Res.* **298**, 183–190 (2006).

9. Havlickova, B. *et al.* A Human Folliculoid Microsphere Assay for Exploring Epithelial–Mesenchymal Interactions in the Human Hair Follicle. *J. Invest. Dermatol.* **129**, 972–983 (2009).

10. Lindner, G., Horland, R., Wagner, I., Ataç, B. & Lauster, R. De novo formation and ultra-structural characterization of a fiber-producing human hair follicle equivalent in vitro. *J. Biotechnol.* **152**, 108–112 (2011).

11. Miao, Y., Sun, Y. Bin, Liu, B. C., Jiang, J. D. & Hu, Z. Q. Controllable Production of Transplantable Adult Human High-Passage Dermal Papilla Spheroids Using 3D Matrigel Culture. *Tissue Eng. Part A* **20**, 2329–2338 (2014).

12. Aasen, T. & Belmonte, J. C. I. Isolation and cultivation of human keratinocytes from skin or plucked hair for the generation of induced pluripotent stem cells. *Nat. Protoc.* **5**, 371–382

(2010).

13.   Ohyama, M. Characterization and isolation of stem cell-enriched human hair follicle bulge cells. *J. Clin. Invest.* **116**, 249–260 (2005).

14.   Moll, I. Proliferative Potential of Different Keratinocytes of Plucked Human Hair Follicles. *J. Invest. Dermatol.* **105**, 14–21 (1995).

15.   Limat, A. & Noser, F. K. Serial Cultivation of Single Keratinocytes from the Outer Root Sheath of Human Scalp Hair Follicles. *J. Invest. Dermatol.* **87**, 485–488 (1986).

16.   Seo, Y.-K. *et al.* Development of isolation and cultivation method for outer root sheath cells from human hair follicle and construction of bioartificial skin. *Biotechnol. Bioprocess Eng.* **8**, 151–157 (2003).

17.   Ehama, R. *et al.* Hair Follicle Regeneration Using Grafted Rodent and Human Cells. *J. Invest. Dermatol.* **127**, 2106–2115 (2007).

18.   Li, A., Simmons, P. J. & Kaur, P. Identification and isolation of candidate human keratinocyte stem cells based on cell surface phenotype. *Proc. Natl. Acad. Sci.* **95**, 3902–3907 (1998).

19.   Cerqueira, M. T., Frias, A. M., Reis, R. L. & Marques, A. P. Boosting and Rescuing Epidermal Superior Population from Fresh Keratinocyte Cultures. *Stem Cells Dev.* **23**, 34–43 (2014).

20.   Gledhill, K., Gardner, A. & Jahoda, C. A. B. Isolation and Establishment of Hair Follicle Dermal Papilla Cell Cultures. in *Methods in molecular biology (Clifton, N.J.)* vol. 989 285–292 (Methods Mol Biol, 2013).

21.   Watt, F., Simon, B. & Prowse, D. Cultivation and Retroviral Infection of Human Epidermal Keratinocytes. in *Cell Biology* 133–138 (Elsevier, 2006).

22.   Jensen, K. B., Driskell, R. R. & Watt, F. M. Assaying proliferation and differentiation capacity of stem cells using disaggregated adult mouse epidermis. *Nat. Protoc.* **5**, 898–911 (2010).

23.   Michel, M. *et al.* Keratin 19 as a biochemical marker of skin stem cells in vivo and in vitro: Keratin 19 expressing cells are differentially localized in function of anatomic sites, and their number varies with donor age and culture stage. *J. Cell Sci.* **109**, 1017–1028 (1996).

24.   Bertolero, F., Kaighn, M. E., Camalier, R. F. & Saffiotti, U. Effects of serum and serum-derived factors on growth and differentiation of mouse keratinocytes. *Vitr. Cell. Dev. Biol.* **22**, 423–428 (1986).

25.   Borowiec, A.-S., Delcourt, P., Dewailly, E. & Bidaux, G. Optimal Differentiation of In Vitro Keratinocytes Requires Multifactorial External Control. *PLoS One* **8**, e77507 (2013).

26.   Ohyama, M., Kobayashi, T., Sasaki, T., Shimizu, A. & Amagai, M. Restoration of the intrinsic

properties of human dermal papilla in vitro. *J. Cell Sci.* **125**, 4114–4125 (2012).

27.   Upton, J. H. *et al.* Oxidative Stress–Associated Senescence in Dermal Papilla Cells of Men with Androgenetic Alopecia. *J. Invest. Dermatol.* **135**, 1244–1252 (2015).

28.   Soma, T., Tajima, M. & Kishimoto, J. Hair cycle-specific expression of versican in human hair follicles. *J. Dermatol. Sci.* **39**, 147–154 (2005).

29.   Takakura, N., Yoshida, H., Kunisada, T., Nishikawa, S. & Nishikawa, S.-I. Involvement of Platelet-Derived Growth Factor Receptor-α in Hair Canal Formation. *J. Invest. Dermatol.* **107**, 770–777 (1996).

30.   Yano, K., Brown, L. F. & Detmar, M. Control of hair growth and follicle size by VEGF-mediated angiogenesis. *J. Clin. Invest.* **107**, 409–417 (2001).

31.   Botchkarev, V. A. *et al.* Noggin is a mesenchymally derived stimulator of hair-follicle induction. *Nat. Cell Biol.* **1**, 158–164 (1999).

32.   Limat, A. *et al.* Soluble factors from human hair papilla cells and dermal fibroblasts dramatically increase the clonal growth of outer root sheath cells. *Arch. Dermatol. Res.* **285**, 205–210 (1993).

33.   Itami, S., Kurata, S., Sonoda, T. & Takayasu, S. Interaction between dermal papilla cells and follicular epithelial cells in vitro: effect of androgen. *Br. J. Dermatol.* **132**, 527–32 (1995).

34.   Li, W. *et al.* VEGF induces proliferation of human hair follicle dermal papilla cells through VEGFR-2-mediated activation of ERK. *Exp. Cell Res.* **318**, 1633–1640 (2012).

35.   Viac, J., Palacio, S., Schmitt, D. & Claudy, A. Expression of vascular endothelial growth factor in normal epidermis, epithelial tumors and cultured keratinocytes. *Arch. Dermatol. Res.* **289**, 158–163 (1997).

36.   Goldman, C. K., Tsai, J.-C., Soroceanu, L. & Gillespie, G. Y. Loss of Vascular Endothelial Growth Factor in Human Alopecia Hair Follicles. *J. Invest. Dermatol.* **104**, 18–20 (1995).

37.   Kulessa, H. Inhibition of Bmp signaling affects growth and differentiation in the anagen hair follicle. *EMBO J.* **19**, 6664–6674 (2000).

38.   Inamatsu, M., Matsuzaki, T., Iwanari, H. & Yoshizato, K. Establishment of rat dermal papilla cell lines that sustain the potency to induce hair follicles from afollicular skin. *J Invest Dermatol* **111**, 767–775 (1998).

39.   Ansel, J. C. *et al.* Human keratinocytes are a major source of cutaneous platelet-derived growth factor. *J. Clin. Invest.* **92**, 671–678 (1993).

40.   Kamp, H., Geilen, C. C., Sommer, C. & Blume-Peytavi, U. Regulation of PDGF and PDGF

receptor in cultured dermal papilla cells and follicular keratinocytes of the human hair follicle. *Exp. Dermatol.* **12**, 662–672 (2003).

41. Karlsson, L., Bondjers, C. & Betsholtz, C. Roles for PDGF-A and sonic hedgehog in development of mesenchymal components of the hair follicle. *Development* **126**, 2611–2621 (1999).

42. Festa, E. *et al.* Adipocyte lineage cells contribute to the skin stem cell niche to drive hair cycling. *Cell* **146**, 761–771 (2011).

43. Tomita, Y., Akiyama, M. & Shimizu, H. PDGF isoforms induce and maintain anagen phase of murine hair follicles. *J. Dermatol. Sci.* **43**, 105–115 (2006).

44. Yang, C.-C. & Cotsarelis, G. Review of hair follicle dermal cells. *J. Dermatol. Sci.* **57**, 2–11 (2010).

45. Jahoda, C. A. B., Reynolds, A. J., Chaponnier, C., Forester, J. C. & Gabbiani, G. Smooth muscle α-actin is a marker for hair follicle dermis in vivo and in vitro. *J. Cell Sci.* **99**, 627–636 (1991).

46. Iida, M., Ihara, S. & Matsuzaki, T. Hair cycle-dependent changes of alkaline phosphatase activity in the mesenchyme and epithelium in mouse vibrissal follicles. *Dev. Growth Differ.* **49**, 185–195 (2007).

47. Botchkarev, V. A. *et al.* Noggin is required for induction of the hair follicle growth phase in postnatal skin. *FASEB J.* **15**, 2205–2214 (2001).

48. Schmidt-Ullrich, R. & Paus, R. Molecular principles of hair follicle induction and morphogenesis. *BioEssays* **27**, 247–261 (2005).

49. Fuchs, E. Scratching the surface of skin development. *Nature* **445**, 834–842 (2007).

50. Chan, C.-C., Fan, S. M.-Y., Wang, W.-H., Mu, Y.-F. & Lin, S.-J. A Two-Stepped Culture Method for Efficient Production of Trichogenic Keratinocytes. *Tissue Eng. Part C Methods* **21**, 1070–1079 (2015).

51. Bak, S. S. *et al.* Restoration of hair-inductive activity of cultured human follicular keratinocytes by co-culturing with dermal papilla cells. *Biochem. Biophys. Res. Commun.* **505**, 360–364 (2018).

52. Kozlowska, U. *et al.* Expression of vascular endothelial growth factor (VEGF) in various compartments of the human hair follicle. *Arch. Dermatol. Res.* **290**, 661–668 (1998).

53. Ferraris, C., Bernard, B. A. & Dhouailly, D. Adult epidermal keratinocytes are endowed with pilosebaceous forming abilities. *Int. J. Dev. Biol.* **41**, 491–498 (1997).

III-7.   SUPPLEMENTARY INFORMATION

III-7.1. Supplementary Materials and Methods

III-7.1.1.   Chromogenic *in situ* hybridization

The presence of human cells within the wound area was assessed using a human-specific DNA oligo probe and the respective detection system (BIO-HRP REMBRANDT® Universal DISH detection kit, PanPath). Briefly, dewaxed sections were blocked with a 3% solution of hydrogen peroxide (15 min, RT) and proteolytic digestion was performed using a pepsin-HCL solution for 30 min at 37°C, followed by the dehydration in graded ethanol series. The specimens were then air-dried and 1 drop of the probe was applied and covered with a coverslip. Denaturation was performed at 95°C for 5 min, and hybridization for 16h at 37°C in a moisturized environment. Samples were then washed in TBS buffer and incubated for 10 min with the stringency wash buffer (PanWash). After rinsing with TBS, the detection was performed by incubation with the BIO-HRP conjugate (30 min, 37°C). The samples were then washed 3 times in TBS and water and the chromogenic detection was performed using the kit AEC substrate detection system, with color development for 10 min at 37°C (dark). The reaction was stopped with water and the samples observed under a DM750 light microscope (Leica).

III-7.2. Supplementary Figures
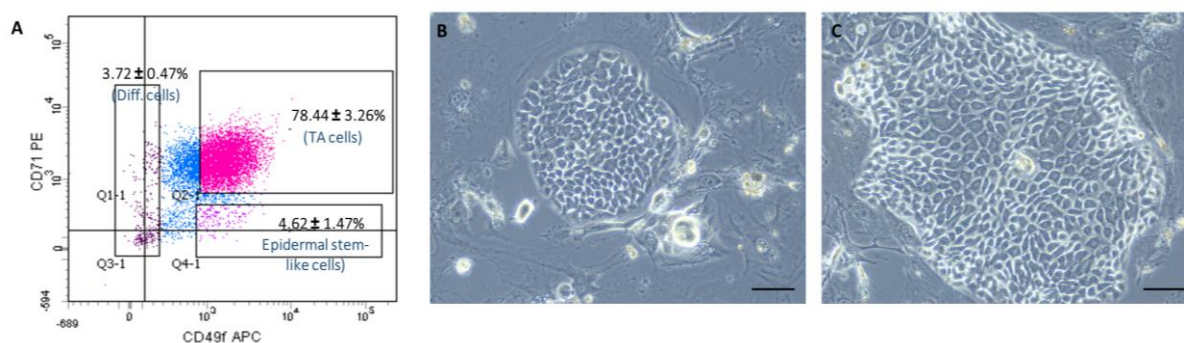
Supplementary Figure III-1 – Phenotype of the CD49f ʰⁱᵍʰ/CD71ᵈⁱᵐ subpopulation. (A) Representative image of fluorescent activated cell sorting (FACS) dotplot of the whole population of epidermal keratinocytes and the gatting of the subpopulations of interest, based on the expression of the CD49f and CD71 markers, accompanied by the respective cellular percentages. CD49f ʰⁱᵍʰ/CD71ᵈⁱᵐ cells represent epidermal stem-like cells, CD49f ʰⁱᵍʰ/CD71ʰⁱᵍʰ subpopulation are transit-amplifying (TA) cells, while differentiated (Diff.) cells are characterized by a CD49f ᵈⁱᵐ phenotype. Epidermal stem-like cells derived colonies growing in the inactivated feeders (B) 4 and (C) 6 days after seeding. Scale bars are 50 μm.
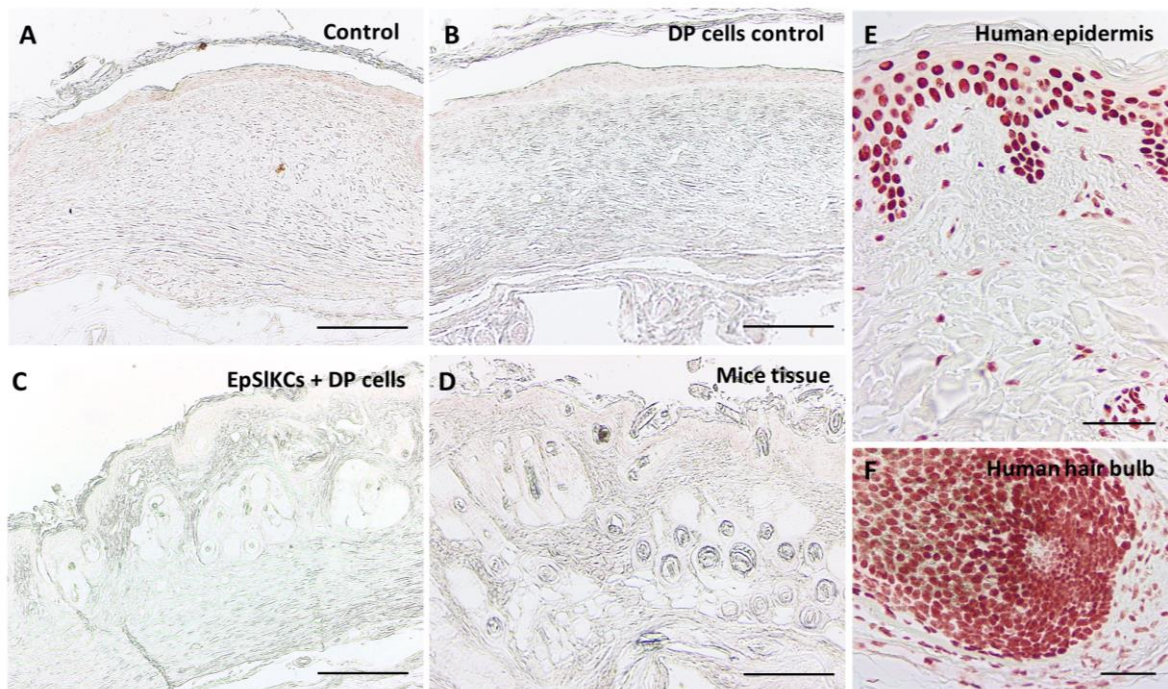
Supplementary Figure III-2 – Human cell detection within skin explants from the hair reconstitution assay. Staining with a human-specific probe demonstrates that, 6 weeks after cells injection, there were no human cells remaining in the wound area in the controls (A, B) and in the condition where interfollicular epidermal stem-like keratinocytes (EpSlKCs) and DP cells were co-grafted (C). Likewise, no staining was observed in the mice tissue (D), whereas nuclear orange-pink staining was observed in human positive control specimens (E, F), demonstrating the specificity of the staining. Scale bars are 200 μm, for (A-D) and 50 μm for (E, F).

CHAPTER IV

RESCUING KEY NATIVE TRAITS IN CULTURED DERMAL PAPILLA CELLS FOR HUMAN HAIR REGENERATION

CHAPTER IV

RESCUING KEY NATIVE TRAITS IN CULTURED
DERMAL PAPILLA CELLS FOR HUMAN HAIR REGENERATION‡

ABSTRACT

The dermal papilla (DP) represents the major regulatory entity within the hair follicle (HF), inducing hair formation and growth through reciprocal interactions with epithelial cells. However, human DP cells rapidly lose their hair inductive ability when removed from their niche and cultured in an epithelium-deficient environment. Here, conditioned medium collected from skin keratinocytes (KCs-CM) was used to culture DP cells both in 2D and 3D culture conditions and investigate how it impacts these cells native properties and inductive phenotype. Further, the hair-inductive capacity of DP cells precultured with KCs-CM was tested in a hair reconstitution assay, after co-grafting with keratinocytes in mice. We demonstrate that KCs-CM contributes to restoring the inductivity of cultured human DP cells in a more effective mode than conventional 3D cultures. This is supported by the higher active alkaline phosphatase (ALP) levels in DP cells, the improved self-aggregative capacity and the reduced expression of α-SMA and the V1-isoform of versican. Moreover, DP cells cultured with KCs-CM displayed a secretome profile (VEGF, BMP2, TGF-β1, IL-6) that matches the one observed during anagen. KCs-CM also enhanced DP cell proliferation, while recovering the cells from a morphology characteristic of high passage cells. The improvement in ALP activity was maintained in 3D spheroidal cultures, even after KCs-CM retrieval, and was superior to the effect of the gold-standard culture conditions. Moreover, DP cells cultured with KCs-CM and grafted with human keratinocytes supported the formation of HF- and sebaceous gland-like structures in mice. The proposed strategy encourages future cell-based strategies for HF regeneration not only in the context of hair-associated disorders but also in the management of wounds to aid in restoring critical skin regulatory appendages.

IV-1. INTRODUCTION

The dermal papilla (DP) is the key mesenchymal compartment involved in hair growth. It is organized as a cluster of highly specialized cells located at the base of the hair follicle (HF), a privileged position from where the DP activates and controls hair growth, through reciprocal interactions with the neighboring epithelium [1–3]. The use of DP cells for HF regenerative approaches relies both on their propagation and in the maintenance of their inductive properties in culture, to ensure that a proper number of functional cells is obtained. However, the quick loss of inductivity that human DP cells experience in culture [4], and from which they don't spontaneously recover, has been hindering the development of DP cell-based strategies for HF regeneration. So far, the most efficient method to restore the inductivity of human DP cells is the artificial recreation of their spatial organization and intercellular contacts using 3D spheroid cultures [4,5]. While it results in a partial recovery of the transcriptome [4] and native signature [5] of human DP cells *in vitro*, the hair-induction rate of these DP spheroids in a human-to-human recombinant assay was only of 15% [4]. This illustrates the difficulty in regenerating human hair, as well as the need to further develop new approaches to improve the inductive properties of human DP cells.

Despite the complexity of the mechanisms that govern hair growth and cycling, the deep involvement of the canonical Wnt/β-catenin, BMP and FGF signaling pathways is well-established [6]. Therefore, attempts to improve human DP cell properties by stimulation of these pathways with specific biomolecules have been reported. The addition of FGF2 and 6-bromoindirubin-39-oxime, a Wnt activator, was shown to improve alkaline phosphatase (ALP) activity [7], a recognized DP cell inductive marker [8]. Another work showed that an optimized combination of 6-bromoindirubin-39-oxime, BMP2 and basic FGF was able to improve ALP activity as well as to maintain the gene expression of freshly isolated DPs however, the obtained cells still failed to form hairs *in vivo* [9].

More recently, Won *et al.* [10] demonstrated that the use of the concentrated conditioned medium (CM) collected from human α6-integrin^high/CD71^low keratinocytes (KCs) has a hair growth-promoting effect in mice. The CM contained different growth factors, namely vascular endothelial growth factor (VEGF) and platelet-derived growth factor-A (PDGF-A), among others. The topical injection of these factors, in telogen-synchronized mice, replicated the CM effect confirming improved hair growth due to earlier telogen-to-anagen transition. This study supports what has been previously shown regarding the importance of epithelial-mesenchymal interactions (EMIs) for hair growth promotion [6]. But whether

the recreation of this complex epithelial signaling *in vitro* is beneficial towards the recovery of the inductive phenotype of human DP cells, and ultimately hair regeneration is yet to be demonstrated. Studies with co-culture systems using human cells [11–13] did not investigate epithelial cell effects on DP cells. In turn, KCs-CM was shown to improve the proliferation of human DP cells [10,14], but its impact on the hair inductive-associated phenotype or trichogenic ability was not addressed. Considering this, we hypothesized that by culturing human DP cells with KCs-CM some of the epithelial-mesenchymal interactions would be recreated, promoting the restoration of an inductive phenotype while simultaneously supporting their proliferation. We uncover the effects of KCs-CM in the recovery of DP cell inductive properties and native phenotype under the standard 2D culture conditions used for their expansion. The persistence of the effect over DP cell inductivity *in vitro* was further demonstrated even after KCs-CM stimulus withdrawal, which is determinant to maximize the effectiveness of DP cells in long term. We propose an efficient and simple approach to attain human DP cells with an improved phenotype and capable of inducing the formation of HF-like structures.

IV-2. MATERIALS AND METHODS

IV-2.1. Cell isolation and culture

J2-3T3 fibroblasts were cultured in DMEM supplemented with 10% adult bovine serum, up to passage 10. Feeders were prepared with 2.4×10^4 cells/cm^2 after inhibition with mitomycin C (4 µg/mL) for 2h 30min at 37°C. KCs were isolated from human skin tissue obtained from patients who underwent abdominoplasty surgery in Hospital da Prelada (Porto, Portugal), as previously described [15], and cultured in Keratinocyte Serum-free Medium (KSFM, Gibco) with Y-27632 (10 µM; STEMCELL Technologies). After the first passage KCs were resuspended in FAD medium [DMEM/Ham's F12 medium (3:1 ratio) supplemented with 1.8×10^4 M adenine, 10% non-inactivated fetal bovine serum (FBS), 0.5 µg/mL hydrocortisone, 10^{-10} M cholera toxin, 10 ng/ml epidermal growth factor, 5 µg/ml insulin and 1.8 mM CaCl$_2$] and $1.0\text{-}1.4 \times 10^5$ cells were seeded onto a feeder layer. Scalp samples were obtained from hair transplantation surgeries performed at Sanare - Unicapilar Clínica (Porto, Portugal) and used to isolate DP cells by standard microdissection technique [16]. Explants were initially cultured in DMEM 20% FBS. After passage, DP cells were cultured in DMEM 10% FBS and used from passage 4 to 6. All cells were cultured in a humidified incubator at 37°C and 5 %CO$_2$, with medium changes every 2-3 days.

IV-2.2. Conditioned medium collection from keratinocytes and usage in dermal papilla cell cultures

KCs (1.0-1.4×10^5) at passage 1 were seeded in 75 cm^2 flasks previously prepared with feeder cells. Approximately after one week, KCs were removed from the feeder layer and 2.5×10^6 cells were cultured in 150 cm^2 culture flasks with 20 mL of KSFM with Y-27632. CM was collected at day 6 of culture, after a medium change at day 4. The collected supernatant was filtered through a 0.22 μm syringe filter and stored at -20°C until further use, up to one month. DP cells were cultured in DMEM with 10% FBS overnight. In the following day, the medium was replaced by the collected CM mixed with an equal volume of fresh DMEM 10% FBS (KCs-CM). DP cells cultured in their standard medium - DMEM 10% FBS - (DMEM), or in DMEM mixed with an equal volume of KSFM with Y-27632 - (Medium CTRL) were prepared as controls. Culture medium was refreshed every two days, up to 5 days.

IV-2.3. DNA and active alkaline phosphatase quantification

DP cells were lysed with ultra-pure water with 0.01% sodium dodecyl sulfate (1h, 37°C), followed by freezing at -80°C. Cells were then scrapped, and DNA levels quantified using the Quant-iT™ PicoGreen® dsDNA Assay Kit (Thermo Fisher Scientific) and the amount of active ALP was quantified using the Alkaline Phosphatase Detection Kit (Sigma-Aldrich).

IV-2.4. Detection of alkaline phosphatase-active cells

Adherent cells were fixed in 10% formalin (15 min, RT) and the *p*-nitro-blue tetrazolium chloride and 5-bromo-4-chloro-3'-indolyphosphate (NBT/BCIP) substrate was prepared by diluting 5 μL of NBT and 3.75 μL of BCIP (Roche) per mL of staining buffer (100 mM NaCl, 100 mM Tris-HCl pH 9.5 and 50 mM MgCl$_2$ in water). The substrate was applied for 20 min (RT, dark) and washed with water before observation.

IV-2.5. Immunocytochemistry

Fixed DP cells were permeabilized with 0.2% Triton X-100 for 15 min at RT (in case of intracellular staining) or with 1% Triton X-100 for 30 min on ice (in case of nuclear staining), and incubated with 3% bovine serum albumin (BSA, Sigma-Aldrich) in PBS for 45 min (RT) to block nonspecific staining.

Primary antibodies (Table IV-1) were diluted in 1% BSA solution containing 0.2% Triton X-100 and incubated for 1h (RT). Samples were then washed with PBS and incubated with Alexa Fluor (AF) (488/594)-conjugated secondary antibodies (1:500; Molecular Probes) prepared in the same conditions as primary antibodies. The cells' F-actin fibers were stained with phalloidin-TRITC (1:100, Sigma-Aldrich) and nuclei with 4',6'-diamino-2-phenylindole (DAPI) (0.02 mg/mL Biotium). Samples were analyzed and images acquired with an Axioplan Imager Z1m microscope (Zeiss).

IV-2.6. Flow cytometry

For cell surface marker analysis, DP cells were resuspended in DMEM 10% FBS and incubated with the CD184-APC (1:20; BioLegend) or the LRP4-PE (1:10; Miltenyi Biotec) antibodies respectively for 30 min (RT) or 10 min (ice). For intracellular staining, the FIX&PERM™ Cell Permeabilization Kit (Thermo Fisher Scientific) was used. Cells were first fixed with reagent A (15 min, RT), washed in PBS, then permeabilized with reagent B and incubated (20 min, RT) with the α-SMA-FITC (1:33; Abcam) or LEF1-AF488 (1:50; Cell Signaling Technology) antibodies. Cell suspensions were analyzed with a FACSCalibur flow cytometer (BD Biosciences) using the Cell Quest Software for data analysis.

IV-2.7. Collagen and non-collagenous protein staining and quantification

The production of collagen (COL) and non-collagenous (NCOL) proteins by DP cells was measured using the Sirius Red/Fast Green Collagen Staining Kit (Chondrex Inc.). Formalin-fixed cells were immersed in the dye solution (30 min, RT) and washed in water until it runs clear. Representative images were acquired with a Leica DM750 microscope (Leica). Further quantification was performed by extracting the die with the kit destaining solution and measuring the samples optical density at 540 nm (Sirius red, COL proteins) and 605 nm (fast green, NCOL proteins). The color equivalences [17] were used to calculate the quantity of COL and NCOL proteins produced.

IV-2.8. Glycosaminoglycans staining and quantification

Fixed cells were rinsed in 3% acetic acid and further stained with 1% Alcian Blue (pH 2.5, Sigma-Aldrich) for 30 min at RT. After washing in water, the presence of GAGs was examined, and representative images were acquired. Sulfated GAGs production was quantified using the 1,9-

dimethylmethylene blue (DMMB) assay [18]. Briefly, DP cells were digested at 60°C (overnight) in a 0.05% of papain and 0.096% of *N*-acetyl cysteine solution prepared in 200 mM of phosphate buffer with 1 mM EDTA (pH 6.8). Samples were then centrifuged (13000 rpm, 10 min) and the supernatants incubated with 250 μl of DMMB solution (16 mg DMMB in 1L water containing 3.04 g glycine and 1.6 g NaCl, pH 3.0). Optical density at 530 nm was read using a microplate reader (Synergy HT, BioTek), and DMMB-GAGs complexes amount was extrapolated using a chondroitin sulfate standard curve.

IV-2.9. Enzyme-linked immunosorbent assay

After 5 days in culture, the DP cell medium was replaced by the equivalent FBS-free media and cultured for 24h. The supernatant was then collected, centrifuged (3000 rpm, 10 min) and stored at -80°C in single-use aliquots. VEGF ELISA Development Kit, BMP2 Standard ELISA Development Kit (Peprotech), PDGF-A DuoSet ELISA, IL-6 DuoSet ELISA (R&D Systems) and TGF-β1 Elisa kit (Invitrogen) were used according to the manufacturer's instructions. Control wells with FBS-free media incubated in the same conditions but without cells were used to determine the amount of each biomolecule in the different media used.

IV-2.10. Self-aggregation assay

Fixed cells were washed in PBS and incubated with DAPI for 15 min at RT. The nuclei were visualized under a Zeiss Axio Observer microscope and 10 pictures/triplicate were taken at different fields. Nuclei staining was used to assess DP cell aggregation using the CellProfiler™ 3.0.0 [19]. Images were first converted to greyscale, and the nuclei signal identified by applying Otsu thresholding algorithm [20] to differentiate signal from background. Cells were regarded as adjacent if the distance between their nuclei was below 8 pixels. Groups of 50 or more adjacent cells were considered an aggregate.

IV-2.11. Spheroid formation assay

After culture with KCs-CM, 1x10^4 DP cells were seeded in round bottom ultra-low attachment 96-well plates (Corning), whereas DP cells cultured in DMEM or Medium CTRL were used as controls. Cells were cultured in the respective culture medium, under standard culture conditions (37°C, 5% CO_2), and

time-lapse microscopy (Axio Observer, Zeiss) was used to record spheroid formation in the center of the well. The 2D area occupied by the cells was quantified at different time points using the ZEN 2 software (Zeiss).

IV-2.12. 3D spheroid culture and analysis

DP cells precultured in KCs-CM were seeded in round bottom ultra-low attachment 96-well plates at a density of 5×10^3 cells/mL, and cultured in 50 µL DMEM 10% FBS. DP cells precultured in control media (DMEM or Medium CTRL) were also used as controls. Upon 4 days of culture, the spheroids were washed in PBS and collected. The quantification of DNA and the amount of active ALP were performed as described. A 5 s sonication step in ice was performed to guarantee the complete disintegration of the spheroid prior quantification. The same cell lysates were used for total protein quantification, using a Bradford-based Protein Dye (BioRad). Briefly, samples were diluted in water with 0.01% Triton X-100, and 4-parts of the diluted sample were added with 1-part of dye reagent. The absorbance was read at 595 nm and protein content was interpolated against a BSA-standard curve.

IV-2.13. Hair reconstitution assay

6 mm full-thickness wounds were made on the back of immunodeficient nude mice (athymic Nude-Foxn1^{nu}, Charles River) and silicon chambers were inserted under the skin (one chamber per animal) [21]. A mixture of 5.0×10^6 CM-precultured DP cells and 2.5×10^6 KCs were injected into the chamber. Cell suspensions of 5×10^6 CM-precultured DP cells or vehicle (FAD medium) were injected as controls. The top of the silicon chambers was cut off after one week and the chamber was completely removed two weeks after the injection of the cells. The animals were euthanized six weeks after surgery and the wound area and surrounding tissue were collected for histological analysis.

IV-2.14. Histological and immunological stainings

Paraffin-embedded sections of 4 µm (*in vivo* samples) or 10 µm (spheroids) were dewaxed in xylene, rehydrated and heat-mediated antigen retrieval (sodium citrate buffer, pH 6.0) was performed before starting the immunolabelling procedure, as previously described in the "Immunocytochemistry" section. For primary antibodies (Table II-5) raised on mice, a mouse-on-mouse kit (Vector Laboratories)

was used to block background caused by endogenous mouse immunoglobulins. Sections stained with Haematoxylin & Eosin (H&E) were analyzed with a Leica DM750 microscope while the remaining specimens were analyzed with an Axio Imager Z1m microscope (Zeiss).

IV-2.15. *In situ* hybridization

The presence of human cells within the wound area was assessed using the human-specific DNA oligo probe of the BIO-HRP REMBRANDT® Universal DISH detection kit (PanPath). Briefly, unspecific staining in dewaxed sections was blocked with a 3% solution of hydrogen peroxide (15 min, RT). Proteolytic digestion was then performed using a pepsin-HCL solution for 30 min at 37°C, followed by dehydration in graded ethanol solutions. Samples were then air-dried and 1 drop of the probe was applied and covered with a coverslip. DNA denaturation was performed at 95°C for 5min, and hybridization was let to occur for 16h at 37°C in a moisturized environment. Samples were then washed in Tris-buffered saline (TBS) and incubated for 10 min with the stringency wash buffer. After rinsing with TBS, the detection was performed using the kit AEC substrate detection system. Color was let to develop for 10 min at 37°C (dark). Samples were washed with water and observed under a DM750 light microscope (Leica).

IV-2.16. Statistical analysis

Experiments were performed using DP cells isolated from three donors and CM variability was ensured by collection from KCs isolated from six donors. When the number of independent experiments was higher than 3, the KCs-CM from cells isolated from 6 different donors was tested with DP cells from the 3 different donors in different combinations. The statistical analysis was performed using the GraphPad Prism 7.03 software. To test if data followed a Gaussian distribution, the D'Agostino & Pearson normality test was used. Nonparametric data were analyzed with a Kruskal-Wallis (unpaired) or a Friedman test (paired), both coupled with Dunn's post-test. For results that did follow a Gaussian distribution, RM one-way ANOVA (paired) or ordinary one-way ANOVA (unpaired) were used in combination with Tukey's post-test. For data where two independent variables were considered, a two-way ANOVA was used (paired) followed by Tukey's post-test. Results are expressed as mean ± SEM and differences with p-values <0.05 were set as significant.

IV-3.   RESULTS

IV-3.1. Improvement of DP cell inductive phenotype by KCs-CM

When deprived of their native milieu and cultured in plain 2D culture conditions, DP cells suffer a rapid loss of their inductive potency [4]. To understand if KCs-CM could restore determinant functional features of DP cells in culture, we assessed the amount of active ALP and the expression of α-SMA and versican, all known markers for DP cells [1]. *In situ*, DP cells do not express α-SMA and the V2-isoform of versican is predominantly expressed, whereas *in vitro* α-SMA and the V1-isoform become widely expressed [22,23]. After culture in KCs-CM a significant increase of active ALP (Figure IV-1A and B), together with a significant reduction in the expression of α-SMA (Figure IV-1C and D) and the deposition of V1-isoform of versican (Figure IV-1D) were observed compared to standard expansion conditions (DMEM). Although KCs-CM did not restore the expression of the V2-isoform of versican (Figure IV-1D, it is evident that it supports a partial recovery of important phenotypic markers of DP cells.

To test if KCs-CM also impacts cell self-aggregative behavior, which is affected in 2D cultures [4], we quantified DP cell aggregation in culture with KCs-CM, which was significantly higher than in control groups (Figure IV-1E and F). Further, we analyzed the kinetics of DP cell aggregation when cultured in round-bottom plates. DP cell aggregates were formed earlier and were more compact in the presence of KCs-CM than controls (Figure IV-1G and H), suggesting a positive effect of KCs-CM on the recovery of DP cells' self-aggregation capacity.

During anagen, the hair cycle phase where DP inductivity is higher [24], the production of the angiogenic factor vascular endothelial growth factor (VEGF) is necessary for the development of a capillary network within the HF dermal compartment [25,26] and promotion of hair growth [27]. Similarly, IL-6 is a multifactorial cytokine strongly expressed in the HF during anagen [28] and known to regulate KCs proliferation and differentiation [29]. In turn, BMP molecules [30] and TGF-β1 [31] are downregulated for anagen onset, to avoid KCs differentiation and even apoptosis. PDGF-A is also known to induce and maintain anagen [32] and to have hair growth-inducing capacity [33]. Considering this signaling network, we investigated if KCs-CM affects the secretion of these hair growth paracrine mediators by DP cells.
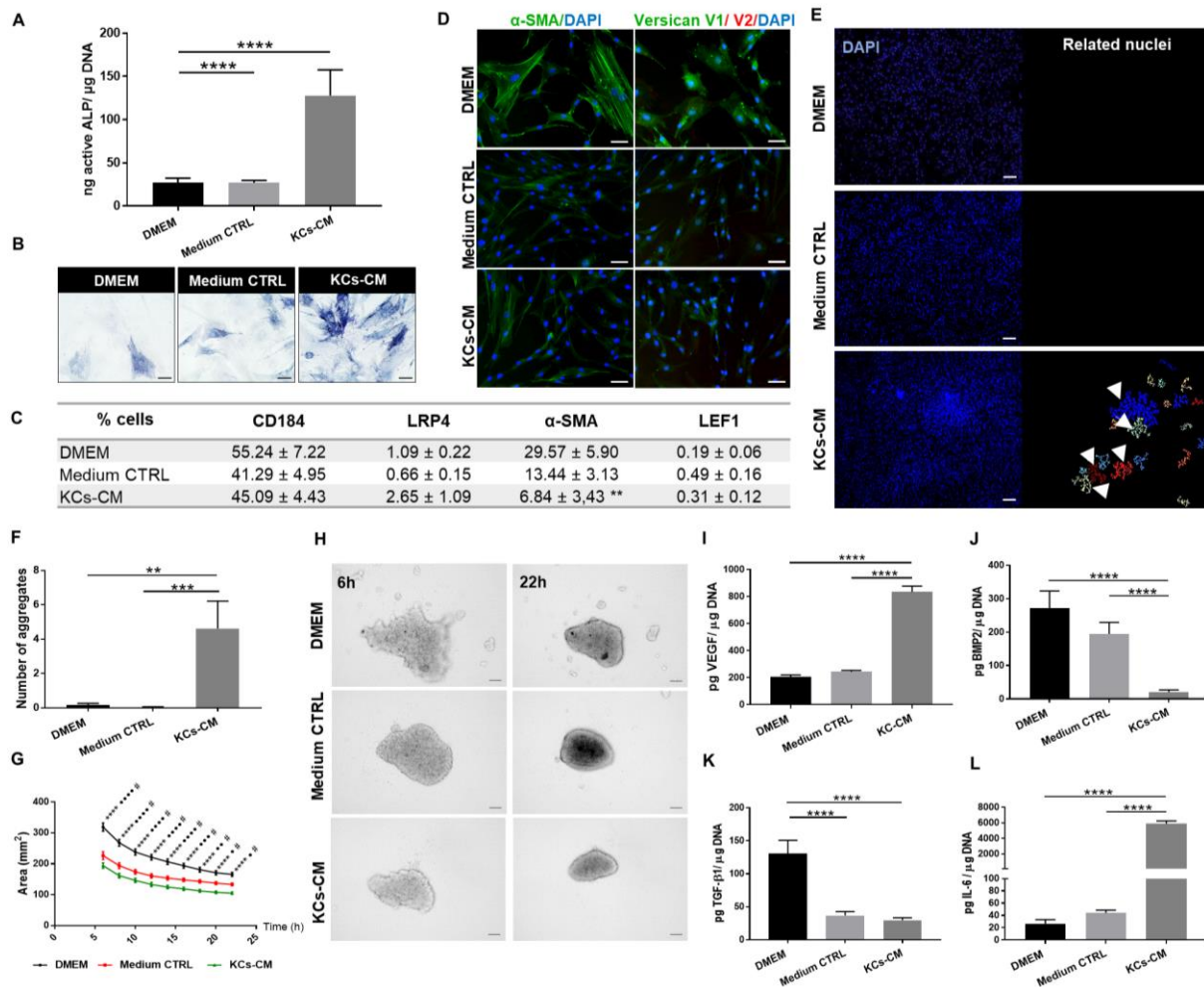
Figure IV-1 –KCs-CM improves DP cell inductive phenotype. (A) Amount of active ALP and (B) respective images of ALP-active DP cells showing an improvement of DP cells inductivity-related phenotype after culture with KCs-CM. (C) Percentage of DP cells expressing CD184, LRP4, α-SMA and LEF1 determined by flow cytometry (** p <0.01 *vs* DMEM). (D) Expression of α-SMA and the V1-isoform of versican in DP cells confirming a decrease after culture with KCs-CM. (E) Representative DAPI-stained nuclei images used to perform image analysis and (F) quantify the number of DP cell aggregates formed after 5 days in culture, showing that DP cells treated with KCs-CM have improved capacity to self-aggregate. (G) Variation of the area occupied by DP cells up to 22h of culture as obtained by the (H) analysis of time-lapse images revealing that DP cell cultured in KCs-CM form more compact spheroids and faster than controls. (I-K) Amount of growth factors and (L) cytokine secreted by DP cells showing the difference of their secretome with culture conditions. Differences are indicated by * KCs-CM *vs* DMEM, • KCs-CM *vs* Medium CTRL and • Medium CTRL *vs* DMEM. * p <0.05; ** p <0.01; *** p <0.00; **** p <0.0001. Scale bars are 50 μm for (B, D), 100 μm for (H) and 200 μm for (E).

DP cells cultured in KCs-CM secreted significantly more VEGF (Figure IV-I), albeit about one-third of this amount could be attributed to the KCs-CM (Supplementary Figure IV-1A). In what concerns BMP2 (Figure IV-1J) and TGF-β1 (Figure IV-1K) secretion, a significant decrease was observed in the culture with KCs-CM. However, the level of TGF-β1 present in the KCs-CM condition and control medium was similar, which seems to indicate that DP cells are responding to the culture medium and not to KCs-

CM. In contrast, BMP2 secretion did not vary among controls, suggesting that the effect observed in the experimental group is mostly related to the KCs-CM. Both factors were absent in KCs-CM (Supplementary Figure IV-1A). The most striking effect of CM treatment was an almost 223-fold increase in the amount of IL-6 (Figure IV-1L), which was undetectable in KCs-CM and present in low amounts in controls. PDGF-A was not detected in cultures with KCs-CM (Supplementary Figure IV-1B), even though it was present in KCs-CM (Supplementary Figure IV-1A). Our findings demonstrate that KCs-CM can modulate DP cell secretome to match in some extent the signaling environment during anagen.

IV-3.2. KCs-CM improves DP cell proliferation and decreases extracellular matrix deposition ability

Another factor preventing the attainment of high numbers of functional DP cells is their low proliferative capacity, probably reminiscent of their quiescent state *in situ*, where less than 2% of the cells are proliferative [5,34]. Moreover, the relatively short lifespan of DP cells in culture [35] further restricts the number of healthy cells obtained. Considering this, we demonstrated that KCs-CM can promote DP cell expansion, as shown by the significantly higher cell number (Figure IV-2A). Further, DP cells cultured in KCs-CM showed a spindle-like shape in opposition to the flat enlarged morphology characteristic of higher passaged cells [36] and observed in the standard DP expansion conditions (Figure IV-2B).

The DP is a densely packed cellular structure surrounded by an extracellular matrix (ECM) comprising mostly fibronectin, laminin, collagen IV and sulfated glycosaminoglycans (GAGs), and minimal collagen I content [37,38]. Culturing DP cells in the presence of KCs-CM lead to a significantly lower capacity to deposit both COL and NCOL proteins (Figure IV-2C, D and E). The COL/NCOL ratio was also significantly lower for CM-cultured DP cells in comparison to standard DMEM culture (Figure IV-2F). The expression of proteins analyzed by immunocytochemistry, seemed to confirm a dimmed signal for DP cells cultured in KCs-CM in comparison to the control (Figure IV-2G). Moreover, collagen I appeared to be less expressed than fibronectin (Figure IV-2G), while the deposition of collagen IV was not detected (data not shown). KCs-CM also negatively affected the deposition of GAGs, which is reflected in the amount of sulfated GAGs produced (Figure IV-2H), as well as in their distribution pattern (Figure IV-2I).

121
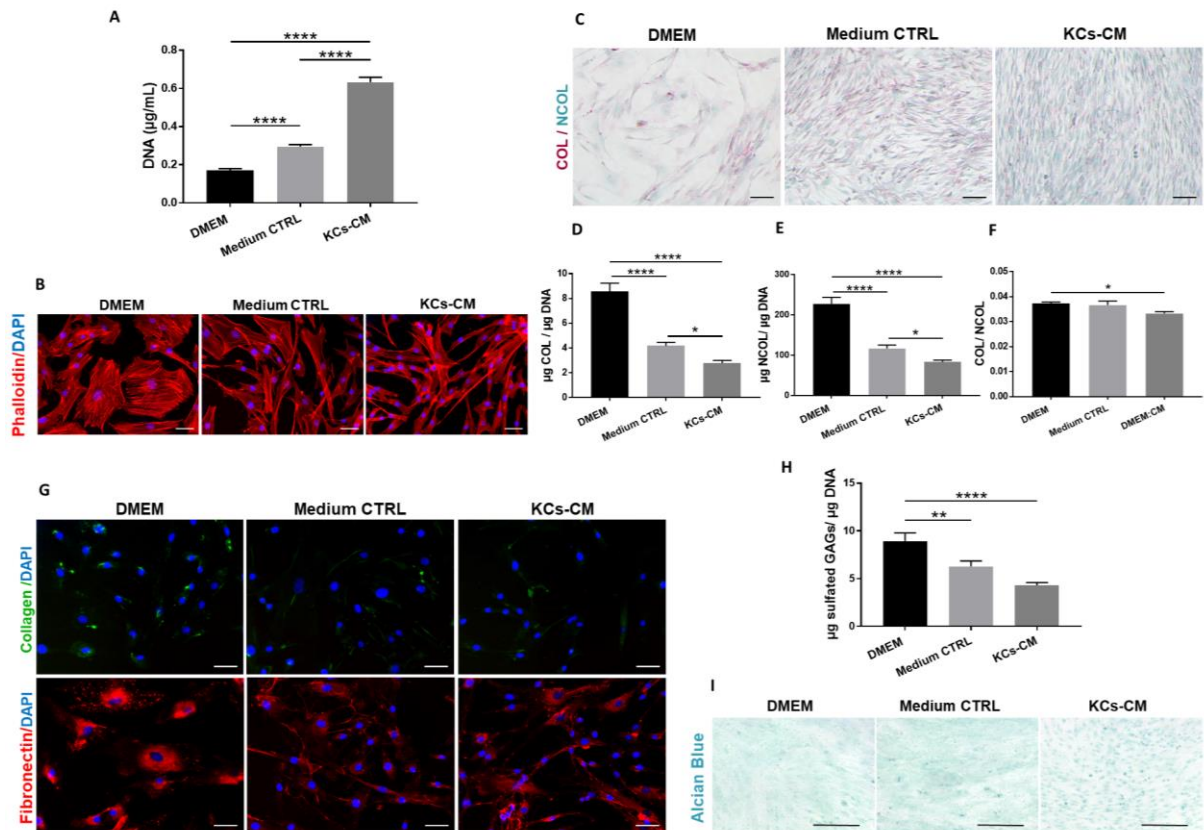
Figure IV-2 – KCs-CM beneficially affects DP cell proliferation but decreases matrix deposition ability. (A) DNA levels demonstrating that KCs-CM increases DP cell numbers. (B) Phalloidin-TRITC stained F-actin cytoskeleton arrangement showing that CM-treatment prevents DP cell enlarged morphology. (C) Representative images of collagen (COL, red) and non-collagenous (NCOL, green) proteins deposition by DP cells and the (D-E) respective quantification showing a reduced secretion by CM-treated DP cells. The same tendency was observed for (F) COL/NCOL proteins ratio. (G) Expression of collagen type I and fibronectin showing a dimmed signal in the condition where DP cells were treated with KCs-CM. (H) Amount of sulfated GAGs showing a reduced production by DP cells cultured with KCs-CM as well as a different (I) deposition pattern of carboxylated and sulfated GAGs compared to controls. * p <0.05; ** p <0.01; **** p <0.0001. Scale bars are 50 μm for (B, G), 100 μm for (C) and 200 μm for (I).

IV-3.3. Preculture with KCs-CM further aids in the recovery of DP cell phenotype

The artificial promotion of DP cell aggregation in spheroids is so far the gold standard strategy to partially recover human DP cell phenotype, characterized by low cellular proliferation and increased ALP activity [5,39]. Thus, we prepared 3D spheroids of DP cells precultured in KCs-CM to understand if the features acquired by DP cells cultured in 2D with KCs-CM were retained upon its removal and were comparable to the current gold-standard. In this 3D environment, spheroids formed from DP cells precultured in KCs-CM displayed significantly lower DNA content than controls (Figure IV-3A), which is indicative of a low proliferative state, further confirmed by the reduced number of Ki67-positive cells (Figure IV-3D). Additionally, preconditioned DP cells maintained high levels of active ALP (Figure IV-3B

and E), while controls showed a small recovery in comparison to the respective 2D cultures (Figure IV-3B *vs* Figure IV-1A). A marked decrease in α-SMA expression (Figure IV-3F) was also observed, as previously demonstrated in DP cell spheroidal cultures [5]. Interestingly, the protein content of spheroids derived from DP cells precultured with KCs-CM was significantly higher than in the respective 3D cultured controls (Figure IV-3C). Independently of the preculture condition, an ECM composed mostly of fibronectin, collagen I and versican V1 (Figure IV-3G to 3I), and a modest amount of the V2-isoform of versican (Figure IV-3J) involved the tightly connected connexin 43 positive DP cells (Figure IV-3K).
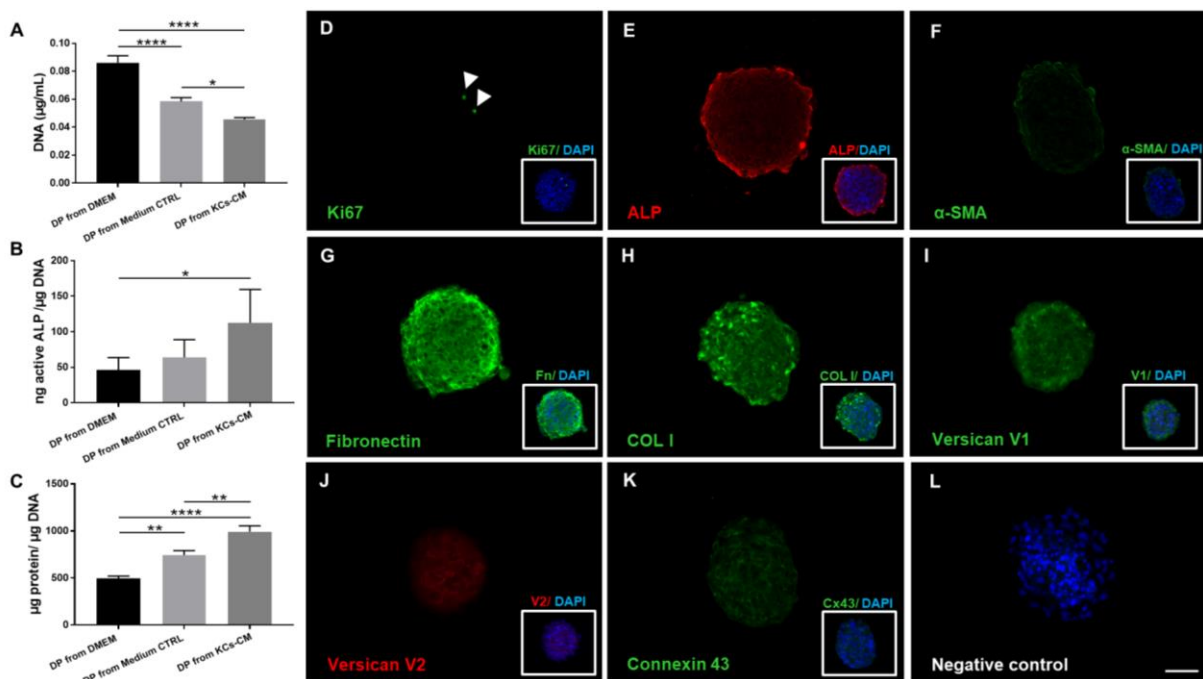
Figure IV-3 – Preconditioning with KCs-CM further enhances DP signature recovery in 3D culture conditions. DP cell spheroids derived from cells previously cultured with KCs-CM had a significantly (A) lower DNA content, (B) higher amount of active ALP and (C) higher protein content. Immunolabelling of DP cell spheroids preconditioned with KCs-CM showing (D) the proliferation-associated marker Ki67 (arrowheads) and the expression of (E) ALP, (F) α-SMA, (G) fibronectin, (H) collagen type I, (I) V1-isoform of versican, (J) V2-isoform of versican and the (K) gap junction protein connexin 43. The negative control is depicted on (I) and DAPI was used as the nuclear counterstaining (merged images, boxes). * p <0.05; ** p <0.01; **** p <0.0001. Scale bars= 50 μm.

Our results showed that in 3D spheroids, DP cells precultured in KCs-CM retain the phenotypic features that are associated to an inductive phenotype, which seems to contribute to the improved recovery of DP signature in comparison to the conventional method.

IV-3.4. Induction of HF- and SG-like structures in mice.

Six weeks after co-grafting the DP cells precultured with KCs-CM and the KCs, we observed the formation of HF- and SG-like structures within the wound area of five out of seven animals (Figure IV-4A). The reformation of a hair bulb (Figure IV-4B, dashed circle, Supplementary Figure IV-2A and B) and shaft elongation (Figure IV-4B, black arrows) were observed in one animal. From the seven animals where the same DP cells were grafted alone, four showed rudimentary structures (Figure IV-4C, Supplementary Figure IV-2C), clearly in inferior number and complexity than the ones observed in the co-grafting group. Three animals did not show any structures (Supplementary Figure IV-2D), like in the control animals (Figure IV-4D).
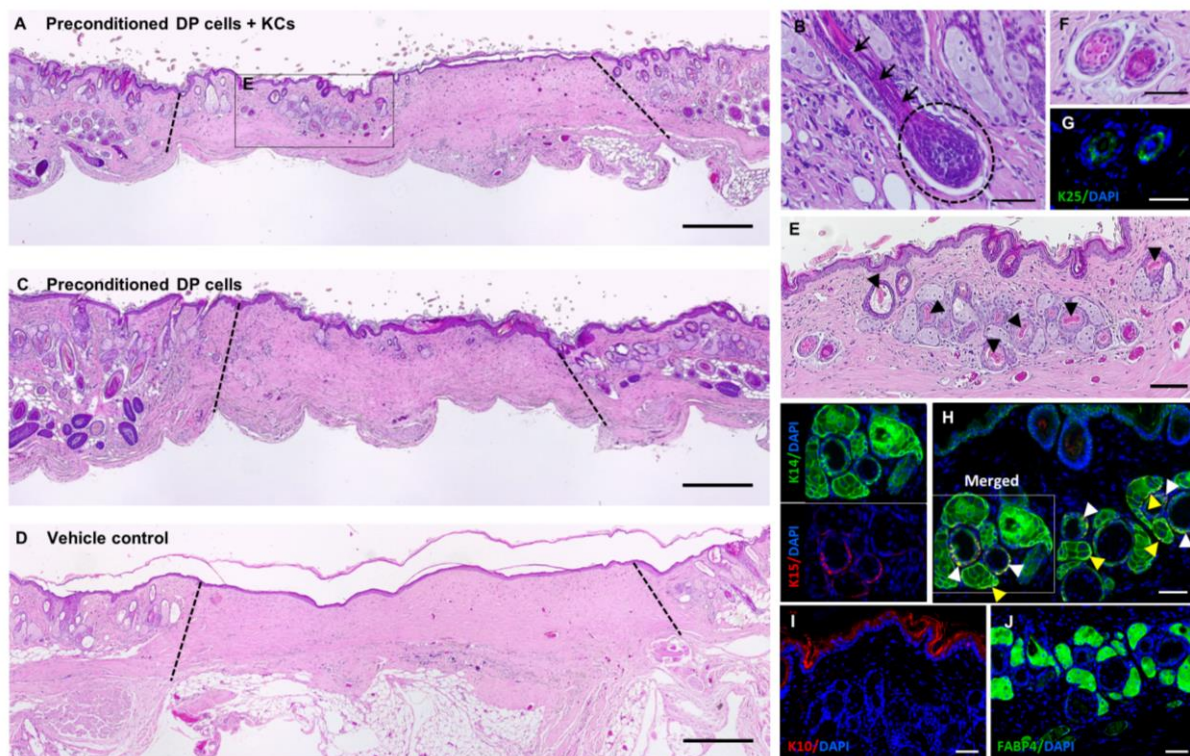
Figure IV-4 – DP cell preconditioning promotes hair induction in mice. (A) H&E staining of the wound sites showing the formation of structures morphologically resembling HFs and SGs 6 weeks after grafting CM-precultured DP cells and KCs in immune-deficient mice. (B) Hair bulb formation (dashed circle) and hair shaft elongation (arrows) were observed in one of the seven co-grafted animals. (C) DP cells grafted alone led to the formation of less complex and abundant structures which (D) were not observed in controls (dotted lines limit the wound area). (E) High magnification image of the recreated structures of the experimental condition demonstrating their complexity, including the presence of a differentiated core morphologically alike to hair shafts (arrowheads). (F) The folliculoid structures featured distinct epithelial layers, including (G) one layer expressing the IRS marker K25, (H) a layer co-expressing both K15 and K14 or layers only positive for K14. Arrowheads indicate K14 and K15 co-expression in HF-like (white) and SG-like structure (yellow). (I) K10 expression was limited to the skin epithelium, whereas (J) the sebocyte marker FABP4 was expressed in the structures resembling SG. Scale bars are 500 µm for (A-C), 100 µm for (D) and 50 µm for (E-J).

The structures found in the experimental group presented a follicular arrangement with multiple epithelial layers, including the presence of a differentiated core layer and some morphologically akin to the hair shaft (Figure IV-4E, arrowheads). The follicular nature of these layered structures (Figure IV-4F) was confirmed by the expression of K25, an IRS-specific marker [40] (Figure IV-4G), and K15 and K14, linked to the hair bulge and ORS. Proliferative areas co-expressing K14 and K15 (Figure IV-4H), as observed in the hair bulge and the immature portions of the ORS, were also identified. Due to the immature nature of the observed structures, K10 staining was only observed in the outermost layers of the skin (Figure IV-4I). Furthermore, analysis of the wound area evidenced the presence of blood vessels surrounding the structures (Supplementary Figure IV-2E, arrowheads). The presence of sebocytes into the SG-like structures was confirmed by FABP4 expression (Figure IV-4J). While human cells were not identified as part of the recreated follicular and SG-like structures, they were occasionally identified within the dermis of some animals where DP cells were grafted alone and no structures were formed (Supplementary Figure IV-3).

IV-4. DISCUSSION

Unlike their rodent counterparts, human DP cells suffer a dramatic loss of their inductive abilities when cultured *in vitro* and do not naturally recover from it when implanted *in vivo* [41]. The loss of contextual microenvironmental cues, especially the surrounding epithelial cells and the paracrine signaling molecules they provide, is commonly appointed as a causing event for this phenomenon [4,42]. Considering this, we took advantage of KCs secretome to rescue DP cell intrinsic properties in culture, therefore enabling their propagation and use for human cell-based HF regenerative approaches.

Cultivation with KCs-CM markedly increased ALP activity in DP cells, a critical hair inductive marker. It also improved DP cell self-aggregative capacity, a distinctive behavior that correlates with their hair induction ability [39,41]. Interestingly, when CM-precultured DP cells were used to form 3D spheroids, the current gold-standard method to restore DP signature [4,5], ALP activity was maintained. This is in line with the modest increase observed also in the conventional 3D spheroid cultures, suggesting that KCs-CM may be a stronger stimulus to restore this phenotypic marker. Furthermore, culture with KCs-CM significantly decreased α-SMA and versican V1 expression, better resembling DP cell native phenotype where these markers are absent or expressed in low levels [22,23], respectively. The low expression of α-SMA expression was kept in spheroids, similarly to what was previously

described for DP cells [5,43]. Moreover, KCs-CM pretreated DP cells secreted lower amounts of ECM proteins when cultured in 2D conditions. Some authors defend that without contextual and positional signals DP cells suffer a de-differentiation event [42] in 2D cultures and behave like dermal fibroblasts, whose main function in the skin is to synthesize and maintain the ECM. Therefore, our results may indicate prevention of this de-differentiation event. Indeed, 2D cultured DP cells are highly effective in replacing dermal fibroblasts in the establishment of the dermal component of engineered skin [44], which further supports those observations. Therefore, the decreased ECM production observed for 2D cultured DP cells in the presence of KCs-CM may indicate prevention of that de-differentiation event, especially when associated with increased ALP activity.

Since DP control over HF development and hair growth is regulated by a well-controlled network of bioactive molecules, the use of human DP cells in HF-regenerative strategies will strongly rely on their capacity to respond in a physiologically relevant manner. Under KCs-CM influence, DP cells produced significantly more VEGF, whereas BMP and TGF-β1 signaling were downregulated, which coincide with what has been reported as necessary for hair induction [27,31,45]. The most impressive effect of KCs-CM was, however, the remarkable increase in IL-6 secretion. Literature concerning the effects of IL-6 in the HF regulation is scant, however, IL-6 expression has been shown higher in the anagen HF in comparison to non-follicular skin [28]. Moreover, Tanabe *et al.* [46] showed that daily injections of 200 ng (1µg/mL) of IL-6 or higher promoted hair growth in rats. On the other hand, Huang and co-workers [47] reported an inhibitory effect of lower doses of IL-6 (250-500 pg/mL) on KCs growth, which seems to indicate a specific dose-dependent effect. Therefore, the dramatic increase of IL-6 secretion that we observed when DP cells were cultured with KCs-CM might be an additional beneficial feature to recover hair inductive phenotype. Taken together, our results demonstrate that after culture with KCs-CM the secretome profile of DP cells matches the one characteristic of the anagen phase.

Despite the encouraging evidence observed *in vitro*, the demonstration of KCs-CM capacity to promote DP cell hair-inductive ability ultimately relies on cellular engraftment *in vivo*. We showed that DP cells precultured with KCs-CM, when combined with adult KCs, were able to induce the formation of follicular structures that recreated the main features of HF and SG structures. Although hair bulb reformation occurred in one of the animals, the presence and elongation of hair fibers were not observed in their majority, demonstrating the immature state of the regenerated structures. Our approach takes advantage of human-epithelial signaling to improve DP cell inductivity, but there are other cellular players involved in hair growth whose lack and/or substantial interspecies differences,

may have prevented complete HF formation. Nevertheless, as far as we know this represents the best result obtained so far entirely using only human cells, both DP cells and KCs, for HF regeneration. Previously, Ehama *et al.* [48] demonstrated the formation of chimeric HFs using murine DP cells and human neonatal KCs, but the combination of both human-origin cells did not show any sign of follicular generation. Later, the combination of cultured human KCs and DP cells led to the formation of what seem to be epithelial structures adjacent to the skin epidermis, but their multicellular epithelial composition was not confirmed and the formation of SG was not observed [49]. We also observed the presence of small vessels around the structures, a functional indicator since follicular and perifollicular vasculature network are intimately coupled with hair growth [27,50,51]. The *in vitro* results demonstrate that KCs produce VEGF and that their CM itself boosted VEGF production by DP cells, therefore both cells may have contributed to the establishment and localization of the observed microvasculature *in vivo*. Remarkably, HF- and SG-like structures were also spotted in most animals where preconditioned DP cells were grafted alone, although their complexity and occurrence were clearly inferior in comparison to the co-grafted animals. Having in consideration previous works showing that DP cells alone do not induce hair formation [47,48], those results further suggest that KCs-CM improve the inductive ability of DP cells, which could induce the host epithelium into a follicular or SG fate.

The absence of human cells within the recreated structures after 6 weeks, might be related to the used model in which cells are not grafted subcutaneously but in the inflicted wound. The chamber assay is characterized by continuous tissue remodeling lead by the wound healing environment, therefore, we can speculate that grafted cells were replaced along the time. In fact, cellular interchangeability and interspecies cooperation leading to grafted epithelial cells replacement by host KCS was previously reported in the same model [48]. This is also in line with another work showing that human cells detected both in the epidermis and in folliculoid structures formed after rabbit DP cell induction, were completely replaced within one month [52].

As hypothesized, and based on previous results demonstrating KCs-CM mitogenic effect over DP cells [10,14], with our strategy we were able to restore DP cell phenotype and inductive properties while supporting their growth in culture. The increase of DP cell proliferative capacity was most likely due to the presence of PDGF-A and VEGF in the KCs-CM, both known mitogenic factors for DP cells [26,53]. Still, spheroids inclosing DP cells precultured with KCs-CM displayed lower proliferative capacity in

comparison to conventionally produced spheroids, demonstrating an improved capacity to recreate the DP quiescent state *in situ* and the importance of different culture conditions (2D vs 3D).

IV-5. CONCLUSIONS

To conclude, our observations demonstrate that CM collected from adult interfollicular KCs represents an effective strategy to improve key human DP cell native features in vitro, including their critical inductivity and self-aggregation capacity. Further, KCs-CM improved DP cell proliferation and the secretion profile of known paracrine mediators of hair growth, better ensuring that a sufficient number of functional cells are obtained. Finally, in vivo testing of CM-precultured DP cells demonstrated their capacity to support the recreation of HF- and SG-like structures, especially in combination with KCs. We believe that the high translational value of our strategy and its easy application hold great promise for supporting upcoming advances in the hair regenerative field.

IV-6. REFERENCES

1. Yang, C.-C. & Cotsarelis, G. Review of hair follicle dermal cells. *J. Dermatol. Sci.* **57**, 2–11 (2010).

2. Driskell, R. R., Clavel, C., Rendl, M. & Watt, F. M. Hair follicle dermal papilla cells at a glance. *J. Cell Sci.* **124**, 1179–1182 (2011).

3. Ohyama, M., Zheng, Y., Paus, R. & Stenn, K. S. The mesenchymal component of hair follicle neogenesis: background, methods and molecular characterization. *Exp. Dermatol.* **19**, 89–99 (2010).

4. Higgins, C. A., Chen, J. C., Cerise, J. E., Jahoda, C. A. B. & Christiano, A. M. Microenvironmental reprogramming by three-dimensional culture enables dermal papilla cells to induce de novo human hair-follicle growth. *Proc. Natl. Acad. Sci.* **110**, 19679–19688 (2013).

5. Higgins, C. A., Richardson, G. D., Ferdinando, D., Westgate, G. E. & Jahoda, C. A. B. Modelling the hair follicle dermal papilla using spheroid cell cultures. *Exp. Dermatol.* **19**, 546–548 (2010).

6. Sennett, R. & Rendl, M. Mesenchymal–epithelial interactions during hair follicle morphogenesis and cycling. *Semin. Cell Dev. Biol.* **23**, 917–927 (2012).

7. Yamauchi, K. & Kurosaka, A. Inhibition of glycogen synthase kinase-3 enhances the expression

of alkaline phosphatase and insulin-like growth factor-1 in human primary dermal papilla cell culture and maintains mouse hair bulbs in organ culture. *Arch. Dermatol. Res.* **301**, 357–365 (2009).

8. McElwee, K. J., Kissling, S., Wenzel, E., Huth, A. & Hoffmann, R. Cultured peribulbar dermal sheath cells can induce hair follicle development and contribute to the dermal sheath and dermal papilla. *J Invest Dermatol* **121**, 1267–1275 (2003).

9. Ohyama, M., Kobayashi, T., Sasaki, T., Shimizu, A. & Amagai, M. Restoration of the intrinsic properties of human dermal papilla in vitro. *J. Cell Sci.* **125**, 4114–4125 (2012).

10. Won, C. H. *et al.* Hair-growth-promoting effect of conditioned medium of high integrin α6 and low CD 71 (α6bri/CD71dim) positive keratinocyte cells. *Int. J. Mol. Sci.* **16**, 4379–4391 (2015).

11. Roh, C., Tao, Q. & Lyle, S. Dermal papilla-induced hair differentiation of adult epithelial stem cells from human skin. *Physiol. Genomics* **19**, 207–217 (2005).

12. Bak, S. S. *et al.* Restoration of hair-inductive activity of cultured human follicular keratinocytes by co-culturing with dermal papilla cells. *Biochem. Biophys. Res. Commun.* **505**, 360–364 (2018).

13. Limat, A. *et al.* Soluble factors from human hair papilla cells and dermal fibroblasts dramatically increase the clonal growth of outer root sheath cells. *Arch. Dermatol. Res.* **285**, 205–210 (1993).

14. Warren, R. & Wong, T. K. Stimulation of human scalp papilla cells by epithelial cells. *Arch. Dermatol. Res.* **286**, 1–5 (1994).

15. Cerqueira, M. T., Frias, A. M., Reis, R. L. & Marques, A. P. Boosting and Rescuing Epidermal Superior Population from Fresh Keratinocyte Cultures. *Stem Cells Dev.* **23**, 34–43 (2014).

16. Gledhill, K., Gardner, A. & Jahoda, C. A. B. Isolation and Establishment of Hair Follicle Dermal Papilla Cell Cultures. in *Methods in molecular biology (Clifton, N.J.)* vol. 989 285–292 (Methods Mol Biol, 2013).

17. López-De León, A. & Rojkind, M. A simple micromethod for collagen and total protein determination in formalin-fixed paraffin-embedded sections. *J. Histochem. Cytochem.* **33**, 737–743 (1985).

18. Kafienah, W. & Sims, T. J. Biochemical Methods for the Analysis of Tissue-Engineered Cartilage. in *Biopolymer Methods in Tissue Engineering* 217–230 (Humana Press, 2003).

19. Lamprecht, M. R., Sabatini, D. M. & Carpenter, A. E. CellProfiler™: free, versatile software for automated biological image analysis. *Biotechniques* **42**, 71–75 (2007).

20. Sankur, B. Survey over image thresholding techniques and quantitative performance evaluation.

J. Electron. Imaging **13**, 146 (2004).

21. Jensen, K. B., Driskell, R. R. & Watt, F. M. Assaying proliferation and differentiation capacity of stem cells using disaggregated adult mouse epidermis. *Nat. Protoc.* **5**, 898–911 (2010).

22. Jahoda, C. A. B., Reynolds, A. J., Chaponnier, C., Forester, J. C. & Gabbiani, G. Smooth muscle α-actin is a marker for hair follicle dermis in vivo and in vitro. *J. Cell Sci.* **99**, 627–636 (1991).

23. Soma, T., Tajima, M. & Kishimoto, J. Hair cycle-specific expression of versican in human hair follicles. *J. Dermatol. Sci.* **39**, 147–154 (2005).

24. Iida, M., Ihara, S. & Matsuzaki, T. Hair cycle-dependent changes of alkaline phosphatase activity in the mesenchyme and epithelium in mouse vibrissal follicles. *Dev. Growth Differ.* **49**, 185–195 (2007).

25. Mecklenburg, L. *et al.* Active Hair Growth (Anagen) is Associated with Angiogenesis. *J. Invest. Dermatol.* **114**, 909–916 (2000).

26. Lachgar, S. *et al.* Vascular Endothelial Growth Factor Is an Autocrine Growth Factor for Hair Dermal Papilla Cells. *J. Invest. Dermatol.* **106**, 17–23 (1996).

27. Yano, K., Brown, L. F. & Detmar, M. Control of hair growth and follicle size by VEGF-mediated angiogenesis. *J. Clin. Invest.* **107**, 409–417 (2001).

28. Yu, M. *et al.* Interleukin-6 cytokine family member oncostatin M is a hair-follicle-expressed factor with hair growth inhibitory properties. *Exp. Dermatol.* **17**, 071117031607006-??? (2007).

29. Taniguchi, K. *et al.* Periostin controls keratinocyte proliferation and differentiation by interacting with the paracrine IL-1α/IL-6 loop. *J. Invest. Dermatol.* **134**, 1295–1304 (2014).

30. Botchkarev, V. A. *et al.* Noggin is a mesenchymally derived stimulator of hair-follicle induction. *Nat. Cell Biol.* **1**, 158–164 (1999).

31. Foitzik, K. *et al.* Control of murine hair follicle regression (catagen) by TGF-β1 in vivo. *FASEB J.* **14**, 752–760 (2000).

32. Tomita, Y., Akiyama, M. & Shimizu, H. PDGF isoforms induce and maintain anagen phase of murine hair follicles. *J. Dermatol. Sci.* **43**, 105–115 (2006).

33. Festa, E. *et al.* Adipocyte lineage cells contribute to the skin stem cell niche to drive hair cycling. *Cell* **146**, 761–771 (2011).

34. Tobin, D. J., Gunin, A., Magerl, M., Handijski, B. & Paus, R. Plasticity and cytokinetic dynamics of the hair follicle mesenchyme: Implications for hair growth control. *J. Invest. Dermatol.* **120**, 895–904 (2003).

35. Messenger, A. G. Isolation, culture and in vitro behavior of cells isolated from papillae of human

hair follicles. in *Trends in Human Hair Growth and Alopecia Research* 57–66 (Springer Netherlands, 1989).

36.   Upton, J. H. *et al.* Oxidative Stress–Associated Senescence in Dermal Papilla Cells of Men with Androgenetic Alopecia. *J. Invest. Dermatol.* **135**, 1244–1252 (2015).

37.   Couchman, J. R. Rat hair follicle dermal papillae have an extracellular matrix containing basement membrane components. *J. Invest. Dermatol.* **87**, 762–767 (1986).

38.   Messenger, A. G., Elliott, K., Westgate, G. E. & Gibson, W. T. Distribution of extracellular matrix molecules in human hair follicles. *Ann. N. Y. Acad. Sci.* **642**, 253–62 (1991).

39.   Young, T.-H., Lee, C.-Y., Chiu, H.-C., Hsu, C.-J. & Lin, S.-J. Self-assembly of dermal papilla cells into inductive spheroidal microtissues on poly(ethylene-co-vinyl alcohol) membranes for hair follicle regeneration. *Biomaterials* **29**, 3521–3530 (2008).

40.   Schweizer, J., Langbein, L., Rogers, M. A. & Winter, H. Hair follicle-specific keratins and their diseases. *Exp. Cell Res.* **313**, 2010–2020 (2007).

41.   Jahoda, C. A. B. & Oliver, R. F. Vibrissa dermal papilla cell aggregative behaviour in vivo and in vitro. *J. Embryol. Exp. Morphol.* **79**, 211–224 (1984).

42.   Ramos, R., Guerrero-Juarez, C. F. & Plikus, M. V. Hair Follicle Signaling Networks: A Dermal Papilla–Centric Approach. *J. Invest. Dermatol.* **133**, 2306–2308 (2013).

43.   Gupta, A. C. *et al.* Establishment of an in vitro organoid model of dermal papilla of human hair follicle. *J. Cell. Physiol.* **233**, 9015–9030 (2018).

44.   Higgins, C. A. *et al.* Multifaceted role of hair follicle dermal cells in bioengineered skins. *Br. J. Dermatol.* **176**, 1259–1269 (2017).

45.   Botchkarev, V. A. *et al.* Noggin is required for induction of the hair follicle growth phase in postnatal skin. *FASEB J.* **15**, 2205–2214 (2001).

46.   Tanabe, A. *et al.* Interleukin 6 induces the hair follicle growth phase (anagen). *J. Dermatol. Sci.* **43**, 210–213 (2006).

47.   Huang, W.-Y. *et al.* Stress-induced premature senescence of dermal papilla cells compromises hair follicle epithelial-mesenchymal interaction. *J. Dermatol. Sci.* **86**, 114–122 (2017).

48.   Ehama, R. *et al.* Hair Follicle Regeneration Using Grafted Rodent and Human Cells. *J. Invest. Dermatol.* **127**, 2106–2115 (2007).

49.   Inoue, K. *et al.* Evaluation of Animal Models for the Hair-Inducing Capacity of Cultured Human Dermal Papilla Cells. *Cells Tissues Organs* **190**, 102–110 (2009).

50.   Lachgar, Charveron, Gall & Bonafe. Minoxidil upregulates the expression of vascular endothelial

growth factor in human hair dermal papilla cells. *Br. J. Dermatol.* **138**, 407–411 (1998).

51. Chew, E. G. Y. *et al.* Differential Expression between Human Dermal Papilla Cells from Balding and Non-Balding Scalps Reveals New Candidate Genes for Androgenetic Alopecia. *J. Invest. Dermatol.* **136**, 1559–1567 (2016).

52. Ferraris, C., Bernard, B. A. & Dhouailly, D. Adult epidermal keratinocytes are endowed with pilosebaceous forming abilities. *Int. J. Dev. Biol.* **41**, 491–498 (1997).

53. Karlsson, L., Bondjers, C. & Betsholtz, C. Roles for PDGF-A and sonic hedgehog in development of mesenchymal components of the hair follicle. *Development* **126**, 2611–2621 (1999).

IV-7. SUPPLEMENTARY IMAGES

A	DMEM	Medium CTRL	KCs-CM
VEGF	nd	19.74 ± 9.57	247.49 ± 67.84
BMP2	nd	nd	nd
TGF-β1	nd	nd	nd
PDGF-A	nd	nd	133.78 ± 43.92
IL-6	nd	nd	nd
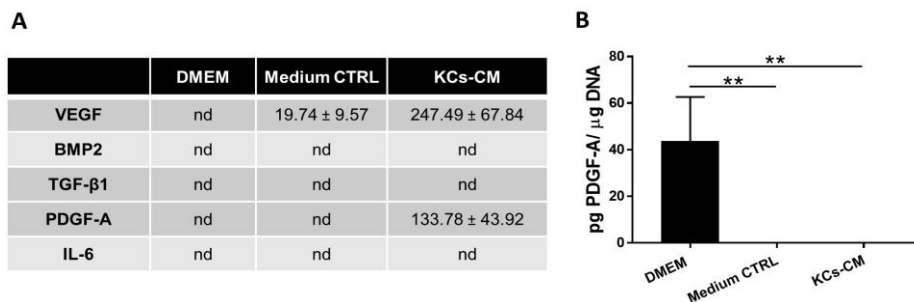
Supplementary Figure IV-1 – (A) Amount (pg/ml) of growth factors and cytokine quantified in the media after 24h of culture without cells. (B) Amount of PDGF-A released by DP cells cultured with KCs-CM and control media.(B). nd – bellow the assay detection level. **$p < 0.01$
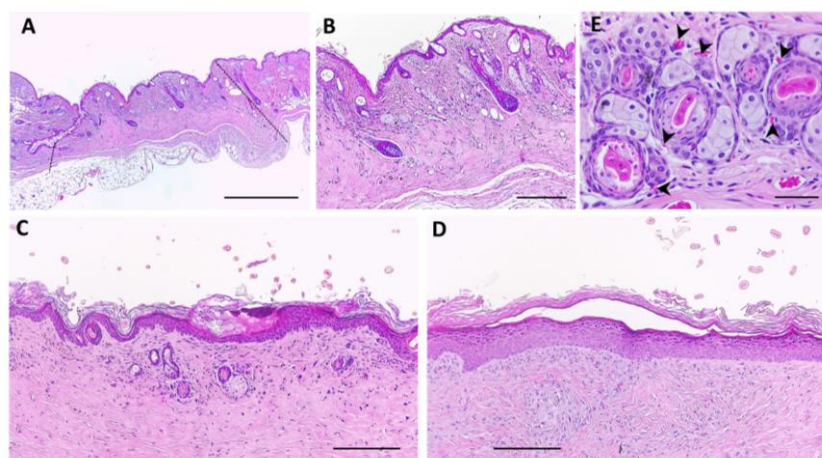
Supplementary Figure IV-2 –Hair reconstitution assay H&E stained wound area where KCs and DP cells precultured with KCs-CM were injected showing (A, B) the reformation of the HF bulb and hair shaft elongation (dashed lines delimitate the wound borders) obtained in one of the animals. When DP cells were injected alone (C) simple structures were formed in four

animals, and (D) hair induction was lacking in the remaining three out of seven animals. (E) High magnification images of the structures observed in the animals where CM-precultured DP cells were co-grafted with KCs demonstrating the presence of microvasculature (arrowheads). Scale bars are 500 μm for (A), 200 μm for (B-D) and 50 μm for (E).
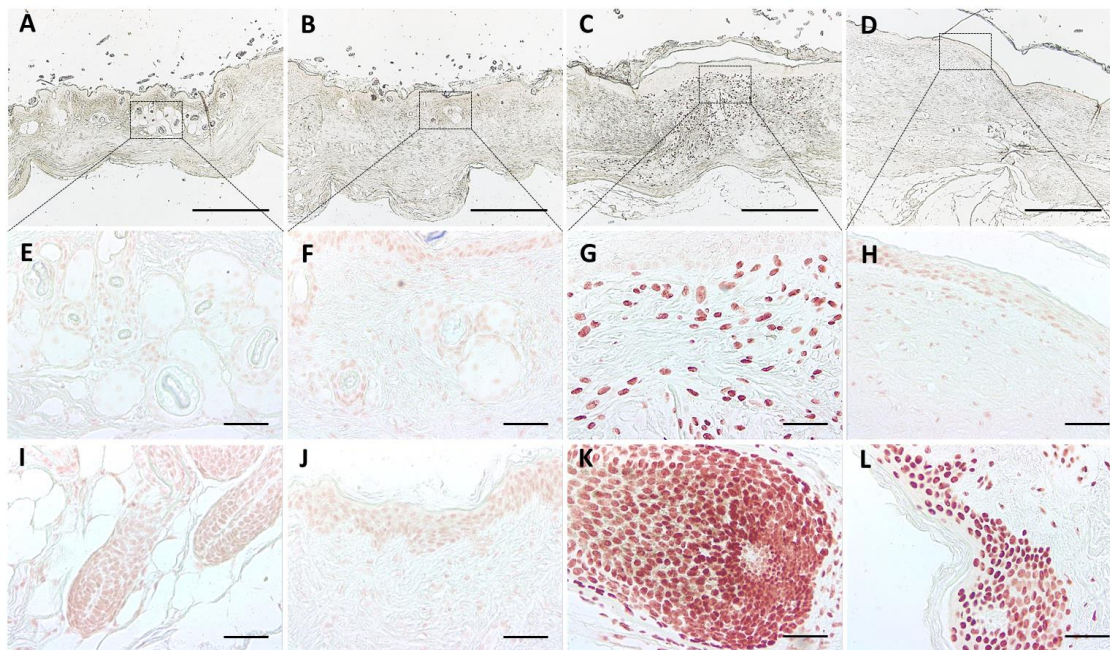
Supplementary Figure IV-3 – Human cell detection. Chromogenic *in situ* hybridization with a human-specific probe failed to detect human cells within the HF- and SG-like structures both in animals where (A, E) CM-precultured DP cells were injected together with KCs or (B, F) alone. (C, G) In some animals where only DP cells were injected and no structures were found, human cells were present in the dermis. (D, H) No human cells were observed in control. The specificity of the staining was confirmed by the absence of positive signal in mice tissue next to the wound margins, including the HFs (I) and epidermis (J). Human scalp samples were used as positive controls, displaying positive staining in both (K) HFs and (L) epidermis. Scale bars are 500 μm for (A-D) and 50 μm for (E-L).

CHAPTER V

GELLAN GUM-DERIVED HYDROGELS SUPPORT THE RECREATION OF THE DERMAL PAPILLA MICROENVIRONMENT

CHAPTER V

GELLAN GUM-DERIVED HYDROGELS SUPPORT THE RECREATION OF THE DERMAL PAPILLA MICROENVIRONMENT§

ABSTRACT

The dermal papilla (DP), a specialized compartment within the hair follicle, regulates hair growth. However, human DP cells rapidly lose their inductivity in 2D culture given the loss of positional and microenvironmental cues. Spheroids have been capable of recreating the 3D intercellular organization of DP cells however, DP cell-matrix interactions are poorly represented. Considering the specific nature of the DP's extracellular matrix (ECM), we functionalized gellan gum (GG) with collagen IV-(HepIII) or fibronectin-(cRGDfC) derived peptide sequences to generate a 3D environment in which the phenotype and physiological functions of DP cells are restored. We further tuned the stiffness of the microenvironments by varying GG amount. Biomimetic peptides in stiffer hydrogels promoted the adhesion of DP cells, while each peptide and amount of polymer independently influenced the type and quantity of ECM proteins deposited. Furthermore, although peptides did not seem to have an influence, stiffer hydrogels improved the inductive capacity of DP cells after short term culture. Interestingly, independently of the peptide, these hydrogels supported the recapitulation of basic hair morphogenesis-like events when incorporated in a human skin *in vitro* model. Our work demonstrates that tailored GG hydrogels support the generation of a microenvironment in which both cell-ECM and cell-cell interactions positively influence DP cells towards the creation of an artificial DP.

V-1.   INTRODUCTION

The hair follicle (HF) is a sophisticated skin appendage endowed with important physiological and aesthetical functions, the reason why its absence or changes in its distribution, can deeply affect the well-being of individuals. Hair loss conditions such as alopecia can be particularly distressing. An efficient treatment involves the autologous transplantation of follicular units, however, a sufficient number of HFs is not always available for translocation.

Hair growth coordination is controlled by a key inductive entity located at the base of the HF, the dermal papilla (DP) [1]. It is organized as a cluster of mesenchymal cells embedded in a dense extracellular matrix (ECM) rich in basement membrane elements such as fibronectin, collagen type IV and laminin, and in sulfated glycosaminoglycans (GAGs) [2,3]. The ECM is continuously remodelled along the hair cycle and plays a role in the HF dermal-epidermal signalling [4,5] and the maintenance of tissue-specific functions and respective cellular differentiation status [6,7].

Advances in the tissue engineering field may allow to *in vitro* recreate functional DPs, which offers the opportunity to screen substances with hair modulation capacity, to investigate the mechanisms underlying HF development, or to be used as follicular units in the treatment of hair loss disorders. However, when retrieved from their niche and cultured two-dimensionally, human DP cells rapidly lose their inductive properties [8,9] and no longer retain the capacity to form HFs after transplantation. A common attempt to overcome this problem has been the recreation of the DP morphological 3D arrangement, by artificially promoting DP cell aggregation and intercellular communication in spheroids using a wide range of techniques [10–17]. However, DP cells' 3D organization in spheroids only accounts for a partial restoration (22%) of the DP transcriptional signature, and to an even lower hair induction rate after *in vivo* implantation [14], demonstrating that the restoration of cell-cell communication is not enough to preserve DP cell functions. Moreover, under these conditions, DP cell-matrix interactions are poorly represented since they mostly rely on the later production of ECM by DP cells. Taking this into consideration, different strategies have been attempted to recreate an ECM-enriched DP environment. Wang *et al.* [18] enclosed mice vibrissae DP cells in successive layers of gelatin and alginate forming microcapsules that self-assembled as DP-like spheroids. In these structures, DP cells showed increased expression of alkaline phosphatase (ALP), neural cell adhesion molecule and versican and were able to promote HF induction *in vivo* when transplanted with mice keratinocytes (KCs). In a different approach, DP cells encapsulated in alginate-derived hydrogels displayed a round morphology and a dormant non-proliferative state *in vitro* [19] and were able to form

structures resembling immature HF-like structures upon transplantation with mice epithelial cells [20,21]. The encapsulation of human DP cells in cell-adhesive collagen type I hydrogels resulted in higher amounts of active ALP, which lead to HF induction in a patch assay when combined with mouse embryonic epithelial cells [22]. Despite demonstrating HF induction *in vivo*, some of those strategies are not using human cells [18], while others have not confirmed the participation of the transplanted human DP cells in the recreated structures [19–22]. Several other works have cultured DP cells in hydrogels with epithelial cells [22–29]. However, these are mostly intended to study epithelial-mesenchymal interactions and how these cells self-organize, whereas matrix influence on DP cells is not explored. Interestingly, most of these strategies rely on collagen type I or Matrigel®, which lack specific features capable of emulating the native ECM of the DP. While Matrigel® combines a cocktail of unknown proteins isolated from a mice-origin tumor [30], collagen type I is not the most abundant or characteristic ECM component of the DP [4]. Therefore, improved approaches capable of providing the necessary environmental cues (3-dimensionality, cell-cell and cell-ECM interactions) to DP cells, for the *in vitro* recovery of their inductive phenotype, are still missing.

We previously proposed a method to chemically modify gellan gum (GG) with an intermediary divinyl sulfone (GGDVS) moiety and covalently immobilize peptides containing cysteine residues [31], enabling GG tailoring to improve, for example, cellular responsiveness. Therefore, in this study, we hypothesized that functionalizing GG with DP ECM-related peptides would contribute not only to support cell-ECM interactions but also subsequent cell-cell connections, generating a 3D environment in which the phenotype and physiological functions of DP cells can be restored. To specifically resemble the ECM of the DP we biofunctionalized GG with the HepIII sequence, a heparin-binding peptide sequence located in the α1 (IV) triple-helical region of collagen IV [32], or with a synthetic cyclic form of RGD (cRGDfC) a peptide motif present within fibronectin and known to mediate cell attachment [33,34]. Besides assessing the effect of the peptides, we further tuned the mechanical properties of the produced GG-derived hydrogels by varying the amount of polymer, to investigate a potential effect of hydrogel stiffness on DP cells, particularly over ECM deposition and the recovery of an inductive phenotype. Finally, the functional ability of the proposed cell-laden hydrogels was tested in an organotypic human skin model. Overall, we propose a promising approach towards the creation of an artificial DP.

V-2.   MATERIALS AND METHODS

V-2.1.   Chemical modification of gellan gum with DVS moieties and post-functionalization with peptide sequences

GGDVS was prepared as previously described and established in our group [31]. The GGDVS-peptide solution was obtained after reacting GGDVS with the peptide in a 0.25 M sucrose solution (pH≥8.3), for 1h at RT under gentle stirring. HepIII (Cys-Gly-Glu-Phe-Tyr-Phe-Asp-Leu-Arg-Leu-Lys-Gly-Asp-Lys >95% purity) or cRGDfC (Cyclo[Arg-Gly-Asp-(D-Phe)-Cys] >95% purity, GeneCust Europe, France) peptides were used.

V-2.2.   Peptide quantification

The Micro Bicinchoninic Acid™ Protein Assay Kit (µBCA, Thermo Fisher Scientific, USA) was used to determine the amount of peptide (HepIII/cRGDfC) that reacted with GGDVS, according to manufacturers' instructions. Calibration curves were prepared with the respective peptide (ranging from 0 to 200 µg/mL), and GGDVS-HepIII and GGDVS-cRGDfC (ranging from 1 and 0.5 mg/mL) solutions. Absorbances were read at 562 nm using a microplate reader (Synergy HT, BioTek, USA). The modification efficiency yield was determined by the ratio of the mass of peptide linked to GGDVS determined by µBCA ($m_{measured\ pept}$) and the mass of peptide that was used for the reaction with GGDVS ($m_{initial\ pept}$), through the following calculation:

$$\text{Efficiency (\%)} = \frac{m_{measured\ pept}}{m_{initial\ pept}} \times 100$$

V-2.3.   Gellan gum-derived hydrogels preparation

GG solution was prepared by dissolving Gelzan (Sigma-Aldrich, USA) in a 0.25 M sucrose solution [35] at 90°C, under stirring. Hydrogels were prepared by mixing an equal volume of GG and GGDVS-

138

peptide solutions (Table V-1) and by pouring the pre-hydrogel solution in cell culture wells, allowing the pre-hydrogel solution to polymerize by temperature crosslinking.

Table V-1 - Nomenclature and composition of the different GG-derived hydrogel formulations

Formulation	Final concentration in the hydrogel		Peptide (concentration)
	GG (w/v)	GGDVS (w/v)	
GG_0.75%	0.75 %	0.375 %	—
GG_1.25%	1.25 %	0.625 %	—
GGDVS_0.75%	0.75 %	0.375 %	—
GGDVS_1.25%	1.25 %	0.625 %	—
GGDVS-HepIII_0.75%	0.75 %	0.375 %	HepIII (400 µM)
GGDVS-HepIII_1.25%	1.25 %	0.625 %	HepIII (400 µM)
GGDVS-cRGDfC_0.75%	0.75 %	0.375 %	cRGDfC (800 µM)
GGDVS-cRGDfC_1.25%	1.25 %	0.625 %	cRGDfC (800 µM)

V-2.4. Analysis of the mechanical properties of gellan gum-derived hydrogels

The unconfined static compressive mechanical properties of GG-derived hydrogels were analyzed using an INSTRON 5543 universal mechanical testing equipment (load cell 1 kN, Instron Int. Ltd., USA). GG-derived hydrogels were prepared in round-shaped molds (10x6 mm) and equilibrated in Dulbecco's Modified Eagle Medium (DMEM) with 10% fetal bovine serum (FBS) for 48h at 37°C prior testing. Samples were submitted to a pre-load of 0.1 N and were tested up to 60% of strain, at a loading rate of 2 mm/min.

V-2.5. Cell isolation and culture

HF samples were collected from occipital scalp areas from patients submitted to hair transplantation surgeries at Sanare Unicapilar (Porto, Portugal) and used to isolate DPs by microdissection [36]. DPs were initially cultured in DMEM supplemented with 20% FBS and 1% antibiotic/antimycotic solution (AB, Gibco, USA). Explant-derived DP cells were then passage into bovine collagen (Sigma-Aldrich, USA) coated-flasks and cultured in DMEM with 10% FBS and 1% AB up to passage 6 at most. Human dermal fibroblasts were isolated as previously described [37] from

discarded skin from plastic surgeries at Hospital da Prelada (Porto, Portugal). Cells were cultured in Minimum Essential Medium Eagle - Alpha Modification (α-MEM, Gibco, USA) supplemented with 10% FBS and 1% AB and used up to passage 4. Human foreskin tissue obtained from Hospital Narciso Ferreira (Braga, Portugal) was used to isolate keratinocytes following the same procedure previously established for adult skin [37]. KCs were cultured in Keratinocyte Serum-free Medium (KSFM, Gibco, USA) supplemented with Y-27632 (10 μM, STEMCELL Technologies, Canada) up to 90% of confluence and used without further expansion. All cultures were conducted in a humidified atmosphere (37°C, 5% CO_2) and with medium changes every 2-3 days.

V-2.6. Cell encapsulation within gellan gum hydrogels

Hydrogels were prepared as described above after re-suspending the DP cells in the GGDVS-peptide solution and mixing with the same volume of unmodified GG at a cellular density of $1x10^4$ cells/μL. DP cells were encapsulated in non-functionalized GG (GG control) or GGDVS (GGDVS control) hydrogels as controls. The cell-laden hydrogels were cultured in DP cell medium up to 7 days with medium changes every 2-3 days.

V-2.7. Analysis of cell viability and cytoskeleton organization

Cell viability was evaluated after calcein-AM and propidium iodide (PI) staining. Briefly, cell-laden hydrogels were incubated with calcein-AM (1 μg/mL; Molecular Probes, USA) and propidium iodide (PI) (2 μg/mL; Molecular Probes, USA) for 1h at 37°C, under standard culture conditions (37°C, 5% CO_2). For the visualization of DP cell F-actin filaments, cell-laden hydrogels were fixed with 10% formalin (1h, RT), washed in phosphate-buffered saline (PBS) and incubated with phalloidin–TRITC (0.1 mg/mL; Sigma-Aldrich, USA) for 1h at RT. Nuclei were counterstained with 4,6-diamidino-2-phenylindole (DAPI) (0.02 mg/mL, Biotium, USA). All samples were observed and images acquired with an Olympus Fluoview FV1000 confocal laser microscope (Olympus, Japan).

V-2.8. Cell cytotoxicity assessment

The lactate dehydrogenase (LDH) amount of encapsulated cells was assessed using the Pierce LDH Cytotoxicity Assay Kit (Thermo Fisher Scientific, USA). Before each experimental time point, the

culture medium was renewed and after 24h the supernatant was collected, centrifuged (250 rcf, 3 min) and directly assayed according to manufacturer instructions. Supernatants collected from acellular hydrogels maintained in the same experimental culture conditions were used as blanks. Maximum LDH activity was established for each experimental condition by promoting total LDH release with the kit lysis buffer (1h, 37°C). The cytotoxicity was then calculated using the following formula:

$$\% \text{ Cytotoxicity} = \frac{(\text{Sample LDH} - \text{blank LDH}) \times 100}{(\text{Maximum LDH} - \text{blank LDH})}$$

V-2.9. Quantification of collagen and non-collagenous protein production

The Sirius Red/Fast Green Collagen Staining Kit (Chondrex Inc, USA) was used to quantify the amount of collagen (COL) and non-collagenous proteins (NCOL) produced by encapsulated DP cells. Briefly, cell-laden hydrogels were fixed with 10% formalin (1h, RT), washed in PBS and incubated with dye solution for 30 min at RT. The solution was then removed, and the samples were washed several times in water under mild stirring until it runs clear, guaranteeing unbounded dye elution. The bound dye was then released with the extraction solution and the absorbance was measured at 540 nm (Sirius Red) and 605 nm (fast green). Control acellular hydrogels were equally processed and used as blanks of the assay.

V-2.10. Immunocytochemistry

Immunostaining of cell-laden hydrogels was carried out after formalin fixation and permeabilization of the DP cells with 0.2% (v/v) Triton X-100 (30 min, ice), and blocking of non-specific binding sites with a 3% (w/v) bovine serum albumin (BSA; Sigma-Aldrich, USA) solution for 1h at RT. Samples were then incubated with the primary antibodies (Table II-5) diluted in 1% BSA with 0.2% Triton and incubated for 24h at 4°C. After washing 3 times with PBS under mild agitation, were incubated with Alexa Fluor (488/594)-conjugated secondary antibodies (1:500; Molecular Probes, USA) overnight at 4°C. Cell-laden hydrogels were then washed with PBS before and after cell nuclei counterstained with DAPI for 1h

at RT. All samples were observed with an Olympus Fluoview FV1000 confocal laser microscope (Olympus, Japan).

V-2.11. Alkaline phosphatase quantification

Encapsulated DP cells were lysed by incubation with ultra-pure water with 0.01% sodium dodecyl sulfate for 1h at 37°C, followed by freezing at -80°C. Before quantification, cell-laden hydrogels were defrosted and sonicated for 5 seconds on ice to ensure a complete disintegration of the hydrogels and full cellular disruption (VCX-130PB-220 ultrasonic processor; Sonics, USA). The amount of active ALP present in the samples was determined using the Alkaline Phosphatase Detection Kit (Sigma-Aldrich, USA) according to the supplier instructions. The lysates were also used to quantify cellular DNA content, using the Quant-iT™ PicoGreen® dsDNA Assay Kit (Thermo Fisher Scientific, USA) as instructed by the kit manufacturer, and used to normalize ALP data. For both quantifications, acellular hydrogels were equally processed and used as blanks of the assay.

V-2.12. Alkaline phosphatase staining

The detection of ALP-active DP cells was performed in formalin-fixed cell-laden hydrogels using the *p*-nitro blue tetrazolium (NBT)/ 5-bromo-4-chloro-3-indolyl phosphate (BCIP) substrate system. The staining solution was prepared by diluting 5 μL of NBT and 3.75 μL of BCIP (Roche, Switzerland) per mL of buffer solution (100 mM NaCl, 100 mM Tris-HCl pH 9.5 and 50 mM $MgCl_2$ in water). The staining solution was applied for 20 min (RT, dark) and samples were washed with water before examination under a bright-field microscope (Axio Imager Z1m; Zeiss, Germany).

V-2.13. Organotypic skin model

The organotypic human skin model established as previously described [38], with some modifications. Firstly, an acellular layer was prepared by mixing basal α-MEM (10x) with 1N sodium hydroxide and rat tail collagen I (3 mg/mL, Invitrogen, USA) at a ratio of 10:2.5:87.5, respectively. Afterwards, 250 μL of the collagen solution was cast onto 12-well polyester inserts (0.4 μm pore, Corning, USA) and left to polymerize (30-40 min, 37°C). The fibroblast cellular layer was prepared by dispensing 750 μL of the collagen solution incorporating dermal fibroblasts at a density of 7.5×10^4

cells/mL, on top of the acellular layer. This layer was allowed to polymerize for 2h in the incubator (37°C) and was then kept in α-MEM with 10% FBS. In the next day, DP cells encapsulated in 1.25% GG-derived hydrogels were incorporated into the dermal equivalent. For that, 1 µL of the pre-hydrogel solution was dispensed inside the collagen cellular gel using a 10 µL viscous pipette (Gilson, USA). At this point, the medium was changed to DMEM with 10% FBS and medium changes were performed every 2-3 days. One week after the formation of the dermal equivalents, 5×10^4 KCs were re-suspended in 50 µL of KSFM and seeded on top of the cellular layer. The whole model was cultured for one week further using KSFM on the insert and DMEM 10% FBS in the bottom well. The model was then lifted to air-liquid interface and cells were fed from bellow with FAD medium - DMEM/Ham's F12 medium (3:1 ratio) supplemented with 1.8×10^4 M adenine, 10% non-inactivated FBS, 0.5 µg/mL hydrocortisone, 10^{-10} M cholera toxin, 10 ng/mL epidermal growth factor, 5 µg/mL insulin and 1.8 mM $CaCl_2$. After two weeks, the model was fixed with 10% formalin and processed for paraffin inclusion and histological analysis.

V-2.14. Histological analysis

5 µm paraffin-embedded sections were prepared and stained with Haematoxylin & Eosin (H&E, Thermo Scientific, USA) according to standard procedures. For the visualization of GAGs, sections were rinsed in a 3% acetic acid solution and stained with 1% Alcian blue 8GX (Sigma-Aldrich, USA) prepared in the rinsing solution (pH 2.5) for 30 min at RT. After washing with water, representative images were acquired with a Leica DM750 microscope (Leica, Germany).

For immunostaining, heat-mediated antigen retrieval (sodium citrate buffer, pH 6.0) was performed on deparaffinized sections. Permeabilization was then performed for 15 min (RT) with 0.2 % Triton X-100, and blocking of non-specific binding sites was done with 3 % BSA for 45 min (RT). Samples were incubated with primary antibodies (Supplementary Table V-1) for 1h at RT, then washed three times with PBS and incubated with secondary antibodies (1:500; Molecular Probes) for 1h at RT. Nuclei were counterstained with DAPI (15 min, RT) and samples were observed using an Axio Imager Z1m microscope.

V-2.15. Statistical analysis

GraphPad Prism 7.03 software (GraphPad Software Inc, USA) was used to perform statistical analysis and data normality was tested with the D'Agostino & Pearson test. All data followed a normal distribution and were analyzed using a one-way ANOVA followed by the Tukey's multiple comparison test. Significance was set to $*p < 0.05$, $**p < 0.01$, $***p < 0.001$; $****p < 0.0001$. All quantitative data refer to $n = 3$ using DP cells from different cell donors and are presented as mean $\pm$ SEM

V-3.   RESULTS

V-3.1.   Effect of polymer concentration and modification on the mechanical properties of the hydrogels

Considering the nature of the native DP's ECM (Figure V-1A), the intermediary moiety DVS was conjugated to the GG backbone and further functionalized with the HepIII and cRGDfC peptide sequences (Figure V-1B). While the conjugation efficiency for the HepIII sequence was $100 \pm 0.8\%$, for cRGDfC it was only $17 \pm 0.2\%$, even though the amount of peptide used was twice (800 µM) the one of HepIII.
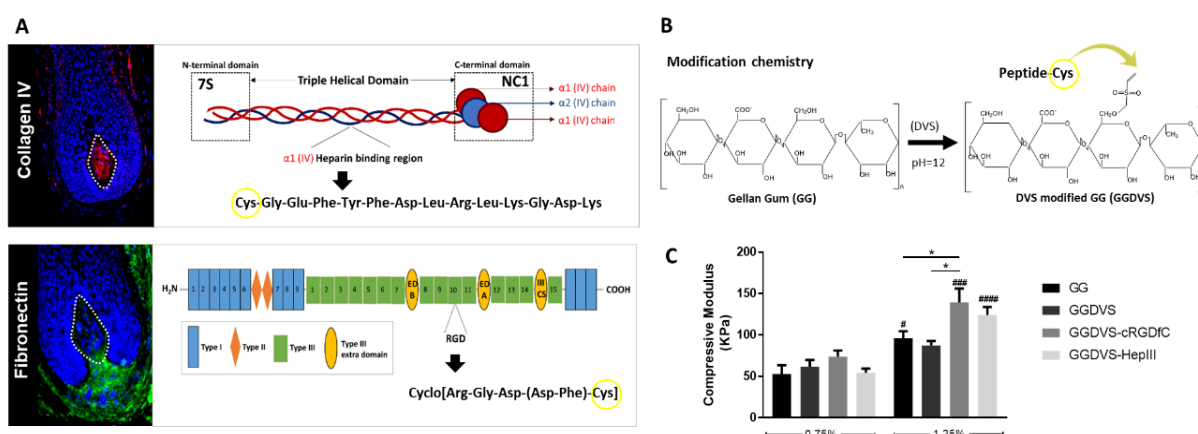
Figure V-1 – Relationship between peptide modification and polymer concentration in the mechanical properties of the hydrogels. (A) Representative immunohistochemical images of the DP (dashed line) stained for collagen type IV and fibronectin, which inspired the (B) conjugation of their respective peptide sequences - HepIII and cRGDfC - into the gellan gum (GG) monomeric structure, using an intermediary DVS moiety to covalently immobilize the peptide through its cysteine residue (yellow circle). (C) Compressive mechanical properties (KPa) of the different GG-derived hydrogels. $*$ $p < 0.05$; $\#$ $p < 0.05$, $\#\#\#$ $p < 0.001$, $\#\#\#\#$ $p < 0.0001$ *vs.* the corresponding formulation with 0.75% GG final concentration.

GG crosslinks through temperature decrease, by the reorganization of its polymeric structure, and the posterior stabilization by ionic-crosslinking, with the cations present in the culture medium. Therefore, peptides conjugation to the GG backbone may affect both GG sol-gel transition during the physical-crosslinking as well as the ionic-crosslinking, thus altering the hydrogels mechanical properties. Therefore, the influence of the polymer amount (0.75% and 1.25%), as well as the conjugation with the different peptides, on the mechanical behavior of the prepared hydrogels was tested under static compression. The stiffness of the hydrogels increased with higher polymer amount, as shown by the significantly higher compressive modulus for GG, GGDVS-cRGDfC and GGDVS-HepIII hydrogels with 1.25% of polymer content, in comparison to the corresponding hydrogels prepared with 0.75% GG (Figure V-1C). Peptide presence did not influence the compressive modulus when 0.75% of GG was used, but in the 1.25% GGDVS-cRGDfC formulation it led to a significantly higher compressive modulus comparably to GG and GGDVS hydrogels with the same polymer concentration. No differences were observed between hydrogels functionalized with the distinct peptides, regardless of the peptide final concentration.

V-3.2.   Effect of polymer concentration and modification on the adhesion and viability of DP cells

Given that both the HepIII [39] and cRGDfC [34] peptides are inspired in sequences that promote cellular adhesion, we studied the response of DP cells to these peptide motifs, after cellular encapsulation. Analysis of the cells' F-actin cytoskeleton organization confirmed that DP cells adhered to the peptides within the biofunctionalized hydrogels with 1.25% GG, in opposition to what was observed for the 0.75% formulations and controls (Figure V-2A). Cells encapsulated in the 0.75% GG derived-hydrogels displayed a round morphology, independently of the linked peptide. Interestingly, after 3 days of culture in the 1.25% GG-hydrogels, cells in hydrogels functionalized with the cRGDfC peptide were significantly less spread than the ones functionalised with the HepIII peptide. In fact, in GGDVS-HepIII_1.25% hydrogels cells formed an interconnected network of highly spread cells populating most of the hydrogel. Similar results were observed one week after encapsulation (Supplementary Figure V-1A). However, cells with a polarized morphology were observed in the 0.75% GG hydrogels functionalized with peptides, suggesting that in these materials cell adhesion may have been delayed. Significant additional morphological changes were not observed.

The effectiveness of the produced hydrogels also depends on their ability to support the basal metabolism of the cells. To confirm that both the chemical modification used to functionalize GG and

the density of the polymeric network, directly related to hydrogels diffusion properties [31,40], did not have a negative influence, we studied the viability of the cells 3 (Figure V-2B) and 7 (Supplementary Figure V-1B) days after encapsulation. The amount of polymer did not affect cell viability except for GGDVS hydrogels after 3 days of culture, which showed cytotoxicity of $15.30 \pm 0.95\%$ and $32.75 \pm 1.89\%$, respectively for the GGDVS_0.75% and GGDVS_1.25% formulations (Figure V-2C). Interestingly, the type of peptide had an impact on DP cell viability. The introduction of the cRGDfC peptide sequence significantly decreased cytotoxicity in comparison to both GG and GGDVS, independently of the amount of GG. In what concerns the effect of GGDVS-HepIII, no significant effects were detected comparably to controls (GG and GGDVS) except for the GGDVS_1.25% formulation, which presented a significantly higher percentage of dead cells. After 7 days of culture, the early differences observed in cell death were annulled, and a common level of cytotoxicity ($\leq 9.03 \pm 1.20\%$) was observed for all hydrogels (Supplementary Figure V-1B and C).
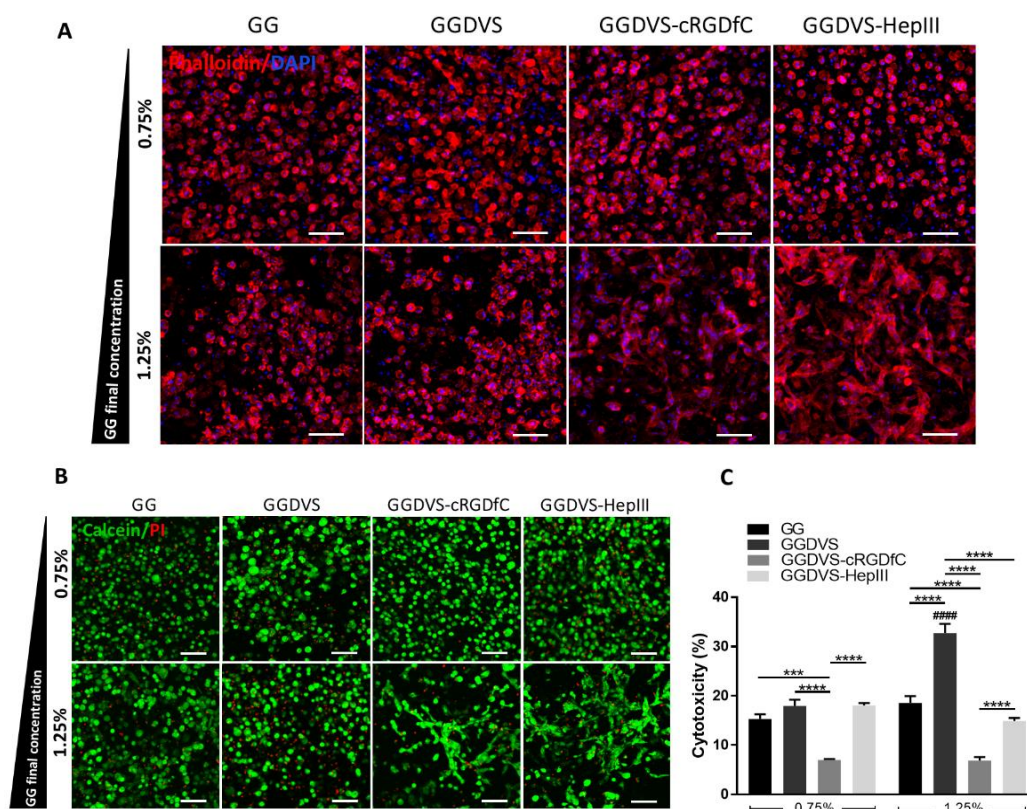
Figure V-2 – Adhesion and viability of DP cells within GG-derived hydrogels. Representative images of (A) β-actin filaments stained with phalloidin-TRITC (red) and B) calcein (green) and PI (red) of DP cells encapsulated within the different hydrogel formulations after 3 days in culture. Nuclei were counterstained with DAPI (blue). (C) Quantification of the cytotoxicity of the different hydrogel formulations over encapsulated DP cells after 3 days in culture. *** $p < 0.001$, **** $p < 0.0001$; #### $p < 0.0001$ *vs.* the corresponding formulation with 0.75% GG final concentration. Scale bars = 100 μm.

V-3.3.   Effect of polymer concentration and modification on ECM deposition

Although the 3D culture in ECM-biomimetic hydrogels may provide DP cells with positional (3D) and contextual (peptides) cues, they should be able to produce their own matrix to further enhance the recreation of their microenvironment.

Analysis of the production and deposition of COL proteins showed that it was higher in GG_1.25 %, GGDVS_1.25% and GGDVS-cRGDfC_1.25% hydrogels than in the corresponding formulations prepared with lower polymer amount at the early time point (Figure V-3A). Along with the culture, differences observed between materials prepared with 0.75% or 1.25% GG became less evident (Figure V-3B) except for GGDVS-HepIII, in which COL deposition was significantly higher in 1.25% GG hydrogels. Interestingly, while the amount of COL proteins in GGDVS-cRGDfC hydrogels was similar to controls, in GGDVS-HepIII hydrogels it was significantly lower than in all the other formulations, regardless of the polymer amount and culture time (Figure V-3A and B). This was also confirmed by immunostaining for collagen type I in the 1.25% GG-derived formulations after 3 days in culture (Figure V-3C).
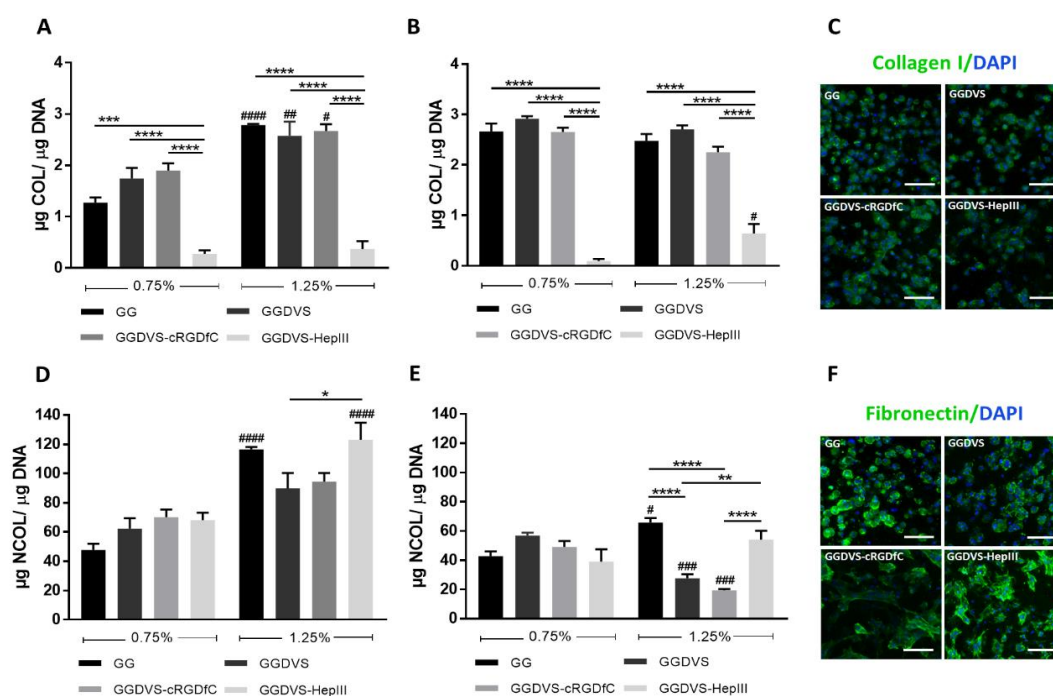
Figure V-3 – Quantification of the production of (A,B) collagen (COL) and (C,D) non-collagenous (NCOL) proteins after (A,D) 3 and (B,E) 7 days in culture.   Representative immunocytochemistry images of (C) collagen type I and (F) fibronectin expression within 1.25% GG-derived hydrogels after 3 days of culture. The cells' nuclei were counterstained with DAPI (blue). *$p < 0.05$, ** $p < 0.01$, *** $p < 0.001$, **** $p < 0.0001$; #$p < 0.05$, ## $p < 0.01$, ### $p < 0.001$, #### $p < 0.0001$ *vs.* the corresponding formulation with 0.75% GG final concentration. Scale bars = 75 μm.

Regarding the production and secretion of NCOL elements in day 3, it was significantly higher in GGDVS-HepIII_1.25% and GG_1.25% (Figure V-3D) formulations than in the corresponding hydrogels prepared with 0.75% GG. At day 7, NCOL proteins production dropped, particularly in 1.25% GG formulations (Figure V-3E). In fact, higher polymer amount continued to be favourable in the case of the unmodified hydrogels, but NCOL proteins production in GGDVS and GGDVS-cRGDfC hydrogels was significantly lower than in the corresponding 0.75% formulations. Concerning the peptide effect, cRGDfC did not affect NCOL production except for longer culture times at which a significantly lower amount was observed for the 1.25% formulation in comparison to GG and GGDVS-HepIII hydrogels prepared with the same amount of polymer. Furthermore, DP cells in GGDVS-HepIII hydrogels produced significantly more NCOL proteins than in GG-DVS controls, independently of the time of culture. This tendency was confirmed by immunocytochemistry for the NCOL fibronectin (Figure V-3F) and laminin (Supplementary Figure V-2) in the 1.25% GG-derived formulations, after 3 days in culture.

V-3.4. Effect of polymer modification on the phenotype of DP dells

The capacity of cultured DP cells to promote hair growth is directly linked with their active ALP [28], thus considered a critical marker of these cells' inductive ability. Moreover, culturing DP cells in 3D spheroids improves their native signature [12], and is considered the gold-standard method to restore the inductive capacity of human DP cells.

The encapsulation of DP cells in GG hydrogels led to a significant increase in the amount of active ALP, independently of the formulation (Figure V-4A, Supplementary Figure V-3A). This is particularly meaningful considering that the amount of active ALP quantified in 3D spheroids was $0.046 \pm 0.173\%$ and similar (p >0.05) to the value quantified in DP cells before encapsulation (0.044 ± 0.012 µg/mL, Control Figure V-4A, Supplementary Figure V-3A). Analysis of the GG final concentration-effect showed that the amount of active ALP in GGDVS and GGDVS-HepIII hydrogels prepared with 1.25% (Figure V-4A) was significantly higher than in the corresponding 0.75% (Supplementary Figure V-4) ones. The presence or type of peptide used for the functionalization did not affect the amount of active ALP in DP cells. However, a dramatic decrease of active ALP levels was observed for longer culture times in all hydrogel formulations, independently of the polymer amount and linked peptide (Figure V-4B, Supplementary Figure V-3B). Given the remarkable increase of DP cells' ALP activity in 1.25% GG-derived hydrogels after 3 days of culture, we further confirmed a higher number of ALP-active DP cells in this formulation, independently of the displayed morphology (Figure V-4C). Moreover, DP cells in

1.25% GG-derived hydrogels retained the expression of the versican V1-isoform and α-SMA (Figure V-4D) and were also able to partially recover the expression of the versican V2-isoform. In the native DP, the V2-isoform of versican is the most abundantly expressed isoform but is lost when cells are cultured *in vitro*, whereas the v1-isoform can be observed *in situ* but its expression is stronger in culture [41]. In turn, α-SMA is only expressed by cultured DP cells, and cannot be observed in the native DP [42]. Therefore, an improved phenotype was observed in the 1.25% GG-derived hydrogels after 3 days of culture.
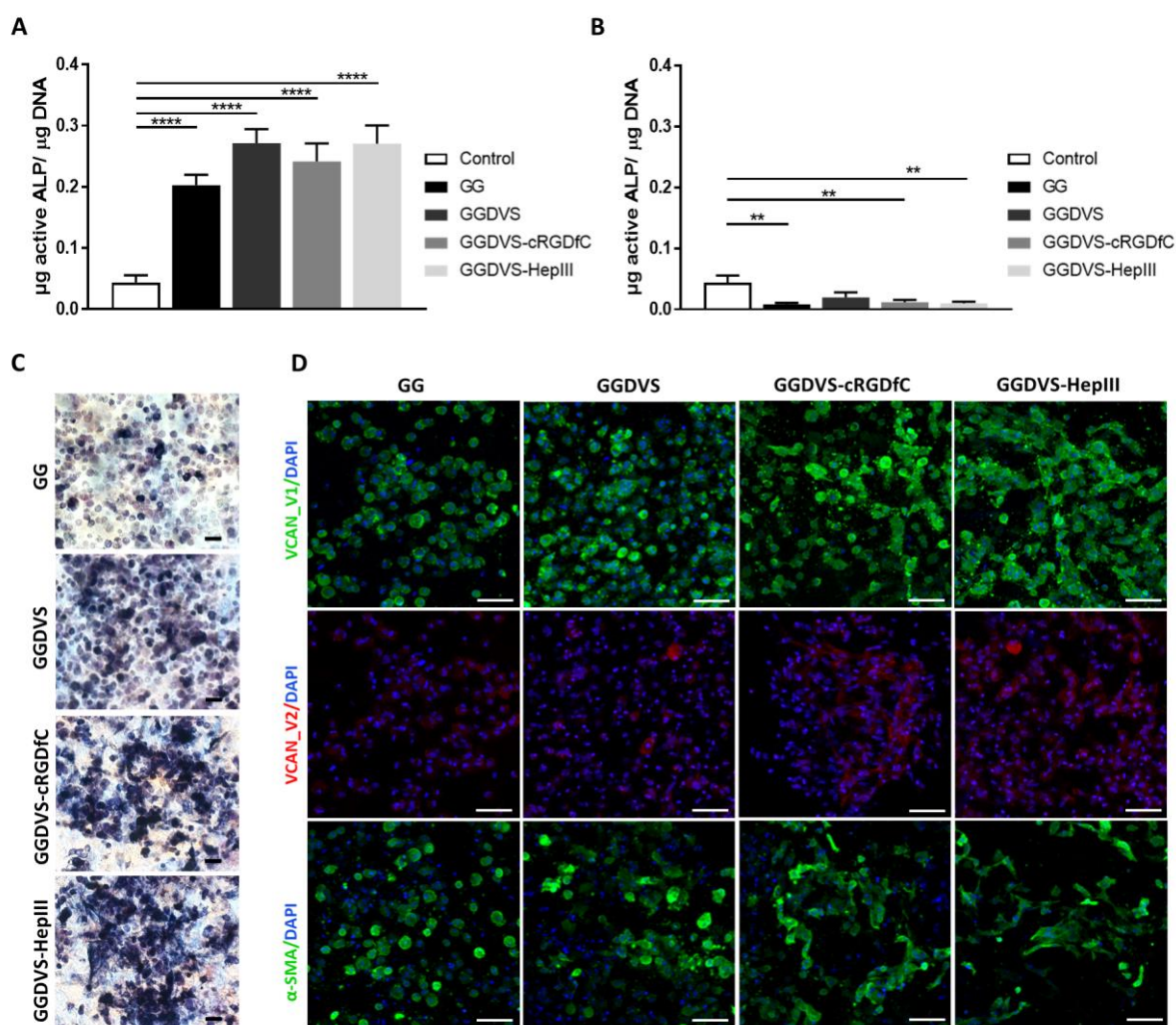
Figure V-4 –Phenotype of DP cell-laden hydrogels. Quantification of active ALP in DP cells before (Control) and after encapsulation in GG-derived hydrogels after 3 (A) and 7 (B) days of culture. C) Staining of ALP-active DP cells within 1.25% GG-derived hydrogels after 3 days in culture. (D) Representative immunocytochemistry images of the expression of the DP cell markers versican isoform V1 (VCAN_V1) (green, upper panel), versican isoform V2 (VCAN_V2) (red, middle panel) and α-SMA (green, lower panel). Nuclei were counterstained with DAPI (blue). **** $p < 0.0001$, **$p < 0.01$; Scale bars are 50 μm for (B) and 75 μm for (D).

V-3.5. Functional capacity of DP cell-laden hydrogels in a human skin model

Despite the demonstrated inductive recovery, the success of the proposed strategy strongly relies on the capacity of DP cells to induce molecular interactions with proximal epithelial cells, since the bidirectional crosstalk between these cells is fundamental to promote hair growth [43,44].

To test the capacity of DP cells to communicate with epithelial cells, we took advantage of the well-established skin organotypic model, in which the DP cell-laden hydrogels prepared with 1.25% GG were incorporated. Within this model, epithelial cells were capable of down growth and surround the DP cell-laden hydrogels in a biomimetic fashion (Figure V-5A). This phenomenon did not occur in the control condition (standard organotypic model), nor when dissociated DP cells (cell slurry) without any support material were directly injected in the dermal layer (Supplementary Figure V-4). Additionally, the epithelial strand surrounding DP cell-laden hydrogels was thicker in the case of GGDVS or GGDVS-peptide hydrogels (Figure V-5A).
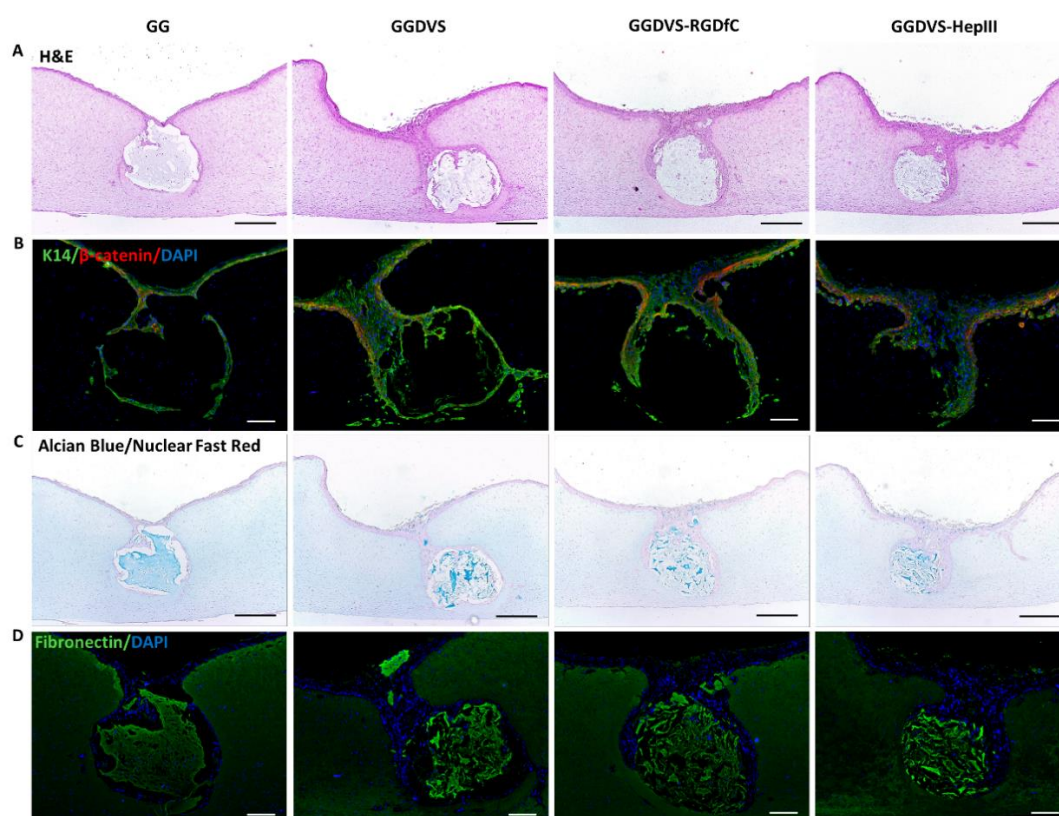
Figure V-5 – Functionality of DP cell-laden hydrogels in an organotypic human skin model. (A) H&E staining of the skin constructs 27 days after inclusion of the cell-laden hydrogels. (B) Representative immunocytochemistry images of keratin (K) 14 (green) and β-catenin (red) expression by keratinocytes. Nuclei were counterstained with DAPI (blue). (C) Alcian Blue staining performed at pH 2.5, with nuclear fast red counterstain, to detect the expression of acidic GAGs. (D) Representative immunocytochemistry images of fibronectin deposition. Scale bars are 500 µm for (A, C) and 200 µm for (B, D).

Interestingly, KCs were kept in an early differentiation state as demonstrated by the expression of the epithelial basal markers keratin(K)14 and β-catenin (Figure V-5B). Analysis of the ECM environment within the DP cell-laden hydrogels demonstrated that DP cells were surrounded by sulfated and carboxylated acidic GAGs, as shown by the Alcian blue staining (Figure V-5C) and as in the native tissue (Supplementary Figure V-5), and by fibronectin (Figure V-5D) in what seems higher amounts comparably to fibroblasts in the non-follicular dermal part.

V-4.   DISCUSSION

Human DP cells are highly specialized cells that rely on positional and contextual cues from their surrounding microenvironment. Standard 2D culture conditions are fairly poor at recreating this rich microenvironment while 3D spheroids, although considered the gold-standard method to restore human DP cell inductivity, are also far from satisfactory given the lack of a supportive ECM.

The encapsulation of DP cells in collagen [22], or hydrogels formed by the self-assembly of synthetic peptides RAD16-I [45], was already demonstrated to improve the inductive capacity of DP cells in comparison to both 2D cultures and 3D spheroids, demonstrating the importance of 3D matrices. However, the specific nature of the DP matrix-microenvironment has been generally overlooked. Bridging this gap, we investigated the effect of GG functionalization with the HepIII and cRGDfC peptides, derived respectively from collagen type IV and fibronectin, in the recreation of cell-ECM interactions, subsequent cell-cell connections and in the generation of a 3D environment in which DP cell phenotype and physiological functions are restored.

We showed that DP cell adhesion within the produced hydrogels was promoted by peptide conjugation to GGDVS. However, this effect was not observed for functionalized hydrogels with lower GG amount, indicating that the hydrogels' stiffness also affected cell behavior, confirming previous findings where an increase in substrate stiffness was directly correlated with increased DP cell attachment and spreading [46]. Furthermore, GGDVS-HepIII_1.25% hydrogels allowed the creation of complex cellular networks and enabled cell-cell interactions. Cellular adhesion was also observed in GGDVS-cRGDfC_1.25% hydrogels but was not as extensive, most likely due to the low conjugation efficiency of cRGDfC. This may be explained by cRGDfC structural parameters, namely the proximity between its cysteine and arginine residues within the peptide cyclic sequence. Cysteines are more reactive near basic amino acids, such as arginine, and therefore promote the effect of conjunct group participation,

151

which in turn can accelerate the oxidation rate of the cysteine thiol molecule and the consequent formation of disulfide-linked dimers [47,48]. Overall, this might lead to a decreased amount of peptide with cysteine groups available for conjugation with GGDVS. Unmodified GG hydrogels did not promote cell adhesion, independently of the concentration used, which was expected given the lack of adhesive motifs in the GG monomeric structure and the high-water-content of the derived hydrogels [49].

It has long been recognized that the mitotic activity of the hair bulb and, consequently, HF bulb and hair fiber volumes correlate with the volume of the DP, to which partially contributes the amount of ECM produced [50]. During anagen, DP ECM production is extensive and decreases afterwards, implying an important role in the regulation of HF morphogenetic events *in vivo* [3,5,51]. Given that cell adhesion is dependent on the mechano-chemical nature of the ECM substrates [52], and that cell adhesion (cell-ECM interaction) was clearly promoted in GGDVS-HepIII_1.25% hydrogels, an improved ECM deposition would be expected in these materials. Nonetheless, a lower COL/NCOL ratio was observed, which might indicate the existence of a negative feedback mechanism from the recognition of the collagen IV peptide and in the predominant production and secretion of NCOL proteins. This effect was not as striking for GGDVS-cRGDfC hydrogels in respect to NCOL proteins production, probably due to the lower conjugation efficiency verified for this peptide, which may have not been enough to modulate DP cell ECM production.

As described before, the amount of active ALP in cultured DP cells directly correlates with these cells' inductivity [28]. DP cells encapsulation in GG-derived hydrogels was enough to increase their active ALP levels, including in comparison to 3D spheroids. Although in spheroidal cultures DP cells can produce ECM molecules [12,53], it is probably insufficient to recreate the DP rich ECM, while in GG-derived hydrogels the higher matrix-to-cell ratio may better support their cellular behaviour and functions. Moreover, the three-dimensionality, together with GG structural similarity with the native ECM GAGs composition, conferred by the presence of glucuronic acid residues in the monomeric units [54], may have contributed to this effect. Indeed, the most abundant GAGs present in the DP – chondroitin sulfate, heparan sulfate and dermatan sulfate [2,55] – have in common with GG the presence of glucuronic acid residues within their structure [56]. Additionally, the amount of active ALP was higher in 1.25% GG cell-laden hydrogels, independently of peptide functionalization, suggesting that the stiffness of the hydrogels played a role in the recovery of DP cell inductivity. Nonetheless, the functionalization with peptides did not further add to this effect. Intriguingly, the recovery in DP cell inductivity in our hydrogels was lost after 7 days in culture, even though the viability of the cells was excellent. An

opposite effect was observed for DP cells encapsulated in collagen [22] or RADA6-I self-assembled hydrogels [45], however, the assessment is either based on ALP gene expression or qualitative results of active ALP.

HF morphogenesis and cycling are dependent on bidirectional epithelial-mesenchymal interactions [44,57] however, even embedded in an ECM-biomimetic matrix, DP cells still lack external signaling which may be preventing them from maintaining the recovered inductivity for longer culture times. Remarkably, when cell-laden hydrogels were incorporated in a well-established human skin organotypic model, epithelial cells from the reconstructed epidermis were capable of migrating and surrounding the artificial DP. This suggests that encapsulated DP cells are capable of creating a chemotactic gradient that promotes epithelial cells down growth, in a process that is reminiscent of the initial steps required for hair development and postnatal cyclical growth [58,59]. This observation was supported by strong β-catenin expression in the epidermis basal layer, a key regulator of the Wnt signalling that needs to be expressed to promote placode formation and HF morphogenesis [60]. The DP GG-derived ECM also had stronger fibronectin and acidic GAGs expression in comparison with the dermal compartment, which are common features of the DP ECM [2–4]. Moreover, the hydrogel structure was kept intact throughout the 27 days of culture that followed their incorporation in the model, despite the continuous remodelling of the surrounding collagen matrix by fibroblasts, which represents an advantage in the compartmentalization of the DP specific ECM microenvironment.

V-5.   CONCLUSIONS

In this work, the HepIII and cRGDfC peptide motifs were conjugated to the GG backbone to produce hydrogels capable of specifically emulating the DP ECM. We demonstrated that the functionalized hydrogels produced with higher GG amount promoted the adhesion of the encapsulated DP cells, whereas the type of peptide and GG amount independently modulated the type and quantity of deposited ECM proteins. Furthermore, stiffer hydrogels were also capable of improving DP cell inductive phenotype and recapitulating basic hair morphogenesis events in an organotypic human skin model, independently of the conjugated peptide. Taken together our results show that GG-derived hydrogels are versatile and promising for the recreation of the DP 3D microenvironment, allowing the production of an artificial DP that can be used as a platform to study the HF mesenchyme, or to evaluate new candidate drugs. Isolated or in more complex model systems, artificial DP may also be used for the therapeutic management of hair loss disorders.

V-6. REFERENCES

1. Yang, C.-C. & Cotsarelis, G. Review of hair follicle dermal cells. *J. Dermatol. Sci.* **57**, 2–11 (2010).

2. Couchman, J. R. Rat hair follicle dermal papillae have an extracellular matrix containing basement membrane components. *J. Invest. Dermatol.* **87**, 762–767 (1986).

3. Messenger, A. G., Elliott, K., Westgate, G. E. & Gibson, W. T. Distribution of extracellular matrix molecules in human hair follicles. *Ann. N. Y. Acad. Sci.* **642**, 253–62 (1991).

4. Link, R. E., Paus, R., Stenn, K. S., Kuklinska, E. & Moellmann, G. Epithelial Growth by Rat Vibrissae Follicles In Vitro Requires Mesenchymal Contact via Native Extracellular Matrix. *J. Invest. Dermatol.* **95**, 202–207 (1990).

5. Jahoda, C. A., Mauger, A., Bard, S. & Sengel, P. Changes in fibronectin, laminin and type IV collagen distribution relate to basement membrane restructuring during the rat vibrissa follicle hair growth cycle. *J. Anat.* **181**, 47–60 (1992).

6. Frantz, C., Stewart, K. M. & Weaver, V. M. The extracellular matrix at a glance. *J. Cell Sci.* **123**, 4195–4200 (2010).

7. Daley, W. P., Peters, S. B. & Larsen, M. Extracellular matrix dynamics in development and regenerative medicine. *J. Cell Sci.* **121**, 255–264 (2008).

8. Rendl, M., Polak, L. & Fuchs, E. BMP signaling in dermal papilla cells is required for their hair follicle-inductive properties. *Genes Dev.* **22**, 543–557 (2008).

9. Ohyama, M., Kobayashi, T., Sasaki, T., Shimizu, A. & Amagai, M. Restoration of the intrinsic properties of human dermal papilla in vitro. *J. Cell Sci.* **125**, 4114–4125 (2012).

10. Osada, A., Iwabuchi, T., Kishimoto, J., Hamazaki, T. S. & Okochi, H. Long-Term Culture of Mouse Vibrissal Dermal Papilla Cells and De Novo Hair Follicle Induction. *Tissue Eng.* **13**, 975–982 (2007).

11. Young, T.-H., Lee, C.-Y., Chiu, H.-C., Hsu, C.-J. & Lin, S.-J. Self-assembly of dermal papilla cells into inductive spheroidal microtissues on poly(ethylene-co-vinyl alcohol) membranes for hair follicle regeneration. *Biomaterials* **29**, 3521–3530 (2008).

12. Higgins, C. A., Richardson, G. D., Ferdinando, D., Westgate, G. E. & Jahoda, C. A. B. Modelling

the hair follicle dermal papilla using spheroid cell cultures. *Exp. Dermatol.* **19**, 546–548 (2010).

13. Driskell, R. R. *et al.* Clonal Growth of Dermal Papilla Cells in Hydrogels Reveals Intrinsic Differences between Sox2-Positive and -Negative Cells In Vitro and In Vivo. *J. Invest. Dermatol.* **132**, 1084–1093 (2012).

14. Higgins, C. A., Chen, J. C., Cerise, J. E., Jahoda, C. A. B. & Christiano, A. M. Microenvironmental reprogramming by three-dimensional culture enables dermal papilla cells to induce de novo human hair-follicle growth. *Proc. Natl. Acad. Sci.* **110**, 19679–19688 (2013).

15. Huang, Y.-C. *et al.* Scalable production of controllable dermal papilla spheroids on PVA surfaces and the effects of spheroid size on hair follicle regeneration. *Biomaterials* **34**, 442–451 (2013).

16. Lin, B. *et al.* Surface Tension Guided Hanging-Drop: Producing Controllable 3D Spheroid of High-Passaged Human Dermal Papilla Cells and Forming Inductive Microtissues for Hair-Follicle Regeneration. *ACS Appl. Mater. Interfaces* **8**, 5906–5916 (2016).

17. Miao, Y., Sun, Y. Bin, Liu, B. C., Jiang, J. D. & Hu, Z. Q. Controllable Production of Transplantable Adult Human High-Passage Dermal Papilla Spheroids Using 3D Matrigel Culture. *Tissue Eng. Part A* **20**, 2329–2338 (2014).

18. Wang, J. *et al.* Bottom-up Nanoencapsulation from Single Cells to Tunable and Scalable Cellular Spheroids for Hair Follicle Regeneration. *Adv. Healthc. Mater.* **7**, 1700447 (2018).

19. Mali, N. M. *et al.* Characterization of Human Dermal Papilla Cells in Alginate Spheres. *Appl. Sci.* **8**, 1993 (2018).

20. Lin, C. *et al.* Microencapsulated human hair dermal papilla cells: a substitute for dermal papilla? *Arch. Dermatol. Res.* **300**, 531–535 (2008).

21. Liu, Y. *et al.* Comparison of Calcium and Barium Microcapsules as Scaffolds in the Development of Artificial Dermal Papillae. *Biomed Res. Int.* **2016**, 1–11 (2016).

22. Kageyama, T., Yan, L., Shimizu, A., Maruo, S. & Fukuda, J. Preparation of hair beads and hair follicle germs for regenerative medicine. *Biomaterials* **212**, 55–63 (2019).

23. Limat, A. *et al.* Outer root sheath (ORS) cells organize into epidermoid cyst-like spheroids when cultured inside Matrigel: a light-microscopic and immunohistological comparison between human ORS cells and interfollicular keratinocytes. *Cell Tissue Res.* **275**, 169–176 (1994).

24. Havlickova, B., Biro, T., Mescalchin, A., Arenberger, P. & Paus, R. Towards optimization of an

organotypic assay system that imitates human hair follicle-like epithelial-mesenchymal interactions. *Br. J. Dermatol.* **151**, 753–765 (2004).

25. Havlickova, B. *et al.* A Human Folliculoid Microsphere Assay for Exploring Epithelial–Mesenchymal Interactions in the Human Hair Follicle. *J. Invest. Dermatol.* **129**, 972–983 (2009).

26. Chermnykh, E. S. *et al.* Dermal papilla cells induce keratinocyte tubulogenesis in culture. *Histochem. Cell Biol.* **133**, 567–576 (2010).

27. Wu, J.-J. *et al.* Hair follicle reformation induced by dermal papilla cells from human scalp skin. *Arch. Dermatol. Res.* **298**, 183–190 (2006).

28. Thangapazham, R. L. *et al.* Dissociated Human Dermal Papilla Cells Induce Hair Follicle Neogenesis in Grafted Dermal–Epidermal Composites. *J. Invest. Dermatol.* **134**, 538–540 (2014).

29. Lim, T. C. *et al.* Follicular dermal papilla structures by organization of epithelial and mesenchymal cells in interfacial polyelectrolyte complex fibers. *Biomaterials* **34**, 7064–7072 (2013).

30. Hughes, C. S., Postovit, L. M. & Lajoie, G. A. Matrigel: A complex protein mixture required for optimal growth of cell culture. *Proteomics* **10**, 1886–1890 (2010).

31. da Silva, L. P. *et al.* Gellan Gum Hydrogels with Enzyme-Sensitive Biodegradation and Endothelial Cell Biorecognition Sites. *Adv. Healthc. Mater.* **7**, 1700686 (2018).

32. Wilke, M. S. & Furcht, L. T. Human Keratinocytes Adhere to a Unique Heparin-Binding Peptide Sequence Within the Triple Helical Region of Type IV Collagen. *J. Invest. Dermatol.* **95**, 264–270 (1990).

33. Hersel, U., Dahmen, C. & Kessler, H. RGD modified polymers: biomaterials for stimulated cell adhesion and beyond. *Biomaterials* **24**, 4385–4415 (2003).

34. D'Souza, S. E., Ginsberg, M. H. & Plow, E. F. Arginyl-glycyl-aspartic acid (RGD): a cell adhesion motif. *Trends Biochem. Sci.* **16**, 246–250 (1991).

35. Carvalho, A. F., Gasperini, L., Ribeiro, R. S., Marques, A. P. & Reis, R. I. Control of osmotic pressure to improve cell viability in cell-laden tissue engineering constructs. *J. Tissue Eng. Regen. Med.* **12**, e1063–e1067 (2018).

36. Topouzi, H., Logan, N. J., Williams, G. & Higgins, C. A. Methods for the isolation and 3D culture of dermal papilla cells from human hair follicles. *Exp. Dermatol.* **26**, 491–496 (2017).

37. Cerqueira, M. T. *et al.* Cell sheet technology-driven re-epithelialization and neovascularization of skin wounds. *Acta Biomater.* **10**, 3145–3155 (2014).

38. Gangatirkar, P., Paquet-Fifield, S., Li, A., Rossi, R. & Kaur, P. Establishment of 3D organotypic cultures using human neonatal epidermal cells. *Nat. Protoc.* **2**, 178–186 (2007).

39. Koliakos, G. G., Kouzi-Koliakos, K., Furcht, L. T., Reger, L. A. & Tsilibary, E. C. The binding of heparin to type IV collagen: Domain specificity with identification of peptide sequences from the α1(IV) and α2(IV) which preferentially bind heparin. *J. Biol. Chem.* **264**, 2313–23 (1989).

40. Figueiredo, L. *et al.* Assessing glucose and oxygen diffusion in hydrogels for the rational design of 3D stem cell scaffolds in regenerative medicine. *J. Tissue Eng. Regen. Med.* **12**, 1238–1246 (2018).

41. Soma, T., Tajima, M. & Kishimoto, J. Hair cycle-specific expression of versican in human hair follicles. *J. Dermatol. Sci.* **39**, 147–154 (2005).

42. Jahoda, C. A. B., Reynolds, A. J., Chaponnier, C., Forester, J. C. & Gabbiani, G. Smooth muscle α-actin is a marker for hair follicle dermis in vivo and in vitro. *J. Cell Sci.* **99**, 627–636 (1991).

43. Schmidt-Ullrich, R. & Paus, R. Molecular principles of hair follicle induction and morphogenesis. *BioEssays* **27**, 247–261 (2005).

44. Sennett, R. & Rendl, M. Mesenchymal–epithelial interactions during hair follicle morphogenesis and cycling. *Semin. Cell Dev. Biol.* **23**, 917–927 (2012).

45. Betriu, N., Jarrosson-Moral, C. & Semino, C. E. Culture and Differentiation of Human Hair Follicle Dermal Papilla Cells in a Soft 3D Self-Assembling Peptide Scaffold. *Biomolecules* **10**, 684 (2020).

46. Tan, J. J. Y. *et al.* Impact of substrate stiffness on dermal papilla aggregates in microgels. *Biomater. Sci.* **6**, 1347–1357 (2018).

47. Wang, Z., Zhang, Y., Zhang, H., Harrington, P. B. & Chen, H. Fast and Selective Modification of Thiol Proteins/Peptides by N-(Phenylseleno)phthalimide. *J. Am. Soc. Mass Spectrom.* **23**, 520–529 (2012).

48. Liu, S. *et al.* Effect of structural parameters of peptides on dimer formation and highly oxidized

side products in the oxidation of thiols of linear analogues of human β-defensin 3 by DMSO. *J. Pept. Sci.* **15**, 95–106 (2009).

49. da Silva, L. P. *et al.* Engineering cell-adhesive gellan gum spongy-like hydrogels for regenerative medicine purposes. *Acta Biomater.* **10**, 4787–4797 (2014).

50. Elliott, K., Messenger, A. G. & Stephenson, T. J. Differences in Hair Follicle Dermal Papilla Volume are Due to Extracellular Matrix Volume and Cell Number: Implications for the Control of Hair Follicle Size and Androgen Responses. *J. Invest. Dermatol.* **113**, 873–877 (1999).

51. Couchman, J. R. & Gibson, W. T. Expression of basement membrane components through morphological changes in the hair growth cycle. *Dev. Biol.* **108**, 290–298 (1985).

52. Ringer, P., Colo, G., Fässler, R. & Grashoff, C. Sensing the mechano-chemical properties of the extracellular matrix. *Matrix Biol.* **64**, 6–16 (2017).

53. Gupta, A. C. *et al.* Establishment of an in vitro organoid model of dermal papilla of human hair follicle. *J. Cell. Physiol.* **233**, 9015–9030 (2018).

54. Bacelar, A. H., Silva-Correia, J., Oliveira, J. M. & Reis, R. L. Recent progress in gellan gum hydrogels provided by functionalization strategies. *J. Mater. Chem. B* **4**, 6164–6174 (2016).

55. Westgate, G. E., Messenger, A. G., Watson, L. P. & Gibson, W. T. Distribution of Proteoglycans During the Hair Growth Cycle in Human Skin. *J. Invest. Dermatol.* **96**, 191–195 (1991).

56. Couchman, J. R. & Pataki, C. A. An Introduction to Proteoglycans and Their Localization. *J. Histochem. Cytochem.* **60**, 885–897 (2012).

57. Botchkarev, V. A. & Kishimoto, J. Molecular Control of Epithelial–Mesenchymal Interactions During Hair Follicle Cycling. *J. Investig. Dermatology Symp. Proc.* **8**, 46–55 (2003).

58. Hardy, M. H. The secret life of the hair follicle. *Trends Genet.* **8**, 55–61 (1992).

59. Millar, S. E. Molecular Mechanisms Regulating Hair Follicle Development. *J. Invest. Dermatol.* **118**, 216–225 (2002).

60. Huelsken, J., Vogel, R., Erdmann, B., Cotsarelis, G. & Birchmeier, W. β-Catenin Controls Hair Follicle Morphogenesis and Stem Cell Differentiation in the Skin. *Cell* **105**, 533–545 (2001).

V-7.   SUPPLEMENTARY IMAGES
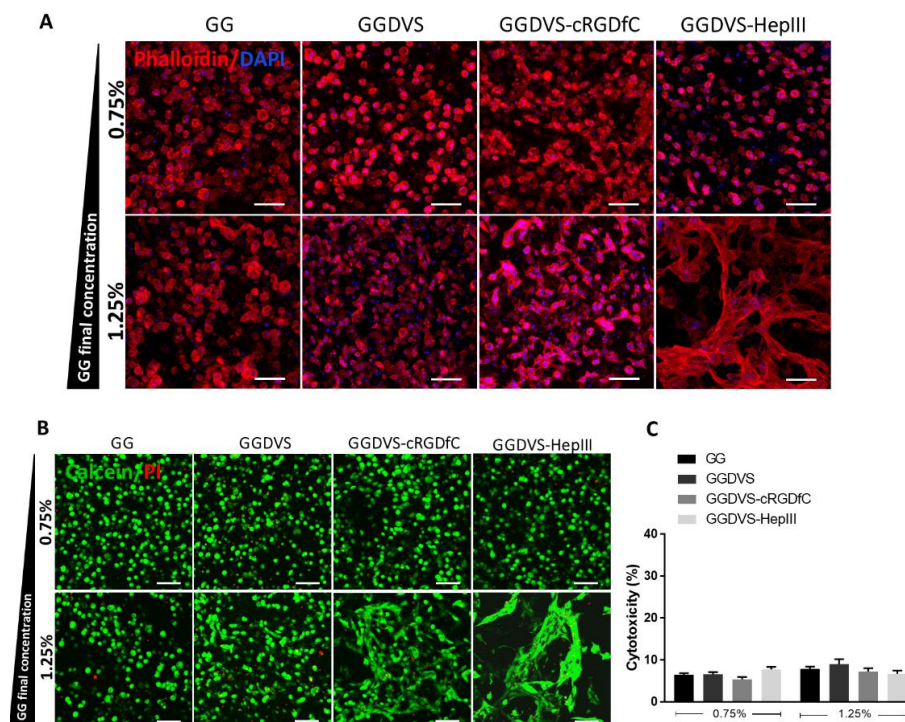
Supplementary Figure V-1 – Adhesion and viability of DP cells within GG-derived hydrogels. (A) β-actin filaments stained with phalloidin-TRITC (red). B) calcein (green)/propidium iodide (PI, red) of DP cells encapsulated within the different hydrogel formulations after 7 days in culture. Nuclei were counterstained with DAPI (blue). (C) Quantification of the cytotoxicity of the different hydrogel formulations over the encapsulated DP cells after 7 days in culture. Scale bars = 100 µm.
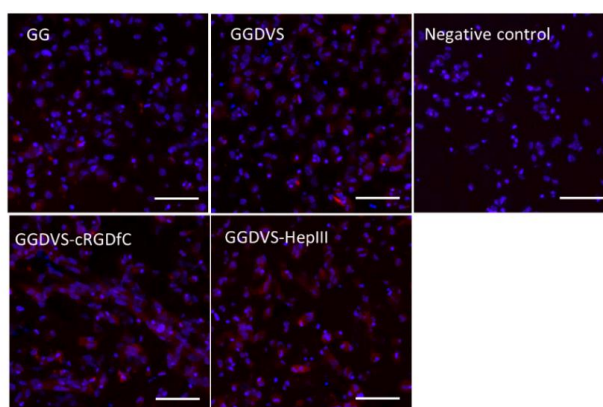
Supplementary Figure V-2 – Representative images of the expression of laminin (red) by DP cells encapsulated in the 1.25% GG-derived hydrogels after 3 days in culture . Nuclei were counterstained with DAPI (blue). Scale bar = 75 µm

159
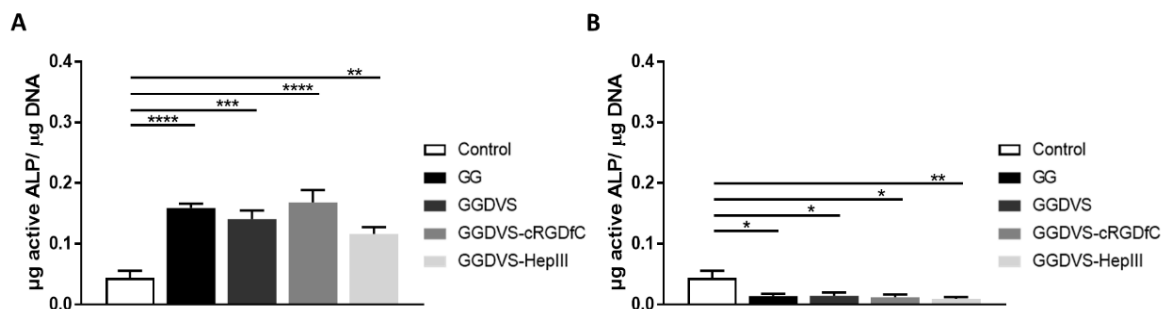
Supplementary Figure V-3 – Inductivity of DP cells within GG-derived hydrogels. Quantification of active ALP in DP cells before (Control) and after encapsulation in the different 0.75% GG-derived hydrogels after 3 (A) and 7 (B) days of culture. * p < 0.05; ** p < 0.01; *** p < 0.001 **** p < 0.0001.
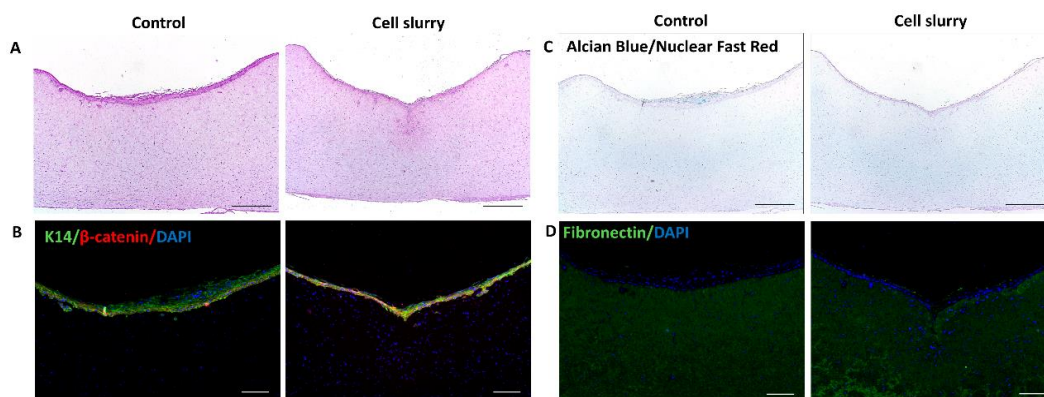
Supplementary Figure V-4 – Organotypic human skin model without (control) and with (cell slurry) the injection of dissociated DP cells. (A) H&E staining and (B) representative immunocytochemistry images of keratin (K) 14 (green) and β-catenin (red) expression by keratinocytes. Nuclei were counterstained with DAPI (blue). (C) Alcian Blue (pH=2.5) was used to stain sulfated and carboxylated GAGs. Nuclear fast red was used as counterstain. (D) Representative immunocytochemistry image of fibronectin expression. Scale bars are 500 μm for (A, C) and 200 μm for (B, D).
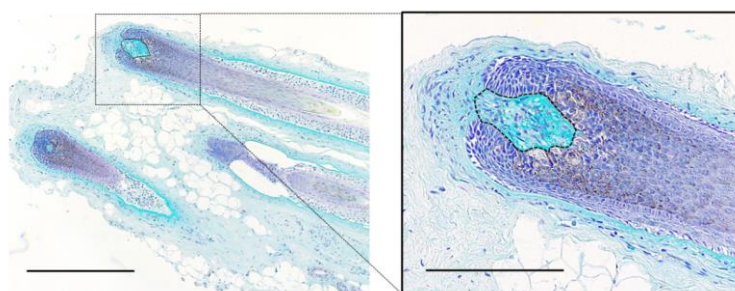
Supplementary Figure V-5 – Alcian blue staining at pH=2.5 of carboxylated and sulfated GAGs within the human scalp DP (dashed line) and non-follicular dermis. Scale bars are 500 μm (left image) and 200 μm (zoomed-in image).

CHAPTER VI

DERMAL PAPILLA CELLS AND MELANOCYTES RESPONSE TO PHYSIOLOGICAL OXYGEN LEVELS DEPENDS ON THEIR INTERACTIONS

CHAPTER VI

DERMAL PAPILLA CELLS AND MELANOCYTES RESPONSE TO PHYSIOLOGICAL OXYGEN LEVELS DEPENDS ON THEIR INTERACTIONS[¨]

ABSTRACT

Dermal papilla (DP) cells and melanocytes (Mel) are central players in hair growth and pigmentation, respectively. In the hair follicle (HF), oxygen levels average about 5% oxygen O_2 (physoxia) and are intimately coupled with the production of reactive oxygen species (ROS), which contribute to hair growth. Considering that oxygen and ROS might have a major role in the maintenance of the HF cellular functions, we studied the effect of physoxia over human DP cells and melanocytes (hMel) and investigated if these cells interaction altered this response. We show that physoxia decreased DP cells senescence and improved their secretome and phenotype, as well as hMel proliferation, migration and tyrosinase activity. In indirect co-cultures, physoxia affected the alkaline phosphatase (ALP) activity of DP cells but their signaling did not influence hMel proliferation or tyrosinase activity. Additionally, ROS production was higher than in the respective monocultures. Considering this, a potential link between the ALP activity of DP cells and ROS levels was addressed, but the treatment of DP cells with hydrogen peroxide did not confirm a direct correlation. In 3D aggregates that recreated these cells native microarchitecture and phenotype, both the tyrosinase activity in hMel and ALP activity in DP cells - their main functional indicators - plus ROS production were higher in physoxia than in normoxia. Overall, we showed that the response to physoxia differs according to hMel-DP cells interactions and that the microenvironment recreated when in direct contact favors their follicular functions.

VI-1. INTRODUCTION

Hair growth is mainly controlled by the dermal papilla (DP), the hair follicle (HF) inductive mesenchymal structure, whereas its pigmentation relies on the melanogenic activity of follicular melanocytes [1,2]. These melanocytes represent the progeny of melanoblasts residing in the bulge, which proliferate and migrate to the hair bulb, surrounding the DP and starting to produce and transfer melanin to the keratinocytes of the growing shaft [3,4]. Although the DP is considered the HF control center, and its anatomical proximity with bulbar melanocytes implies a role also in hair pigmentation, little is known about the capacity of DP cells to regulate melanocytes. Rodent studies indicate that DP cells can influence melanocytes proliferation/differentiation, migration and affect pigment formation and hair coat color [5]. *In vitro* studies confirmed a chemotactic effect of DP cell-conditioned medium towards human melanocytes (hMel) [6], further suggesting mediation of melanocytes location and migration in the HF by DP cells. Interestingly, DP cell extracellular matrix (ECM) was also suggested to stimulate tyrosinase activity [7,8], the rate-limiting step for melanin production [9].

Oxygen (O_2) is a basic component of the tissue microenvironment and its fluctuation can deeply affect cellular metabolism, signaling, proliferation, differentiation and reactive oxygen species (ROS) formation [10,11]. Physiological ROS play a regulatory role in several cellular signaling events [12,13] however, ROS imbalance has been linked to the etiopathogenesis of several conditions, including androgenetic alopecia and hair greying [14,15]. It is well known that ROS accumulate at supraphysiological oxygen levels [16]. Previous studies demonstrated that in cultures performed under 21% O_2 (normoxia) both HF mesenchymal (DP and dermal sheath cells) [17] and epithelial [18] populations proliferate at lower rates than when respectively cultured at 6% O_2 or 4% O_2. Moreover, under hypoxic conditions (2% O_2), the viability, phenotype and inductivity of DP cells are improved [15,19]. Further, hMel proliferation and melanin production are also higher at 1-5% O_2 comparably to normoxia [20]. Overall, these studies indicate that low oxygen levels are beneficial for DP cells and melanocytes, which seem to agree with the oxygen tension measured in the human DP (4.0-5.2% O_2) [21] or skin (average 5.3% O_2) [22]. Nevertheless, the anagen hair bulb is a ROS-enriched microenvironment [23], in which ROS directly activates proliferation and differentiation programs, stimulating hair growth [24]. Therefore, the involvement of multiple oxygen-associated responses, potentially by the different cells implicated in hair growth is expected, but yet to be elucidated.

Considering this, we investigated the response of hMel and DP cells to physiological oxygen levels (5% O_2, physoxia) and if this response was influenced by their interaction, aiming at mirroring their

potential communication within the HF. We demonstrate that under physiological culture conditions, together with an expected decrease in ROS levels, both DP cells and hMel showed increased proliferative capacity and functionality. Interestingly, DP cells and hMel response to physoxia varied not only if these were co-cultured, but also whether they were indirectly or directly interacting. When hMel and DP cells were directly contacting in 3D cell aggregates resembling their native organization, the microenvironment recreated under physoxia favored their highly specialized follicular functions.

VI-2. MATERIALS AND METHODS

VI-2.1. Cell culture

Human scalp samples were obtained from consenting patients who underwent hair transplantation procedures at Sanare Unicapilar (Porto, Portugal) and used to isolate DPs [25]. DP cells were subcultured on bovine collagen-coated (Sigma-Aldrich) surfaces in DMEM (Sigma-Aldrich) with 10% fetal bovine serum (FBS) and 1% antibiotic-antimycotic solution (Gibco). hMel were purchased from Cell Applications (San Diego, USA) and cultured in the recommended complete HEM medium. Unless otherwise stated, the cell densities used to establish the monocultures were $2x10^4$ cells/cm^2 (DP cells and hMel).

Physoxia cultures were established with 5% O_2 in a hypoxic chamber (Coy O2 Control Glove Box; Coy Laboratory Products, USA). Cells cultured under normoxia were used as controls. Cells were used up to passage 4 (hMel) or passage 7 (DP cells).

To assess the link between ROS and alkaline phosphatase activity (ALP), DP cells were cultured overnight and then treated with H_2O_2 (300 μM, PanReac AppliChem), with N-acetyl cysteine (NAC; 1 mM, Sigma-Aldrich) or with NAC for 2h before H_2O_2.

VI-2.2. Morphology and aggregation analysis

After 3 days of culture, DP cells were fixed with 10% formalin for 15 min at room temperature (RT) and their F-actin filaments stained with phalloidin-TRITC 300 (0.1 mg/mL, Sigma-Aldrich) for 1h at RT. Nuclei were counterstained with 4,6-diamidino-2-phenylindole (DAPI) (0.02 mg/mL, Biotium) for 15 min at RT. Images (six per triplicate) were acquired with an Axio Observer microscope (Zeiss) and used for

the quantification of cell area, perimeter and major axis length, with the software module "*MeasureObjectSizeShape*" of CellProfiler™ 3.0.0 [26].

Cell aggregation was analyzed after 7 days of culture, after labelling the cells' nuclei with DAPI. Images (ten per triplicate) were acquired (Axio Observer, Zeiss) and analyzed with the CellProfiler™ 3.0.0 module "*RelabeledNuclei*". Cells were considered adjacent if the distance between their nuclei was below 8 pixels. Groups of 30 or more adjacent cells were counted as one aggregate.

VI-2.3. Senescence-associated-β-galactosidase assay

DP cells were seeded at a density of $1x10^4$ cells/cm^2 and cultured overnight. Next day, the cells medium was replaced by serum-free DMEM and DP cells were kept in culture for 5 days. The detection of senescence cells was performed using the Senescence β-Galactosidase Staining Kit (Cell Signaling Technology) following manufacturer instructions. Images (12 per each triplicate) used to quantify the percentage of senescent cells were taken using an AxioVert.A1 microscope (Zeiss)

VI-2.4. Quantification of collagen and non-collagenous proteins

The total amount of collagen (COL) and non-collagenous (NCOL) proteins were quantified using the Sirius Red/Fast Green Staining Kit (Chondrex) according to the supplier instructions. DNA values were used to normalize data.

VI-2.5. Migration assay

hMel ($4x10^4$ cells/cm^2) were seeded in 8.0 μm pore size inserts (Corning) in non-supplemented HEM medium, whilst complete medium was added to the bottom well. After 48h of culture under normoxia or physoxia, cells that migrated from the insert to the bottom well were fixed with 10% formalin (15 min, RT). Images were acquired with an AxioVert.A1 (Zeiss) for quantification (12 per triplicate) or with an Axio Observer (Zeiss) microscope after staining the cells' nuclei with DAPI.

VI-2.6. Tyrosinase activity quantification

hMel were incubated for 5 min (ice) with 20 mM Tris(hydroxyethyl) aminomethane (pH 7.5) containing 0.1% Triton X-100 and a protease inhibitor cocktail (1:100, Sigma-Aldrich). Cell lysates were then centrifuged at 14500 rcf (10 min, 4°C) and 70 µL of the supernatant transferred into transparent 96-well plates. As a substrate for tyrosinase, a 0.1% (w/v) L-Dopa (Sigma-Aldrich) solution was prepared in sodium phosphate buffer (pH 6.8) and 140 µL were added to each well. Plates were incubated for 2h at 37°C, and the absorbance measured at 475 nm using a microplate reader (Synergy HT, BioTek). Data are presented as relative tyrosinase activity after normalization with DNA values.

VI-2.7. Co-cultures

DP cells resuspended in DMEM with 10% FBS were seeded at a density of $2x10^4$ cell/cm^2 and cultured overnight before establishing the co-culture with hMel, seeded at $2x10^4$ cell/cm^2 in HEM in 0.4 µm pore size inserts (Corning). Monocultures of each cell-type were prepared as controls, either by culturing cells in their regular medium, or in the medium used in to establish the co-culture, DMEM with HEM (1:1), to control possible medium effects. Direct co-cultures were established by seeding $3x10^3$ DP cells in round bottom ultra-low attachment 96-wells (Corning) in 50 µL of DMEM with 10% FBS for 24h before the addition of $1.5x10^3$ hMel resuspended in 25 µL of HEM medium. Both co-cultures were performed for 3 days.

VI-2.8. DNA, active alkaline phosphatase and reactive oxygen species quantification

Cells were lysed in water with 0.01% sodium dodecyl sulfate. A 1h incubation at 37°C was followed by freezing at -80°C. DNA content was quantified using the Quant-iT™ PicoGreen® dsDNA kit (Thermo Fisher Scientific), and ROS levels were measured using the OxiSelect™ *In vitro* ROS/RNS assay kit (Cell Biolabs Inc.). Cell lysates were also used to quantity active ALP in DP cells, using the Alkaline Phosphatase Detection Kit (Sigma-Aldrich). For DNA and ALP quantification in cell aggregates, a 5 s sonication step (ice) was first performed to ensure the complete disintegration of the 3D aggregates prior quantification. All commercial kits were used according to the manufacturer instructions. DNA values were used to normalize ROS and ALP results.

VI-2.9. Alkaline phosphatase staining

The detection of active ALP was performed by incubating formalin-fixed DP cells (15 min, RT) for 20 minutes with a solution prepared with 5 μL of NBT and 3.75 μL of BCIP (Roche) in 1 mL of NTMT buffer (100 mM NaCl, 100 mM Tris-HCl (pH 9.5) and 50 mM $MgCl_2$ in water). Representative images were acquired with an AxioVert.A1 microscope (Zeiss).

VI-2.10. Ezime-linked immunsorbent assay

After co-culture, inserts containing the hMel were removed and DP cells were cultured in serum-free DMEM for 24h. The cells supernatant was then collected, centrifuged (3000 rpm, 10 min) and single-use aliquots were stored at -80°C. Human vascular endothelial growth factor (VEGF) ELISA Development Kit (Peprotech) and human bone morphogenetic protein 2 (BMP2) Standard ELISA Development Kit (Petrotech) were then used following the manufacturer instructions to determine VEGF and BMP2 levels. DNA values were used to normalize data.

VI-2.11. Immunofluorescence staining

DP-hMel aggregates were fixed in 10% formalin (overnight, 4°C), embedded in HistoGel™ (Thermo Scientific) and processed for paraffin inclusion. 4 μm paraffin-embedded sections were then dewaxed and heat-mediated antigen retrieval was performed with sodium citrate buffer (pH 6.0). Primary antibodies (Table II-5) were detected with Alexa Fluor 488/594 (1:500, Molecular Probes) secondary antibodies and nuclear counterstain was performed with DAPI. Images were acquired using an Axio Imager Z1m microscope (Zeiss).

Haematoxylin and eosin (H&E) staining was performed according to standard protocols and representative images acquired with a DM750 microscope (Leica). Images were used to count cell nuclei and determine the DP cell/hMel ratio present within the cell aggregates for normalization of tyrosinase and ALP activity using the DNA amount of the corresponding cells.

VI-2.12. Statistical analysis

Statistical analysis and data visualization were performed using the GraphPad Prism 7.03 (San Diego, USA). The D'Agostino & Pearson normality test was used to determine if data followed a Gaussian distribution. Nonparametric data were analyzed with a two-tailed Mann-Whitney test (two groups, unpaired) or with a Friedman (paired) or Kruskal-Wallis test (unpaired) when more than 2 groups were compared. Parametric data were analyzed with a two-tailed Student's t-test (two groups, paired or unpaired). The comparison of more than two groups was performed with an ordinary (unpaired) or RM (paired) one-way ANOVA (one independent variable) or two-way ANOVA (two independent variables). Data are presented as mean ± standard error of the mean (SEM). For data displayed as dot plots, black dots represent data points and red bars indicate the mean. Differences with p-values < 0.05 were considered significant.

VI-3.   RESULTS

VI-3.1. Physoxia reduces the negative impact of *in vitro* culture conditions on DP Cells

DP cell cultures are typically established under normoxia, rapidly losing their native phenotype and intrinsic properties [27,28], including their key self-aggregation capacity [29,30]. Moreover, they also have a short lifespan [31] in culture, which is accompanied by morphological changes such as shifting from a small polygonal morphology to a spindle-like shape [32,33], before acquiring an enlarged morphology [15]. Therefore, we investigated if those changes also occurred under physoxia to understand how the O_2 level impacts DP cell phenotype in culture. DP cells under physoxia depicted a polygonal and less spindle-like shape and higher nuclei-to-cytoplasm ratio, as demonstrated by the significant decrease in the cells' area, perimeter and major axis length in comparison to normoxia (Figure VI-1A to D).
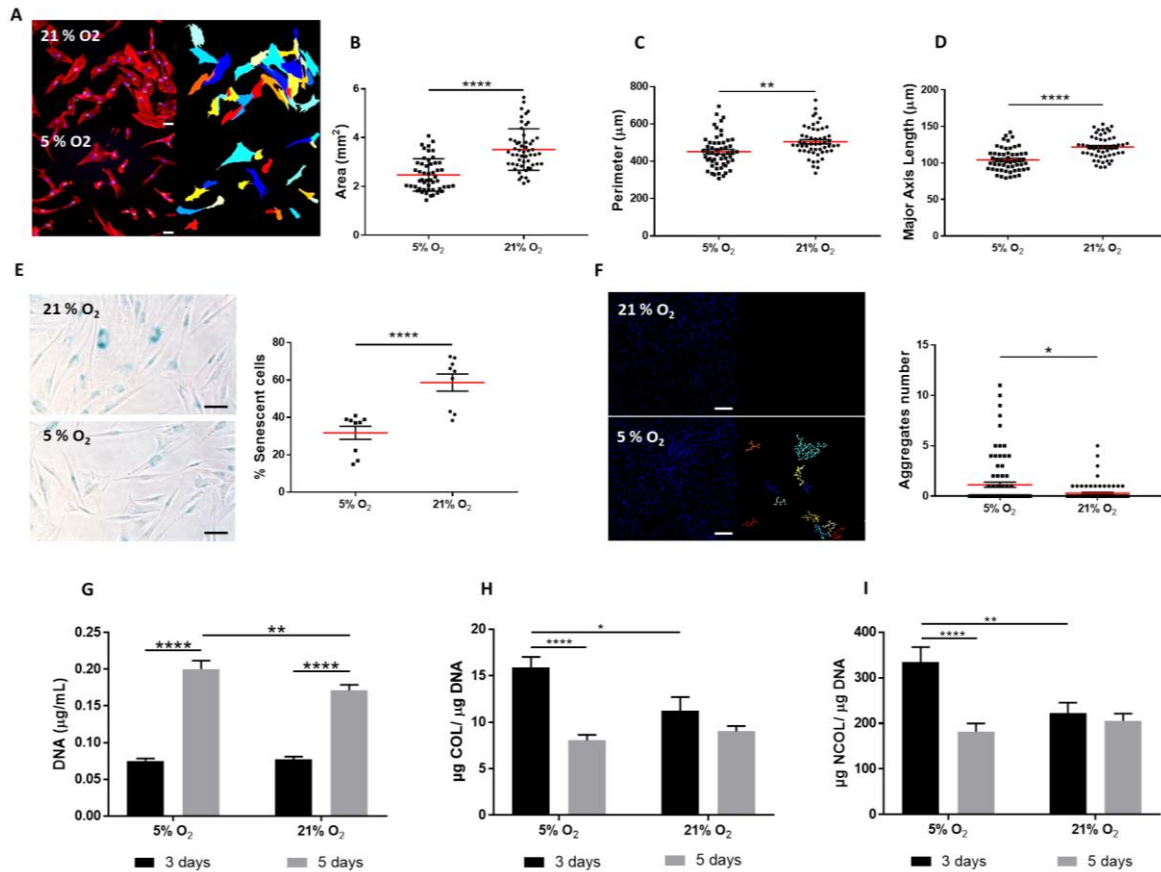
Figure VI-1 – Phenotype of DP cells under physoxia. (A) Representative images of DP cells' F-actin cytoskeleton labelled with phaloidin-TRITC (left panel) and respective CellProfiler™ output (right panel) used to quantify morphological features such as (B) cell area, (C) perimeter and (D) major axis length. (E) Representative images of the β-galactosidase staining used to quantify the percentage of senescent DP cells. (F) Representative images from DAPI-stained nuclei of DP cells (left panel) and CellProfiler™ output of subsequent grouping of related nuclei (distance < 8 pixels) used to count the number of cell aggregates (≥ 30 related nuclei). (G) DNA quantification used to evaluate cellular proliferation. Quantification of (H) collagen (COL) and (I) non-collagenous (NCOL) proteins secretion. Nuclei were counterstained with DAPI. Statistical differences are indicated as * $p < 0.05$; ** $p < 0.01$; **** $p < 0.0001$. Scale bars are 50 μm for (A and E) and 200 μm for (F).

Physoxia also significantly decreased the percentage of senescent DP cells in culture (Figure VI-1E) and improved their aggregative capacity (Figure VI-1F). Moreover, it enhanced cell proliferation, albeit the DNA amount at day 3 was similar in normoxia and physoxia (Figure VI-1G). Interestingly, an opposite effect was observed regarding COL (Figure VI-1H) and NCOL (Figure VI-1I) proteins secretion under physoxia, beneficial only after 3 days in culture. Altogether, these results suggest that physoxia promotes a healthier state in cultured DP cells, which featured characteristics typically associated with low passage cells.

VI-3.2. Physoxia enhances hMel migration, tyrosinase activity and proliferation within short culture times

Although hMel are normally cultured under normoxia, there are indications that their proliferation and tyrosinase activity are favored under lower oxygen tensions [20]. We found that physoxia significantly increased both the migration (Figure VI-2A) and tyrosinase activity (Figure VI-2B) of hMel, although this last effect was not sustained along with the culture.
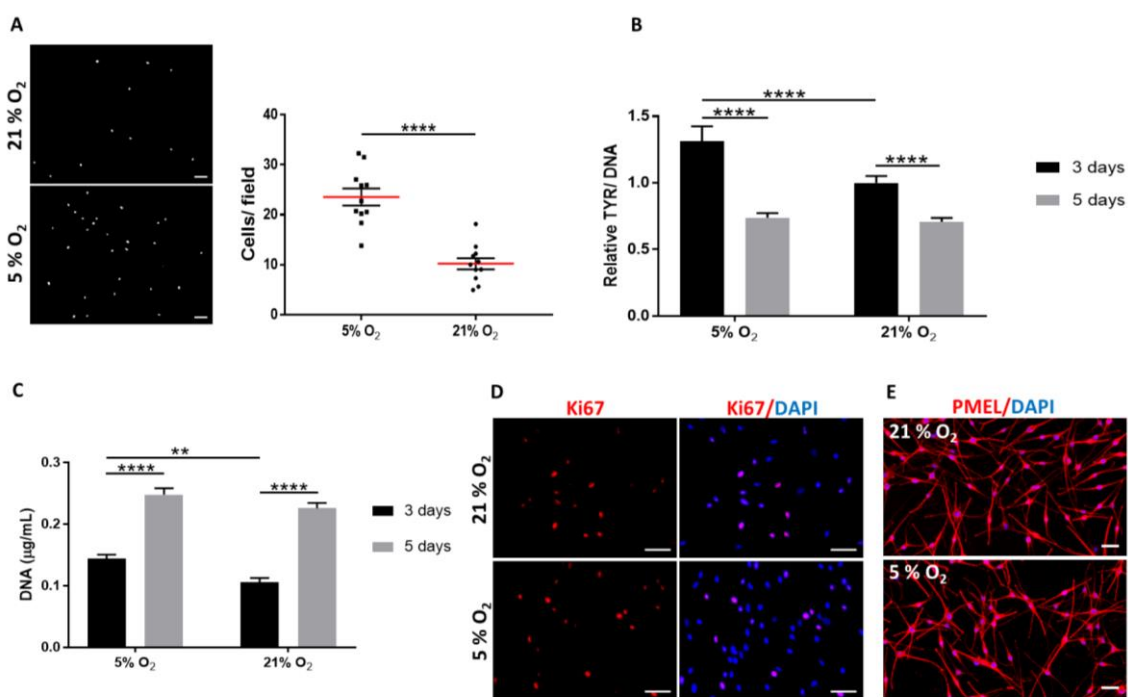
Figure VI-2 – Characterization of hMel behavior under physoxia. (A) Representative fluorescence microscopy images of DAPI-labelled hMel that migrated over 48h and respective quantification. (B) Quantification of tyrosinase activity (TYR) in hMel. Relative values in comparison to cells cultured under 21% O_2 at day 3 of culture are presented. (C) DNA quantification used to assess the proliferation of hMel. (D) Representative immunofluorescence images showing Ki67-positive hMel. Nuclei were counterstained with DAPI. (E) PMEL immunostaining showing the morphology of hMel. Nuclei were counterstained with DAPI. Statistical differences are indicated as ** $p < 0.01$; **** $p < 0.0001$. Scale bars= 50 µm.

Similarly, significantly higher DNA levels were observed for hMel cultured under physoxia at day 3 of culture (Figure VI-2C), suggesting an improved proliferative capacity. This effect was lost with the culture time, despite the high number of Ki67-positive cells (Figure VI-2D). Physoxia did not seem to affect hMel morphology (Figure VI-2E). Collectively, these results indicate that physoxia supports hMel functional features better than normoxia but only for short culture periods.

VI-3.3. DP cell and hMel response to physoxia depends on their type of interaction

Although residing in close vicinity in the hair bulb and having their functions coupled to anagen [34,35], little is known about how human DP cells and hMel interact and potentially affect each other's functionality. Knowing that physoxia individually improved hMel and DP cell functional features after 3 days in culture, we next explored its effect when these cells were indirectly co-cultured (Figure VI-3A). The co-culture with DP cells did not add to the increased hMel proliferation induced by physoxia (Figure VI-3B), in opposition to normoxia. Like for proliferation, co-culture with DP cells under physoxia did not affect the tyrosinase activity of hMel, contrarily to normoxia, which promoted recovery from the negative effect of the co-culture medium (Figure VI-3C).

Regarding DP cells, they proliferated significantly more under physoxia than in normoxia but only when cultured in their conventional medium. Thus, the higher DNA amount detected in co-culture might be due to the medium used. This is also sustained by the results similar to the control condition, both under physoxia and normoxia (Figure VI-3D). The amount of active ALP cells in the co-culture was not affected by physoxia but, as for proliferation, the medium used led to a significant increase of this inductive marker. In the presence of hMel, a significant decrease of DP cells´ active ALP was observed under physoxia, but not in normoxia (Figure VI-3E).

In the HF, hMel and DP cells are separated only by a thin and permeable basal lamina [2]. Therefore, we sought to investigate if physoxia effects were different from those observed in the indirect co-cultures, assuming a direct interaction between hMel and DP cells. When hMel were cultured with DP cell spheroids, they organized themselves around the spheroid in a biomimetic fashion, displaying a polarized positioning over one-half of the DP spheroid, independently of the oxygen level (Figure VI-3F). Highly-stable aggregates with similar DNA content were obtained (Figure VI-3G). Interestingly, the phenotype of both cell types was improved under physoxia, as demonstrated by a significant increase on the tyrosinase activity of hMel (Figure VI-3H) and by the higher amount of active ALP in DP cells (Figure VI-3I), respectively their main functional markers. Moreover, COL and NCOL proteins production by aggregates cultured in physoxia were significantly higher than in normoxia (Figure VI-3J). Physoxia benefits hMel and DP cell functionality when both cells types are directly contacting. Interestingly, the response of hMel to physoxia does not seem to be indirectly affected by DP cells, while its signaling appears to have an impact on the ALP activity of DP cells.

171
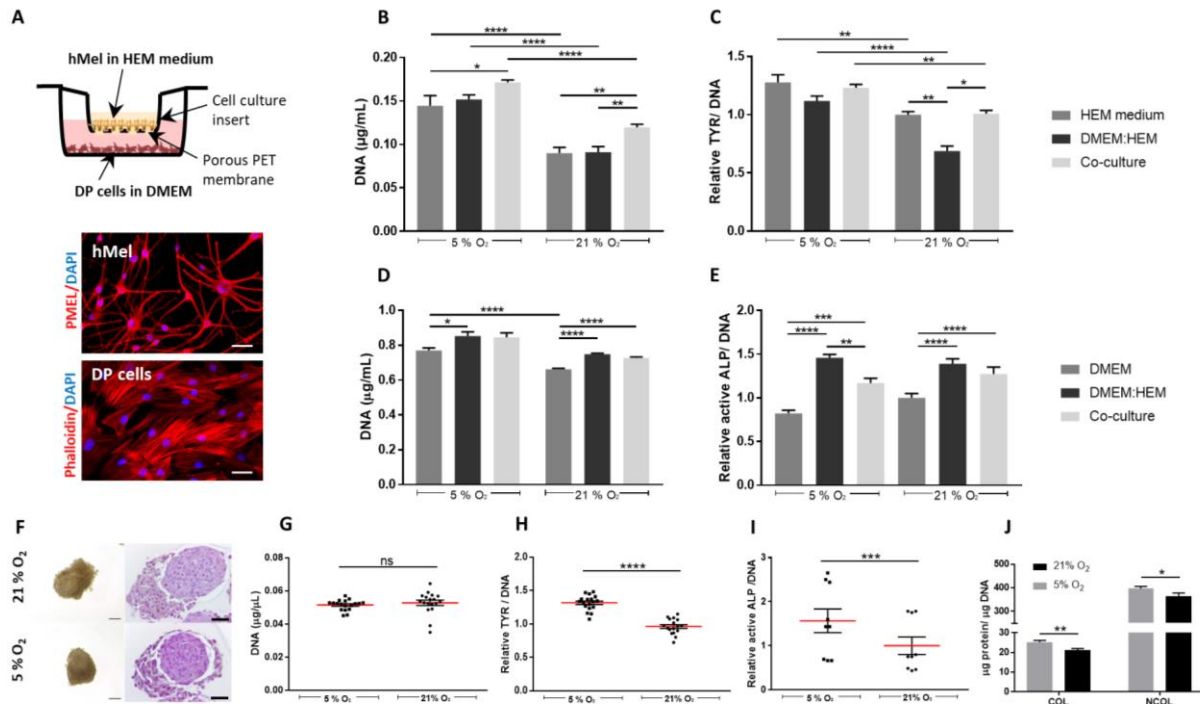
Figure VI-3 – Physoxia effects on co-cultured hMel and DP cells. (A) Schematic representation of the indirect co-culture system used to study hMel and DP cell interactions, accompanied by images displaying the morphology of each cell type, respectively immunolabelled with PMEL and stained with phalloidin-TRITC. **(B)** DNA quantification used to assess hMel cell numbers in the co-culture with DP cells, and in the respective homotypic controls – hMel cultured in standard conditions (HEM medium) or in the medium used for the co-culture (DMEM: HEM). **(C)** Quantification of tyrosinase activity (TYR) in hMel in the different culture conditions. Quantification of **(D)** DNA and **(E)** active ALP of DP cells co-cultured with hMel and in the respective control media. **(F)** Representative phase contrast (left panel) and H&E (right panel) images of the cell aggregates formed after hMel direct culture with DP spheroids. **(G)** Quantification of the amount of DNA of the aggregates. **(H)** Quantification of TYR in the multicellular aggregates. **(I)** Quantification of active ALP in the DP 3D spheroids. **(J)** Quantification of COL and NCOL proteins present in the aggregates. Relative values are presented in comparison to the cells standard culture conditions at 21% O_2 (C, D) or in comparison to aggregates formed at 21% O_2 (H, I). Nuclei were counterstained with DAPI. Statistical differences are indicated as *p <0.05; **p <0.01; ***p <0.001; ****p <0.0001. Scale bars are 50 μm for (A, F-right image) and 100 μm for (F-left image).

VI-3.4. ROS generation due to hMel and DP cell interaction does not directly correlate with DP cell functionality

During hair growth and pigmentation the bulb is a ROS-enriched environment [23] therefore, in addition to the functionality of hMel and DP cells, we addressed the involvement of ROS in their response. The production of ROS by hMel was significantly lower under physoxia, although this effect was significant only for the co-cultures (Figure VI-4A). Moreover, hMel in co-culture produced significantly more ROS than in the control conditions, regardless of the oxygen level. Physoxia also led to a reduction of the ROS levels in DP cells in comparison to normoxia, independently of the culture

conditions (Figure VI-4B). The indirect co-culture with hMel under physoxia also resulted in significantly higher amounts of ROS than in control conditions (Figure VI-4B). Surprisingly, when cells were directly cultured, ROS production in physoxia was significantly higher than in normoxia (Figure VI-4C), the opposite of what was observed in indirect co-cultures.
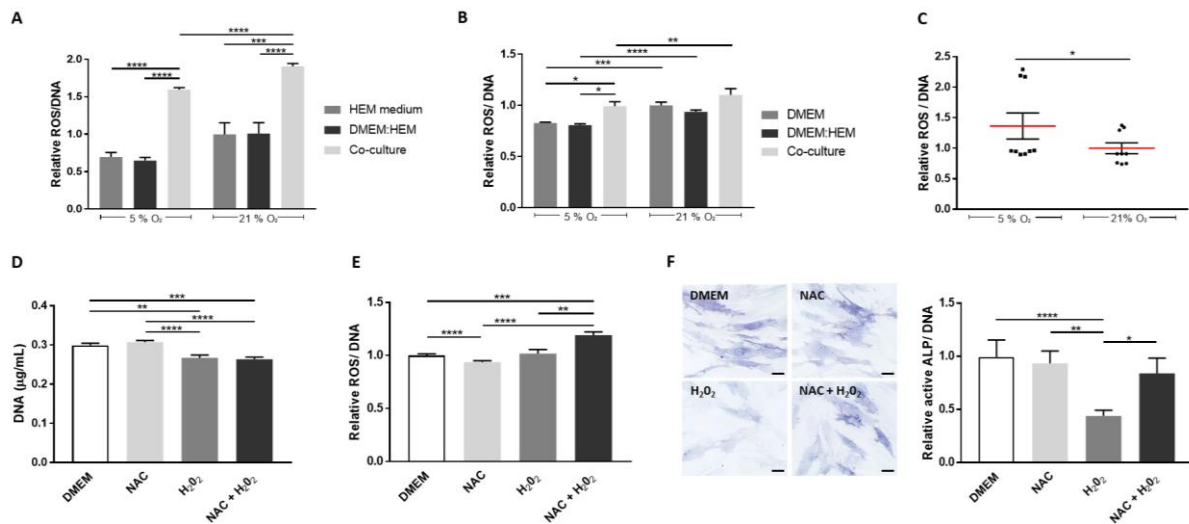
Figure VI-4 – ROS production by co-cultured hMel and DP cells and analysis of its association to active ALP in DP cells. ROS quantification in (A) hMel and (B) DP cells co-cultured indirectly and in the respective control conditions. (C) Amount of ROS in the DP-hMel cell aggregates. (D) Quantification of the DNA amount in conventionally cultured DP cells (DMEM, 21% O_2) in the presence of the ROS-scavenger *N*-acetyl cysteine (NAC), hydrogen peroxide (H_2O_2) or the combination of both (NAC+H_2O_2). (E) Quantification of ROS production by DP cells after NAC, H_2O_2 or both treatments. (F) Representative light microscopy images of ALP staining in DP cells and respective quantification of active ALP levels. Relative values are presented in comparison to standard cell culture conditions at 21% O_2 (A, B, E, F) or in comparison to aggregates formed at 21% O_2 (C). *p < 0.05; ** p < 0.01; *** p < 0.001; **** p < 0.0001. Scale bars= 100 μm

Considering that in indirect (Figure VI-3E and Figure VI-4B) or direct (Figure VI-3I and Figure VI-4C) co-cultures the effect of physoxia over the amount of active ALP and ROS followed a common trend, we then investigated if there was a correlation between these responses. For that, DP cells were treated H_2O_2 to increased oxidative stress, with the ROS inhibitor NAC or both. Treatment with the exogenous ROS (H_2O_2) led to a significant decrease in the amount of DNA (Figure VI-4D) but surprisingly, it did not affect ROS intracellular levels observed for DP cells (Figure VI-4E) while a significant decrease of active ALP was observed (Figure VI-4F). Moreover, NAC pre-treatment before H_2O_2 addition further enhanced ROS production in comparison to H_2O_2 alone, but it also reduced the H_2O_2 effect on the amount of active ALP. Although it is not clear the mechanism by which H_2O_2 decreases ALP activity in DP cells, these results suggest that it is not directly correlated with an increase in ROS levels.

VI-3.5. Physoxia and 3D co-culture support the native phenotype of DP cells and hMel

To further explore both physoxia and hMel influence on DP cell hair regenerative potential, we looked at the production of a known promoter [36,37] or inhibitor factor [38] of hair induction, respectively VEGF and BMP2. In physoxia, the amount of VEGF released by DP cells was significantly higher than in normoxia independently of the culture condition (Figure VI-5A).
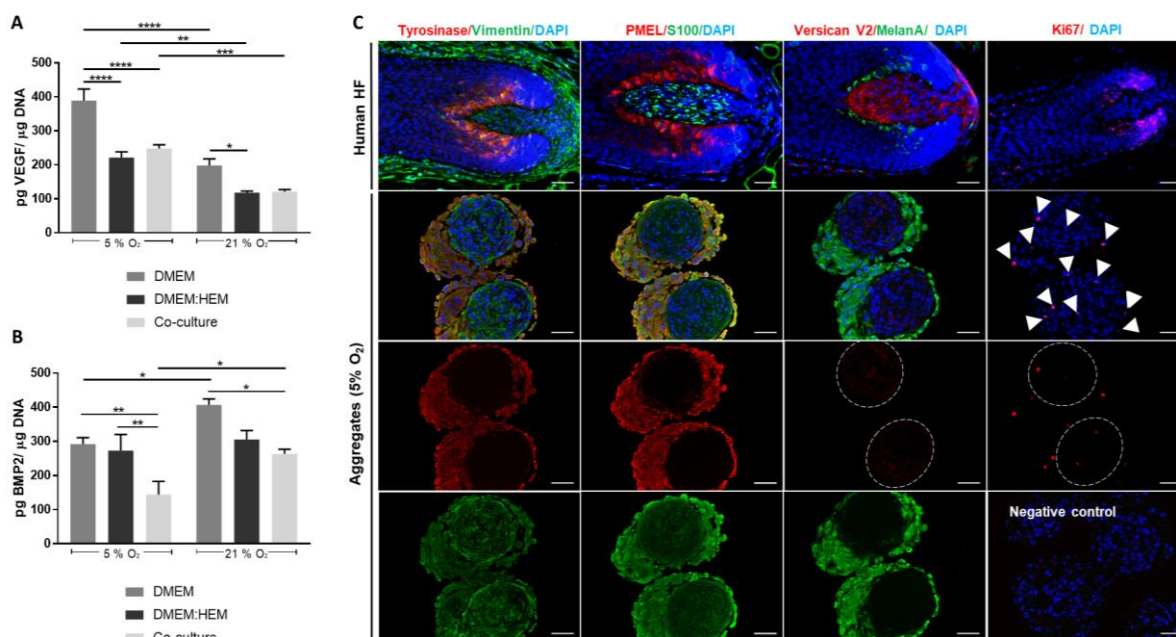
Figure VI-5 – Phenotypic assessment of co-cultured DP cells and hMel. ELISA quantification of (A) VEGF and (B) BMP2 released by DP cells indirectly co-cultured with hMel and the respective control conditions. Significant are indicated as * p < 0.05; ** p < 0.01; *** p < 0.001; **** p < 0.0001. (C) Representative immunofluorescence images showing the expression of different DP cell and hMel markers in the native hair follicle (HF) tissue and in the DP-hMel aggregates prepared under physoxia. Nuclei were counterstained with DAPI. White arrowheads indicate Ki67-positive cells and dotted circles delimitate the DP spheroid area. Scale bars= 50 μm

The co-culture medium negatively impacted VEGF release by DP cells, which was not overcome with the co-culture with hMel. In opposition, the amount of BMP2 in physoxia was significantly lower than in normoxia, for both co-cultures and conventional DP culture medium (Figure VI-5B). As this effect was not seen in the control established with the co-culture medium, it suggests that hMel presence was essential for the observed result.

Considering hMel-DP cell aggregates 3D architectural resemblance with the HF bulb and the observed advantages regarding their functionality under physoxia, we then investigated the rescue of these cells native phenotype under these conditions. The expression profile of different markers of DP

cell and hMel in the 3D aggregates (Figure VI-5c, lower panel) showed that the cells display a phenotype and organization identical to the native HF (Figure VI-5C, upper panel). The identification of the hMel markers tyrosinase, PMEL and MelanA, and vimentin and S100 also expressed by DP cells, showed clear compartmentalization between the cell types. Moreover, Ki67 immunolabelling confirmed a low number of proliferative cells within both cellular compartments (Figure VI-5C). Noteworthy, tyrosinase expression in the cellular aggregates was higher than in conventionally cultured hMel (Supplementary Figure VI-1). Moreover, the *in vivo* predominant V2-isoform of versican [39], a DP inductive marker typically absent in 2D cultured cells (Supplementary Figure VI-1) was weakly expressed in the cellular aggregates, confirming what was previously described for DP spheroids [27].

Overall, these results indicate that under physoxia the DP cell inductive secretome is promoted which, in conjunction with 3D culture conditions, allows the recovery of critical melanocytes and DP cell native markers.

VI-4. DISCUSSION

Besides ensuring overall cellular survival, oxygen levels are responsible for regulating a wide range of tissue functions, the reason why each organ, or even tissue, has its oxygenation status [10]. In the HF and skin, oxygen ranges about 5% O_2, however, the anagen hair bulb is a ROS-enriched microenvironment [26], which seems to indicate the involvement of multiple oxygen-associated responses, potentially by the different cells implicated in hair growth. Therefore, we aimed to explore the response of DP cells and hMel to physiological oxygen levels, and if this response was influenced by either their indirect signaling or direct contact, as it happens in the native tissue.

When cultured at standard atmospheric levels, DP cells have a characteristic short lifespan before entering growth arrest [31] and gradually lose their native properties [1]. This has been associated with premature senescence *in vitro*, triggered by excessive ROS production and oxidative stress [15]. We show that DP cells cultured under physoxia featured an early-culture morphology and phenotype, characterized by decreased senescence and increased proliferative and aggregative capacity. Moreover, under physoxia ROS levels were lower, which is expected given the reduced oxygen availability for the mitochondrial respiratory chain [40], the main toxic ROS producer. When exposed to excessive ROS DP cell capacity to support hair growth is severely compromised and they lose their hair inductive ability [41]. Interestingly, DP cells cultured under physoxia released higher amounts of VEGF and reduced

175

levels of BMP2, which corresponds to the necessary trend to promote anagen induction and hair growth initiation [37,38,42,43], suggesting that physoxia stimulates DP cell inductive secretome. Further, also in agreement with what referred above to DP cells, hMel cultures under physoxia showed lower ROS levels. This was also associated with an increase of hMel migration, proliferative capacity and tyrosinase activity, confirming the results of a previous study showing higher hMel growth and pigmentation in cultures established under 1-5% O_2 [20].

During the hair growth phase, hMel mature into tyrosinase-active cells after migrating to the hair bulb and surrounding the DP, and indirect evidence suggest that DP may be involved in this process [9]. In a previous study, DP cell-conditioned medium was shown to enhance tyrosinase activity in hMel under normoxic conditions [8]. We show that, in the presence of DP cells and under physoxia, tyrosinase activity in hMel was higher than in normoxia, yet similar to the homotypic controls, suggesting that the influence of factors released by DP cells on hMel do not surpass physoxia benefits. Interestingly, in our work tyrosinase activity in the 3D aggregates cultured under physoxia also correlated with a higher ECM deposition, which is in agreement with a previous study [8], which showed improved tyrosinase activity in both hMel direct co-cultured with DP cells and with their ECM. These seem to support a link between tyrosinase activity in hMel and the ECM produced by DP cells, in addition to their secretome.

In the HF, DP cells are mitotically quiescent [44,45] and the differentiated tyrosinase-active hMel are less committed to cell division [46,47]. In indirect co-cultures, hMel proliferated more in response to physoxia while DP cells remained unaffected, contrarily to the proliferative capacity shown before for both DP cells and hMel cultured under normoxia [17,20]. Further, the proliferative capacity of cells in the 3D aggregates was lower than in the indirect co-cultures that were established in 2D standard conditions, evidencing a mitotic profile that more closely emulates the native behavior.

Despite the generically accepted deleterious effects of supraphysiological ROS accumulation, there is a thin line separating beneficial and detrimental effects, which is associated with the tissue physiological ROS levels. In the hair bulb, a transient and physiological elevation of ROS [23] is necessary to promote hair growth and differentiation programs [24] during anagen. Interestingly, although ROS levels in co-cultured hMel and DP cells were lower under physoxia than in normoxia, potentially as a consequence of lower oxygen availability, they were higher than in the corresponding homotypic controls, which was observed independently of the oxygen level. This seems to suggest that there is an indirect interaction between the two cell types that influence ROS formation. Intriguingly, and

unlike what was observed in the co-cultures, in the 3D cellular aggregates ROS generation was higher in physoxia than in normoxia. While this seems to contradict the expected relation between the available oxygen and ROS formation, it is also known that spheroids represent a hypoxic environment [48,49]. Thus, the oxygen levels in the highly compact DP-hMel aggregates are also likely to be below 5% O_2 and lead to the formation of ROS by an alternative mechanism [16], which was previously demonstrated to play a key role in the stimulation of DP cell inductivity [19]. Moreover, ROS increase in the 3D cellular aggregates may also be a consequence of improved tyrosinase activity which is, by itself, a ROS-generating oxidative step [50,51]. Moreover, albeit a direct correlation was not observed in flat cultures, in the 3D cell aggregates both ROS levels and ALP activity were higher in physoxia than in normoxia demonstrating that, in a more complex environment, interactions between hMel and DP cells can be better represented.

VI-5. Conclusions

In summary, our results demonstrate that the recreation of the HF oxygen levels and the associated decrease of intracellular ROS benefit both hMel and DP cells, improving their proliferative capacity and functional features. Furthermore, we show that the type of interaction occurring between these cells also affects their response to physoxia and that, within the 3D aggregates, both hMel and DP cell-type functions and ROS generation are increased. Taken together, our results demonstrate that hMel-DP cells direct interaction under physiological oxygen levels has a superior capacity to recreate a microenvironment that more closely simulates the anagen bulb milieu, consequently enhancing their follicular cell-specific functions.

VI-6. References

1. Driskell, R. R., Clavel, C., Rendl, M. & Watt, F. M. Hair follicle dermal papilla cells at a glance. *J. Cell Sci.* **124**, 1179–1182 (2011).

2. Slominski, A. *et al.* Hair Follicle Pigmentation. *J. Invest. Dermatol.* **124**, 13–21 (2005).

3. Tobin, D. J. The cell biology of human hair follicle pigmentation. *Pigment Cell Melanoma Res.* **24**, 75–88 (2011).

4. Slominski, A. *et al.* Hair follicle pigmentation. *J Invest Dermatol* **124**, 13–21 (2005).

5.   Lim, J., Ng, K. J. & Clavel, C. Dermal papilla regulation of hair growth and pigmentation. in *Advances in Stem Cells and their Niches* vol. 3 115–138 (Elsevier, 2019).

6.   Ideta, R., Soma, T., Tsunenaga, M. & Ifuku, O. Cultured human dermal papilla cells secrete a chemotactic factor for melanocytes. *J. Dermatol. Sci.* **28**, 48–59 (2002).

7.   Balafa, C. *et al.* Dopa oxidase activity in the hair, skin and ocular melanocytes is increased in the presence of stressed fibroblasts. *Exp. Dermatol.* **14**, 363–372 (2005).

8.   Buffey, J. A. *et al.* Extracellular matrix derived from hair and skin fibroblasts stimulates human skin melanocyte tyrosinase activity. *Br. J. Dermatol.* **131**, 836–842 (1994).

9.   Tobin, D. J. The cell biology of human hair follicle pigmentation. *Pigment Cell Melanoma Res.* **24**, 75–88 (2011).

10.   Carreau, A., Hafny-Rahbi, B. El, Matejuk, A., Grillon, C. & Kieda, C. Why is the partial oxygen pressure of human tissues a crucial parameter? Small molecules and hypoxia. *J. Cell. Mol. Med.* **15**, 1239–1253 (2011).

11.   Place, T. L., Domann, F. E. & Case, A. J. Limitations of oxygen delivery to cells in culture: An underappreciated problem in basic and translational research. *Free Radic. Biol. Med.* **113**, 311–322 (2017).

12.   Dröge, W. Free Radicals in the Physiological Control of Cell Function. *Physiol. Rev.* **82**, 47–95 (2002).

13.   Sena, L. A. & Chandel, N. S. Physiological Roles of Mitochondrial Reactive Oxygen Species. *Mol. Cell* **48**, 158–167 (2012).

14.   Trueb, R. Oxidative stress in ageing of hair. *Int. J. Trichology* **1**, 6 (2009).

15.   Upton, J. H. *et al.* Oxidative Stress–Associated Senescence in Dermal Papilla Cells of Men with Androgenetic Alopecia. *J. Invest. Dermatol.* **135**, 1244–1252 (2015).

16.   Jagannathan, L., Cuddapah, S. & Costa, M. Oxidative Stress Under Ambient and Physiological Oxygen Tension in Tissue Culture. *Curr. Pharmacol. Reports* **2**, 64–72 (2016).

17.   Kanayama, K. *et al.* Hair Regeneration Potential of Human Dermal Sheath Cells Cultured Under Physiological Oxygen. *Tissue Eng. Part A* ten.tea.2019.0329 (2020).

18.   Xia, L. *et al.* Enhanced proliferation and functions of in vitro expanded human hair follicle outer root sheath cells by low oxygen tension culture. *Tissue Eng. - Part C Methods* **18**, 603–613 (2012).

19.   Zheng, M. *et al.* Hypoxia improves hair inductivity of dermal papilla cells via nuclear NADPH oxidase 4-mediated reactive oxygen species generation'. *Br. J. Dermatol.* **181**, 523–534

(2019).

20. Horikoshi, T., Balin, A. K. & Carter, D. M. Effects of Oxygen Tension on the Growth and Pigmentation of Normal Human Melanocytes. *J. Invest. Dermatol.* **96**, 841–844 (1990).

21. Wang, W., Winlove, C. P. & Michel, C. C. Oxygen Partial Pressure in Outer Layers of Skin of Human Finger Nail Folds. *J. Physiol.* **549**, 855–863 (2003).

22. Lartigau, E. *et al.* Intratumoral oxygen tension in metastatic melanoma. *Melanoma Res.* **7**, 400–406 (1997).

23. Lemasters, J. J. *et al.* Compartmentation of Mitochondrial and Oxidative Metabolism in Growing Hair Follicles: A Ring of Fire. *J. Invest. Dermatol.* **137**, 1434–1444 (2017).

24. Carrasco, E. *et al.* Photoactivation of ROS Production In Situ Transiently Activates Cell Proliferation in Mouse Skin and in the Hair Follicle Stem Cell Niche Promoting Hair Growth and Wound Healing. *J. Invest. Dermatol.* **135**, 2611–2622 (2015).

25. Gledhill, K., Gardner, A. & Jahoda, C. A. B. Isolation and Establishment of Hair Follicle Dermal Papilla Cell Cultures. in *Methods in molecular biology (Clifton, N.J.)* vol. 989 285–292 (Methods Mol Biol, 2013).

26. Lamprecht, M. R., Sabatini, D. M. & Carpenter, A. E. CellProfiler™: free, versatile software for automated biological image analysis. *Biotechniques* **42**, 71–75 (2007).

27. Higgins, C. A., Richardson, G. D., Ferdinando, D., Westgate, G. E. & Jahoda, C. A. B. Modelling the hair follicle dermal papilla using spheroid cell cultures. *Exp. Dermatol.* **19**, 546–548 (2010).

28. Higgins, C. A., Chen, J. C., Cerise, J. E., Jahoda, C. A. B. & Christiano, A. M. Microenvironmental reprogramming by three-dimensional culture enables dermal papilla cells to induce de novo human hair-follicle growth. *Proc. Natl. Acad. Sci.* **110**, 19679–19688 (2013).

29. Young, T.-H., Lee, C.-Y., Chiu, H.-C., Hsu, C.-J. & Lin, S.-J. Self-assembly of dermal papilla cells into inductive spheroidal microtissues on poly(ethylene-co-vinyl alcohol) membranes for hair follicle regeneration. *Biomaterials* **29**, 3521–3530 (2008).

30. Rushan, X., Fei, H., Zhirong, M. & Yu-zhang, W. Identification of proteins involved in aggregation of human dermal papilla cells by proteomics. *J. Dermatol. Sci.* **48**, 189–197 (2007).

31. Messenger, A. G. Isolation, culture and in vitro behavior of cells isolated from papillae of human hair follicles. in *Trends in Human Hair Growth and Alopecia Research* 57–66 (Springer Netherlands, 1989).

32. Messenger, A. G., Jennifer, H. & Bleehen, S. S. The in vitro properties of dermal papilla cell lines established from human hair follicles. *Br. J. Dermatol.* **114**, 425–430 (1986).

33. Ohyama, M., Kobayashi, T., Sasaki, T., Shimizu, A. & Amagai, M. Restoration of the intrinsic properties of human dermal papilla in vitro. *J. Cell Sci.* **125**, 4114–4125 (2012).

34. Slominski, A. & Paus, R. Melanogenesis is coupled to murine anagen: Toward new concepts for the role of melanocytes and the regulation of melanogenesis in hair growth. *J. Invest. Dermatol.* **101**, S90–S97 (1993).

35. Iida, M., Ihara, S. & Matsuzaki, T. Hair cycle-dependent changes of alkaline phosphatase activity in the mesenchyme and epithelium in mouse vibrissal follicles. *Dev. Growth Differ.* **49**, 185–195 (2007).

36. Lachgar, Charveron, Gall & Bonafe. Minoxidil upregulates the expression of vascular endothelial growth factor in human hair dermal papilla cells. *Br. J. Dermatol.* **138**, 407–411 (1998).

37. Yano, K., Brown, L. F. & Detmar, M. Control of hair growth and follicle size by VEGF-mediated angiogenesis. *J. Clin. Invest.* **107**, 409–417 (2001).

38. Botchkarev, V. A. *et al.* Noggin is a mesenchymally derived stimulator of hair-follicle induction. *Nat. Cell Biol.* **1**, 158–164 (1999).

39. Soma, T., Tajima, M. & Kishimoto, J. Hair cycle-specific expression of versican in human hair follicles. *J. Dermatol. Sci.* **39**, 147–154 (2005).

40. Wagner, B. A., Venkataraman, S. & Buettner, G. R. The rate of oxygen utilization by cells. *Free Radic. Biol. Med.* **51**, 700–712 (2011).

41. Huang, W.-Y. *et al.* Stress-induced premature senescence of dermal papilla cells compromises hair follicle epithelial-mesenchymal interaction. *J. Dermatol. Sci.* **86**, 114–122 (2017).

42. Mecklenburg, L. *et al.* Active Hair Growth (Anagen) is Associated with Angiogenesis. *J. Invest. Dermatol.* **114**, 909–916 (2000).

43. Botchkarev, V. A. *et al.* Noggin is required for induction of the hair follicle growth phase in postnatal skin. *FASEB J.* **15**, 2205–2214 (2001).

44. Tobin, D. J., Gunin, A., Magerl, M., Handijski, B. & Paus, R. Plasticity and cytokinetic dynamics of the hair follicle mesenchyme: Implications for hair growth control. *J. Invest. Dermatol.* **120**, 895–904 (2003).

45. Jahoda, C. A. B. & Oliver, R. F. Vibrissa dermal papilla cell aggregative behaviour in vivo and in vitro. *J. Embryol. Exp. Morphol.* **79**, 211–224 (1984).

46. Commo, S. & Bernard, B. A. Melanocyte Subpopulation Turnover During the Human Hair Cycle: An Immunohistochemical Study. *Pigment Cell Res.* **13**, 253–259 (2000).

47. Randall, V. A., Jenner, T. J., Hibberts, N. A., De Oliveira, I. O. & Vafaee, T. Stem cell factor/c-Kit

signalling in normal and androgenetic alopecia hair follicles. *J. Endocrinol.* **197**, 11–23 (2008).

48. Kim, J. W., Ho, W. J. & Wu, B. M. The role of the 3D environment in hypoxia-induced drug and apoptosis resistance. *Anticancer Res.* **31**, 3237–3245 (2011).

49. Leek, R., Grimes, D. R., Harris, A. L. & McIntyre, A. Methods: Using three-dimensional culture (spheroids) as an in vitro model of tumour hypoxia. *Adv. Exp. Med. Biol.* **899**, 167–196 (2016).

50. Diehl, C. Melanocytes and Oxidative Stress. *J. Pigment. Disord.* **1**, 1512–1518. (2014).

51. Denat, L., Kadekaro, A. L., Marrot, L., Leachman, S. A. & Abdel-Malek, Z. A. Melanocytes as Instigators and Victims of Oxidative Stress. *J. Invest. Dermatol.* **134**, 1512–1518 (2014).

VI-7.   SUPPLEMENTARY INFORMATION
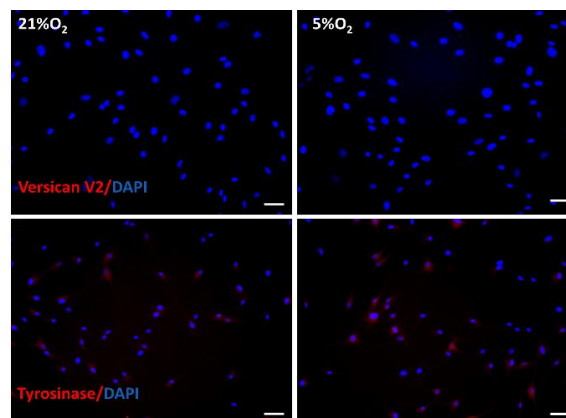
Supplementary Figure VI-1 - Representative immunofluorescence images showing lack of expression of the V2-isoform of versican by DP cells (upper panel) and the low tyrosinase expression by hMel (lower panel) in 2D cultures under normoxia and physoxia. Nuclei were counterstained with DAPI. Scale bars = 50 µm.

CHAPTER VII

MICROSCOPY-GUIDED LASER ABLATION FOR THE CREATION OF COMPLEX SKIN MODELS WITH FOLLICULOID APPENDAGES

CHAPTER VII

MICROSCOPY-GUIDED LASER ABLATION FOR THE CREATION OF COMPLEX SKIN MODELS WITH FOLLICULOID APPENDAGES††

ABSTRACT

Engineering complex tissues requires the use of advanced biofabrication techniques that allow the replication of the tissue 3D microenvironment, architecture and cellular interactions. In the case of skin, the most successful strategies to introduce the complexity of hair follicle appendages have highlighted the importance of facilitating direct interaction between dermal papilla (DP) cells and keratinocytes (KCs) in organotypic skin models. In this work, we took advantage of microscopy-guided laser ablation (MGLA) to microfabricate a fibroblast-populated collagen hydrogel and create a subcompartment that guides the migration of KCs and lead their interaction with DP cells to recreate follicular structures. Upon definition of the processing parameters (laser incidence area and power), MGLA was used to create 3D microchannels from the surface of a standard organotypic human skin model up to the aggregates containing DP cells and KCs, previously incorporated into the dermal-like fibroblast-collagen layer. Analysis of the constructs showed that the fabricated microfeatures successfully guided the fusion between epidermal and aggregates keratinocytes, which differentiated into follicular-like structures within the organotypic human skin model, increasing its functionality. In summary, we demonstrate the fabrication of a highly-structured 3D hydrogel-based construct using MGLA to attain a complex skin model bearing folliculoid structures, highlighting its potential use as an *in vitro* platform to study the mechanisms controlling HF development or for the screening of bioactive substances

---

VII-1. Introduction

Complex tissue models that replicate human biological interactions and the tissues' 3D architecture and function are a requirement for the development of accurate and reliable *in vitro* systems. Recent advances in biofabrication techniques, such as 3D printing, micromolding and soft lithography have contributed to the production of 3D tissue constructs with increased complexity [1,2], but many features remain unaccomplished.

In the case of skin, currently available models are far from replicating its complexity, representing an oversimplified version composed only by the epidermal and dermal layers. Contrastingly, the skin is an organ endowed with important physiological functions, which are conferred by the presence of specialized cell populations and by functional skin appendages. The hair follicle (HF) critically contributes to the most important physiological functions attributed to the skin, including barrier function, thermoregulation, sensory perception and immunosurveillance. Consequently, the lack of HFs in skin models has hampered their translational value in the pharmaceutical and biomedical fields. In particular, given the HF high cosmetic value, there is a great deal of interest in promoting HF regenerative therapies, which cannot be dissociated from the development of appropriate test systems representative of the HF formation events, to find novel targeted treatments/drugs.

It is well-established that HF development depends on reciprocal interactions between its epithelial and mesenchymal compartments (EMIs), in which the inductive dermal papilla (DP) cells stimulate the overlying epithelial cells to proliferate and differentiate into the distinct HF epithelial layers [3]. The recreation of these processes *in vitro* faces some challenges, such as the loss of inductivity that DP cells suffer upon 2D culture, partially recovered in 3D spheroids [4], as well as the need of adequate positional and microenvironmental conditions in which EMIs can be re-established. The most successful strategies achieved so far rely on the modification of a standard organotypic human skin model, either by the incorporation of DP spheroids within the dermal-like fibroblast-collagen layer [5] or by creating *in situ* conditions that allow DP cells to self-organize as spheroids prior the seeding of keratinocytes (KCs) [6]. While the first showed a potential communication between DP cells and epidermal KCs, which resulted in epidermal invaginations towards the spheroids but no HF-like structures formation [5], the second approach confirmed the need for a direct interaction between these cells to promote follicular differentiation in organotypic skin models [6].

184

Laser ablation is a non-contact technique that allows the removal of successive fractions of material by irradiation with a pulsed laser beam. In this process, the energy of the laser photons is transferred to the electrons of the target material increasing the temperature until the material vaporizes [7]. Laser ablation techniques have a wide range of applications, which include laser surgery, selective cell ablation in basic research, patterning/modification of surfaces and the engineering of the cell microenvironment [8]. Moreover, it enables the precise micropatterning of three-dimensional scaffolds with a high degree of control and precision over degraded features, the reason why it has emerged as a promising tool in the bioengineering field [8]. Among others, laser-based hydrogel degradation allows the production of scaffolds with channels capable of guiding the cellular organization and migration [8]. For example, Sarig-Nadir *et al.* [9] ablated channels in a PEGylated fibrinogen hydrogel to direct neurites growth and create 3D neuronal networks *in vitro*. Ilina and coworkers [10] created 3D microtracks in collagen matrices to support and guide breast cancer cells extracellular matrix (ECM) invasion.

Here we report the use of microscopy-guided laser ablation (MGLA) for the microscale manipulation of a fibroblast-populated collagen hydrogel and the fabrication of microfeatures that enable the recreation of HFs in an organotypic human skin model. We defined the laser incidence area and power parameters to successfully ablate collagen material with minor impact in the viability of the cells already growing within it. Considering previous findings, regarding the importance of DP-KCs interactions [6], cell aggregates formed by DP cells spheroids enclosed by KCs were incorporated into the fibroblast-collagen layer. MPGA was used to create 3D microchannels from the surface of the model up to the aggregates to guide the migration of the KCs seeded on top. Morphological analysis of the constructs demonstrated that the created MPGA microchannels successfully allowed recreating the DP and epithelial cells arrangement as observed in the HF, and the establishment of the necessary interactions to generate HF-like structures. Overall, a skin model with follicular appendages was biofabricated using MGLA to fine-tune both the model biological and spatial properties, ultimately increasing its level of complexity and functionality.

VII-2. MATERIALS AND METHODS

VII-2.1. Cell isolation and culture

DP cells were manually microdissected [11] from scalp samples of patients undergoing hair transplant surgery at Sanare Unicapilar (Porto, Portugal) after the patients' informed consent. Cells were cultured in Dulbecco's Modified Eagle Medium (DMEM, Sigma-Aldrich) supplemented with 10% fetal bovine serum (FBS, Gibco) and 1% antibiotic and antimycotic solution (AB, Gibco). KCs were isolated from foreskin samples obtained at Hospital Narciso Ferreira (Braga, Portugal) after the patients' informed consent and isolated according to a previously described procedure for the isolation of skin cells [12]. KCs were directly plated onto 3T3-fibroblast feeders previously inactivated with 4 µg/mL mitomycin C (Sigma-Aldrich) [13] and cultured in complete FAD medium [DMEM/Ham's F12 medium (3:1 ratio) supplemented with 10% non-inactivated FBS, 5 µg/mL insulin, 1.8×10^{4} M adenine, 0.5 µg/mL hydrocortisone, 10^{10} M cholera toxin (Sigma-Aldrich), 10 ng/mL epidermal growth factor (Peprotech), 1.8 mM $CaCl_2$ (Merck) and 1% AB]. Dermal fibroblasts (DFbs) were isolated from discarded skin collected from consenting patients undergoing routine abdominoplasty surgery at Hospital da Prelada (Porto, Portugal) and cultured in Eagle's Minimum Essential Medium-alpha modification (α-MEM, Sigma-Aldrich) supplemented with 10% FBS and 1% AB.

Cells were maintained under standard cultures conditions (37°C, 5% CO_2) in a humidified incubator and the medium was changed every 2-3 days. DFbs (passage 3-4), KCs (passage 1-2) and DP cells (passage 4-5) were used for the experiments.

VII-2.2. Multicellular aggregates formation

Spheroids were formed by seeding 3×10^3 DP cells in round bottom ultra-low attachment 96-wells (Corning) in 50 µL of DMEM with 10% FBS for 2 days. Afterwards, 7.5×10^3 KCs were resuspended in 125 µL of Keratinocyte Serum-Free Medium (KSFM, Gibco), added to the wells and further cultured for 2 days. Phase-contrast images of DP spheroids after KCs seeding, and of the formed multicellular aggregates, were acquired with an AxioVert.A1 microscope (Zeiss, Germany). The diameter of the cellular aggregates and DP spheroids was analyzed using the ZEN 2 software (blue edition; Zeiss, Germany) and presented as mean ± standard error of the mean (SEM).

VII-2.3. Aggregates incorporation in a dermal equivalent

The organotypic human skin model was prepared in 12 mm Transwell® (0.4 µm pore, Corning) as previously described [14], with some modifications. Briefly, a collagen solution was prepared by mixing basal α-MEM (10x) with 1N NaOH and rat tail collagen I (3 mg/mL, Invitrogen) at a ratio of 10:2.5:87.5 and 250 µL were cast onto the inserts to prepare an acellular layer. This layer was then covered with 500 µL of the same collagen solution containing hDFbs at a concentration of 7.5×10^4 cells/mL, forming the first cellular layer. After polymerization, 1-2 DP-KCs aggregates were placed on top and a second cellular layer (250 µL) was slowly added. The constructs were cultured submerged in DP cells culture medium for 5 days before starting the MGLA procedure.

VII-2.4. Laser ablation

Laser ablation was performed with a UGA-42 Caliburn motorized laser focus and a 355 nm, 1 kHz, 42 µJ/pulse pulsed laser (Rapp Optoelectronic, Germany) directly coupled to an Axio Observer 7 inverted microscope (Zeiss, Germany). Before ablation, the motorized laser focus was calibrated following the procedure provided by the manufacturer. Different diameters that limit the ablation area were tested to confirm the accuracy of the process. Moreover, different laser powers, other than its full power (42 µJ/pulse, 1 kHz), were tested to determine the minimum necessary power to successfully ablate collagen-based hydrogels.

The dermal constructs were turned upside down in a sterile three-well chamber microscopy glass slide (Ibidi, Germany) with culture medium and sealed under sterile conditions. For each construct, the end ablation plan (*x*, *y* and *z* position) was fixed by focusing the center of the cellular aggregate (20 x magnification). Then, the focus plan was moved to the surface of the construct in contact with the glass slide. To determine the starting ablation *z*-plane we first focused the microscope on the glass slide and ablated a small spot, easily confirmed by the presence of corrugations and the change in the transparency of the ablated surface. The focus plan was then moved 5 µm away to ablate another area. This procedure was repeated until no sign of ablated glass was seen, thus establishing the starting plan for the ablation of the hydrogel. The ablation of 150 µm diameter sections was repeated along different planes towards the cellular aggregate and up to the end ablation plan. Each ablation removed 30 µm of material, in depth.

After ablation, the constructs were placed back in the inserts and 5×10^4 KCs were seeded on top in 30 μL of KSFM. Constructs were then cultured in KSFM from the top and in DP cell medium from bellow for one week, to allow KCs proliferation. Afterwards, they were air-lifted and cultured in complete FAD medium to promote KCs differentiation and epidermis stratification [14]. The medium was changed every 1-2 days for two weeks, after which the samples were harvested and processed for histology analysis.

VII-2.5. Viability assay

One day after the ablation, dermal constructs were incubated with 1 μg/mL calcein-AM and 2 μg/mL propidium iodide (PI, Molecular Probes, USA) for 1h at 37°C. Samples were observed, and images were acquired with an Olympus Fluoview FV1000 laser confocal microscope (Olympus, Japan). Image analysis for cell viability was performed using the CellProfiler™ 3.0.0 software [15]. In brief, the maximum 2D projection of all the image stacks was thresholded using the most satisfactory method: Otsu for PI and Robust Background for calcein [16]. Dead and living cells were counted and the percentage of live cells was expressed as the ratio of living cells per the total number of cells in the total area or in non-ablated areas around the microchannels. Results were presented as mean and SEM (n=3).

VII-2.6. Histological analysis

Histological (hematoxylin and eosin, H&E) and immunocytochemistry stainings were performed in 5 μm paraffin-embedded sections according to routine protocols. For immunodetection, sections were deparaffinized and heat-mediated antigen retrieval was performed using citrate buffer (pH=6.0). The sections were then permeabilized with 0.2% Triton X-100 for 15 min at room temperature (RT) and blocked with 3% bovine serum albumin (Sigma-Aldrich) for 45 min a RT. The incubation with the primary antibodies against vimentin (1:50; ab92547, Abcam), keratin (K) 10 (1:100; ab9026, Abcam), K14 (1:800; PRB-155P, BioLegend), involucrin (1:25, ab68, Abcam), fibronectin (1:100, ab2413, Abcam), K15 (1:50, ab80522, Abcam), β-catenin (1:100, 610154, BD Transduction Laboratories) and α-SMA (1:200, ab7817, Abcam) was carried out overnight at 4°C. Next day, sections were incubated with Alexa Fluor 488/594-conjugated secondary antibodies (1:500, Molecular Probes) for 1h at RT. Nuclei were counterstained with 4′,6-diamidino-2-phenylindole (DAPI) (0.02 mg/mL, Biotium) for 15

min at RT. H&E staining illustrative images were taken with a DM750 microscope (Leica, Germany) whereas immunofluorescent images were acquired with an AxioVert.A1 microscope (Zeiss, Germany).

VII-3.   RESULTS AND DISCUSSION

During laser ablation, when a high-peaked power pulsed laser is focused on a sample the material in the area affected by the laser vaporizes. The laser causes a photoinduced breaking of bonds and a thermal decomposition of the material with very little damage to the surrounding area [17]. Thus, micro-laser ablation allows ablating a selected portion of material delimited by the spot size of the laser. The laser can then scan a predefined area of the sample, instantaneously removing the material along the path. Once all the area is ablated, the *z*-plane focus is moved to repeat the scan and ablate in depth the successive layer of material (Figure VII-1A). Laser-based ablation has been mostly used in hard materials, and knowing that the resolution and efficiency of the process in hydrogels is both dependent on the laser characteristic and the material properties [8,18], we first optimized the ablation parameters. To confirm the accuracy of the ablation, we first set different ablation diameters in the software – from 50 μm to 300 μm with 50 μm increments – and assessed the real diameter of the holes created in a black microscopy slide (Figure VII-1B). The results showed that the diameter of the ablated spots corresponded to the settings. Then, we proceeded with the identification of the laser power suitable to ablate our target material, fibroblast cell-laden collagen hydrogels. We adjusted the software to ablate 4 separate holes (150 μm diameter) of the same sample, at different laser powers from 25% to 100%, with 25% increments. Histological analysis demonstrated that collagen ablation requires the use of the laser at full power, since other conditions did not remove any portion of the surface of the construct (Figure VII-1C). Given that the diameter of the hole obtained at full power corresponds to the one set in the software, this experiment also allowed confirming the accuracy of the process in the collagen gel, as it was observed for the glass slide. After defining the working conditions, we assessed if a continuous ablation in the *z*-axis would result in the successive removal of the material and formation of a continuous channel. The ablation at different depths towards the opposite side of the hydrogel surface was confirmed (Figure VII-1D). The ablation of the first layer was associated with the formation of bubbles between the collagen gel and the glass slide and was also confirmed by a change in the hydrogel transparency. The observed bubbles may be due to the effects of the laser ablation on our water-rich samples [19]. The channels showed the presence of some of the ablated material, which might be associated to losses in the laser beam power along the optical path, through processes such

as energy diffusion or collision with heavier particles [8], therefore impacting the laser efficiency in deeper areas. Moreover, we also observed slight variations regarding the microchannel dimension and shape, which might be due to histological processing [20].
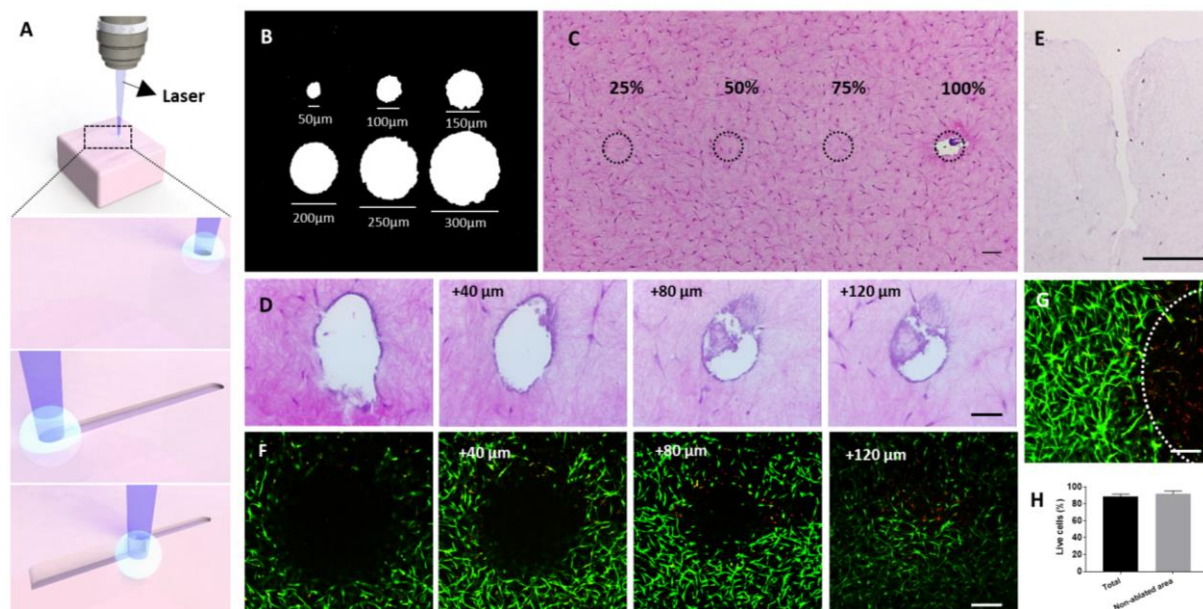

Figure VII-1 – Microscopy-guided laser ablation (MGLA) principle and conditions. (A) At the focus and delimited spot of the laser the material is vaporized due to thermal decomposition, creating an ablation point. A continuous scan allows creating continuous microfeatures that can be deepened by changing the z-plane of focus and repeating the ablation scanning. (B) Diameter of the holes attained in a glass slide when different ablation diameters were set in the software. (B) Top view of an H&E stained collagen cell-laden hydrogel showing the potential ablation areas (dashed circle) using laser with different powers, demonstrating that the laser full power (100%) is required to ablate the collagen matrices. (D) H&E images of successive sections of a 300 μm depth channel done in the collagen cell-laden hydrogel, showing the void space created by the channel along with increasing depth. (E) Transversal cut of the channel done in the collagen cell-laden hydrogel after 7 days in culture confirming that it was kept open, despite the changes in relation to the initial dimensions. Representative images of calcein (live cells, green) and propidium iodide (dead cells, red) stained fibroblast populating the hydrogels 24h after ablation (up to 120 μm depth) showing the presence of dead cells only in the (F) border and (G) near the bottom of the ablated area (dashed circle), and (H) the percentage of viable cells quantified considering the ablated area (total) or not (non-ablated area). Scale bars are 250 μm for (F, G), 100 μm for (C, E) and 50 μm for (D).

Since our strategy involves the seeding of KCs on top of the ablated hydrogels and their migration and proliferation inside the void space of the channels, we assessed if the dimensions of the channel were affected by collagen contraction. In fibroblast-laden collagen hydrogels cultured for 7 days, the size of the channel was considerably affected (Figure VII-1E), probably due to matrix contraction [14]. The channel, initially with 150 μm in diameter and 510 μm in depth, suffered a higher contraction in the deepest part widening towards the surface and ending up with 135 μm diameter at the surface and 300 μm in depth. This demonstrates that even if the matrix contracts, KCs will still be able to infiltrate

the channels. A potential side effect of MGLA in the encapsulated cells was also assessed by testing cellular viability on the day after the procedure. As expected, we verified the presence of some dead cells around the ablated channel (Figure VII-1F) and in the proximity of the bottom but without impacting the viability of the surrounding cells (Figure VII-1G and H).

Having determined the laser ablation parameters that allow the removal of collagen with minimal impact on cell viability, we next used MPGA to create 3D microchannels in the cell-laden hydrogels (Figure VII-2A). DP cell spheroids were prepared and directly cultured with KCs, forming compartmentalized aggregates (Figure VII-2B) with a mean diameter of 258.5 ± 2.5 µm (Figure VII-2C), that replicated the cells 3D positional relationship *in vivo* during hair growth [21]. These DP-KCs aggregates were then incorporated in the dermal equivalents, between the cellular collagen layers, working as hair-forming units. The fibroblasts were let to populated the collagen, produce ECM and remodel the collagen, causing its contraction [22]. After contraction, samples maintained transparency, which allowed the localization of the aggregates within their collagen bed. During the whole culture and contraction of the model, the overall structure and compartmentalization of the multicellular aggregates were kept (Figure VII-2D; Figure VII-2E, upper image). On the contrary, the diameter of the control DP spheroids without KCs decreased and DP cells outgrew into the hydrogels (Figure VII-2E, lower image). While representing a specialized follicular population, DP cells can easily suffer a dedifferentiation process and successfully replace fibroblasts as the dermal cellular source in skin constructs [23]. Therefore, the preculture of DP cells with KCs, and consequent aggregate formation, is of critical importance for the generation of individual and compartmentalized HF units. During the ablation procedure, a channel with 150 µm diameter was created from the collagen surface to the cellular aggregates. For an unequivocal demonstration that the created channels reached up to the spheroid we created channels slightly off-centered (Figure VII-2F), however, in our constructs, the channels were aligned with the aggregate (Figure VII-2G).
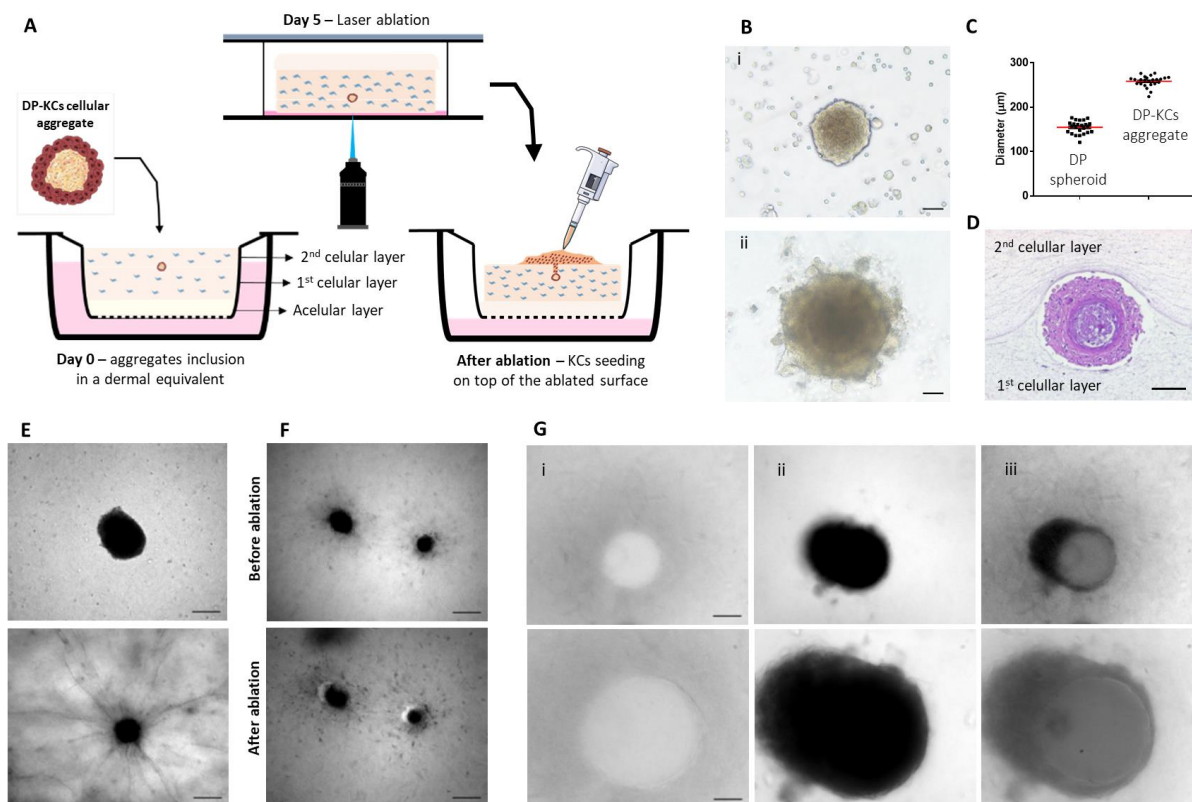
Figure VII-2 – Ablation of 3D microchannels in the fibroblast-laden hydrogels. (A) Schematic representation of the procedure adopted to incorporate DP-KCs aggregates between fibroblast-embedded collagen layers, the ablation of a microchannel connecting the hydrogel surface to the aggregate and the subsequent seeding of KCs on top of the ablated surface. (B) Phase-contrast image of DP spheroids co-cultured with a suspension of KCs (i) and the DP-KCs aggregates formed after 2 days of culture (ii). (C) Quantification of the diameter of DP-KCs aggregates and DP spheroids. (D) Representative H&E image of a DP-KCs cellular aggregate 5 days after its incorporation in the dermal-like collagen layer. (E) Representative light microscopy images of a DP-KCs aggregate (top) and a DP spheroid (bottom) inside the collagen matrices after 5 days in culture, respectively showing maintenance of the structure and the outgrowth of the DP cells into the collagen. (F) Light microscopy images of DP spheroids before and after the creation of an off-centered microchannel by MGLA. (G) Light microscopy images of the microchannel at the top of the hydrogel (i) and just before the DP-KCs aggregate (ii), and the corresponding overlap (iii), denoting the position of the ablated microchannels in relation to the DP-KCs aggregate. Bottom images are higher magnifications of the top ones. Scale bars are 200 µm for (E-top image, F), 100 µm for (D, G-top image) and 50 µm for (B, E and G-bottom images).

KCs were able to infiltrate the ablated channel and form a multilayered epithelium that integrated with the DP-KCs aggregates, leading to the formation of structures (Figure VII-3A i) that morphologically resembled an immature hair bulb (Supplementary Figure VII-1A). The epithelium of the formed HF-like structures exhibited a complexity by far higher than the epidermis on the dermal equivalents without the channels (Figure VII-3B). The formation of channels in hydrogels without aggregates also enabled KCs to grow downward, but the resultant epithelial strand shared the same simple morphological features of the epidermis of the standard organotypic model, with the difference that terminal differentiation was orientated inward (Figure VII-3C). The complexity of the HF-like structures was further confirmed by the

presence of a multilayered epithelium that was positive for the epithelial basal marker keratin(K)14 (Figure VII-3A ii). Interestingly, distinct morphologies were observed within K14-positive cells. These were arranged in regimented layer(s) of cuboidal-shaped cells located proximal to the dermal portion, which were adjacent to cells with a large cytoplasm and these, in turn, connected to flattened cells towards the core of the HF-like structure. This last flattened layer already denoted a certain degree of differentiation, as demonstrated by the absence of staining against the epidermal basal marker β-catenin (Figure VII-3A iii) and by the presence of the late differentiation marker K10 (Figure VII-3A iv), revealing an expression profile similar to the human HF (Supplementary Figure VII-1B to D). Moreover, terminal differentiation was also demonstrated by involucrin-positive staining (Figure VII-3A ii). Remarkably, vimentin staining revealed the presence of a dense and organized mesenchymal layer surrounding the HF-like structure, suggesting the organization of a dermal sheath-mimetic layer (Figure VII-3A iv). Analysis of the vimentin staining seems to indicate that the cells from this layer were originated from the dermal compartment (Figure 3A iv, dashed rectangle), suggesting a signaling within the environment around the follicular structures that also impact dermal fibroblasts. Interestingly, these fibroblasts are not positive for α-smooth muscle actin (α-SMA) as the dermal sheath cells (Supplementary Figure VII-2), which can be indicative of an underway dedifferentiation process. This also seems to corroborate that the ablation laser is not inducing phenotypic alterations in the fibroblasts since they retain their original phenotype (vimentin positive cells) being able to respond to the environment with a specific spatial organization within the dermis and around the follicular structures. The area where the DP cells are located appears as a dense agglomerate of cells (Figure VII-3A iv, dashed circle) embedded in a fibronectin-rich matrix (Figure VII-3A v). This basement membrane glycoprotein is prominently produced and expressed in the DP compartment (Supplementary Figure VII-1E), including in DP spheroids [24], and believed to play an essential role in the mechanisms regulating EMIs, including enabling signal transduction [25,26]. The expression of K15, initially described as an epidermal stem cell marker [27] present in the hair bulge, but whose presence was later also confirmed in the outermost outer root sheath layer (ORS) and in the epidermis basal layer [28], was equally studied. Interestingly, in our model cells positive for K15 (Figure VII-3A v) were present in a pattern that replicated the *in vivo* expression, in the epidermis basal layer and the most immature areas of the HF epithelium, but not in the lower hair bulb (Supplementary Figure VII-1E).
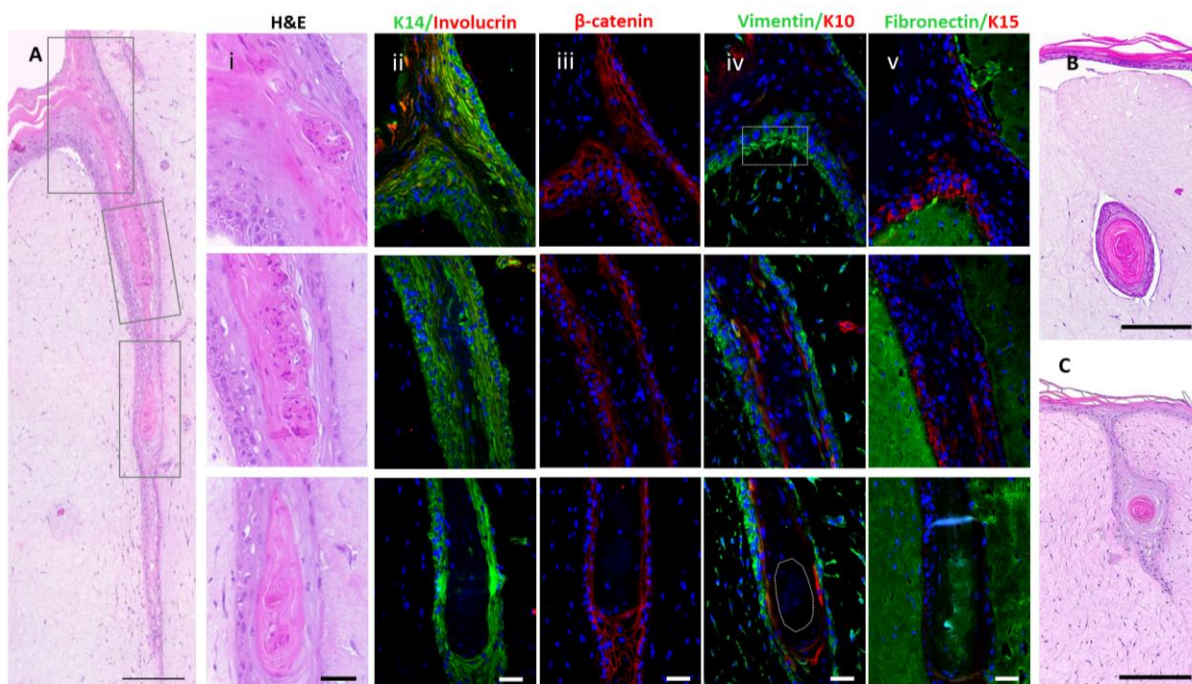
Figure VII-3 – Organotypic human skin model with follicular units. (A) Representative H&E images of the HF-like structures replicating the native tissue architecture and including (i) an epidermal invagination (top), a middle portion (middle) and a hair bulb mimetic area (bottom). Representative immunohistochemistry images showing the expression of (ii) K14 (green), involucrin (red), (iii) β-catenin (red), (iv) vimentin (green), K10 (red), (v) fibronectin (green) and K15 (red) within the recreated follicular structures. Nuclei were counterstained with DAPI. Representative images of control organotypic human models (B) with DP-KCs aggregates incorporated in the fibroblast-seeded hydrogels but without the microchannel, and (C) with the microchannel but without the DP-KCs aggregates. Scale bars are 250 μm for (A), 200 μm for (B, C) and 50 μm for (i-v).

Hair shaft formation was not observed, either because of insufficient culture time or, most likely, given the lack of additional paracrine signals involved in hair growth, such as the ones derived from the adipose tissue [29]. However, it is worth noting that the KCs used in this study were isolated from a hairless skin source, which requires the influence of inductive DP cells to acquire a follicular fate [4,6,30]. Therefore, the formation of the folliculoid structures in our model clearly demonstrates that they are influenced and respond to DP cells' signals, demonstrating our strategy ability to elicit EMIs. Finally, the microenvironment where the cellular aggregates were inserted, namely the reconstructed dermis and even the DP ECM rich in fibronectin, may have also synergistically modulated EMIs [25] and allowed the maintenance of the DP-KCs positional relationship, therefore also contributing to the success of this strategy.

VII-4. Conclusions

In conclusion, we demonstrate that the controlled 3D microprocessing of soft hydrogels with an emergent biofabrication tool – MGLA – supported the induction of follicular structures within a reconstructed human skin. The features microfabricated in the fibroblast-populated collagen hydrogels led the integration of KCs with DP cells and the subsequent formation of structures that morphologically resembled an immature hair bulb. The biofabricated human skin bearing follicular units opens new avenues in skin and hair research, providing not only an *in vitro* platform for studying the mechanisms controlling the HF early development but also a more complex and sophisticated alternative skin *in vitro* model for cosmetic testing and drug development.

VII-5. References

1. Abaci, H., Guo, Z., Doucet, Y., Jacków, J. & Christiano, A. Next generation human skin constructs as advanced tools for drug development. *Exp. Biol. Med.* **242**, 1657–1668 (2017).

2. Yanagawa, F., Sugiura, S. & Kanamori, T. Hydrogel microfabrication technology toward three dimensional tissue engineering. *Regen. Ther.* **3**, 45–57 (2016).

3. Sennett, R. & Rendl, M. Mesenchymal–epithelial interactions during hair follicle morphogenesis and cycling. *Semin. Cell Dev. Biol.* **23**, 917–927 (2012).

4. Higgins, C. A., Chen, J. C., Cerise, J. E., Jahoda, C. A. B. & Christiano, A. M. Microenvironmental reprogramming by three-dimensional culture enables dermal papilla cells to induce de novo human hair-follicle growth. *Proc. Natl. Acad. Sci.* **110**, 19679–19688 (2013).

5. Vahav, I. *et al.* Reconstructed human skin shows epidermal invagination towards integrated neopapillae indicating early hair follicle formation in vitro. *J. Tissue Eng. Regen. Med.* **14**, 761–773 (2020).

6. Abaci, H. E. *et al.* Tissue engineering of human hair follicles using a biomimetic developmental approach. *Nat. Commun.* **9**, 5301 (2018).

7. Hashida, M., Mishima, H., Tokita, S. & Sakabe, S. Non-thermal ablation of expanded polytetrafluoroethylene with an intense femtosecond-pulse laser. *Opt. Express* **17**, 13116 (2009).

8. Pradhan, S., Keller, K. A., Sperduto, J. L. & Slater, J. H. Fundamentals of Laser-Based Hydrogel Degradation and Applications in Cell and Tissue Engineering. *Adv. Healthc. Mater.* **6**, 1700681 (2017).

9. Sarig-Nadir, O., Livnat, N., Zajdman, R., Shoham, S. & Seliktar, D. Laser Photoablation of Guidance Microchannels into Hydrogels Directs Cell Growth in Three Dimensions. *Biophys. J.* **96**, 4743–4752 (2009).

10. Ilina, O., Bakker, G.-J., Vasaturo, A., Hofmann, R. M. & Friedl, P. Two-photon laser-generated microtracks in 3D collagen lattices: principles of MMP-dependent and -independent collective cancer cell invasion. *Phys. Biol.* **8**, 015010 (2011).

11. Gledhill, K., Gardner, A. & Jahoda, C. A. B. Isolation and Establishment of Hair Follicle Dermal Papilla Cell Cultures. in *Methods in molecular biology (Clifton, N.J.)* vol. 989 285–292 (Methods Mol Biol, 2013).

12. Cerqueira, M. T. *et al.* Cell sheet technology-driven re-epithelialization and neovascularization of skin wounds. *Acta Biomater.* **10**, 3145–3155 (2014).

13. Watt, F., Simon, B. & Prowse, D. Cultivation and Retroviral Infection of Human Epidermal Keratinocytes. in *Cell Biology* 133–138 (Elsevier, 2006).

14. Gangatirkar, P., Paquet-Fifield, S., Li, A., Rossi, R. & Kaur, P. Establishment of 3D organotypic cultures using human neonatal epidermal cells. *Nat. Protoc.* **2**, 178–186 (2007).

15. Lamprecht, M. R., Sabatini, D. M. & Carpenter, A. E. CellProfiler™: free, versatile software for automated biological image analysis. *Biotechniques* **42**, 71–75 (2007).

16. Sankur, B. Survey over image thresholding techniques and quantitative performance evaluation. *J. Electron. Imaging* **13**, 146 (2004).

17. Srinivasan, R. & Braren, B. Ultraviolet Laser Ablation of Organic Polymers. *Chem. Rev.* **89**, 1303–1316 (1989).

18. Vogel, A. & Venugopalan, V. Mechanisms of Pulsed Laser Ablation of Biological Tissues. *Chem. Rev.* **103**, 577–644 (2003).

19. Lam, J. *et al.* Dynamical study of bubble expansion following laser ablation in liquids. *Appl. Phys. Lett.* **108**, 074104 (2016).

20. Caliari, S. R. & Burdick, J. A. A practical guide to hydrogels for cell culture. *Nat. Methods* **13**,

405–414 (2016).

21. Schneider, M. R., Schmidt-Ullrich, R. & Paus, R. The Hair Follicle as a Dynamic Miniorgan. *Curr. Biol.* **19**, R132–R142 (2009).

22. Carlson, M. W., Alt-Holland, A., Egles, C. & Garlick, J. A. Three-Dimensional Tissue Models of Normal and Diseased Skin. *Curr. Protoc. Cell Biol.* **41**, 19.9.1-19.9.17 (2008).

23. Higgins, C. A. *et al.* Multifaceted role of hair follicle dermal cells in bioengineered skins. *Br. J. Dermatol.* **176**, 1259–1269 (2017).

24. Gupta, A. C. *et al.* Establishment of an in vitro organoid model of dermal papilla of human hair follicle. *J. Cell. Physiol.* **233**, 9015–9030 (2018).

25. Link, R. E., Paus, R., Stenn, K. S., Kuklinska, E. & Moellmann, G. Epithelial Growth by Rat Vibrissae Follicles In Vitro Requires Mesenchymal Contact via Native Extracellular Matrix. *J. Invest. Dermatol.* **95**, 202–207 (1990).

26. Jahoda, C. A., Mauger, A., Bard, S. & Sengel, P. Changes in fibronectin, laminin and type IV collagen distribution relate to basement membrane restructuring during the rat vibrissa follicle hair growth cycle. *J. Anat.* **181 (Pt 1**, 47–60 (1992).

27. Bose, A., Teh, M.-T., Mackenzie, I. & Waseem, A. Keratin K15 as a Biomarker of Epidermal Stem Cells. *Int. J. Mol. Sci.* **14**, 19385–19398 (2013).

28. Abbas, O., Richards, J. E., Yaar, R. & Mahalingam, M. Stem cell markers (cytokeratin 15, cytokeratin 19 and p63) in in situ and invasive cutaneous epithelial lesions. *Mod. Pathol.* **24**, 90–97 (2011).

29. Schmidt, B. & Horsley, V. Unravelling hair follicle-adipocyte communication. *Exp. Dermatol.* **21**, 827–830 (2012).

30. Thangapazham, R. L. et al. Dissociated Human Dermal Papilla Cells Induce Hair Follicle neogenesis in Grafted Dermal–Epidermal Composites. J. Invest. Dermatol. 134, 538–540 (2014).

VII-6. SUPPLEMENTARY IMAGES
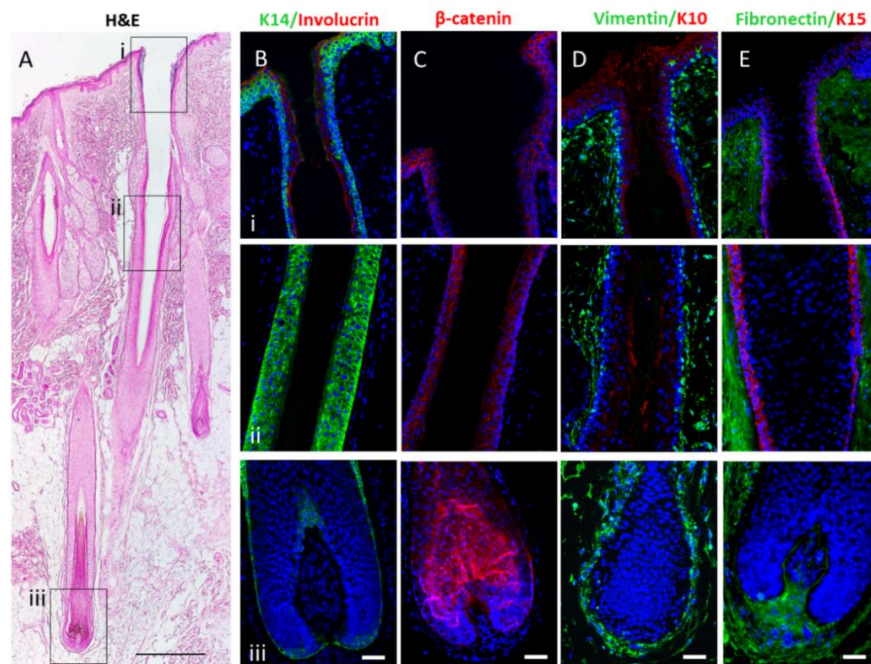
Supplementary Figure VII-1 - Histological analysis of human scalp skin and respective HFs. A) H&E images demarking the (i) invagination area, (ii) an upper middle portion and (iii) the hair bulb. Representative images showing expression of (B) K14 (green), involucrin (red), (C) β-catenin (red), (D) vimentin (green), K10 (red), (E) fibronectin (green) and K15 (red) within the HF and surroundings. Nuclei were counterstained with DAPI. Scale bars are 500 µm for (A) and 50 µm for (B-E).
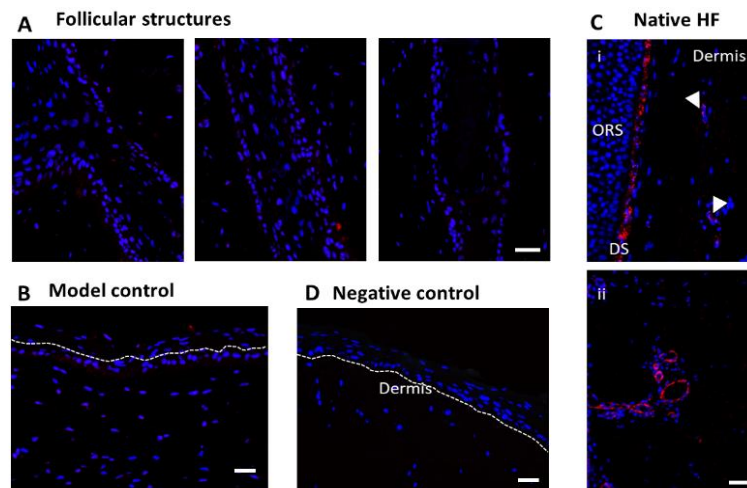
Supplementary Figure VII-2 Expression of α-SMA in the created model and native tissue. Representative immunocytochemistry images of the expression of α-SMA (red) in (A) the recreated HF-like structures and adjacent fibroblasts, and in (B) a control organotypic skin model without the DP-KCs aggregates and without ablation. (C) In human skin, α-SMA (red) expression can be observed in the HF dermal sheath (i) and blood vessels present within the dermis (i-arrowhead, ii). (D) Represents the negative control. Nuclei were counterstained with DAPI (blue). Scale bars = 50 µm.

CHAPTER VIII

GENERAL CONCLUSIONS

AND FUTURE PERSPECTIVES

CHAPTER VIII

GENERAL CONCLUSIONS AND FUTURE
PERSPECTIVES

The hair follicle (HF) critically contributes to the most important physiological functions attributed to the skin and has an elevated aesthetical and social role in humans. So far, HF regeneration has been mainly attempted through the combination of key cellular players as a strategy to elicit the epithelial-mesenchymal interactions that promote hair development and growth. In spite of the few reports demonstrating hair reformation following the use - total or partial - of children/neonatal tissue cell sources, HF regeneration using adult cells remains defiantly unmet. This limits the use of autologous therapies, making it difficult to satisfy the needs of patients suffering from significant skin losses, disfigurement or hair disorders.

Relevant trichogenic adult human cells rapidly lose their capacity to support hair growth after isolation and expansion in culture, which are indispensable for any cell-based regenerative strategy. This creates a paradox that can only be overcome with the development of alternative *in vitro* approaches to maintain or recover human cells' trichogenic capacity throughout the culture. It was under this context that the work reported in this thesis was developed, to tackle those issues and with the expectation of contributing with relevant knowledge to support the development of new or improved strategies.

Facing the need of a large number of receptive epithelial cells for regenerative strategies, we proposed the use of epidermal keratinocytes (KCs) with stem-like features (EpSIKCs) as a direct alternative to follicular KCs, usually obtained from small tissue portions such as plucked or excised HFs. EpSIKCs were obtained after selection of the $\alpha6^{high}/CD71^{dim}$ cellular subfraction from the whole interfollicular keratinocyte population, and subsequently cultured onto feeder cells to sustain their undifferentiated status. Although displaying a proliferative capacity and an expression profile of epithelial markers similar to their follicular counterparts, EpSIKCs represent a more available epithelial cell source that can be obtained from surgically discarded skin. Moreover, EpSIKCs paracrine signaling improved dermal papilla (DP) cell phenotypic profile, inductivity and even morphology, particularly for short culture times. In turn, DP cells markedly promoted EpSIKCs proliferation and supported a tight balance

between EpSIKCs division and differentiation over the culture time, as it is their function within the native tissue. Ultimately, EpSIKCs co-grafting with DP cells in mice led to the recreation of immature structures resembling HFs and sebaceous glands (SGs). Despite the promising results, EpSIKCs application in human regenerative strategies will require changes in the experimental protocol, namely the replacement of the mice feeder cells used for their culture. Human dermal fibroblasts were previously shown to be suitable feeders for an effective expansion of KCs *in vitro* thus, and since they can be isolated from the same skin samples as EpSIKCs, they might be used as an alternative source, overcoming safety restrictions.

Tackling the most ubiquitous problem encountered in the field of HF regeneration - the rapid loss of hair inductive properties that human DP cells undergo in culture - three independent strategies were explored in this thesis:

(i) Use of KCs conditioned medium (KCs-CM), as representative of the epithelial compartment paracrine signaling, to culture DP cells. Culturing DP cells with KCs-CM improved these cells' alkaline phosphatase (ALP) activity and the respective self-aggregation capacity, two important properties directly related to DP cell hair-inductive capacity. DP cell secretome profile was also altered after culture with KCs-CM, showing a profile that matches the one observed during anagen, further sustaining an inductive recovery. Likewise, KCs-CM treatment promoted cell proliferation and rescued DP cell morphology to one representative of lower passages. Considering that DP cells cultured in 3D spheroids partially recover their native signature, we showed that spheroids from DP precultured with KCs-CM have higher active ALP levels than the conventional ones, demonstrating the superiority of our strategy. *In vivo* experimentation further supported CM-pretreatment as an effective method to improve DP cell native properties, as shown by the development of HFs- and SGs-like structures. The reformation of a hair bulb and shaft elongation observed in one animal further reinforces the benefit of KCs-CM, whose potential can be further expanded after an in-depth analysis of its composition and correlation with other culture conditions, particularly the culture time and medium.

(ii) DP cell 3D culture in extracellular matrix (ECM)-mimicking hydrogels. Using a biomaterial-based approach, DP ECM biomimicry was pursued with gellan gum (GG) hydrogels after functionalization with peptides of collagen IV (HepIII) and fibronectin (cRGDfC), both preeminently expressed in the DP's ECM. Both peptides promoted cell adhesion within GG hydrogels with higher polymer concentration (1.25% *vs* 0.75% GG), although the cellular network and extension of cell-cell interaction were higher in HepIII functionalized hydrogels. Moreover, stiffer hydrogels (1.25% GG) were

also capable of improving DP cell inductive phenotype (active ALP levels and markers expression) and recapitulating basic hair morphogenesis events in an organotypic human skin model, independently of the conjugated peptide. This suggests that the three-dimensionality and GG similarity with the native DP ECM glycosaminoglycans composition (conferred by the presence of glucuronic acid residues) *per se*, contribute to the generation of a microenvironment in which the phenotype and physiological functions of DP cells are supported. Considering these results, we propose the use of the developed cell-laden hydrogels as an artificial DP for *in vitro* testing.

(iii) Recreation of HF physiological oxygen levels in DP cell culture. Under a 5% O_2 atmosphere, DP cell senescence and reactive oxygen species (ROS) levels decreased, which was also associated with an improvement in the cells' morphological parameters and proliferative capacity. Moreover, their self-aggregative properties were partially rescued, although no apparent effect was observed in ALP activity. DP cells and melanocytes (hMel) are in close proximity *in situ* and, interestingly, the type of interactions *in vitro* influenced their response to physoxia. When in indirect co-culture, the cells did not seem to affect each other, except for the higher ROS levels observed in comparison to normoxia (21% O_2). Curiously, when directly interacting, ROS levels were unexpectedly higher in physoxia than in normoxia, suggesting ROS formation by an alternative mechanism other than just oxygen availability. Indeed, during anagen, a transient elevation in ROS levels is required to sustain hair growth, which seemed to be replicated *in vitro*. Cells in direct co-culture also organized in a microarchitecture and had a phenotype that mimicked the native one. Moreover, both hMel tyrosinase and DP cell ALP activities, their main functional indicators, were significantly improved. Overall, we showed that the response to physoxia differs according to hMel-DP cells type of interaction and that the microenvironment recreated when these cells are in direct contact favors their follicular functions.

Although representing distinct strategies, it is relevant to highlight that these three approaches can be easily combined in culture. DP cell expansion is a necessary step to obtain cell numbers suitable for regenerative applications, and both DP cell culture with KCs-CM or under physoxia maintain the cells in a healthy proliferative state. However, CM treatment has the advantage of improving ALP activity in 2D cultured cells. DP cell encapsulation in stiffer GG-derived hydrogels shows a similar effect but for a short culture time which means that, similarly to DP spheroids, this strategy does not sustain long-term *in vitro* culture, requiring a fast application. Considering this, an integrated strategy would be to expand DP cells with KCs-CM under a 5% O_2 atmosphere until an adequate number of cells is obtained and, only then produce the artificial DPs, either for *in vitro* testing or clinical applications. Although it is difficult to

ascertain at which extent the developed strategies may provide a cumulative effect without further experimentation, it is safe to conclude that some advantages will be obtained by combining these strategies.

At last, the inadequacy of animal models to test human-dedicated HF regenerative approaches and the lack of skin *in vitro* models capable of sustaining HF development, inspired the fabrication of a more complex skin model containing HF-like structures. Our model was established considering two of the most important hallmarks for HF development - the promotion of epidermal invaginations and the epithelial engulfment of DP cell condensates. To foster these events, compartmentalized aggregates containing DP cell spheroids surrounded by KCs were incorporated in the dermal equivalents of a standard skin organotypic model. Then, microscopy-guided laser ablation (MGLA) was used to create 3D microchannels from the surface of the model up to the cell aggregates, to promote epithelial cell migration and downward movement. As a result, follicular structures that recapitulated the HF physiology and architecture were recreated. The developed construct containing HF-like structures holds great potential to be used either as an *in vitro* platform to study the mechanisms controlling HF development or as a more complex and functional skin model. Nevertheless, they still offer opportunities for improvement. To broaden the range of applications of the model other important cell types, including neuronal and immune cells and melanocytes could be incorporated. The later is necessary for pigmentation and could be easily incorporated together with KCs in the compartmentalized DP-KCs aggregates. Moreover, during anagen, the hair bulb is deeply embedded in the subcutaneous tissue, which in turn is increasingly associated with the regulation of hair growth. Thus, the inclusion of a hypodermis-mimetic layer at the base of the model, and in closer contact with the DP-KCs aggregates to allow their communication, might have a role in the maturation of the attained follicular structures, possibly even allowing hair shaft formation.

Besides *in vitro* applications, the use of the produced constructs as skin substitutes is equally realistic. The model was inbuilt in a reconstructed skin equivalent whose production is similar to the ones already used in the clinics. The exception was the use of rat tail collagen instead of bovine or porcine collagen matrices which, however, can be easily replaced to comply with safety regulations. Nonetheless, to reach clinical applications with a significant impact, other modifications capable of improving its functionality should be implemented. For example, vasculature - whose network construction may be equally introduced in the model using a MGLA strategy and subsequent endothelial cell seeding - would certainly improve the model integration within the patient's skin wounds and

improve its survival. Moreover, it would also be relevant to replace the skin KCs used in the reconstructed epidermis by EpSIKCs. Their higher immature status may improve the constructs' self-renew capacity, as well as possibly supporting the maturation of the attained folliculoid structures and, ultimately, hair formation.

Notwithstanding their promising application as skin substitutes for wound management, these constructs are not expected to be equally applied in the context of hair loss disorders, in which a high density of HFs is required to provide aesthetically acceptable solutions. Previous results demonstrated that human HF reformation can occur when DP cell spheroids are placed between the epidermis and dermis of human skin and then placed on mice, in a "human-to-human inductive assay". This demonstrates that the maintenance of DP cell in 3D culture conditions and in close contact with human (and not animal) epidermis and respective species-matched signaling, may prove enough to support hair growth. In this thesis, we demonstrated that the increase of ALP activity in DP cells encapsulated within 1.25% GG-derived hydrogels (artificial DP) is higher than the one observed in spheroids, offering clues of an improved hair-inductive capacity. Moreover, and as previously mentioned, this increase may even be boosted by simultaneous culture with KCs-CM. Considering this, it is feasible to envisage a direct application of the injectable artificial DPs as hair-forming units. The use of GG hydrogels would be less invasive than the currently used hair transplantation procedure, which represents the only available treatment for baldness.

Although the discussed perspectives can only be considered theoretical for now, further testing is expected to generate important contributions in the field of hair regeneration representing another step towards the development of successful autologous trichogenic cell-based therapies.